

TWO CENOZOIC FLORAS FROM SOUTH AMERICA: PALEOCLIMATIC AND  
PALEOALTIMETRY INFERENCES

A Dissertation

Presented to the Faculty of the Graduate School

of Cornell University

In Partial Fulfillment of the Requirements for the Degree of

Doctor of Philosophy

by

Camila Martinez Aguillon

May 2019

© 2019 Camila Martinez Aguillon

# TWO CENOZOIC FLORAS FROM SOUTH AMERICA: PALEOCLIMATIC AND PALEOALTIMETRY INFERENCES

Camila Martinez Aguillon, Ph. D.

Cornell University 2019

Tropical America contains more plant species than any other continental area.

Understanding the origins of its flora and its adaptations to dynamic climate and topography during the Cenozoic are fundamental not only to studying its evolutionary history but also to predicting the effects of contemporary anthropogenic climate change. Here, I describe two floras from Tropical America, one from the Neogene of Peru and another one from the Paleogene of Colombia. Using detailed stratigraphic context, I collected numerous plant fossils that included leaves, fruits, seeds, flowers, cuticles, and wood, in addition to collecting rock samples for relative and absolute dating purposes, and for palynological (pollen and spores) analysis. The fossil material collected at each locality was carefully prepared, morphotyped, described, and when possible, formally named. Quantitative paleoclimatic and paleoelevation analyses were performed for each fossil locality and, in addition, I compared them with extant ecosystems and their characteristic taxa.

The results from the Neogene of Peru support hypotheses that suggest that the plant fossil record indicates a rapid surface uplift of approximately 2500 m in the northern part of Central Andean Plateau during the late Miocene to early Pliocene. Estimations based on these analyses also suggest that, contrary to what paleoclimate models have predicted for this region, the precipitation of the Central Andean Plateau was higher during the early Pliocene and late

Miocene. The evidence presented here for this site also documents the earliest Puna-like ecosystem during the early Pliocene, and the existence of a montane ecosystem without modern analogs during the late Miocene.

The results from the late Eocene of Colombia provide the earliest evidence of a seasonally dry tropical forest ecosystem based on both paleoclimatic analyses and taxonomic affinities of the floral elements. This site also includes the earliest confirmed record of Passifloraceae based on fossil seeds in addition to a legume samara from the clade Dalbergieae; a clade that is today mostly restricted to tropical dry forest ecosystems.

## BIOGRAPHICAL SKETCH

Camila Martínez is a Colombian Paleobotanist. She attended the Universidad de los Andes, Bogota, Colombia from 2004–2011. There she received her Bachelor of Science degree in Biology in 2009, and a Master of Science degree in Biological Sciences in 2011. Since 2009 she has been working in close collaboration with the Center of Tropical Paleoecology and Archaeology from the Smithsonian Tropical Research Institute in different research projects. In 2013, she was awarded a Fulbright-Colciencias Doctoral Fellowship to pursue her Ph.D. in the Plant Biology Section, from the School of Integrative Plant Sciences from Cornell University. In 2019, she was awarded with the Smithsonian Institution Fellowship Program for starting a postdoctoral project at the Smithsonian Tropical Research Institute in Panama.

Dedicated to the memory of Margarita Gómez whom I will always carry in my heart, may her  
memory bring peace

## ACKNOWLEDGMENTS

I would like to thank the members of my committee W.L. Crepet, M.A. Gandolfo, T.E. Jordan, and K.C. Nixon, and also M. Carvalho, N. Jud, J. Svitko for their help and support during the course of my dissertation research. I especially thank C. Jaramillo for his constant support and advice throughout my professional career as a Paleobotanist.

I thank my family, in particular my parents for their unconditional love and support. I also thank all my friends from around the world for making my time at Cornell such an enjoyable period of my life and who taught me so much about life.

I deeply in debt with Fulbright-Colciencias for granting me a Doctoral Fellowship and the Plant Biology Section, School of Integrative Plant Science, Cornell University; and the Harold E. Moore Jr. Memorial and Endowment Funds from Cornell University, for funding and support.

Additional acknowledgments for specific sub-sections of this dissertation are given below:

*Chapter 1*—The authors thank R. Salas-Guismondi, J. Tejada, M. Arakaki for providing help in the field and space at the Museum of Natural History of Lima, Peru; G. Umasi for his valuable help in the field; the community of the Espinar Province for welcoming us and letting us to explore the area. C. Martinez thanks the Cornell Graduate School Research Travel Grant.

*Chapters 2, 3 and 4*— I thank W. Crepet, M. A. Gandolfo, T. Jordan, and C. Jaramillo, for guidance throughout the duration of project; M. Carvalho and N. Jud for support and advice at different stages of the project. F. Moreno, A. Cárdenas, L. Espitia, C. Monje, H. Garcia, L. Bueno, A. Zuñiga, K. Jiménez, S. Gómez, and C. Rosero for valuable help in the field; C. Montes and the Geoscience Department of the Universidad de los Andes, Colombia for

providing work space; the Bailey Hortorium Herbarium for access to plant material; and the Mapuka Museum of the Universidad del Norte, Colombia for providing storage space for the collection. This project was supported by the Howard T. Corrigan Fund of the Asociación Colombiana de Geólogos y Geofísicos del Petroleo, Harold E. Moore Jr. Memorial and Endowment Funds from Cornell University, Latin American Studies Association and the Einaudi Center from Cornell University, the Smithsonian Tropical Research Institute, Servicio Geológico Colombiano, and Isagen.

## TABLE OF CONTENTS

Biographical Sketch .....	v
Dedication .....	vi
Acknowledgments .....	vii
Table of Contents .....	ix
List of Figures .....	xi
List of Tables .....	xiv
<b>CHAPTER 1: Neogene climate, vegetation, and elevation history of the Central Andean</b>	
Plateau .....	6
Abstract .....	7
Main text .....	8
References .....	18
Supplementary materials .....	22
Materials and methods .....	22
Supplementary text .....	31
Supplementary references .....	95
Supplementary figures .....	99
<b>CHAPTER 2: The paleobotanical record from the Middle to Late Eocene Esmeraldas Formation</b>	
from Colombia .....	139
Abstract .....	139
Introduction .....	140
Methods .....	148
Results .....	152
Discussion .....	206
Conclusions .....	215
References .....	216
Supplementary material .....	222
<b>CHAPTER 3: Dalbergieae (Fabaceae) samara fruits from the late Eocene of Colombia.....</b>	<b>231</b>
Abstract .....	231
Introduction .....	233
Materials and methods .....	235
Results .....	240
Discussion .....	252
References .....	256
Supplementary material .....	259
Appendix A1 .....	259
Table A1 .....	261

Appendix A2 .....	263
<b>CHAPTER 4: Passifloraceae seeds from the late Eocene of Colombia.....</b>	<b>264</b>
Abstract .....	264
Introduction .....	265
Materials and methods .....	268
Results .....	274
Discussion .....	284
References .....	288
Supplementary material .....	297
Appendix S1 .....	297
References appendix S1 .....	298
Appendix S2 .....	301

#### **SUPPLEMENTARY DATA**

- Data S1. Library of modern pollen taxa distribution along the environmental space  
(Chapter 1)
- Data S2. Library of modern macrofossil taxa distribution along the environmental space  
(Chapter 1)

## LIST OF FIGURES

### INTRODUCTION

Fig. 1. Fossiliferous outcrops.....	3
-------------------------------------	---

### CHAPTER 1

Fig. 1. Geographic location and precipitation of the CAP .....	9
Fig. 2. Environmental space .....	13
Fig. 3. Floristic comparison.....	17

### SUPPLEMENTARY MATERIAL

Fig. S1. Geological map of the Descanso-Yauri Basin.....	99
Fig. S2. Geological setting of the Descanso-Yauri Basin.....	100
Fig. S3. Cathodoluminescence images of zircon .....	101
Fig. S4. Wetherill concordia diagrams.....	102
Fig. S5. Micrographs of palynomorphs.....	103
Fig. S6. Micrographs of palynomorphs.....	104
Fig. S7. Micrographs of palynomorphs.....	105
Fig. S8. Micrographs of palynomorphs.....	106
Fig. S9. Micrographs of palynomorphs.....	107
Fig. S10. Micrographs of palynomorphs.....	108
Fig. S11. Micrographs of palynomorphs.....	109
Fig. S12. Micrographs of palynomorphs.....	110
Fig. S13. Micrographs of palynomorphs.....	111
Fig. S14. Micrographs of palynomorphs.....	112
Fig. S15. Micrographs of palynomorphs.....	113
Fig. S16. Wood anatomy DSB1.....	114
Fig. S17. Wood anatomy DSB2.....	115
Fig. S18. Topographic map and structural section, from the San Miguel region. ....	116
Fig. S19. Wood anatomy DSB3.....	117
Fig. S20. Wood anatomy DSB4.....	118
Fig. S21. Leaf fragments DSB5.....	119
Fig. S22. Macrofossil compressions and impressions from Member C. ....	120
Fig. S23. Palynological counts and number of taxa.....	121
Fig. S24. Correction of temperature estimates by global temperature anomaly.....	122
Fig. S25. Probability density for environmental space.....	123
Fig. S26. Elevation and precipitation estimates under the mixture model.....	124
Fig. S27. Marginal probability density for elevation and precipitation.....	125
Fig. S28. Credible distribution of elevation and precipitation.....	126

Fig. S29. Generalized linear model comparison for plant habit. ....	127
Fig. S30. Comparison of the relative abundance of angiosperm and fern taxa.....	128
Fig. S31 Modern palynological dataset.....	129
Fig. S32. Palynoflora composition along an altitudinal gradient.....	130

## CHAPTER 2

Fig. 1. Location of fossil plant outcrops. ....	144
Fig. 2. Chronostratigraphic correlation Llanos section .....	147
Fig. 3. Stratigraphic section .....	155
Fig. 4. Chronostratigraphic correlation Nuevo Mundo Syncline .....	157
Fig. 5. Fossil leaf morphotype exemplars.....	167
Fig. 6. Micrographs of cuticles .....	169
Fig. 7. Fossil leaf morphotype exemplars.....	178
Fig. 8. Fossil leaf morphotype exemplars.....	185
Fig. 9. Fossil leaf morphotype exemplars.....	189
Fig. 10. Morphotype ES49.....	191
Fig. 11. Morphotype ES50.....	192
Fig. 12. Morphotype ES51.....	193
Fig. 13. Morphotype ES52.....	195
Fig. 14. Morphotype ES53.....	197
Fig. 15. Phylogenetic tree for Solanaceae .....	198
Fig. 16. Morphotype ES54.....	200
Fig. 17. Morphotype ES55 AND ES56 .....	202
Fig. 18. Morphotype ES57.....	203

## SUPPLEMENTARY MATERIAL

Fig. S1. Stratigraphic section for the Paleogene of the Nuevo Mundo Syncline .....	222
--	-----

## CHAPTER 3

Fig. 1. Geographic and geological location .....	236
Fig. 2 Stratigraphic section .....	237
Fig. 3. Extant samaras of the clade Dalbergieae .....	245
Fig. 4. Phylogenetic placement of the fossil samara.....	246
Fig. 5. Fossil samara fruit <i>Luckowcarpa gunnii</i> gen. and sp. nov. ....	250
Fig. 6. Dissected modern Dalbergieae samaras. ....	251

## CHAPTER 4

Fig. 1. Geographic and geological location. ....	270
Fig. 2. Stratigraphic section. ....	272
Fig. 3. Fossil seed of <i>Passifloroidesperma sogamosense</i> sp. nov. ....	277

Fig. 4. Extant seeds of Passifloroideae. ....	281
Fig. 5. Phylogenetic tree of Passifloraceae. ....	283

## LIST OF TABLES

### CHAPTER 1

#### SUPPLEMENTARY MATERIAL

Table S1. U-Pb geochronological analyses.....	131
Table S2. Palynological samples.....	132
Table S3. Macrofossil samples. ....	134
Table S4. Fossil pollen taxa identified at family level.....	135
Table S5. Fossil pollen taxa identified at genus level.....	136
Table S6. Elevation and precipitation estimates. ....	137
Table S7. Taxa present in the macrofossil record.....	138

### CHAPTER 2

Table 1. Mean leaf area estimation. ....	205
Table 2. Results of leaf margin and leaf area analysis .....	206

#### SUPPLEMENTARY MATERIAL

Table S1. Isotopic analysis results of $\delta^{13}\text{C}_{\text{TOM}}$ .....	225
Table S2. Values of in-house standards .....	226

### CHAPTER 3

Table 1. Leguminosae genera with samara fruits.....	241
Table 3. Morphologic characters of Leguminosae samaras.....	242

### CHAPTER 4

Table 1. Fossil record of Passifloroideae .....	267
Table 2. Families with ruminant endosperm.....	278
Table 3. Families with palisade seed coat.....	279

## INTRODUCTION

Efforts to understand the history of Neotropical (Tropical America) ecosystems and their past climates have been constrained by the scarce fossil record. The Neotropical region, contains an estimated 90,000 plant species, more than any other continental area (Thomas, 1999).

Understanding the origins of its flora and the history of their adaptations to a dynamic climate and topography during the Cenozoic are fundamental for predicting world floral changes under similarly dynamic climatic conditions that apply today. Tropical regions, however, represent a challenge for paleontologists, since most of the tropical terrestrial surface is covered by vegetation and therefore, there are fewer outcrops available for paleontological exploration. In addition, there has been a disparity in the geographic concentration of scientists interested in collecting botanical fossils. Only today are we seeing higher numbers of interested South American paleobotanists. In spite of this exciting development, there are still challenges in evaluating South American paleofloras. Access to rural areas is also often difficult due to the complex topography, road access, and safety concerns. Even with this exciting increase in the number of interested scientists, the number of researchers in this region remains lower compared to those in temperate regions as a result of the sociopolitical situations, funding resources, and education access.

The current anthropogenic climate change has already caused an increase in the global temperature of 1.5°C and an increase in atmospheric CO<sub>2</sub> concentration (*p*CO<sub>2</sub>) of more than 410 ppm (IPCC, 2018). During the last 800,000 years, Earth did not experience *p*CO<sub>2</sub> above 300 ppm, not even during interglacial periods. Consequently, to understand and compare the changes that the Earth could have faced during warmer periods with higher *p*CO<sub>2</sub>, it is important to go

further back in time, to the Paleogene and Neogene periods, in order to improve future predictions.

Working in paleontology has constraints relative to experimental sciences. Although we work within the boundaries of existing knowledge with some predictive power, when exploring new areas, we cannot always imagine what questions will be addressable from the material that we might discover. Additionally, the exploration of new localities often involves failed field trips without fossil material from new potential localities. With the aim of studying Cenozoic records of the Neotropics, I chose to explore three new sites in which ongoing related projects were being undertaken by collaborators and for which there was some previous knowledge of their potential value for the questions I was interested in pursuing. These three sites are located in the Peruvian Central Andean Plateau, the Peruvian Amazon, and the piedmont of the eastern cordillera from Colombia.

The Peruvian Central Andean Plateau is characterized by low vegetation cover, therefore a large area around the Espinar municipality was explored, and large outcrops and fossil material were found along a Miocene and Pliocene section (Fig. 1). The Peruvian Amazon, as expected, is densely covered by vegetation, and restricted our exploration to rock exposures along roads that were recently broadened near the Tarapoto town in the San Martín region (Fig. 1). Despite the efforts in this site, the material found was not abundant and did not have sufficient preservation for a detailed study. The site from northeastern Colombia was also densely covered by vegetation. There, I had the opportunity to participate in a paleontological salvage project during the construction of the Topocoro dam, in which one of the most important findings was the Eocene macroflora I studied here (Fig. 1). After evaluating the potential of each site in early stages of the exploration, I decided to focus additional work in the Neogene site from the Central

Andean Plateau and the Eocene locality from the Piedmont of the eastern cordillera of Colombia. The plant fossil record from each site allowed me to not only describe new taxa but also to address research questions related to paleoclimate, paleoelevation, biogeography, and evolution of Neotropical lineages.



**Fig. 1.** Fossiliferous outcrops. (a) Side of a road in the Peruvian Amazon, Huallaga Basin, San Martín, Peru. (b–d) Outcrops around the Topocoro Dam, Middle Magdalena Valley Basin, Santander, Colombia. (e–h) Outcrops around the Espinar Region in the Central Andean Plateau, Descanso-Yauri Basin, Cusco, Peru.

Hitherto, there are some macrofossil records of plant taxa from the Neotropics, however, most of those were published before the 60s and their ages and geologic settings were often not described accurately or in detail, and often the taxonomic affinities proposed did not include broad comparisons with extant material. A careful re-examination of those records is necessary

in most cases to obtain an accurate age determination and taxa identifications (Burnham and Johnson, 2004). In addition, quantitative climatic analyses have only been performed in a few Neotropical localities (Kowalski, 2001; Gregory-Wodzicki, 2002; Wing et al., 2009).

Aiming to overcome inaccuracy in the age determination in this study, radiometric dating techniques from igneous samples were implemented when these were available, and performed chemostratigraphic and biostratigraphic analyses in other cases. To perform quantitative analyses, fossils were collected systematically in each locality and then described following standard procedures. Finally, in order to propose taxonomic affinities with confidence, we made comparisons with abundant extant material and only named taxa formally when there was enough evidence to support these proposed taxonomic affinities.

Predicting the future climate of the Neotropics under our current global warming scenario requires a deep understanding of the modern climate of the region and the implications of the Andean cordillera as a topographic barrier for atmospheric circulation. This dissertation project allowed me to approach this important topic from different perspectives, methods and time frames. To perform this dissertation project, I had the collaboration and advice from numerous people and institutions. Chapter 1 includes the paleobotanical record, geologic setting, and paleoclimatic and paleoelevation inferences from the Neogene Descanso-Yauri Basin from the Central Andean Plateau of Peru. In Chapter 2 I described the plant macrofossil record from the Eocene Esmeraldas Formation of Colombia, its geologic setting and paleoclimatic inferences. In Chapter 3 I formally described a samara fossil fruit from the legume Dalbergieae clade from the Esmeraldas Formation. And in Chapter 4 I also formally described a Passifloroideae seed from the Esmeraldas Formation.

## REFERENCES

- Burnham, R. J., and K. R. Johnson. 2004. South American palaeobotany and the origins of neotropical rainforests. *Philosophical Transactions of the Royal Society B: Biological Sciences* 359: 1595–1610.
- Gregory-Wodzicki, K. M. 2002. A late Miocene subtropical-dry flora from the northern Altiplano, Bolivia. *Palaeogeography, Palaeoclimatology, Palaeoecology* 180: 331–348.
- IPCC. 2018. Global warming of 1.5°C. World Meteorological Organization, Geneva.
- Kowalski, E. A. 2001. Middle to late Miocene environments of southern Ecuador: Temperature, elevation, and fossil plants of the Nabón Basin. Ph.D. University of Michigan, United States -- Michigan.
- Thomas, W. W. 1999. Conservation and monographic research on the flora of Tropical America. 8: 1007–1015.
- Wing, S. L., F. Herrera, C. A. Jaramillo, C. Gómez-Navarro, P. Wilf, and C. C. Labandeira. 2009. Late Paleocene fossils from the Cerrejón Formation, Colombia, are the earliest record of Neotropical rainforest. *Proceedings of the National Academy of Sciences* 106: 18627–18632.

## CHAPTER 1

### NEOGENE CLIMATE, VEGETATION, AND ELEVATION HISTORY OF THE CENTRAL ANDEAN PLATEAU

**Authors:** C. Martínez<sup>1,2\*</sup>, C. Jaramillo<sup>2</sup>, A. Correa-Metrío<sup>3</sup>, W. Crepet<sup>1</sup>, E. Moreno<sup>2</sup>, A. Aliaga<sup>4</sup>,  
F. Moreno<sup>5</sup>, M. Ibañez-Mejía<sup>5</sup>, M. Bush<sup>6</sup>

**Affiliations:**

<sup>1</sup>Plant Biology Section, School of Integrative Plant Sciences, Cornell University, 412 Mann Library Building, Ithaca, NY, USA 14853.

<sup>2</sup>Smithsonian Tropical Research Institute, Unit 0948, APO AA 34002, Balboa, Ancon, 0843-03092, Panama.

<sup>3</sup>Instituto de Geología, Universidad Nacional Autónoma de México, Ciudad de México 04520, México

<sup>4</sup>Departamento de Paleontología de Vertebrados, Museo de Historia Natural Lima- UNMSM, Av. Arenales 1256, Jesús María, Lima, Perú

<sup>5</sup>Earth & Environmental Sciences, University of Rochester, 227 Hutchison Hall, University of Rochester, Rochester, NY, USA 14627

<sup>6</sup>Ocean Engineering and Marine Sciences, Florida Institute of Technology, 225 Harris Building, Melbourne, FL, USA 32901

## ABSTRACT

A rapid surface uplift of approximately 2500 m occurred in the Central Andean Plateau (CAP) during the Neogene. Understanding the impact of this event on climate and biota is fundamental to predict the effects of future rapid climate change on regional biomes. We investigated the fossil record from the Neogene of this region (pollen, leaves, fruits, wood). Our estimations suggest that compared with modern CAP, regional precipitation was higher during the early Pliocene when the area was near modern elevations, and was even wetter during the late Miocene, when the cordillera was around ~1700 m.a.s.l. By the early Pliocene there existed a Puna-like ecosystem with a higher abundance of ferns than today, and a late Miocene montane ecosystem without modern analogs.

**One Sentence Summary:** Neogene climate of the Central Andean Plateau

## MAIN TEXT

The Andean mountain range, with an average elevation of 4000 m, exerts vast influence on the regional climate and biogeography of South America. The Central Andean Plateau (CAP), inclusive of the Altiplano, is the second largest plateau in the world after Tibet, and preserves an outstanding Cenozoic (*i.e.*, syn-uplift) sedimentary record. Paleo-elevation reconstructions based on stable isotopes, tectonics, paleobotany, and geodynamics suggest that the northernmost part of the CAP (NCAP) experienced a rapid surface uplift of approximately 2500 m during the Late Miocene and attained near-modern elevations by the early Pliocene (Saylor and Horton, 2014; Kar et al., 2016; Garzzone et al., 2017) (Fig. 1). In the NCAP, the Descanso-Yauri Basin preserves Miocene and Pliocene fossils in a sequence that spans the time before and after the uplift event, thus offering a unique opportunity to study the timing and magnitude of uplift, and its effects on regional ecosystems and climates. A previous study from this basin, using mainly stable isotopes, suggests that until the Late Miocene (~9 Ma) paleo-elevations ranged from ~ 900 to 2100 m, and by the early Pliocene (~ 4.8 Ma) near-modern elevations were attained (Kar et al., 2016).

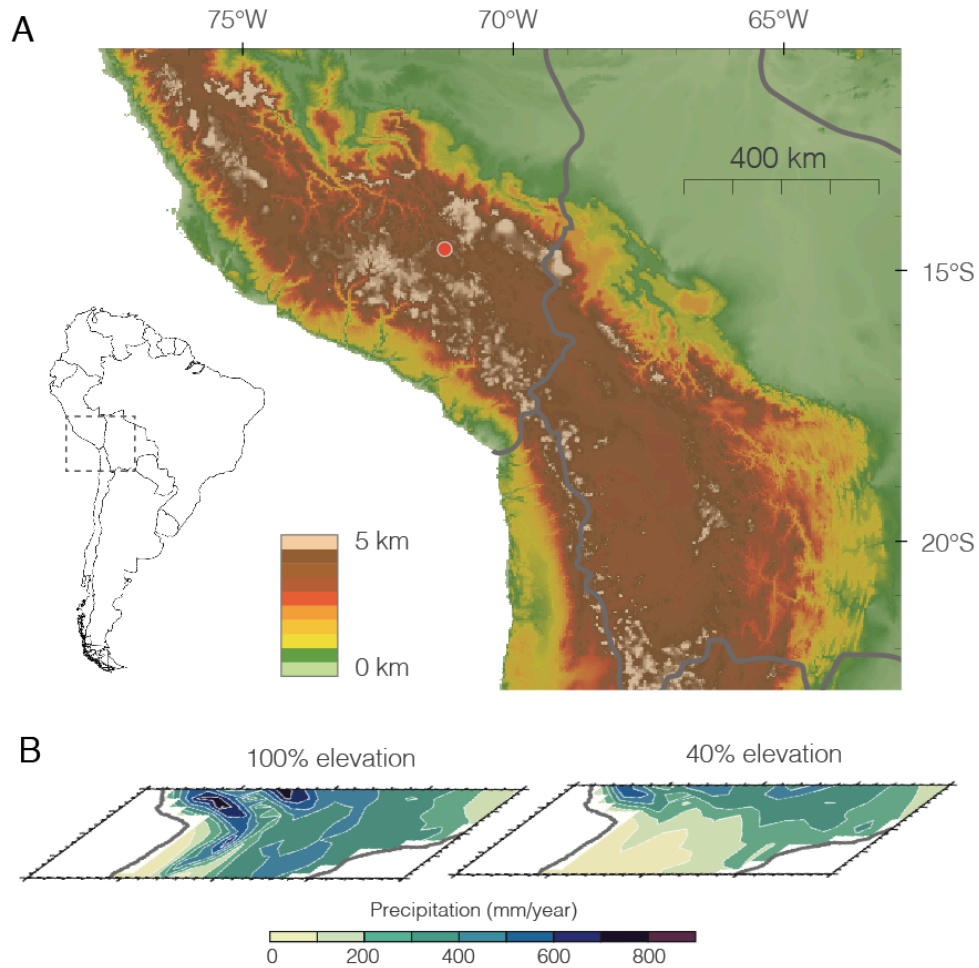


**Fig. 1. Geographic location and precipitation of the CAP**

Geographic location of the CAP, summary of paleoprecipitation estimates from previous studies. (A) Topographic map showing the CAP (GTOPO30 1 km data set) and the location of the Descanso-Yauri Basin (red dot). (B) Simulated response of precipitation when the CAP had 40% its current elevation (Figure taken from *I*).

Assessing the impact of this rapid surface uplift on atmospheric circulation patterns and past climate is fundamental for predicting future climate changes of the region. Predictions on temperature and atmospheric CO<sub>2</sub> concentration ( $p\text{CO}_2$ ) by the end of this century, under our current global warming scenario (Zachos et al., 2008), suggest that these parameters will be similar to those found in the Late Miocene and Early Pliocene. Precipitation predictions under these higher temperature and  $p\text{CO}_2$  scenarios are far more difficult to assess, especially in the

neotropics where global climate models yield contradictory predictions regarding precipitation (Joetzjer et al., 2013). The CAP paleobotanical record provides physical evidence that can be used to reconstruct paleo-precipitation during past warmer global environments, which can in turn be used to test climate model predictions. The modern NCAP sits at ~ 4000 m of elevation, has a mean annual temperature (MAT) ~ 8 – 9 °C, and a mean annual precipitation (MAP) ~ 500 – 800 mm. CAP is characterized by cold and strong winds all year long and it experiences extreme diurnal and nocturnal temperature changes reaching up to 30 °C (Arroyo and Cavieres, 2013). Most of its precipitation falls during the austral summer and its source is predominantly easterly from the Amazon region (Garreaud et al., 2003). Today, this climatic pattern has resulted in a regional vegetation dominated by grasses and shrubs, a type of highland ecosystem called Puna (Kuentz et al., 2012).

Here, we used the Neogene paleobotanical record of the Descanso-Yauri Basin in the NCAP (Fig. 1) to estimate regional paleoelevation and paleoprecipitation. The plant fossil record studied included palynological (pollen and spores), and macrofossil samples (permineralized wood, and compressions and impressions of leaves and fruits) of Middle to Late Miocene and early Pliocene age. This record provides a unique opportunity to: 1) estimate the Neogene paleoprecipitation in the CAP in comparison with previous climate modeling studies; and 2) reconstruct the regional vegetation of both Middle to Late Miocene and early Pliocene. We studied two members from the Descanso Formation: the Middle to Late Miocene Member B ( $18.7 \pm 0.2 - 9.1 \pm 0.7$  Ma) and the early Pliocene Member C ( $4.8 \pm 1 - 3.9 \pm 0.1$  Ma). We determined the age of these localities using previously published stratigraphic information (Kar et al., 2016), together with zircon U-Pb geochronology of two tuff samples within Member B that yielded ages of  $10.03 \pm 0.16/0.18$  Ma and  $12.07 \pm 0.73/0.74$  Ma (SOM). A total of 191

paleobotanical samples were collected from 88 localities from Members B and C. Thirteen samples corresponded with permineralized wood assigned to four morphotypes. Ninety-nine samples corresponded with macrofossil compressions and impressions of leaves and fruits assigned to eight morphotypes. Seventy-five corresponded with palynological samples that included 183 palynomorph taxa and 5428 individual occurrences.

Wood samples were preserved as silica permineralizations and were only found at the top of Member B. Eight specimens had taxonomic affinities with Fabaceae and one with the fossil genus *Anacardioxylon* (Anacardiaceae; Fig. S19). Within Fabaceae two samples were identified within the Tribe Ingeae (Fig. S16), five samples within the mimosoid clade (Fig. S20), and one as the fossil genus *Andiroxylon* sp (Fig. S17). Tree-height was estimated for the *Andiroxylon* sp. sample based on its diameter (Fig. S17A), and estimates ranged from 29.8 to 34.6 m (SOM). All the samples had simple perforation plates. Twelve out of the 13 samples collected had diffuse porous wood and non-distinct growth-rings. Six out of the seven identified samples had large vessel diameters  $>150$  ( $-270$   $\mu\text{m}$ ), and high proportions of axial parenchyma cells (SOM). Leaves were found in both members; Member B had palm leaf fragments, whereas Member C had leaves with taxonomic affinities to five genera and one family that are today present in the Puna: *Ribes* (Scrophulariaceae), *Berberis* (Berberidaceae), *Polylepis* (Rosaceae), *Polystichum* (Dryopteridaceae), *Equisetum* (Equisetaceae), and Juncaceae (Fig. S22). Based on the palynological record, the floristic composition of Member B is dominated ( $>50$  counts) by several families including Podocarpaceae, Cyatheaceae, Polygonaceae, Asteraceae, and Chloranthaceae, while Member C is dominated by the families Poaceae and Cyatheaceae.

Using this paleobotanic record, we performed a quantitative coexistence analysis to reconstruct paleoprecipitation and paleoelevation. The analysis uses climate and elevation

information associated with the nearest living relatives of the identified palynomorphs and macrofossil taxa (SOM). Two distribution datasets (palynological and macrofossil data) were described through bivariate probability density distributions of modern taxon occurrence along elevation and precipitation gradients. Global temperatures during both Middle to Late Miocene and Early Pliocene times were warmer than pre-industrial temperatures. Therefore, we performed a correction of temperature estimates that resulted in average displacements of the elevation estimates by ~650 and 440 m for Members B and C, respectively (Fig. S15). For Member B, the average corrected modal elevation based on palynological and macrofossil data was 1745 m (interquartile range: 1300 – 2210 m), and for Member C was 4005 m (3580 – 4110 m) (Fig. 2). Estimated MAPs based on palynological and macrofossil data were 1619 mm (1192 – 2124 m) for Member B, and 851 mm (593 – 1099 m) for Member C. These estimates of environmental space show a trend that progressed in time towards ascending elevation and decreasing precipitation (Fig. 2). Changes in the environmental space from Miocene to Pliocene were far more drastic than changes from Pliocene to Holocene (Fig. 2 and S18).

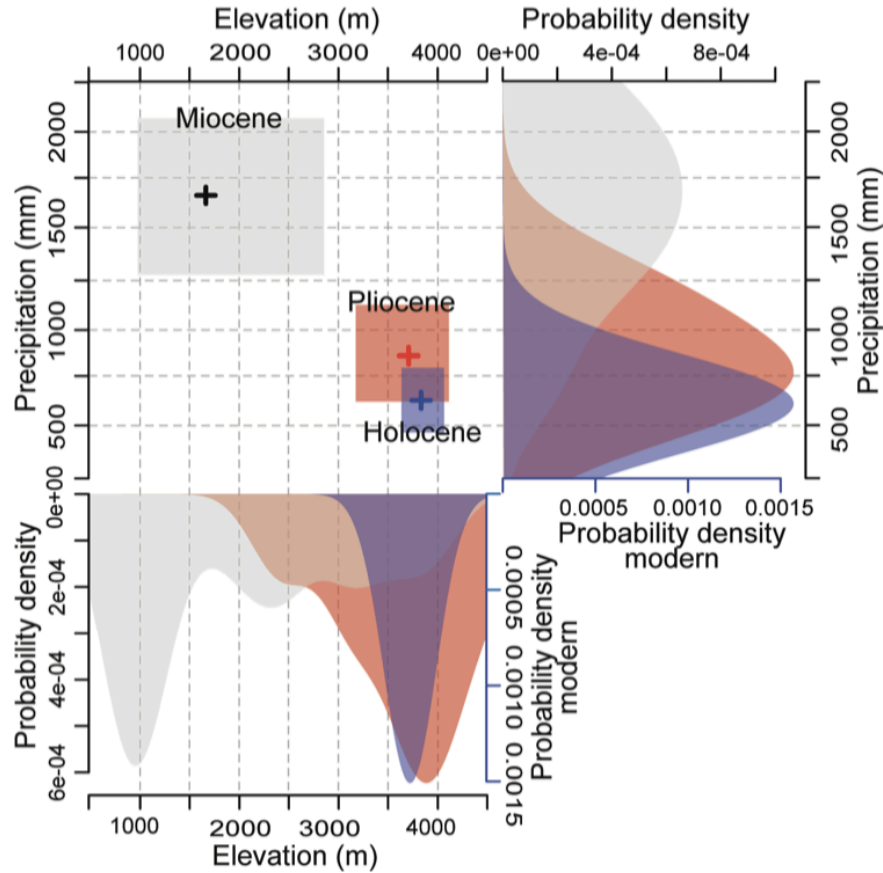


**Fig. 2. Environmental space.**

Estimated environmental space for the Middle to Late Miocene (Member B; grey), the early Pliocene (Member C; red), and the Holocene (blue) at Descanso-Yauri Basin, showing PDFs for precipitation (right) and elevation (bottom). These estimations are based on a mixture of micro- and macrofossil sets.

Wood anatomy and tree diameter also support the aforementioned estimates of elevation and precipitation. In tropical high elevation ecosystems plant growth is dependent on the number of hours of freezing per day (Simpson, 1983). A correlation between tree-height and elevation across six modern Andean elevation transects shows that trees taller than 30 m are not found above ~1100 m of elevation in the Andean region (Girardin et al., 2014). A temperature correction for the Middle to Late Miocene would thus produce higher estimates; assuming that plants shift their distribution upwards when the temperature increases (Fadrique et al., 2018), we

expect that trees of equivalent size would not be found above ~1750 m during the Late Miocene. These observations support a low elevation deposition for Member B, since the fossil log was around 30 m in length. Wood anatomical characters in other petrified fossils such as diffuse porosity, non-distinct growth-rings, vessels with a large diameter, simple perforation plates and a large proportion of axial parenchyma cells (Fig. S16, S17, FS20; SOM), also suggest the presence of tall trees, with lowland affinities, growing in sites with high MAP regimes and low seasonality (Wheeler et al., 2007; Fichtler and Worbes, 2012).

Our reconstructions for the Middle to Late Miocene indicate that when the southern Peruvian Andes were at half of their modern elevation (~1745 m), MAP was about three times higher (~1619 mm) than today. In contrast, regional climate models (ECHAM, GENESIS, LMDz4, PLASIM, RegCM3) predict that half-modern CAP elevations would lead to much-drier-than-modern conditions (Insel et al., 2009, 2012; Garreaud et al., 2010; Poulsen et al., 2010; Sepulchre et al., 2011; Lease and Ehlers, 2013). For example, the global ECHAM model indicates that when the Andes were at 40% of their modern elevation, MAP was 100 – 200 (Garzzone et al., 2017) (Fig. 1). Previous paleobotanical studies also suggest that during the Middle to Late Miocene, the CAP had a paleoelevation between 1200 and 2000 m, a MAT of ~20 to 22°C, and a MAP of ~550 to 1500 mm (Gregory-Wodzicki et al., 1998; Gregory-Wodzicki, 2000; Graham et al., 2001). The incongruence between the paleobotanical evidence from the Middle to Late Miocene and climate models for the CAP is a major question that needs to be addressed in order to predict the impact of future climate change in South America.

Our early Pliocene reconstructions indicate that, around 4.8 Ma the NCAP had already attained near-modern elevations (~ 3800 m) with a MAP slightly higher than modern (~ 851 mm). This higher-than-modern MAP is further supported by the fossil lacustrine biota (diatoms

and ostracods) (Vélez et al., 2018), the stratigraphic (Vélez et al., 2018), and isotopic data (Garziona et al., 2008; Kar et al., 2016). Given that ferns have higher water requirements than angiosperms (Brodribb et al., 2005), the high proportion of fern taxa present in Member C of the Descanso basin compared with the modern Puna (SOM) offers additional evidence to support the high MAP estimations for the Early Pliocene.

The Pliocene climate have two warming phases, the Early Pliocene warm period (4.6 – 3.1 Ma), the mid-Pliocene warm period (or ‘warm blip’ around 3 Ma) (Haywood, 2009). Numerous high magnitude regional sea surface temperatures (SST) excursions (Dekens et al., 2007; Rousselle et al., 2013) and short-term climate perturbations (Jordan et al., 2014) have also been reported for the Pliocene. The time spanned by Member C overlaps with the Early Pliocene warm period. The wetter conditions inferred here for the NCAP during the Early Pliocene contradict some global climate models that report "permanent" El Niño-like conditions during the Early Pliocene warm period—which implies lower-than-modern precipitation for the CAP—(Wara et al., 2005; Fedorov et al., 2006, 2010). However, whether these wetter conditions correspond to a large scale or a permanent state for the Altiplano during the Early Pliocene is unknown. SSTs from the Peru margin during the Pliocene warm period indicate a cooling trend of approximately  $\sim 1.3^{\circ}\text{C}$ .

Separately, when comparing Pleistocene with Pliocene climate data, evidence from Pleistocene cores in the Altiplano suggest that glacial (interglacial) periods were wetter (drier) than modern (Baker, 2001; Fritz et al., 2007; Baker and Fritz, 2015). Considering that SST for the Peru margin show that the early Pliocene was  $3.3^{\circ}\text{C}$  warmer than the late Pleistocene (Dekens et al., 2007), and that the elevation of the CAP was similar to modern values since in the Early Pliocene, paleoprecipitation would be expected to follow the interglacial pattern —drier

regional conditions. However, our wetter CAP estimates for the early Pliocene suggest that this time period does not represent an extended interglacial period.

To address the similarities of paleofloras in Members B and C to modern ecosystems, we used the Chao's dissimilarity index (CDI) (SOM) (Chao et al., 2005). We first calculate CDI for all extant sites in each elevation range to estimate the overall heterogeneity of the ecosystem, and then we compared the extant sites with the fossil palynological record from each member. The median CDI between the Member B palynoflora and extant lower montane sites was 0.8. This value is significantly higher than the median CDI of 0.4 obtained by all pairs of extant lower montane modern sites (Fig. 3, Table S9). The median CDI between the Member B palynoflora and all extant upper montane sites was 0.7. This value differs significantly from the median CDI of 0.2 obtained by all pairs of extant upper montane modern sites (Fig. 3, Table S9). Thus, our results suggest that Member B palynoflora is not similar to extant montane sites. The Member B paleoflora is composed of common montane forest indicators such as Podocarpaceae, Chloranthaceae, Papaveraceae, and Cyatheaceae (Homeier et al., 2008) but also has components that are typical of extant highland (e.g. Ericaceae, Rosaceae, and Poaceae.) and lowland (e.g. large legume trees and palms) ecosystems. Therefore, we propose that the Member B paleoflora does not have a modern analog, and was more heterogeneous than modern montane ecosystems.

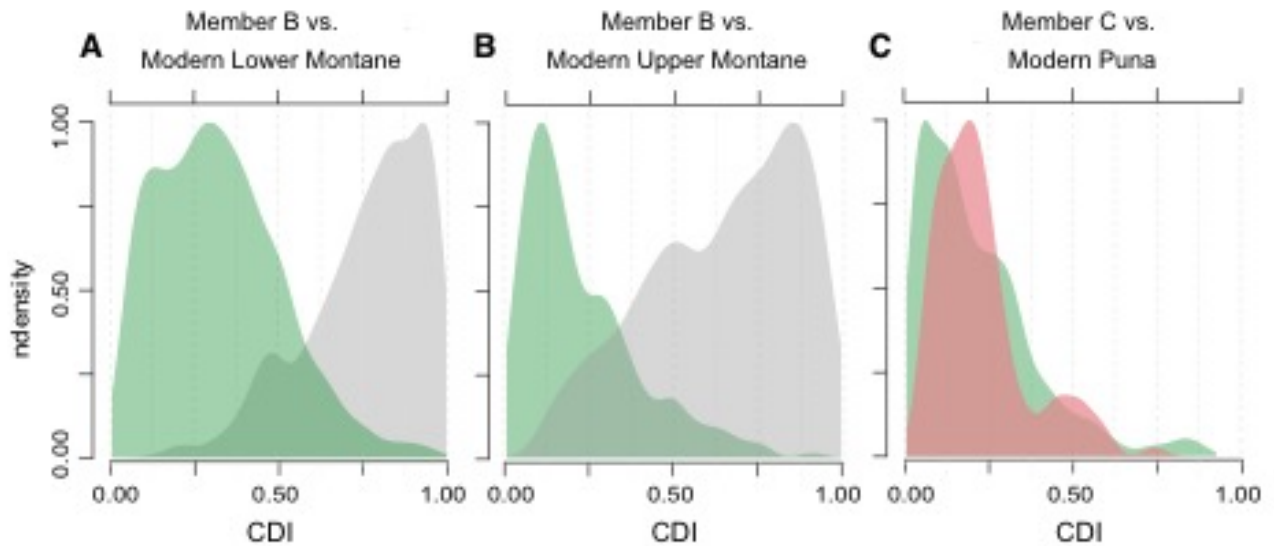


**Fig. 3. Floristic comparison.**

Floristic comparison of Member B and C palynoflora and modern pollen data from South America. The density plots show the probability distribution of the Chao Dissimilarity Index (CDI) for modern sites (green curves) for each altitudinal range, and the CDI between the fossil assemblage from the Member B (gray curves) and the Member C (red curve). In the CDI 0 is the least dissimilar and 1 the most dissimilar **A.** CDI for modern lower montane sites and Member B versus the modern dataset. **B.** CDI for modern upper montane sites and Member B versus the modern dataset. **C.** CDI estimated for modern puna sites and Member C versus the modern dataset.

The median CDI between the Member C palynoflora and all extant sites from the Puna was 0.19. This value did not differ significantly from the mean CDI of 0.16 obtained by all pairs of Puna modern sites (Fig. 3, Table S9). The macrofossil record of Member C also indicates a Puna biome by the presence of *Polylepis*, *Berberis*, *Ribes*, and *Polystichum*. Therefore, the Member C flora represents the earliest record of the Puna, appearing shortly after the landscape is inferred to have reached near-modern elevations. This early Puna would differ from the modern Puna by having a higher diversity and abundance of ferns.

The present-day  $p\text{CO}_2$  levels and future predictions under our current climate change scenario are more similar to those from the Neogene than those from the Pleistocene. Enhancing our understanding of the Neogene climate would therefore be essential to predicting future

changes, especially in tropical regions, where less data are available. The plant fossil record studied here allowed us to identify incongruences with past precipitation predictions from global and regional model simulations. Understanding the source of these discrepancies can help us better elucidate the driving forces controlling the climate of the CAP and the overall climate in South America, considering that the topographic barrier for atmospheric circulation resulting from the Andean uplift exerts a strong influence on climate on a continental scale. The deeper understanding of the uplift of the CAP, and its importance in shaping biomes and climate, highlights the dynamic nature of montane ecosystems and how these can adapt to dramatic changes in elevation and climate.

## REFERENCES

- Arroyo, M. T. K., and L. A. Cavieres. 2013. High-Elevation Andean Ecosystems. *Encyclopedia of Biodiversity*, 96–110. Elsevier.
- Baker, P. A. 2001. The History of South American Tropical Precipitation for the Past 25,000 Years. *Science* 291: 640–643.
- Baker, P. A., and S. C. Fritz. 2015. Nature and causes of Quaternary climate variation of tropical South America. *Quaternary Science Reviews* 124: 31–47.
- Brodribb, T. J., N. M. Holbrook, M. A. Zwieniecki, and B. Palma. 2005. Leaf hydraulic capacity in ferns, conifers and angiosperms: impacts on photosynthetic maxima. *New Phytologist* 165: 839–846.
- Chao, A., R. L. Chazdon, R. K. Colwell, and T.-J. Shen. 2005. A new statistical approach for assessing similarity of species composition with incidence and abundance data. *Ecology Letters* 8: 148–159.
- Dekens, P. S., A. C. Ravelo, and M. D. McCarthy. 2007. Warm upwelling regions in the Pliocene warm period. *Paleoceanography* 22.
- Fadrique, B., S. Báez, Á. Duque, A. Malizia, C. Blundo, J. Carilla, O. Osinaga-Acosta, et al. 2018. Widespread but heterogeneous responses of Andean forests to climate change. *Nature* 564: 207–212.
- Fedorov, A. V., C. M. Brierley, and K. Emanuel. 2010. Tropical cyclones and permanent El Niño in the early Pliocene epoch. *Nature* 463: 1066–1070.

- Fedorov, A. V., P. S. Dekens, M. McCarthy, A. C. Ravelo, P. B. deMenocal, M. Barreiro, R. C. Pacanowski, and S. G. Philander. 2006. The Pliocene Paradox (Mechanisms for a Permanent El Niño). *Science* 312: 1485–1489.
- Fichtler, E., and M. Worbes. 2012. Wood anatomical variables in tropical trees and their relation to site conditions and individual tree morphology. *IAWA Journal* 33: 119–140.
- Fritz, S. C., P. A. Baker, G. O. Seltzer, A. Ballantyne, P. Tapia, H. Cheng, and R. L. Edwards. 2007. Quaternary glaciation and hydrologic variation in the South American tropics as reconstructed from the Lake Titicaca drilling project. *Quaternary Research* 68: 410–420.
- Garreaud, R. D., A. Molina, and M. Farias. 2010. Andean uplift, ocean cooling and Atacama hyperaridity: A climate modeling perspective. *Earth and Planetary Science Letters* 292: 39–50.
- Garreaud, R., M. Vuille, and A. C. Clement. 2003. The climate of the Altiplano: observed current conditions and mechanisms of past changes. *Palaeogeography, Palaeoclimatology, Palaeoecology* 194: 5–22.
- Garzzone, C. N., G. D. Hoke, J. C. Libarkin, S. Withers, B. MacFadden, J. Eiler, P. Ghosh, and A. Mulch. 2008. Rise of the Andes. *Science* 320: 1304–1307.
- Garzzone, C. N., N. McQuarrie, N. D. Perez, T. A. Ehlers, S. L. Beck, N. Kar, N. Eichelberger, et al. 2017. Tectonic Evolution of the Central Andean Plateau and Implications for the Growth of Plateaus. *Annual Review of Earth and Planetary Sciences* 45: 529–59.
- Girardin, C. A. J., W. Farfan-Rios, K. Garcia, K. J. Feeley, P. M. Jørgensen, A. A. Murakami, L. Cayola Pérez, et al. 2014. Spatial patterns of above-ground structure, biomass and composition in a network of six Andean elevation transects. *Plant Ecology & Diversity* 7: 161–171.
- Graham, A., K. M. Gregory-Wodzicki, and K. L. Wright. 2001. Studies in Neotropical Paleobotany. XV. A Mio-Pliocene Palynoflora from the Eastern Cordillera, Bolivia: Implications for the Uplift History of the Central Andes. *American Journal of Botany* 88: 1545–1557.
- Gregory-Wodzicki, K. M. 2000. Uplift history of the Central and Northern Andes: A review. *Geological Society of America Bulletin* 112: 1091–1105.
- Gregory-Wodzicki, K. M., W. McIntosh, and K. Velásquez. 1998. Climatic and tectonic implications of the late Miocene Jakokkota flora, Bolivian Altiplano. *Journal of South American Earth Sciences* 11: 533–560.
- Haywood, A. M. 2009. Pliocene CLimates. *Encyclopedia of Paleoclimatology and Ancient Environments*, 804–813. Springer, Dordrecht.
- Homeier, J., F. A. Werner, and S. R. Gradstein. 2008. Potential Vegetation and Floristic Composition of Andean Forests in South Ecuador, with a Focus on the RBSF. *Gradients*

- in a tropical mountain ecosystem of Ecuador, *Ecological Studies*, 14. Springer, Heidelberg, Germany.
- Insel, N., C. J. Poulsen, and T. A. Ehlers. 2009. Influence of the Andes Mountains on South American moisture transport, convection, and precipitation. *Climate Dynamics* 35: 1477–1492.
- Insel, N., C. J. Poulsen, T. A. Ehlers, and C. Sturm. 2012. Response of meteoric  $\delta^{18}\text{O}$  to surface uplift — Implications for Cenozoic Andean Plateau growth. *Earth and Planetary Science Letters* 317–318: 262–272.
- Joetzjer, E., H. Douville, C. Delire, and P. Ciais. 2013. Present-day and future Amazonian precipitation in global climate models: CMIP5 versus CMIP3. *Climate Dynamics* 41: 2921–2936.
- Jordan, T. E., N. E. Kirk-Lawlor, N. P. Blanco, J. A. Rech, and N. J. Cosentino. 2014. Landscape modification in response to repeated onset of hyperarid paleoclimate states since 14 Ma, Atacama Desert, Chile. *Geological Society of America Bulletin* 126: 1016–1046.
- Kar, N., C. N. Garziona, C. Jaramillo, T. Shanahan, V. Carlotto, A. Pullen, F. Moreno, et al. 2016. Rapid regional surface uplift of the northern Altiplano plateau revealed by multiproxy paleoclimate reconstruction. *Earth and Planetary Science Letters* 447: 33–47.
- Kuentz, A., M.-P. Ledru, and J.-C. Thouret. 2012. Environmental changes in the highlands of the western Andean Cordillera, southern Peru, during the Holocene. *The Holocene* 22: 1215–1226.
- Lease, R. O., and T. A. Ehlers. 2013. Incision into the Eastern Andean Plateau During Pliocene Cooling. *Science* 341: 774–776.
- Poulsen, C. J., T. A. Ehlers, and N. Insel. 2010. Onset of Convective Rainfall During Gradual Late Miocene Rise of the Central Andes. *Science* 328: 490–493.
- Rousselle, G., C. Beltran, M.-A. Sicre, I. Raffi, and M. De Rafélis. 2013. Changes in sea-surface conditions in the Equatorial Pacific during the middle Miocene–Pliocene as inferred from coccolith geochemistry. *Earth and Planetary Science Letters* 361: 412–421.
- Saylor, J. E., and B. K. Horton. 2014. Nonuniform surface uplift of the Andean plateau revealed by deuterium isotopes in Miocene volcanic glass from southern Peru. *Earth and Planetary Science Letters* 387: 120–131.
- Sepulchre, P., L. C. Sloan, and F. Fluteau. 2011. Modelling the Response of Amazonian Climate to the Uplift of the Andean Mountain Range. In C. Hoorn, and F. P. Wesselingh [eds.], *Amazonia: Landscape and Species Evolution*, 211–222. Wiley-Blackwell Publishing Ltd., Oxford, UK.
- Simpson, B. B. 1983. An Historical Phytogeography of the High Andean Flora. *Revista Chilena de Historia Natural* 56: 109–122.

- Vélez, M. I., C. Jaramillo, A. Salazar-Ríos, X. Benito, S. Fritz, P. Tapia, D. Lubiniecki, et al. 2018. Aquatic ecosystems in a newly formed ecospace: Early Pliocene lakes in the Central Andean Altiplano. *Palaeogeography, Palaeoclimatology, Palaeoecology* 490: 218–226.
- Wara, M. W., A. C. Ravelo, and M. L. Delaney. 2005. Permanent El Niño-Like Conditions During the Pliocene Warm Period. *Science* 309: 758–761.
- Wheeler, E. A., P. Baas, and S. Rodgers. 2007. Variations In Dicot Wood Anatomy: A Global Analysis Based on the Insidewood Database. *IAWA Journal* 28: 229–258.
- Zachos, J. C., G. R. Dickens, and R. E. Zeebe. 2008. An early Cenozoic perspective on greenhouse warming and carbon-cycle dynamics. *Nature* 451: 279–283.

## SUPPLEMENTARY MATERIALS

### Neogene climate and elevation history of the Central Andean Plateau

C. Martínez<sup>1,2\*</sup>, C. Jaramillo<sup>2</sup>, A. Correa-Metrío<sup>4</sup>, W. Crepet<sup>1</sup>, E. Moreno<sup>2</sup>, A. Aliaga<sup>3</sup>, F. Moreno<sup>5</sup>, M. Ibáñez-Mejía<sup>5</sup>, M. Bush<sup>6</sup>

#### MATERIALS AND METHODS

##### *Geologic setting*

The Descanso-Yauri Basin has today an average elevation of 4000 m, an approximate area of 2000 km<sup>2</sup>, and is located in the northern-most part of the CAP (Cerpa and Meza, 2001). The El Descanso Formation of the Descanso-Yauri Basin has approximately 1800 m of thickness (Kar et al., 2016) and is divided in three members: A, B and C (Cerpa and Meza, 2001). The Member A, at the base of the Formation is ~500 m thick, and is dominated by conglomerates and sandstones exposed in a narrow zone at the north of the basin (Kar et al., 2016). The Member B is exposed along most of the basin and is the thickest unit with approximately 1100 m (Kar et al., 2016). The lithology of this Member is characterized by the presence of conglomerates, sandstones, mudstones, siltstones and a few limestone beds at the top. Members A and B are inferred to be deposited in an environment of braided rivers (Kar et al., 2016). Between Members B and C there is an angular unconformity that spans approximately 4 Ma (Kar et al., 2016). The Member C is approximately less than 100 m thick and is dominated by diatomaceous mudstones, but also thick sandstone beds of more than 3 m, with cross stratification, conglomerate units of

less than 1 m or more of thickness, and muddy sandstone beds occasionally with carbonaceous root traces (Kar et al., 2016; Vélez et al., 2018). Plant fossil remains were found in numerous diatomaceous beds, but also in clay and fine sandstone beds in four different sections from this Member. Member C was deposited in a fluvial-lacustrine system (Kar et al., 2016; Vélez et al., 2018). Syn-depositional volcanic eruptions deposited tuffs that have been used to constraint the age of the three members. The top of the Member A is  $18.7 \pm 0.2$  Ma ( $^{40}\text{Ar}/^{39}\text{Ar}$  biotite; Cerpa and Meza 2001). The top of the Member B is  $9.1 \pm 0.7$  Ma ( $^{206}\text{Pb}/^{238}\text{U}$  igneous zircons; 2). Member C had a tuff deposited at  $4.8 \pm 1.1$  Ma ( $^{206}\text{Pb}/^{238}\text{U}$  igneous zircons; Kar et al. 2016; Fig. S1). Two other detrital zircon ages were estimated for Member C, one was deposited  $5.4 \pm 1.0$  Ma and the other one at  $3.9 \pm 0.1$  Ma (Kar et al., 2016). Since the older age ( $5.4 \pm 1.0$ ) was estimated from a reworked tuff, we opt for a more conservative age range for Member C, spanning at least from  $4.8 \pm 1.1$  Ma to  $3.9 \pm 0.1$  Ma. Although the stratigraphic sections from Member C studied by Kar et al. (2016) and revisited here could not be completely correlated due to the strong lateral variation of the strata, and the presence of tuffs that cannot be followed laterally, we estimate that Member C was not deposited during a short-lived event. Instead, we interpret that it spanned more than 2 My, based on the known radiometric ages, its stratigraphic separation ( $\sim 20$  m), the lithology, and the erosional contacts.

### ***Zircon U-Pb geochronology methods***

Two tuff samples with abundant pumaceous fragments were collected to correlate two wood localities of the Colpamayo and San Miguel region using U-Pb geochronology. The sample from the Colpamayo region (STRI-MUSM 44449) was collected from a 60 cm conglomerate rich in pumaceous fragments, and the sample from the San Miguel region (STRI-MUSM 44448) was collected from a 50 cm-thick ash-fall tuff.

Zircon separates were performed by standard magnetic and gravity-based methods at the University of Rochester, using a Frantz LB-1 separator and methylene iodide. Prior to U-Pb analysis by LA-ICP-MS, zircons were mounted in 1" epoxy plugs and characterized by cathodoluminescence (CL) imaging using a JEOL JSM-7100 electron microscope equipped with a field-emission gun and a Deben Centaurus CL detector at the University of Nevada, Reno. All U-Pb isotopic measurements were performed by LA-ICP-MS at the Arizona Laserchron center, University of Arizona, using a Photon Machines *Analyte-G2* Excimer laser system coupled to a Thermo-Finnigan Element2 single collector ICP-MS.

Analytical methods for the U-Pb analyses are outlined in Ibañez-Mejía et al. (2015) and Pullen et al. (2018). In brief, analyses of unknown zircon were bracketed by U-Pb isotopic measurements of fragments from the SL2 (Gehrels et al., 2008), R33 (Black et al., 2004), and FC-1 (Paces and Miller, 1993), zircon reference materials, which were used to correct for elemental- and mass-dependent instrumental fractionation as a function of beam intensity. Non-radiogenic Pb (*i.e.*, Pb<sub>c</sub>) in all analyses was assumed to be initial (*i.e.*, from co-crystallized inclusions) and was corrected for using the measured <sup>204</sup>Pb and the isotopic composition of crustal Pb at the age of crystallization after Stacey and Kramers (1975). Further details about data processing and uncertainty propagation for U-Pb results are described in Pullen et al. (2018).

### ***Paleobotanical samples***

The Descanso-Yauri basin was explored during three field trips done during the dry season of years 2014, 2015 and 2016. All the samples were collected from Members B and C. During the collection process, we kept a stratigraphic control by visiting the localities previously described by Kar et al. (2016) and then by correlating stratigraphically the new localities found.

We collected palynological samples, tuffs and compressions and impressions of fossil leaves and fertile parts, and permineralized wood. To correlate stratigraphically two of the new localities, we used radiometric dating of igneous samples present near the fossiliferous region.

Palynological sample preparation was done following conventional methods (Wood et al., 1996). Sieving and panning was used to recover the fraction rich in palynomorphs. Slides were mounted with polyvinyl alcohol and sealed with Canada balsam. Samples were processed at the laboratory of Paleoflora, Bucaramanga, Colombia. Palynomorphs were counted aiming for a minimum of 300 specimens per slide.

Macrofossil compressions and impressions were studied at the Paleontological Collection of the Museo de Historia Natural de la Universidad Nacional Mayor de San Marcos Lima, Peru (DPV-MHN-UNMSM). Sediment was carefully removed using an air scribe to expose possible attachments and the maximum number of features. Specimens were observed using a LEICA EZ4 HD coupled to an integrated camera 5.0 Mega Pixel CMOS. Photographs were taken with varied low-angle light. Each leaf morphotype was described following the terminology of the Manual of Leaf Architecture (Ellis et al., 2009). Comparisons with extant taxa were made with herbarium material from the San Marcos Herbarium (MHN-UNMSM; Lima, Peru), virtual collections accessed through the JSTOR Global Plants database, and literature.

Permineralized wood were initially cut with diamond saws at the Museum of Natural History of the Universidad de San Marcos of Lima (MUSM). Thin sections were prepared following standard techniques described in detail in Boonchai (2012). The anatomy of the samples was described following the International Association of Wood Anatomists (IAWA) list of microscopic features for hardwood identification (IAWA, 1989). Preliminary comparisons

with modern and fossil wood were done using the InsideWood database (Wheeler, 2011), additional comparisons were done based on literature.

Macrofossil compressions and impressions and permineralized wood, were organized and described by morphotypes following the method described by Peppe et al. (2008). Each morphotype has a three-letter prefix (DSB or DSC) based on the name of the formation and the member which they belong to, plus a number starting from one. A systematic affinity was proposed for each morphotype. Species names were not proposed for any of the morphotypes described because this required extensive research into the nomenclature of the taxon, previous fossil descriptions, and phylogenetic relationships (Peppe et al., 2008), which were topics out of the scope of this paper.

### *Paleoclimatic analyses*

Given that palynological counts were uneven because of differential preservation of samples, and also aiming to make palynology and macrofossil estimates comparable, palynological relative abundance was not considered representative of environmental conditions, and the dataset was therefore transformed to presence-absence. Palynological samples were filtered to consider only samples that met the following criteria: i) the sample was composed of taxa that were represented in the modern pollen and spore dataset, ii) at least three taxa were represented in the sample, and iii) at least one of the taxa present in the sample was identified at genus level.

The distribution of taxa found in the fossil datasets (palynology and macrofossils) was described through bivariate probability density distributions (PDF) of modern taxon occurrence along elevation and precipitation gradients. These distributions were described through a bivariate Gaussian kernel density estimator (S15) defined by:

$$\hat{f}(x; H) = \frac{1}{n} \sum_{i=1}^n K_H(x - \mathbf{X}_i)$$

where:

$\hat{f}(x; H)$  defines the probability density at a point  $x = (x_1, x_2)^T$

$\mathbf{X}_i = (X_{i1}, X_{i2})^T$  is the vector of realizations at points  $i = 1, 2, \dots, n$ , for variables  $X_1$  (elevation) and  $X_2$  (precipitation).

$H = \begin{bmatrix} h_1 & 0 \\ 0 & h_2 \end{bmatrix}$  is a matrix of bandwidths; in our case  $h_1 = h_2 = 250$ .

$K(x) = \frac{1}{2\pi} e^{-\frac{1}{2}x^T x}$  is the Gaussian kernel smoother

Georeferenced occurrence of modern both pollen and vegetation taxa (data from BIEN R-package, S16) present in the fossil dataset were described in terms of the elevation and mean annual precipitation at the occurrence points (data from WordClim; S17). Thus, two reference libraries of bivariate environmental distributions were built, one for palynology (PDFpaly), and one for macrofossils (PDFmacro,). In instances of taxonomic uncertainty in the identification of macrofossils, PDFmacro were based on the modern distribution of multiple taxa. The paleoenvironmental reconstruction for a given fossil palynology sample consisted of a  $PDF_{fossil\ paly_j}$  derived from a non-weighted finite mixture (Peel and Mclachlan, 2000) of the modern PDFpaly of  $s_j$  pollen and spore taxa present in the fossil sample  $j$ . Individual sample estimates from the same stratigraphic member (T) were in turn mixed to obtain a PDF<sub>T</sub>.

$$PDF_{fossil\ paly_j} = \sum_{k=1}^{s_j} PDF_{paly_k} \xrightarrow{\text{leads}} PDF_T = \sum_{j=1}^{n_T} PDF_{fossil\ paly_j}$$

where

$PDF_{fossil\ paly_j}$  is the probability density function of sample j composed of  $s_j$  pollen taxa.

$PDF_{paly_k}$  is the probability density function of modern pollen taxon k with  $k = 1, 2, \dots, s$ .

$PDF_T$  is the probability density function of stratigraphic member T, represented by  $n_T$  samples.

The paleoenvironmental reconstruction based on macrofossils consisted of a single probability density function for each stratigraphic member ( $PDF_{macro_B}$  and  $PDF_{macro_C}$ ), as follows:

$$PDF_{macro} = \sum_{i=1}^s PDF_{macro_k}$$

where:

$PDF_{macro_k}$  is the probability density function of modern pollen taxon k with  $k = 1, 2, \dots, s$ .

$PDF_{paly}$  and  $PDF_{macro}$  of each sample represents the probability distribution of data pairs of precipitation and elevation conditioned to the presence of a given set of taxa  $s$ . The credible environmental area within each PDF was obtained by trimming the margins of the bivariate surface, keeping the area of the distribution associated with a cumulative probability higher than 0.5. Based on the probability densities of this area, the marginal distribution of elevation and precipitation for each sample was extracted, obtaining one macrofossil-based marginal distribution per variable per stratigraphic member, and nB and nC palynology-based marginal distributions per variable. For summarizing palynology-based estimates, marginal distributions were subsequently mixed.

Marginal distributions of elevation estimates based on palynology and macrofossils were corrected taking into account global temperature within the estimated age range for each stratigraphic member (between 12.87 and 8.4 Ma for Member B, and from 4.3 and 5.3 Ma for Member C, global temperature anomaly data from (Hansen et al., 2013) Observed global temperature anomalies within the time period of each stratigraphic member were randomly sampled, converted to elevation using a lapse rate of 0.6 °C (Graham, 2010), and added to our estimates (global temperature was warmer).

Final estimates of both elevation and precipitation per stratigraphic member resulted from mixing palynology- and macrofossil-based marginal distributions. Modern estimates were based on mixing palynology -based, cross-validated estimates with distributions of actual climatic data (this latter step was necessary because of the lack of macrofossils for the Holocene). Such mixture resulted from an addition of individual densities weighted by a proportion factor, as follows

$$MD_{parameter} = \lambda_1 * MD_{paly} + \lambda_2 * MD_{macro}$$

where,

$MD_{parameter}$  is the marginal distribution of temperature or precipitation.

$MD_{paly}$  is the pollen-based marginal distribution of temperature or precipitation.

$MD_{macro}$  is the macrofossil-based marginal distribution of temperature or precipitation.

$\lambda_1$  and  $\lambda_2$  are the representation factors for palynology and macrofossils, respectively, with  $\lambda_1 + \lambda_2 = 1$ .

Given the lack of information regarding the relative reliability of palynology and macrofossils, and therefore the proportion that the information provided by each proxy should weight,  $\lambda_1$  was set to vary from zero (estimation based exclusively on macrofossils) to one (estimation based exclusively on palynology) aiming to evaluate the stability of estimates. When estimates varied monotonically with  $\Delta$ , we selected a solution based on a completely proportional mixture (i.e.  $\lambda_2 = \lambda_1 = 0.5$ ), whereas when the estimation was notoriously affected by the selection of  $\lambda$ , the inflection point was preferred. The environmental space for each time period was represented as the conjunction of the interquartile range of elevation and precipitation.

Differential both elevation and precipitation was calculated by randomly sampling the distribution of estimates and subtracting time-contiguous members (Member B to Member C, and Member C to Modern). These differences in turn were summarized through a univariate PDF.

### ***Palynological analyses and comparison with modern ecosystems***

Fossil palynological data from Members B and C were used for a comparison with modern pollen data. The modern pollen dataset consisted of palynological counts grouped by family from South American sites that span an elevation gradient from 100 to 4700 m. We used the Chao's dissimilarity index (CDI) (Chao et al., 2005) to estimate similarities between modern data and modern versus fossil palynological data. The parameters used to estimate the CDI used here were the asymmetric Sorensen-type, using probability estimations and taxa abundance data. This analysis was implemented in R using the CommEcol package (Melo, 2017).

Since the modern pollen dataset did not include spore counts, we also did a comparison of the proportion of angiosperms and ferns present in the palynological record from the Members B

and C, and modern data from the Global Biodiversity Information Facility (GBIF.org, 2018) using relative abundances. Modern data were extracted from a polygon that included the Altiplano region and the eastern and western flanks of the Andes. The polygon was between -17 and -11° of latitude, and -74 and -69° of longitude. Within the analysis a Quaternary sample that was collected in the Espinar region was also included in the comparison. Finally, the inferred habit from the taxa represented in the fossil palynological samples was also compared to evaluate changes in the ecosystems.

## **SUPPLEMENTARY TEXT**

### ***Zircon U-Pb geochronology***

Zircons from tuffaceous horizons in the Colpamayo region (STRI-MUSM 44449) and San Miguel region (STRI-MUSM 44448) are characterized by internal oscillatory-zoned textures (Fig. S3), which are indicative of magmatic crystallization. U-Pb results of 59 zircons analyzed from both samples are reported in Table S1U-Pb data, whereas only the populations used to determine the eruption age of both samples are graphically shown as traditional (Wetherill) concordia diagrams in Fig. S3. Uncertainties in the reported  $^{206}\text{Pb}/^{238}\text{U}$  weighted means for each sample are in the form  $\pm X/Y$  Ma, where the first uncertainty level 'X' only represents analytical uncertainty and the second term 'Y' includes propagation of the reproducibility of the zircon reference materials measured during the same analytical session.

Sample 16ES04Z from the Colpamayo region yielded zircons ranging in age from ~11.4 to 130 Ma, suggesting some degree of sedimentary reworking in this unit. From 29 zircons that were analyzed, the five youngest define a cluster with a weighted mean  $^{206}\text{Pb}/^{238}\text{U}$  date of  $12.07 \pm 0.73/0.74$  Ma (95% conf., MSWD= 2.5) that we interpret as reflecting the age of eruption of this tuff. Sample 16ES13Z from the San Miguel region yielded zircons ranging in age from ~9.3

to 572 Ma, also indicative of some reworking. Nevertheless, a larger proportion of crystals in this sample yielded ages around 10 Ma (Fig. S4), and a group defined by the 18 youngest analyses yields a weighted mean  $^{206}\text{Pb}/^{238}\text{U}$  date of  $10.03 \pm 0.16/0.18$  Ma (95% conf., MSWD= 0.7) which is also interpreted as the age of eruption.

### ***Paleobotanical samples***

One hundred and ninety-nine samples were collected from 88 localities from Members B and C of El Descanso Formation. The material collected included palynological samples, tuffs and macrofossil samples of leaves, fruits and permineralized wood. Due to its higher thickness and lithology, more material was collected from the Miocene Member B. However, from the Pliocene Member C, palynological samples and macrofossil samples of leaves and fruits were also found.

Seventy-five palynological samples were analyzed, from those 5,428 palynomorphs were counted and 183 morphospecies were identified (Table S2). From the analyzed samples, 8 were barren and 10 have only one or two counts (Table S2). Fifty-three samples were collected in Member B, 16 from the Member C and 2 samples were collected from a modern swamp. Four samples from the Palpatamayo region were collected possibly from the Member B, however, their stratigraphic position could not be determined, so they were excluded from the analyses (Table S2). The identified palynomorphs were categorized in 4 groups: arboreal, shrubs, herbs and ferns.

### ***Palynology***

#### **Angiosperms-Eudicotyledoneae**

Amaranthaceae

*Amaranthus* sp.1 L. (equivalent morphotype: Fenestrites “baculoides”)

Grains monad, apolar, radially symmetric, inaperturate, reticulate; brochus having lumina ample resembling fenestrate condition; murus thin, less than 1  $\mu\text{m}$  thick, columellate, columellae long, baculae-pattern, simplibaculate; exine tectate ca. 5  $\mu\text{m}$  thick; outline circular; grains spheroidal, 19  $\mu\text{m}$  in size (Fig. S5.1) [Sample: Peru, Espinar, ID-39726, Paleo-12606, El Descanso Fm., Member C. England Finder: F29]

*Amaranthus* sp.2 L. (equivalent morphotype: Parsoncidites “homogeneous”)

Grains monad, apolar, radially symmetric, periporate, baculate; baculae less than 1  $\mu\text{m}$  length, inconspicuous; six circular and equidistant pores, 5  $\mu\text{m}$  in diameter ea.; exine intectate ca. 5  $\mu\text{m}$  thick; ambitus circular; grains spheroidal, 24  $\mu\text{m}$  in size (Fig. S5.2) [Sample: Peru, Accocunca North, ID-36584/B47-R16, El Descanso Fm., Member B. England Finder: P49/Q50]

*Chenopodium* sp. L. (equivalent morphotype: Scabraperiporites “minutus”)

Grains monad, apolar, radially symmetric, periporate, subtly scabrate; ca. 50 circular and regularly distributed pores, 3  $\mu\text{m}$  in diameter each one, slightly annulate; exine tectate, 3  $\mu\text{m}$  thick; ambitus circular; grains spheroidal, 15 to 19  $\mu\text{m}$  in size (Fig. S5.3) [Sample: Peru, Espinar, ID-39726, Paleo-12606, El Descanso Fm., Member C. England Finder: K38/L39]

Anacardiaceae

*Anacardium* sp. L. (equivalent morphotype: Retitricolporites “striatus”)

Grains monad, isopolar, radially symmetric, tricolporate, reticulate; homobrochate, brochus ca. 1  $\mu\text{m}$  wide, longitudinally oriented, resembling striate pattern; murus thin, less than 1  $\mu\text{m}$  thick, simplicolumellate, columellae baculae-typed; colpus as long as grain, wide, having costae ecto-colpi, exhibiting “exitus digitatus” condition; pores endexinic, inconspicuous; exine tectate,

3  $\mu\text{m}$  thick; ambitus probably circular; grains subprolate, 31  $\mu\text{m}$  length x 24  $\mu\text{m}$  wide (Fig. S5.4)

[Sample: Peru, Espinar, ID-40127, Paleo-12609, El Descanso Fm., Member C. England Finder: C45-4]

*Schinus* sp. L. (equivalent morphotype: Retitricolporites sp. 1 aff. “zigzaguenensis”)

Grains monad, isopolar, radially symmetric, tricolporate, reticulate; homobrochate, brochus less than 1  $\mu\text{m}$  wide, murus thin, less than 1  $\mu\text{m}$  thick, simplicolumellate, columellae baculae-typed; colpus as long as grain, thin, straight, marginate, margo subtle; colpus exhibiting “exitus digitatus” condition; pores apparently circular, ca. 7  $\mu\text{m}$  in diameter; exine tectate, 1.5  $\mu\text{m}$  thick; ambitus circular; grains probably prolate-spheroidal, 25  $\mu\text{m}$  length x 22  $\mu\text{m}$  wide (Fig. S5.5)

[Sample: Peru, Checa, ID-36582/B47-R12, England Finder: G12-4]

Araliaceae

*Schefflera* sp. J.R. Forst. & G. Forst. (equivalent morphotype: Retitricolporites “radiatus”)

Grains monad, isopolar, radially symmetric, tricolporate, reticulate; homobrochate, brochus fine ca. 1  $\mu\text{m}$  thin; murus very thin, simplicolumellate, columellae dense, baculae-typed; colpus as long as grain, thin; pores endexinic, inconspicuous; exine tectate, 3  $\mu\text{m}$  thick; ambitus circular-semi triangular; grains probably oblate (description based on polar view), 21  $\mu\text{m}$  in size.

(Fig. S5.6) [Sample: Peru, Espinar, ID-40127, Paleo-12609, El Descanso Fm., Member C. England Finder: H25-3]

Asteraceae

*Ambrosia* sp. L. (equivalent morphotype: Echitricolporites mneilly)

Grains monad, isopolar, radially symmetric, tricolporate, echinate; echinae short, acute-end, wide-based; apertures inconspicuous, colpus as long as grain, thin; pores endexinic, apparently circular; exine tectate, 1.5  $\mu\text{m}$  thick, columellate, caveate, caveae conspicuous, wide; ambitus circular-trilobate; grains spheroidal 17  $\mu\text{m}$  in size (Fig. S5.7) [Sample: Peru, Espinar, ID-39721, Paleo-

12601, El Descanso Fm., Member C. England Finder: Q32-3]

*Baccharis* sp. L. (equivalent morphotype: *Echitricolporites spinosus*)

Grains monad, isopolar, radially symmetric, tricolporate, echinate; echinae ca. 1.5  $\mu\text{m}$  length, acute-end, wide-based; colpus  $2/3$  as long as grain, wide; pores endexinic inconspicuous, probably lalongate; exine tectate, 2  $\mu\text{m}$  thick (echini excluded), columellate; ambitus circular; grains subprolate 32  $\mu\text{m}$  length x 21  $\mu\text{m}$  wide (Fig. S5.8) [Sample: Peru, Espinar, ID-39726, Paleo-12606, El Descanso Fm., Member C. England Finder: G30-4]

*Barnadesia* sp. Mutis ex. L. f. (equivalent morphotype: Fenestrites “ampliporicus”)

Grains monad, apolar, radially symmetric, periporate, psilate; pores circular 4  $\mu\text{m}$  in diameter, resembling fenestrate condition; exine tectate, coarse, ca. 4  $\mu\text{m}$  thick; ambitus circular; grains spheroidal, 25  $\mu\text{m}$  in size (Fig. S5.9) [Sample: Peru, Espinar, ID-39458, Paleo-12571, El Descanso Fm., Member B. England Finder: L21-1]

*Hypochoeris* sp. L. (equivalent morphotype: *Cichoreacidites longispinosus*)

Grains monad, apolar, radially symmetric, fenestrate, echinate; ca. 20 fenestrae/grain not well defined and masked by sculpture; echinae acute, long, dense, 3.5  $\mu\text{m}$  length; exine tectate, 2.5  $\mu\text{m}$  thick; (all = 6  $\mu\text{m}$ ); ambitus circular; grains spheroidal, 26  $\mu\text{m}$  in size (Fig. S5.10) [Sample: Peru, Espinar, ID-39456, Paleo-12562, El Descanso Fm., Member B. England Finder: H16]

*Mutisia* sp. L. f. (equivalent morphotype: *Echitricolporites* “mutis”)

Grains monad, isopolar, radially symmetric, tricolporate, echinate; echinae flat, wide, inconspicuous; colpus as long as grain, 2  $\mu\text{m}$  wide; pores lalongate becoming to join at apices forming a continuous equatorial ring, 1.5  $\mu\text{m}$  height; exine tectate, 3.5  $\mu\text{m}$  thick, strongly columellate; ambitus circular-trilobate; grains spheroidal 30  $\mu\text{m}$  in size (Fig. S5.11) [Sample: Peru, Accocunca North, ID-36569/B47-R17, El Descanso Fm., Member B. England Finder: H8]

Undetermined (equivalent morphotype: *Echitricolporites* “magnus”)

Grains monad, isopolar, radially symmetric, tricolporate, echinate; echinae 3.5  $\mu\text{m}$  length x 2.5  $\mu\text{m}$  wide, acute-end, wide-based; colpus as long as grain, irregular; pores endexinic inconspicuous; exine tectate, 1.2  $\mu\text{m}$  thick (between echini) and 5  $\mu\text{m}$  thick (including echini), densely columellate; ambitus circular; grains subprolate 47  $\mu\text{m}$  length x 33  $\mu\text{m}$  wide (Fig. S5.12)

[Sample: Peru, Accocunca North, El Descanso Fm., Member B, ID-36584/B47-R16. England Finder: Q46/R47]

#### Betulaceae

*Alnus* sp. Mill. (equivalent morphotype: *Alnipollenites verus*)

Grains monad, isopolar, radially symmetric, stephanoporate, psilate; 5 small, circular and equidistant pores (occasionally having 4 pores), inconspicuous; exine tectate, variable in size from 1.5 to 3  $\mu\text{m}$  thick at apertures, displaying a continuous arc between opposite apertures; ambitus pentagonal; grains apparently oblate, 21  $\mu\text{m}$  in size (Fig. S5.13) [Sample: Peru, Espinar, ID-

39364, Paleo-12549, El Descanso Fm., Member C. England Finder: Y8]

#### Brassicaceae

*Brassica* sp. Burnett (equivalent morphotype: *Tricolporites* “*bacularis*”)

Grains monad, isopolar, radially symmetric, tricolporate, baculate; baculae long, thin, rounded-end; colpus as long as grain, wide, having a conspicuous equatorial “bridge”; pores endexinic, inconspicuous, apparently circular, masked by presence of bridge; exine intectate, 3.5  $\mu\text{m}$  thick; ambitus circular-trilobate; grains slightly subprolate, 25  $\mu\text{m}$  length x 19  $\mu\text{m}$  wide (Fig.

S5.14) [Sample: Peru, Espinar, ID-39726, Paleo-12606, El Descanso Fm., Member C. England Finder: T12 & G13-4]

#### Buxaceae

*Styloceras* sp. Kunt ex. A. Juss. (equivalent morphotype: *Retiperiporites* “*poriannulatus*”)

Grains monad, apolar, radially symmetric, periporate, reticulate; slightly heterobrochate, brochus fine ca. 1  $\mu\text{m}$  thin; murus very thin, less than 1  $\mu\text{m}$  wide; ca. 12 circular pores/grain, 2

$\mu\text{m}$  in diameter each one, annulate, ca. 1  $\mu\text{m}$  wide; exine tectate, ca. 1  $\mu\text{m}$  thick; ambitus circular; grains spheroidal, 27  $\mu\text{m}$  in size (Fig. S5.15) [Sample: Peru, Accocunca North, ID-36566/B47-R20, El Descanso Fm., Member B. England Finder: W9-1]

#### Cactaceae

*Opuntia* sp. (*O. corotilla*?) Mill. (equivalent morphotype: Magnaperiporites “irregularis”)

Grains monad, apolar, radially asymmetric, periporate, baculate; ca. 20 circular pores/grain, irregular, 6  $\mu\text{m}$  in diameter each one, not well defined; baculae 1.5  $\mu\text{m}$  length x less than 1  $\mu\text{m}$  wide, thin; exine intectate, ca. 2.5  $\mu\text{m}$  thick; ambitus circular; grains spheroidal, 69  $\mu\text{m}$  in size (Fig. S6.16) [Sample: Peru, Accocunca North, ID-36569-S2/B48-R4, El Descanso Fm., Member B. England Finder: S4]

#### Cannabaceae

*Celtis* sp. L. (equivalent morphotype: Verrutripurites “celtoides”)

Grains monad, apolar, radially symmetric, triporate, sometimes appearing as diporate, verrucate; verrucae subtle, flat, homogeneous, ca. 1.5  $\mu\text{m}$  wide; pores apparently circular, small, inconspicuous; exine tectate, ca. 2.5  $\mu\text{m}$  thick; ambitus circular; grains spheroidal, 22  $\mu\text{m}$  in size (Fig. S6.17) [Sample: Peru, Espinar, ID-39361, Paleo-12548, El Descanso Fm. Fm., Member C. England Finder: F45-2]

#### Caprifoliaceae

*Valeriana* sp. L. (equivalent morphotype: Echitricolpites “microechinatus”)

Grains monad, isopolar, radially symmetric, tricolpate, echinate; echinae less than 1  $\mu\text{m}$  length; colpus as long as grain, thin, tortuous; exine tectate, 2.5  $\mu\text{m}$  thick, surface between echinae slightly scabrate; ambitus probably circular; grains subprolate, 31  $\mu\text{m}$  length x 22  $\mu\text{m}$  wide (Fig. S6.18) [Sample: Peru, Accocunca North, ID-36569/B47-R17, El Descanso Fm. Fm., Member B. England Finder: V39-4]

#### Caryophyllaceae

*Arenaria* sp. L. (equivalent morphotype: *Psilaperiporites robustus*)

Grains monad, apolar, radially symmetric, periporate, scabrate; scabrae fine, dense; ca. 50 circular and equidistant pores, 3 µm in diameter each one; exine tectate, 2 µm thick, densely columellate; ambitus circular; grains spheroidal, 22.5 µm in size (Fig. S6.19) [Sample: Peru, Espinar, ID-39364, Paleo-12549, El Descanso Fm., Member C. England Finder: W9-3]

Convolvulaceae

*Evolvulus* sp. L. (equivalent morphotype: *Pericolpites* “*baculatus*”)

Grains monad, apolar, radially asymmetric, pericolpate, baculate; baculae long, coarse, dense; ca. 8 colpi/grain, irregular, transversally oposite, irregular; exine intectate; ambitus circular-irregular; grains probably spheroidal, 40 µm in size (Fig. S6.20) [Sample: Peru, Espinar, ID-39460, Paleo-12573, El Descanso Fm., Member B. England Finder: J20-2]

*Iseia* sp. O’Donell (equivalent morphotype: *Psilatricolporites digitatus*)

Grains monad, apolar, radially symmetric, tricolporate, apparently tricolpate, baculate; baculae long, coarse, dense; pores, if present, inconspicuous; exine intectate, coarse, 3.5 µm thick; ambitus circular-trilobate; grains oblate to suboblate, 64 µm in size (Fig. S6.21) [Sample: Peru, Espinar, ID-39461, Paleo-12574, El Descanso Fm., Member B. England Finder: G32-2]

Ericaceae

*Gaultheria* sp. L. (equivalent morphotype: *Ericipites* “*perfectus*”)

Grains grouped as tetrad, 4 grains ordered in a tetrahedral pattern, ca. 26 µm in size. Isolated grains isopolar, radially symmetric, tricolporate, psilate; colpus  $\frac{3}{4}$  as long as grain, thin, straight; pores inconspicuous apparently lalongate-linear; exine tectate, 1.2 µm thick; ambitus circular; grains suboblate, 26 µm in size (Fig. S6.22) [Sample: Peru, Accocunca North, ID-36569/B47-R17, El Descanso Fm., Member B. England Finder: O35]

## Euphorbiaceae

*Acalypha* sp. L. (equivalent morphotype: *Psilastephanocolporites* “acalyphus”)

Grains monad, isopolar, radially symmetric, stephanocolporate, psilate; 5 small, inconspicuous and equidistant colpi; colpus very thin, short, acute-end; pores apparently circular, slightly protruding; exine tectate, very thin, less than 1  $\mu\text{m}$  thick; ambitus circular-pentagonal; grains apparently oblate, 13  $\mu\text{m}$  in size (Fig. S6.23) [Sample: Peru, Espinar, ID-39443, Paleo-12550, El Descanso Fm., Member B. England Finder: N17]

*Croton* sp. L. (equivalent morphotype: *Clavaperiporites* “crotonoides”)

Grains monad, apolar, radially symmetric, periporate, clavate; clavae ca. 1.5  $\mu\text{m}$  length x 1  $\mu\text{m}$  wide, rounded-head, sometimes resembling bifurcate ends, densely present; more than 20 inconspicuous pores/grain, apparently circular ca. 1.5  $\mu\text{m}$  in diameter each one, masked by sculpture; exine intectate, nexine very thin; ambitus circular; grains spheroidal, 35  $\mu\text{m}$  in size (Fig. S6.24) [Sample: Peru, Accocunca North, ID-36569/B47-R17, El Descanso Fm., Member B. England Finder: R10-3]

*Sapium* sp. Jacq. (equivalent morphotype: *Foveotricolporites* *cingulatum*)

Grains monad, isopolar, radially symmetric, tricolporate, finely reticulate; homobrochate, brochus less than 1  $\mu\text{m}$  wide; murus thin; colpus as long as grain, thin, marginate; pores endexinic, lalongate-linear almost joined at apices, ca. 2.5  $\mu\text{m}$  height x 17  $\mu\text{m}$  wide; exine tectate, 3.5  $\mu\text{m}$  thick (nexine 1.2, columellae 1, tectum 1.3), simplicolumellate, columellae baculae-typed, dense; ambitus probably circular; grains prolate, 42.5  $\mu\text{m}$  length x 17  $\mu\text{m}$  wide (Fig. S6.25) [Sample: Peru, Accocunca North, El Descanso Fm., Member B, ID-36569/B47-R17. England Finder: O49/O50]

*Tetrorchidium* sp. Poepp. (equivalent morphotype: *Baculitricolpites* “perfectus”)

Grains monad, isopolar, radially symmetric, apparently tricolpate, baculate; baculae long, rounded-head, dense; colpus as long as grain, straight, thin; pores, if present, inconspicuous;

exine intectate, 2.5 µm thick; ambitus circular; grains prolate, 40 µm length x 2.5 µm wide (Fig. S6.26) [Sample: Peru, Accocunca North, El Descanso Fm., Member B, ID-36569/B47-R17. England Finder: T18 & L22-1]

Undetermined 1 (equivalent morphotype: *Baculatricolpites* “trilobatus”)

Grains monad, isopolar, radially symmetric, tricolpate, baculate; baculae thin, short, densely distributed; colpus  $\frac{3}{4}$  as long as grain, wide, deep; exine intectate, 1.5 µm thick; ambitus circular-trilobate; grains subprolate, 32 µm length x 28 µm wide (Fig. S7.27) [Sample: Peru, Espinar, ID-39449, Paleo-12555, El Descanso Fm., Member B. England Finder: H42-4]

Undetermined 2 (equivalent morphotype: *Baculatricolporites* “densus”)

Grains monad, isopolar, radially symmetric, tricolporate, baculate; baculae coarse, long; colpus as long as grain, apparently marginate; pores lalongate, acute-ends; exine intectate, 3 µm thick; ambitus probably circular; grains spheroidal, 24 to 26 µm in size (Fig. S7.28) [Sample: Peru, Espinar, ID-39458, Paleo-12571, El Descanso Fm., Member B. England Finder: M34/M35]

Fabaceae-Caesalpinioideae

*Jacqueshuberia* sp. Ducke (equivalent morphotype: *Spyrosyncolpites* “medius”)

Grains monad, apolar, radially symmetric, apparently inaperturate, reticulate; heterobrochate, brochus coarse, irregular, undulating, lumina variable, murus thin, 1 µm thick, simplicolumellate, columellae baculae-typed; exine tectate 3 µm thick; outline circular; grains spheroidal, 27 µm in size (Fig. S7.29) [Sample: Peru, Espinar, ID-39449, Paleo-12555, El Descanso Fm., Member B. England Finder: U11-4]

Fabaceae-Faboideae

*Trifolium* sp. L. (equivalent morphotype: *Psilatricolporites* “fabaciformis”)

Grains monad, apolar, radially symmetric, tricolporate, psilate; apertures thin, inconspicuous, colpus as long as grain; pores apparently circular to elongate; exine tectate 2 µm

thick; ambitus circular; grains subprolate, 19  $\mu\text{m}$  length x 15  $\mu\text{m}$  wide (Fig. S7.30) [Sample: Peru, Espinar, ID-39726, Paleo-12606, El Descanso Fm., Member C. England Finder: M41-4]

Undetermined (equivalent morphotype: *Psilatricolporites* “communis”)

Grains monad, apolar, radially symmetric, tricolporate, psilate; colpus as long as grain, 1.5 to 2  $\mu\text{m}$  wide, displaying equatorial constriction, acute-ends; pores inconspicuous, probably lalongate; exine tectate 1  $\mu\text{m}$  thick, densely columellae; ambitus circular; grains spheroidal, 21  $\mu\text{m}$  in size (Fig. S7.31) [Sample: Peru, San Miguel, Field Station, ID-36583, Paleo-10699. England Finder: T11]

Fabaceae-Mimosoideae

*Acacia* sp. Mill. (equivalent morphotype: *Polyadopollenites mariae*)

Grains grouped as polyad, ca. 34  $\mu\text{m}$  in size, having 16 grains symmetrically arranged. Isolated grains anisopolar, asymmetric, apparently inaperturate, psilate; if apertures present then inconspicuous; exine tectate, less than 1  $\mu\text{m}$  thick; outline trapezoidal; grains oblate, 13  $\mu\text{m}$  in size (Fig. S7.32) [Sample: Peru, Accocunca North, El Descanso Fm., Member B, ID-36569/B47-R17. England Finder: X41/Y41]

*Inga* sp. Mill. (equivalent morphotype: *Polyadopollenites* “ingis”)

Grains grouped as polyad, ca. 115  $\mu\text{m}$  in size, having 24 grains symmetrically arranged. Isolated grains anisopolar, asymmetric, periporate, scabrate; ca. 5 pores, apparently circular, inconspicuous located at proximal face of grain; exine tectate, 2.5  $\mu\text{m}$  thick at distal face to less than 1  $\mu\text{m}$  thick at proximal face; ambitus trapezoidal; grains oblate, variable in size, 20 to 36  $\mu\text{m}$  (Fig. S7.33) [Sample: Peru, Espinar, ID-39702, Paleo-12585, El Descanso Fm., Member B. England Finder: P43]

Fagaceae

*Quercus* sp. L. (equivalent morphotype: *Fagacipollis* “quercoides”)

Grains monad, isopolar, radially symmetric, tricolporate, irregularly scabrate; colpus as long as grain, thin, straight; pores apparently circular to lolongate, sometimes inconspicuous; exine tectate 2  $\mu\text{m}$  thick, densely columellate; ambitus circular; grains subprolate, 18  $\mu\text{m}$  length x 14  $\mu\text{m}$  wide (Fig. S7.34) [Sample: Peru, Espinar, ID-40127, Paleo-12609, El Descanso Fm., Member C. England Finder: H17-3]

#### Hypericaceae

*Vismia* sp. Vand. (equivalent morphotype: *Retitricolporites* “luminibaculosus”)

Grains monad, isopolar, radially symmetric, tricolporate, reticulate; heterobrochate, brochus ca. 1  $\mu\text{m}$  wide, lumina rounded having free exinic elements, muri thin ca. 1  $\mu\text{m}$  thick; colpus as long as grain, thin; pores endexinic, inconspicuous, apparently circular; exine semitectate 1.5  $\mu\text{m}$  thick; ambitus circular; grains subprolate, 22.5  $\mu\text{m}$  length x 19  $\mu\text{m}$  wide (Fig. S7.35) [Sample: Peru, Espinar, ID-40127, Paleo-12609, El Descanso Fm., Member C. England Finder: Q29]

#### Juglandaceae

*Juglans* sp. L. (equivalent morphotype: *Ulmoideipites*? “brevicolporatus”)

Grains monad, isopolar, radially symmetric, stephanoporate, scabrate; 5 small and equidistant pores, circular, 3  $\mu\text{m}$  in diameter, annulate, annulus 2.5  $\mu\text{m}$  wide, slightly protruding; exine tectate, very thin, at inter-apertures areas, ca. 1  $\mu\text{m}$  thick, becoming to be thicker at pore area; ambitus pentagonal; grains apparently oblate, 27  $\mu\text{m}$  in size (polar view) (Fig. S7.36)

[Sample: Peru, Espinar, ID-39443, Paleo-12550, El Descanso Fm., Member B. England Finder: R5/S6]

#### Lamiaceae

*Salvia* sp. L. (equivalent morphotype: *Jandufouria* seamrogiformis)

Grains monad, isopolar, radially symmetric, stephanocolpate, reticulate; homobrochate, brochus less than 1  $\mu\text{m}$  wide; 6 colpus/grain, thin, acute-ends, deep; exine tectate, ca. 1  $\mu\text{m}$  thick,

simplicolumellate; ambitus circular-hexalobulate; grains apparently oblate, 39  $\mu\text{m}$  in size (polar view) (Fig. S7.37) [Sample: Peru, Espinar, ID-39460, Paleo-12573, El Descanso Fm., Member B. England Finder: R49]

#### Malpighiaceae

*Tetrapterys* sp. Cav. (equivalent morphotype: *Perisyncolporites pokorny*)

Grains monad, apolar, radially asymmetric, pericorporate, psilate; 6 to 8 pores subtle and irregularly connected between them by pseudocolpi; pores circular, ectecxinic, 2.5  $\mu\text{m}$  in diameter; exine tectate, 2  $\mu\text{m}$  thick; ambitus circular; grains spheroidal, 22.5  $\mu\text{m}$  in size (Fig. S7.38) [Sample: Peru, Huanu Huanu, El Descanso Fm., Member C, ID-36592/B47-R13. England Finder: H34]

#### Malvaceae-Bombacoideae

*Pseudobombax* sp. Dugand (equivalent morphotype: *Bombacidites* “bombaciformis”)

Grains monad, isopolar, radially symmetric, tricolporate, reticulate; homobrochate, brochus fine less than 1  $\mu\text{m}$  wide diminishing towards apices; apertures inter subangular, brevicorporate, colpus acute-ends; pores endexinic, apparently lalongate, annulate, slightly protruding; exine tectate 1.5  $\mu\text{m}$  thick; ambitus triangular; grains oblate, 31  $\mu\text{m}$  in size (polar view) (Fig. S8.39) [Sample: Peru, Espinar, ID-39542, Paleo-12588, El Descanso Fm., Member B. England Finder: W20]

*Mortoni dendron* sp. Standl. & Steyerl. (equivalent morphotype: *Bombacidites brevis*)

Grains monad, isopolar, radially symmetric, apparently tricolporate, reticulate; heterobrochate, brochus fine diminishing from polar areas towards intercolpium areas; apertures inter subangular, brevicorporate, colpus rounded-ends, marginate; polar area distance between colpi 12  $\mu\text{m}$ ; exine tectate 1  $\mu\text{m}$  thick, sometimes resembling semitectate condition; ambitus circular-trilobate; grains oblate, 33  $\mu\text{m}$  in size (polar view) (Fig. S8.40) [Sample: Peru, Checa, ID-39587/B48-R15. England Finder: W24]

#### Malvaceae-Malvoideae

*Acaulimalva* sp. Krapov. (equivalent morphotype: *Echitriporites* “malviscus”)

Grains monad, isopolar, radially symmetric, triporate, sometimes resembling periporate condition, echinate; echinae short, acute, wide-based, densely distributed; pores circular, masked by ornamentation, annulate; exine tectate, 1  $\mu\text{m}$  thick, surface between echinae scabrate; ambitus circular; grains spheroidal 44  $\mu\text{m}$  in size (Fig. S8.41) [Sample: Peru, Espinar, ID-39443, Paleo-12550, El Descanso Fm., Member B. England Finder: K39-2]

Undetermined (equivalent morphotype: *Malvacipollis mariestelae*)

Grains monad, isopolar, radially symmetric, triporate, echinate; echinae short, conical, acute ends, 1.5  $\mu\text{m}$  length x 1.5  $\mu\text{m}$  wide at base; pores circular, strongly annulate, costae pori 3.5  $\mu\text{m}$  thick, pores slightly protuberant; exine tectate, 1.2  $\mu\text{m}$  thick (excluding echinae); ambitus circular; grains spheroidal 28  $\mu\text{m}$  in size (Fig. S8.42) [Sample: Peru, Accocunca North, El Descanso Fm., Member B, ID-36579/B47-R21. England Finder: D37-1]

Melastomataceae/Combretaceae

Undetermined (equivalent morphotype: *Heterocolpites rotundus*)

Grains monad, isopolar, radially symmetric, heterocolpate, scabrate; three colpi alternating with three colpi; colpi inconspicuous; colpi as long as grain, thin; pores endexinic, apparently circular, annulate; exine tectate, 2  $\mu\text{m}$  thick; ambitus circular-hexalobulate; grains apparently spheroidal, 22  $\mu\text{m}$  in size (Fig. S8.43) [Sample: Peru, Espinar, ID-40127, Paleo-12609, El Descanso Fm., Member C. England Finder: K32-4]

Meliaceae

*Trichilia* sp. P. Browne (equivalent morphotype: *Tetracolporites* “trichiloides”)

Grains monad, isopolar, radially symmetric, stephanocolporate, 4-colporate, reticulate; heterobrochate, brochus very fine less than 0.5  $\mu\text{m}$  wide; colpus straight,  $\frac{3}{4}$  as long as grain,

marginate, displaying equatorially exitus digitatus condition, opposite colpus crossed; pores endexinic, circular to slightly oval; exine tectate 2  $\mu\text{m}$  thick, strongly columellate, columellae very thin; ambitus circular to square; grains subprolate, 26  $\mu\text{m}$  length x 20  $\mu\text{m}$  wide (Fig. S8.44)

[Sample: Peru, Accocunca North, El Descanso Fm., Member B, ID-36569-S2/B48-R4. England Finder: F19]

#### Nyctaginaceae

*Mirabilis* sp. L. (equivalent morphotype: *Annuperiporites* “diornamented”)

Grains monad, apolar, radially symmetric, periporate, echinate; echinae thin, fine, small, less than 1  $\mu\text{m}$  length, acute; ca. 20 circular and equidistant pores/grain, 3  $\mu\text{m}$  in diameter, annulate; exine tectate, 2  $\mu\text{m}$  thick, densely columellate; ambitus circular; grains spheroidal, 33  $\mu\text{m}$  in size (Fig. S8.45) [Sample: Peru, Espinar, ID-39443, Paleo-12550, El Descanso Fm., Member B. England Finder: G19-3]

#### Onagraceae

*Fuchsia* sp. L. (equivalent morphotype: *Crassitriporites* “fuchsicus”)

Grains monad, isopolar, radially symmetric, triporate, scabrate; scabrae fine and becoming to be irregular verrucae around aperture areas; pores circular, protruding, vestibulate, 15  $\mu\text{m}$  in diameter; exine tectate, 1  $\mu\text{m}$  thick; ambitus triangular; grains oblate 50  $\mu\text{m}$  in size (Fig. S8.46)

[Sample: Peru, Espinar, ID-39458, Paleo-12571, El Descanso Fm., Member B. England Finder: D11/E12]

#### Papaveraceae

*Bocconia* sp. L. (equivalent morphotype: *Retiperiporites* “papaveraceous”)

Grains monad, apolar, radially symmetric, periporate, reticulate; homobrochate, brochus fine, lumina circular less than 1  $\mu\text{m}$  wide; more than 30 circular and equidistant pores/grain, 3  $\mu\text{m}$  in diameter ea.; exine tectate, 1  $\mu\text{m}$  thick, columellate, columellae baculae-shaped; ambitus circular; grains spheroidal, 35  $\mu\text{m}$  in size (Fig. S8.47) [Sample: Peru, San Miguel, Field Station, ID-

36583/B47-R11. England Finder: T23]

## Polygonaceae

*Polygonum* sp. L. (equivalent morphotype: *Retiperiporites* “*luminiporosus*”)

Grains monad, apolar, radially symmetric, apparently periporate, reticulate; heterobrochate, per-reticulate, brochus ample, irregular, lumina variable from 2 to 4  $\mu\text{m}$  wide, having free and short columellae; muri thin less than 1  $\mu\text{m}$  thick, undulating; pores inconspicuous, not well defined; exine semitectate, 3.5  $\mu\text{m}$  thick (nexine 1, columellae 2, tectum 0.5  $\mu\text{m}$  thick), columellae baculae-shaped; ambitus circular; grains spheroidal, 35  $\mu\text{m}$  in size (Fig. S8.48)

[Sample: Peru, San Miguel, Field Station, ID-36583/B47-R11. England Finder: G16]

## Portulacaceae (Montiaceae)

*Calandrinia* sp. Kunth (equivalent morphotype: *Annuperiporites* “*densibacularis*”)

Grains monad, apolar, radially symmetric, periporate, reticulate; homobrochate, brochus fine, less than 1  $\mu\text{m}$  wide; ca. 20 pores/grain, circular, 2.5  $\mu\text{m}$  in diameter, slightly annulate; exine tectate, 2  $\mu\text{m}$  thick, simplicolumellate, columellae baculae-shaped; ambitus circular; grains spheroidal, 35  $\mu\text{m}$  in size (Fig. S8.49) [Sample: Peru, Espinar, ID-39705, Paleo-12588, El Descanso Fm., Member

B. England Finder: R17]

## Primulaceae

*Myrsine* sp. L. (equivalent morphotype: *Pericolpites* “*baculatus*”)

Grains monad, apolar, radially asymmetric, pericolpate, 6-aperturate, baculate; baculae 2  $\mu\text{m}$  long; sculpture resembling reticulate pattern; colpus elongated, short, 12  $\mu\text{m}$  length, slightly marginate, opposite colpus crossed; exine intectate 2.5  $\mu\text{m}$  thick, diminishing towards apertures; ambitus circular-square; grains probably oblate, 25  $\mu\text{m}$  in size (Fig. S9.50) [Sample: Peru, Accocunca

North, El Descanso Fm., Member B, ID-36569-S2/B48-R4. England Finder: M22-3]

## Rosaceae

*Polylepis* sp. Ruiz & Pav. (equivalent morphotype: *Byttnerisporis regulate*)

Grains monad, isopolar, radially symmetric, tricolporate, sculpture not well define, resembling striate-rugulate pattern; colpus as long as grain, thin; pores endexinic, circular to slightly elongate, appearing as vestibulate, ca. 5  $\mu\text{m}$  in diameter; exine intectate, thin, 1  $\mu\text{m}$  thick; ambitus circular; grains subprolate, 28  $\mu\text{m}$  length x 23  $\mu\text{m}$  wide (Fig. S9.51) [Sample: Peru, Espinar, ID-39726, Paleo-12606, El Descanso Fm., Member C. England Finder: N39-1]

### Sapotaceae

Unknown (*Pouteria* sp. Aubl.?) (equivalent morphotype: *Retitricolporites* “sapoticus”)

Grains monad, isopolar, radially symmetric, tricolporate, reticulate; homobrochate, brochus very fine less than 0.5  $\mu\text{m}$  wide; colpus thin, as long as grain; pores endexinic, circular to slightly elongate, having a subtle costae pori (annulus); exine tectate, 2  $\mu\text{m}$  thick; ambitus circular; grains subprolate, 27  $\mu\text{m}$  length x 20  $\mu\text{m}$  wide (Fig. S9.52) [Sample: Peru, Espinar, ID-40127, Paleo-12609, El Descanso Fm., Member C. England Finder: T46-4]

### Solanaceae

*Solanum* sp. L. (equivalent morphotype: *Retitricolporites* “solaniformis”)

Grains monad, isopolar, radially symmetric, tricolporate, reticulate; homobrochate, brochus very fine less than 1  $\mu\text{m}$  wide; muri thin, simplibaculate, baculae fine, rounded-head; colpus thin, straight, as long as grain, marginate, margo ca. 2.5  $\mu\text{m}$  thick; pores lalongate becoming to join at apices forming a continuous equatorial ring, ca. 5  $\mu\text{m}$  height; exine tectate, 1  $\mu\text{m}$  thick; ambitus probably circular; grains subprolate, 24  $\mu\text{m}$  length x 19  $\mu\text{m}$  wide (Fig. S9.53) [Sample: Peru, Accocunca North, El Descanso Fm., Member B, ID-36569/B47-R17. England Finder: L34-3]

### Thymelaeaceae

*Daphnopsis* sp. Mart. (equivalent morphotype: *Retiperiporites* “thymelaceous”)

Grains monad, apolar, radially symmetric, periporate, reticulate; homobrochate, brochus fine, 1  $\mu\text{m}$  wide; muri coarse 1  $\mu\text{m}$  thick, simplicolumellate, columellae baculae-shaped, 2.5  $\mu\text{m}$  length; 6 pores/grain, circular, 1  $\mu\text{m}$  in diameter, inconspicuous; exine tectate, 3.5  $\mu\text{m}$  thick; ambitus circular; grains spheroidal, 28  $\mu\text{m}$  in size (Fig. S9.54) [Sample: Peru, Espinar, ID-39456, Paleo-12562, El Descanso Fm., Member B. England Finder: G12-3]

### Vochysiaceae

*Vochysia* sp. Aubl. (equivalent morphotype: *Margotricolporites fastigiatus*)

Grains monad, isopolar, radially symmetric, tricolporate, psilate to slightly scabrate; colpus as long as grain, rounded-end, marginate, margo coarse 2.0  $\mu\text{m}$  thick; pores apparently lalongate, inconspicuous; exine tectate, 1  $\mu\text{m}$  thick; ambitus circular; grains spheroidal, 24  $\mu\text{m}$  in size (polar view) (Fig. S9.55) [Sample: Peru, Accocunca North, El Descanso Fm., Member B, ID-36589/B47-R18. England Finder: P43-1]

### Other eudicotyledoneae

Undetermined 1 (equivalent morphotype: *Retitricolporites* “*solaniformis*”)

Grains monad, isopolar, radially symmetric, tricolporate, reticulate; homobrochate, brochus fine, 1  $\mu\text{m}$  wide; colpus as long as grain, thin; pores lalongate, displaying a subtle equatorial constriction; exine tectate, 2  $\mu\text{m}$  thick, simplicolumellate; ambitus probably circular; grains subprolate, 30  $\mu\text{m}$  length x 21  $\mu\text{m}$  wide (Fig. S9.56) [Sample: Peru, Accocunca North, El Descanso Fm., Member B, ID-36579/B47-R21. England Finder: G17]

Undetermined 2 (equivalent morphotype: *Retitricolporites* “*marginatus*”)

Grains monad, isopolar, radially symmetric, tricolporate, reticulate; homobrochate, brochus fine, less than 1  $\mu\text{m}$  wide, muri thin, lumina circular; colpus as long as grain, thin, marginate, margo ca. 1.5  $\mu\text{m}$  thick, exhibiting equatorially exitus digitatus condition; pores lalongate to

oval, 2  $\mu\text{m}$  length x 2.5  $\mu\text{m}$  wide; exine tectate, 1.2  $\mu\text{m}$  thick, simplicolumellate, columellae baculae-shaped; ambitus circular; grains subprolate, 21  $\mu\text{m}$  length x 16.5  $\mu\text{m}$  wide (Fig. S9.57)

[Sample: Peru, Accocunca North, El Descanso Fm., Member B, ID-36569-S2/B48-R4. England Finder: R22-1/2]

Undetermined 3 (equivalent morphotype: *Psilatricolporites* “annulatus”)

Grains monad, isopolar, radially symmetric, tricolporate, psilate; colpus as long as grain, thin, straight; pores endexinic, circular, annulate, annulus coarse; exine tectate, 2  $\mu\text{m}$  thick; ambitus circular; grains subprolate, 28  $\mu\text{m}$  length x 20  $\mu\text{m}$  wide (Fig. S9.58) [Sample: Peru, Espinar,

ID-40127, Paleo-12609, El Descanso Fm., Member C. England Finder: G35-1]

Undetermined 4 (equivalent morphotype: *Psilatricolpites* “complicatus”)

Grains monad, isopolar, radially symmetric, apparently tricolporate, if pores present then inconspicuous, reticulate; subtly homobrochate, brochus fine, less than 1  $\mu\text{m}$  wide; colpus as long as grain, marginate, margo irregular; exine tectate, 1.5  $\mu\text{m}$  thick; ambitus probably circular; grains prolate, 25  $\mu\text{m}$  length x 15  $\mu\text{m}$  wide (Fig. S9.59) [Sample: Peru, Espinar, ID-40127, Paleo-12609, El

Descanso Fm., Member C. England Finder: M41-1]

Undetermined 5 (equivalent morphotype: *Retitriporites* “amplibrochate”)

Grains monad, isopolar, radially symmetric, triporate, reticulate; heterobrochate, per-reticulate; brochi wide, irregular, variable in size; muri ca. 1  $\mu\text{m}$  thick, simplicolumellate, columellae baculae-shaped; lumina sporadically having free exinic elements; pores circular, not well defined, ample, inconspicuous, ca. 6  $\mu\text{m}$  in diameter; exine semitectate, 1  $\mu\text{m}$  thick; ambitus circular; grains spheroidal, 22  $\mu\text{m}$  in size (Fig. S9.60) [Sample: Peru, Espinar, ID-39452, Paleo-12558, El

Descanso Fm., Member C. England Finder: Q23/R23]

Undetermined 6 (equivalent morphotype: *Retitricolporites* “confusus”)

Grains monad, isopolar, radially symmetric, tricolporate, reticulate; homobrochate, brochus fine, ca. 1  $\mu\text{m}$  wide, muri thin; colpus as long as grain, marginate, margo coarse 2  $\mu\text{m}$  thick;

pores endexinic, lalongate; exine tectate, 2  $\mu\text{m}$  thick, simplicolumellate, columellae baculae-shaped; ambitus circular; grains subprolate to prolate, 31  $\mu\text{m}$  length x 18  $\mu\text{m}$  wide (Fig. S9.61)

[Sample: Peru, Espinar, ID-39452, Paleo-12558, El Descanso Fm., Member C. England Finder: M6-1]

Undetermined 7 (equivalent morphotype: *Retitricolporites* “pseudodigitatus”)

Grains monad, isopolar, radially symmetric, tricolporate, reticulate; homobrochate, brochus less than 1  $\mu\text{m}$  wide, muri very thin; colpus as long as grain, thin; pores endexinic, circular, inconspicuous; exine tectate, 2  $\mu\text{m}$  thick; ambitus circular; grains subprolate, 32  $\mu\text{m}$  length x 27  $\mu\text{m}$  wide (Fig. S9.62) [Sample: Peru, Espinar, ID-39458, Paleo-12571, El Descanso Fm., Member B. England Finder: Q16-3]

Undetermined 8 (equivalent morphotype: *Retitricolporites* “incognitus”)

Grains monad, isopolar, radially symmetric, tricolporate, reticulate; homobrochate, brochus fine, muri thin; colpus as long as grain, slightly marginate; pores endexinic, lalongate; exine semitectate, 1  $\mu\text{m}$  thick, simplicolumellate, columellae baculae-shaped; ambitus circular; grains subprolate to spheroidal, 23  $\mu\text{m}$  in size (Fig. S9.63) [Sample: Peru, Espinar, ID-39459, Paleo-12572, El Descanso Fm., Member B. England Finder: K30]

## **Angiosperms-Monocotyledoneae**

### *Alismataceae*

*Echinodorus* sp. Rich. (equivalent morphotype: *Echiperiporites* *akanthos*)

Grains monad, apolar, radially asymmetric, periporate sometimes resembling pericorporate condition, echinate; echinae conical, acute-ends, 1.8  $\mu\text{m}$  long x 1.5  $\mu\text{m}$  wide; surface scabrate between echinae, scabrae fine less than 1  $\mu\text{m}$  thick, densely distributed; 7 to 8 pores/grain, circular, 1.5  $\mu\text{m}$  in diameter, annulate, annulus ca. 1  $\mu\text{m}$  thick; colpus if present very short, inconspicuous, linear; exine tectate, 2  $\mu\text{m}$  thick, densely columellate; outline circular; grains

spheroidal, 33  $\mu\text{m}$  in size (Fig. S10.64) [Sample: Peru, Accocunca North, El Descanso Fm., Member B, ID-36589/B47-R18. England Finder: J45-3]

*Sagittaria* sp. L. (equivalent morphotype: Echiperiporites “sagittarianus”)

Grains monad, apolar, radially asymmetric, periporate, echinate; echinae conical, short, acute-ends, 1.5  $\mu\text{m}$  long; 8 pores/grain, circular, irregular, 2.5  $\mu\text{m}$  in diameter; exine intectate; outline circular-irregular; grains spheroidal, 31  $\mu\text{m}$  in size (Fig. S10.65) [Sample: Peru, Accocunca North, El Descanso Fm., Member B, ID-36569-S2/B48-R4. England Finder: R16-4]

Araceae

*Anthurium* sp. 1 Schott (equivalent morphotype: Retiinaperturites “araceiformis”)

Grains monad, apolar, radially symmetric, inaperturate, reticulate; homobrochate, brochus fine, lumina circular, muri 1  $\mu\text{m}$  thick; exine tectate, 1  $\mu\text{m}$  thick, strongly columellate, columellae baculae-shaped; outline circular; grains spheroidal, 22  $\mu\text{m}$  in size (Fig. S10.66) [Sample: Peru, Checa, ID-36582/B47-R12. England Finder: T42-2]

*Anthurium* sp. 2 Schott (equivalent morphotype: Verruinaperturites “anthuricus”)

Grains monad, apolar, radially symmetric, inaperturate, verrucate; verrucae spheroidal resembling gemmae condition, small, less than 1  $\mu\text{m}$  wide; exine tectate, masked by sculpture, 1.5  $\mu\text{m}$  thick; outline circular; grains spheroidal, 12  $\mu\text{m}$  in size (Fig. S10.67) [Sample: Peru, Espinar, ID-39726, Paleo-12606, El Descanso Fm., Member C. England Finder: K40-3/L40-1]

*Spathiphyllum* sp. Schott (equivalent morphotype: Stephanocolpites “longistriate”)

Grains monad, isopolar, radially symmetric, stephanocolpate but could be interpreted as inaperturate due to colpi are not well defined (pseudocolpi? Striae?); colpus longitudinally oriented resembling striate condition; exine tectate, thin; outline circular; grains spheroidal, 14  $\mu\text{m}$  in size (Fig. S10.68) [Sample: Peru, Espinar, ID-39726, Paleo-12606, El Descanso Fm., Member C. England Finder: R48]

Arecaceae

*Lepidocaryum* sp. Mart. (equivalent morphotype: *Mauritiidites franciscoi*)

Grains monad, heteropolar, bilaterally symmetric, monocolpate, echinate; echinae short, rounded-ends, 1  $\mu\text{m}$  length, scarcely distributed, echini inserted into sexine based in a conspicuous depression; colpus irregular, inconspicuous, 2/3 as long as grain; exine tectate, less than 1  $\mu\text{m}$  thick; outline oval irregular; grains 47  $\mu\text{m}$  in size (Fig. S10.69) [Sample: Peru, Espinar, ID-39703, Paleo-12586, El Descanso Fm., Member B. England Finder: H38]

*Socratea* sp. H. Karst. (equivalent morphotype: *Echimonocolpites "socratensis"*)

Grains monad, heteropolar, bilaterally symmetric, monocolpate, echinate; echinae conical, acute-ends, 1  $\mu\text{m}$  length; surface between echinae slightly scabrate; colpus irregular, marginate, as long as grain; exine tectate, 1  $\mu\text{m}$  thick; outline oval; grains 27  $\mu\text{m}$  length x 20  $\mu\text{m}$  wide (Fig. S10.70) [Sample: Peru, Accocunca North, El Descanso Fm., Member B, ID-36579/B47-R21. England Finder: Q34-1]

Undetermined 1 (equivalent morphotype: *Psilamonocolpites "giganteus"*)

Grains monad, heteropolar, bilaterally symmetric, monocolpate, psilate; colpus thin, as long as grain; exine tectate, 1  $\mu\text{m}$  thick, strongly columellate, columellae very thin, linear, pilum-shaped; outline oval; grains 62  $\mu\text{m}$  length x 42.5  $\mu\text{m}$  wide (Fig. S10.71) [Sample: Peru, San Miguel, Field Station, ID-36583/B47-R11. England Finder: J10]

Undetermined 2 (equivalent morphotype: *Baculimonocolpites "microbaculatus"*)

Grains monad, heteropolar, bilaterally symmetric, monocolpate, baculate; baculae short, less than 1  $\mu\text{m}$  length, thin, densely distributed on surface; colpus thin, as long as grain, inconspicuous; exine intectate, 1  $\mu\text{m}$  thick; outline oval to circular; grains 22.5  $\mu\text{m}$  length x 18  $\mu\text{m}$  wide (Fig. S10.72) [Sample: Peru, San Miguel, Field Station, ID-36583/B47-R11. England Finder: J32]

Undetermined 3 (equivalent morphotype: *Psilamonocolpites ovatus*)

Grains monad, heteropolar, bilaterally symmetric, monocolpate, psilate; colpus 3/4 as long as grain, wide, ca. 28  $\mu\text{m}$  long x 12  $\mu\text{m}$  wide, irregular; exine tectate, 1  $\mu\text{m}$  thick, columellate,

columellae fine; outline oval; grains 34  $\mu\text{m}$  length x 27  $\mu\text{m}$  wide (Fig. S10.73) [Sample: Peru, Accocunca North, El Descanso Fm., Member B, ID-36584/B47-R16. England Finder: J15-1]

#### Bromeliaceae

*Tillandsia* sp. L. (equivalent morphotype: *Retiinaferturites* “communis”)

Grains monad, apolar, radially symmetric, inaperturate, reticulate; heterobrochate, brochus irregular, lumina wide, muri thin; exine tectate, 2  $\mu\text{m}$  thick; outline spheroidal; grains 50  $\mu\text{m}$  in size (Fig. S10.74) [Sample: Peru, Espinar, ID-40127, Paleo-12609, El Descanso Fm., Member C. England Finder: F40-3/4]

#### Cyperaceae

*Rhynchospora* sp. Vahl (equivalent morphotype: *Pseudoperiporites* “asymmetricus”)

Grains monad, apolar, radially asymmetric, periporate, scabrate, scabrae fine; pores irregular, resembling vestigial colpus, ca. 4 pores irregularly distributed, variables in size; exine tectate, 2.5  $\mu\text{m}$  thick; outline trapezoidal; grains 25  $\mu\text{m}$  in size (Fig. S10.75) [Sample: Peru, Espinar, ID-39361, Paleo-12548, El Descanso Fm., Member C. England Finder: J20-2/4]

#### Poaceae

*Calamagrostis* sp. Adans. (equivalent morphotype: *Monoporopollenites annulatus* < 35  $\mu\text{m}$ )

Grains monad, apolar, radially asymmetric, monoporate, scabrate, scabrae fine; pore circular, annulate, small, annulus 1.5  $\mu\text{m}$  thick; exine tectate, 1  $\mu\text{m}$  thick; outline circular; grains 34  $\mu\text{m}$  in size (Fig. S10.76) [Sample: Peru, Huanu Huanu, El Descanso Fm., Member C, ID-36563/B47-R15. England Finder: M40-1]

*Hordeum* sp. L. (equivalent morphotype: *Monoporopollenites annulatus* > 35  $\mu\text{m}$ )

Grains monad, apolar, radially asymmetric, monoporate, psilate; pore circular, 4.5  $\mu\text{m}$  in diameter, annulate, annulus 2.5  $\mu\text{m}$  thick; exine tectate, 1  $\mu\text{m}$  thick; outline circular irregular, folded; grains 45  $\mu\text{m}$  in size (Fig. S10.77) [Sample: Peru, San Miguel, Field Station, ID-36583/B47-R11. England Finder: S34-4]

## Angiosperms-Basal Angiosperms

### Chloranthaceae

*Hedyosmum* sp. Sw. (equivalent morphotype: *Clavainaperturites microclavatus*)

Grains monad, apolar, radially symmetric, inaperturate, clavate; clavae resembling small baculae, short, fine, rounded-end, ca. 1  $\mu\text{m}$  long; exine intectate, very thin, ca. 1  $\mu\text{m}$  thick; outline circular; grains 21  $\mu\text{m}$  in size (Fig. S10.78) [Sample: Peru, Accocunca North, El Descanso Fm., Member B, ID-36589/B47-R18. England Finder: M48-3]

### Winteraceae

*Drimys* sp. J.R. Forst. & G. Forst. (equivalent morphotype: *Tetradites* “tetraporosus”)

Grains grouped as tetrad, 4 grains ordered in a tetrahedral pattern, ca. 24  $\mu\text{m}$  in size, ambitus circular. Isolated grains heteropolar, radially asymmetric, monoporate, psilate; pores on distal face, ample, rounded, borders do not well defined, apparently annulate, annulus densely scabrate; exine tectate, thin; ambitus circular; grains apparently suboblate, 20  $\mu\text{m}$  in size (polar view) (Fig. S10.79) [Sample: Peru, Espinar, ID-39726, Paleo-12606, El Descanso Fm., Member C. England Finder: N5-3]

## Gnetophyta

### Ephedraceae

*Ephedra* sp. L. (equivalent morphotype: *Ephedripites* “problematicus”)

Grains monad, isopolar, radially symmetric, apparently inaperturate, striate; striae coarse, irregular, longitudinally oriented; if apertures present then inconspicuous; exine tectate, ca. 1  $\mu\text{m}$  thick; ambitus probably circular; grains subprolate 26  $\mu\text{m}$  length x 15  $\mu\text{m}$  wide (Fig. S11.80) [Sample: Peru, Espinar, ID-39458, Paleo-12571, El Descanso Fm., Member B. England Finder: H49]

## Pinophyta

### Podocarpaceae

*Podocarpus* sp. L'Hér. ex Pers. (equivalent morphotype: Podocarpites “normalis”)

Grains monad, vesiculate (bissacate), diploxilonoid, 47  $\mu$  in size; vesiculae globose, translucent, psilate to slightly reticulate, 26 x 38  $\mu$ m in size, angularly oriented; corpus apolar, radially asymmetric, inaperturate, psilate; exine tectate, 2  $\mu$ m thick (nexine 0.5, columellae and tectum 1.5  $\mu$ m thick); ambitus probably circular; grains spheroidal 38  $\mu$ m in size (Fig. S11.81)

[Sample: Peru, San Miguel, Field Station, ID-36583/B47-R11. England Finder: M20-1]

## Tracheophyta

### Anemiaceae

*Anemia* sp. Sw. (equivalent morphotype: Striatriletes saccolomoides)

Spore trilete, heteropolar, radially symmetric, striate; striae fine, irregular, 1  $\mu$ m thick, concentrically oriented on proximal face; laesurae irregular, as long as proximal face; sclerine thin, less than 1  $\mu$ m thick; outline triangular-irregular; spores 42  $\mu$ m in size (Fig. S11.82) [Sample:

Peru, Espinar, ID-39460, Paleo-12573, El Descanso Fm., Member B. England Finder: G40-1]

### Aspleniaceae

*Asplenium* sp.1 L. (equivalent morphotype: Perimonoletes “simplex”)

Spore monolete, heteropolar, bilaterally symmetric; sclerine psilate 1.2  $\mu$ m thick, having a continuous undulating perine, translucent, sessile, displaying irregular projections resembling echinulate condition; laesurae inconspicuous, apparently as long as spore; outline convex-convex; spores 33  $\mu$ m length x 24  $\mu$ m wide (excluding perine) and becoming to 45  $\mu$ m in size including it (Fig. S11.83) [Sample: Peru, Huanu Huanu, El Descanso Fm., Member C, ID-36594/B47-R14. England

Finder: U20-2]

*Asplenium* sp.2 L. (equivalent morphotype: Perimonoletes “circularis”)

Spore monolete, heteropolar, bilaterally symmetric; sclerine psilate, thin, having a continuous undulating perine, translucent, resembling reticulate pattern; laesurae inconspicuous,

masked by perine; outline circular; spores 35  $\mu\text{m}$  in size (excluding perine) (Fig. S11.84) [Sample: Peru, Espinar, ID-39726, Paleo-12606, El Descanso Fm., Member C. England Finder: M39-1]

*Asplenium* sp.3 L. (equivalent morphotype: Perinotriletes “caoticus”)

Spore trilete, heteropolar, radially symmetric; sclerine psilate, thin, masked by a continuous undulating perine, translucent, irregularly reticulate, 5  $\mu\text{m}$  length; laesurae inconspicuous, masked by perine; outline triangular-rounded; spores 30  $\mu\text{m}$  in size (excluding perine) and 40  $\mu\text{m}$  including it (Fig. S11.85) [Sample: Peru, Espinar, ID-39443, Paleo-12550, El Descanso Fm., Member B. England Finder: O15]

*Asplenium* sp.4 L. (equivalent morphotype: Perinotriletes “giganteous”)

Spore trilete, heteropolar, radially symmetric; sclerine psilate, thin, masked by a continuous and folded perine, translucent, slightly reticulate, 7  $\mu\text{m}$  length; laesurae inconspicuous, masked by perine; outline circular; spores 65  $\mu\text{m}$  in size (excluding perine) and 79  $\mu\text{m}$  including it (Fig. S11.86) [Sample: Peru, Espinar, ID-39456, Paleo-12562, El Descanso Fm., Member B. England Finder: M42-1/2]

#### Blechnaceae

*Blechnum* sp. L. (equivalent morphotype: Perimonoletes “ondulosus”)

Spore monolete, heteropolar, bilaterally symmetric; sclerine psilate 2.5  $\mu\text{m}$  thick, having a continuous undulating perine, granular; laesurae inconspicuous; outline convex-convex; spores 41  $\mu\text{m}$  in size (excluding perine) and becoming to 50  $\mu\text{m}$  in size including it (Fig. S11.87) [Sample: Peru, Accocunca North, El Descanso Fm., Member B, ID-36569/B47-R17. England Finder: L30]

#### Cyatheaceae

*Cyathea* sp.1 Sm. (equivalent morphotype: Psilatrilletes sp. < 50  $\mu\text{m}$ )

Spore trilete, heteropolar, radially symmetric; sclerine psilate, very thin, less than 1  $\mu\text{m}$  thick; laesurae thin, marginate, as long as proximal face; outline triangular-rounded; spores 39  $\mu\text{m}$  in size (Fig. S12.88) [Sample: Peru, San Miguel, Field Station, ID-36583/B47-R11. England Finder: D34-1]

*Cyathea* sp.2 Sm. (equivalent morphotype: *Verrucatotriletes etayoi*)

Spore trilete, heteropolar, radially symmetric; sclerine verrucate, coarse, verrucae densely distributed, rounded, ca. 2.5  $\mu$  length x 5  $\mu$ m wide, variable in size; laesurae masked by sculpture; outline triangular-straight; spores 33  $\mu$ m in size (Fig. S12.89) [Sample: Peru, Checa, ID-36582/B47-R12. England Finder: K33-4]

*Cyathea* sp.3 Sm. (equivalent morphotype: *Verrutriteles* “homogeneous”)

Spore trilete, heteropolar, radially symmetric; sclerine 3  $\mu$ m thick, verrucate, verrucae densely distributed, coarse, rounded, ca. 2.5  $\mu$  length x 3.5  $\mu$ m wide, variable in size; laesurae wide, as long as proximal face; outline triangular-convex; spores 19 to 28  $\mu$ m in size (Fig. S12.90) [Sample: Peru, Espinar, ID-39361, Paleo-12548, El Descanso Fm., Member C. England Finder: N25]

*Cyathea* sp.4 Sm. (equivalent morphotype: *Verrutriteles* “medianus”)

Spore trilete, heteropolar, radially symmetric; sclerine 5  $\mu$ m thick, verrucate, verrucae big, flat, amply distributed on surface; laesurae straight, thin, as long as proximal face; outline triangular-convex; spores 55  $\mu$ m in size (Fig. S12.91) [Sample: Peru, Espinar, ID-39456, Paleo-12562, El Descanso Fm., Member B. England Finder: H23-3]

*Hemitelia* sp. R. Br. (equivalent morphotype: *Kuylisporites* “irregularis”)

Spore trilete, heteropolar, radially symmetric; spores having thin, translucent and sessile perine; perine oradate resembling circular and annulate “pores”; holes irregularly dispersed on surface of spore, variables in size, 2 to 4  $\mu$ m in diameter; sclerine coarse, variable, thicker at oral areas resembling small foveae; laesurae inconspicuous; outline triangular (proximal face); spores 31  $\mu$ m in size (Fig. S12.92) [Sample: Peru, Espinar, ID-39713, Paleo-12594, El Descanso Fm., Member B. England Finder: F6]

Dennstaedtiaceae

*Hypolepis* sp. Bernh. (equivalent morphotype: *Retimonoletes* “microechinatus”)

Spore monolete (sporadically trilete), heteropolar, bilaterally symmetric; sclerine psilate 2  $\mu\text{m}$  thick, having a very thin and continuous perine, sessile, reticulate-echinate; laesurae inconspicuous; outline plano-convex; spores 38  $\mu\text{m}$  length x 31  $\mu\text{m}$  wide (Fig. S12.93) [Sample: Peru, Accocunca North, El Descanso Fm., Member B, ID-36584/B47-R16. England Finder: X35 & O33-1]

#### Hymenophyllaceae

*Hymenophyllum* sp. Sm. (equivalent morphotype: Baculatriletes “irregularis”)

Spore trilete, heteropolar, radially symmetric; sclerine thin, densely baculate, baculae short, rounded, sometimes arranged as reticulate pattern; laesurae as long as proximal face, rounded ends, marginate; outline triangular-convex (proximal face); spores 15  $\mu\text{m}$  in size (Fig. S12.94) [Sample: Peru, Huanu Huanu, El Descanso Fm., Member C, ID-36592/B47-R13. England Finder: G15]

#### Lycopodiaceae

*Lycopodium* sp.1 L. (equivalent morphotype: Foveotriletes “variabilis”)

Spore trilete, heteropolar, radially symmetric; sclerine apparently foveolate, foveolae irregular, becoming to be circular, ca. 5  $\mu\text{m}$  in diameter; distance between foveolae (bridges) irregular, thin, ca. 1  $\mu\text{m}$  thick; spores displaying a subtle, hyaline and sessile perine; laesurae thin, irregular, as long as proximal face; outline triangular-convex (proximal face); spores 48  $\mu\text{m}$  in size (Fig. S12.95) [Sample: Peru, San Miguel, Field Station, ID-36583/B47-R11. England Finder: L48]

*Lycopodium* sp.2 L. (equivalent morphotype: Retitriletes “sessile”)

Spore trilete, heteropolar, radially symmetric; sclerine apparently psilate (laevigate), thin, 1  $\mu\text{m}$  thick, having thin and irregular perine; perine reticulate; laesurae as long as proximal face, irregular, thin; outline triangular-convex (proximal face); spores 62  $\mu\text{m}$  in size (Fig. S12.96) [Sample: Peru, Accocunca North, El Descanso Fm., Member B, ID-36584/B47-R16. England Finder: M9-3]

*Lycopodium* sp.3 L. (equivalent morphotype: Foveotriletes ornatus)

Spore trilete, heteropolar, radially symmetric; sclerine thin, psilate, 1.2  $\mu\text{m}$  thick, perforate, holes regular, circular, 1  $\mu\text{m}$  in diameter, resembling a foveolate condition; laesurae as long as proximal face, thin, straight, subtly marginate; outline triangular-convex (proximal face); spores 40  $\mu\text{m}$  in size (Fig. S12.97) [Sample: Peru, Accocunca North, El Descanso Fm., Member B, ID-36590/B47-R19.

England Finder: Z43-1]

*Lycopodium* sp.4 L. (equivalent morphotype: Retitriletes “fungiformis”)

Spore trilete, heteropolar, radially symmetric; sclerine not well defined, masked by a persistent perine, sessile, reticulate, irregular; laesurae as long as proximal face, masked by perine; outline triangular-convex (proximal face); spores 80  $\mu\text{m}$  in size (Fig. S12.98) [Sample: Peru,

Espinar, ID-39443, Paleo-12550, El Descanso Fm., Member B. England Finder: T13]

Polypodiaceae

*Grammitis* sp.1 Sw. (equivalent morphotype: Scabratriletes “sphericus”)

Spore trilete, heteropolar, radially symmetric; sclerine 1  $\mu\text{m}$  thick, scabrate, scabrae irregular, scarce; laesurae coarse, slightly marginate, as long as proximal face; outline circular (proximal face); spores 27  $\mu\text{m}$  in size (Fig. S13.99) [Sample: Peru, Accocunca North, El Descanso Fm., Member B, ID-

36579/B47-R21. England Finder: F41]

*Polypodium* sp.1 L. (equivalent morphotype: Psilamonoletes tibui)

Spore monolete, heteropolar, bilaterally symmetric; sclerine psilate (laevigate), 1  $\mu\text{m}$  thick, sometimes surface appear to have subtle verrucae; laesurae irregular,  $\frac{3}{4}$  as long as spore; outline plano-convex; spores 39  $\mu\text{m}$  length x 30  $\mu\text{m}$  wide (Fig. S13.100) [Sample: Peru, San Miguel, Field Station,

ID-36583/B47-R11. England Finder: G37-3]

*Polypodium* sp.2 L. (equivalent morphotype: Polypodiisporites “verruplanatus”)

Spore monolete, heteropolar, bilaterally symmetric; sclerine verrucate, verrucae uniform, flat, abundant, wide, 1  $\mu\text{m}$  height x 3  $\mu\text{m}$  wide; sclerine 3.5  $\mu\text{m}$  thick; laesurae  $\frac{2}{3}$  as long as

spore, ca 30  $\mu\text{m}$  length, marginate, margo conspicuous, coarse; outline plano-convex; spores 54  $\mu\text{m}$  length x 34  $\mu\text{m}$  wide (Fig. S13.101) [Sample: Peru, Accocunca North, El Descanso Fm., Member B, ID-36584/B47-R16. England Finder: K41-4]

*Polypodium* sp.3 L. (equivalent morphotype: *Polypodiisporites* “spinosus”)

Spore monolete, heteropolar, bilaterally symmetric; sclerine verrucate, verrucae irregular, scarce, dispersed, 1.5  $\mu\text{m}$  height x 3  $\mu\text{m}$  wide; sclerine thin, 1  $\mu\text{m}$  thick; laesurae thin, as long as spore, slightly marginate; outline plano-convex; spores 37  $\mu\text{m}$  length x 22  $\mu\text{m}$  wide (Fig. S13.102) [Sample: Peru, Accocunca North, El Descanso Fm., Member B, ID-36566/B47-R20. England Finder: W46-3]

*Polypodium* sp.4 L. (equivalent morphotype: *Verrumonoletes usmensis*)

Spore monolete, heteropolar, bilaterally symmetric; sclerine verrucate, verrucae uniform, 2.5  $\mu\text{m}$  height x 3.5  $\mu\text{m}$  wide; sclerine 3  $\mu\text{m}$  thick; laesurae inconspicuous, apparently as long as spore, marginate; outline plano-convex; spores 28  $\mu\text{m}$  length x 19  $\mu\text{m}$  wide (Fig. S13.103) [Sample: Peru, Espinar, ID-39361, Paleo-12548, El Descanso Fm., Member C. England Finder: J20]

*Polypodium* sp.5 L. (equivalent morphotype: *Polypodiisporites* “insignificant”)

Spore monolete, heteropolar, bilaterally symmetric; sclerine verrucate, verrucae flat, wide, dense; sclerine coarse, 5  $\mu\text{m}$  thick; laesurae inconspicuous; outline plano-convex; spores 56  $\mu\text{m}$  length x 38  $\mu\text{m}$  wide (Fig. S13.104) [Sample: Peru, Espinar, ID-39721, Paleo-12601, El Descanso Fm., Member C. England Finder: R13-3]

*Polypodium* sp.6 L. (equivalent morphotype: *Polypodiisporites* “disastrous”)

Spore monolete, heteropolar, bilaterally symmetric; sclerine verrucate, verrucae flat, dense; sclerine thin, 1.5  $\mu\text{m}$  thick; laesurae inconspicuous, irregular; outline concave-convex; spores 66  $\mu\text{m}$  length x 37  $\mu\text{m}$  wide (Fig. S13.105) [Sample: Peru, Espinar, ID-39443, Paleo-12550, El Descanso Fm., Member C. England Finder: G11]

Pteridaceae

*Ceratopteris* sp. Brongn. (equivalent morphotype: *Magnastriatites grandiosus*)

Spore trilete, heteropolar, radially symmetric; sclerine striate, striae coarse, granulate, 5 µm thick concentrically oriented at proximal face; laesurae thin, as long as proximal face; outline triangular (proximal face); spores 67 µm in size (Fig. S13.106) [Sample: Peru, Accocunca North, El Descanso Fm., Member B, ID-36569/B47-R17. England Finder: M33-2/4]

*Jamesonia* sp. Hook. & Grev. (equivalent morphotype: *Cingulatisporites* “psilatus”)

Spore trilete, heteropolar, radially symmetric; sclerine psilate, variable 1.8 µm at apices and 6 µm thick to the side; laesurae wide, having a coarse and strongly margo ca. 6 µm thick, as long as proximal face; outline triangular-concave (proximal face); spores 34 µm in size (Fig. S13.107) [Sample: Peru, Checa, ID-36582/B47-R12. England Finder: G23]

#### Selaginellaceae

*Selaginella* sp.1 P. Beauv. (equivalent morphotype: *Echitriletes* “selaginelloides” type “regularis”)

Spore trilete, heteropolar, radially symmetric; sclerine 1 µm thick, undulating, echinate; echinae thin, straight, acute ends, ca. 3 µm length; laesurae thin, as long as proximal face; outline triangular-convex (proximal face); spores 50 µm in size (Fig. S13.108) [Sample: Peru, Accocunca North, El Descanso Fm., Member B, ID-36569/B47-R17. England Finder: X15-2]

*Selaginella* sp.2 P. Beauv. (equivalent morphotype: *Echitriletes* “selaginelloides” type “spinosus”)

Spore trilete, heteropolar, radially symmetric, echinate; echinae long, acute, conical, ca. 5 µm length x 1 µm wide; laesurae inconspicuous; sclerine 1.5 to 2 µm thick (echini excluded); outline circular (proximal face); spores 28 to 30 µm in size (Fig. S13.109) [Sample: Peru, Accocunca North, El Descanso Fm., Member B, ID-36569-S2/B48-R4. England Finder: U12]

*Selaginella* sp.3 P. Beauv. (equivalent morphotype: *Verrutriletes* “selaginellaceous”)

Spore trilete, heteropolar, radially symmetric, verrucate; verrucae flat, wide, irregular; laesurae straight, thin,  $\frac{3}{4}$  as long as proximal face, marginate, margin coarse; sclerine ca. 2.5  $\mu\text{m}$  thick diminishing at apices; outline triangular-convex (proximal face); spores 28  $\mu\text{m}$  in size (Fig. S13.110) [Sample: Peru, Espinar, ID-39447, Paleo-12554, El Descanso Fm., Member B. England Finder: E9-4]

*Selaginella* sp.4 P. Beauv. (equivalent morphotype: Echitriletes “selaginelloides” type “muelleri”)

Spore trilete, heteropolar, radially symmetric, echinate; echinae long, irregular, densely distributed on surface; laesurae inconspicuous, masked by ornamentation; sclerine coarse; outline circular (proximal face); spores 28  $\mu\text{m}$  in size (Fig. S13.111) [Sample: Peru, Espinar, ID-39450, Paleo-12556, El Descanso Fm., Member B. England Finder: V46]

*Selaginella* sp.5 P. Beauv. (equivalent morphotype: Echitriletes “selaginelloides” type “bacularis”)

Spore trilete, heteropolar, radially symmetric, baculate; baculae irregular, scarce, long, ending head-shaped, sometimes resembling irregular echinae; laesurae inconspicuous; sclerine thin, ca. 1  $\mu\text{m}$  thick; outline circular (proximal face); spores 25  $\mu\text{m}$  in size (Fig. S13.112) [Sample: Peru, Espinar, ID-40129, Paleo-12611, El Descanso Fm., Member B. England Finder: H40-3]

#### Thelypteridaceae

*Thelypteris* sp. Schmidel (equivalent morphotype: Perinomonoletes reticuloacicularis)

Spore monolete, heteropolar, bilaterally symmetric; spore covered by a persistent thin and irregular perine, microechinate-reticulate; laesurae inconspicuous; sclerine thin, psilate; outline plano-convex; spores 47  $\mu\text{m}$  length x 27  $\mu\text{m}$  wide (Fig. S13.113) [Sample: Peru, Espinar, ID-39704, Paleo-12587, El Descanso Fm., Member B. England Finder: Y11]

#### Other tracheophyta

Undetermined 1 (equivalent morphotype: Retitriletes “fossulatus”)

Spore trilete, heteropolar, radially symmetric; sclerine reticulate sometimes resembling foveolate condition, ca. 1.8  $\mu\text{m}$  thick; brochi variable, lumina circular, muri coarse; laesurae triangular, wide, marginate,  $\frac{1}{2}$  as long as proximal face; outline circular (proximal face); spores 34  $\mu\text{m}$  in size (Fig. S13.114) [Sample: Peru, Accocunca North, El Descanso Fm., Member B, ID-36566/B47-R20. England Finder: R22-4]

Undetermined 2 (equivalent morphotype: *Echimonoletes* “spiniiformis”)

Spore monolete, heteropolar, bilaterally symmetric; sclerine 1.5  $\mu\text{m}$  thick, covered by a persistent thin and irregular perine (?); perine displaying irregular and thick projections ca. 3.5  $\mu\text{m}$  length, resembling vestigial echini; laesurae wide, as long as spore; sclerine thin, psilate; outline biconvex; spores 40  $\mu\text{m}$  length x 32  $\mu\text{m}$  wide (Fig. S14.115) [Sample: Peru, Accocunca North, El Descanso Fm., Member B, ID-36566/B47-R20. England Finder: R19-4]

Undetermined 3 (equivalent morphotype: *Retitriletes* “inciertus”)

Spore trilete, heteropolar, radially symmetric, psilate to irregularly scabrate; laesurae coarse, as long as proximal face, ending in a circular and protruding elongation; sclerine 2.5  $\mu\text{m}$  thick; outline circular to slightly triangular (proximal face); spores 38  $\mu\text{m}$  in size (Fig. S14.116) [Sample: Peru, Accocunca North, El Descanso Fm., Member B, ID-36579/B47-R21. England Finder: L46]

Undetermined 4 (equivalent morphotype: *Retitriletes* *sommeri*)

Spore trilete, heteropolar, radially symmetric, rugulate; rugulae irregular, ca. 1  $\mu\text{m}$  thick, sinuous; laesurae coarse, as long as proximal face; sclerine 2  $\mu\text{m}$  thick; outline circular (proximal face); spores 33  $\mu\text{m}$  in size (Fig. S14.117) [Sample: Peru, Accocunca North, El Descanso Fm., Member B, ID-36579/B47-R21. England Finder: P43-1]

Undetermined 5 (equivalent morphotype: *Retitriletes* “uniformis”)

Spore trilete, heteropolar, radially symmetric, reticulate; brochi uniform, fine, less than 1  $\mu\text{m}$  wide, resembling perforate pattern; laesurae linear, irregular, as long as proximal face;

sclerine 2  $\mu\text{m}$  thick; outline triangular-convex (proximal face); spores 25  $\mu\text{m}$  in size (Fig. S14.118) [Sample: Peru, Espinar, ID-39364, Paleo-12549, El Descanso Fm., Member C. England Finder: Y10]

Undetermined 6 (equivalent morphotype: Retitriletes “fungosus”)

Spore apparently trilete, heteropolar, radially symmetric, reticulate; brochi irregular; laesurae and sclerine not well defined; spore looks as fungal spore; outline triangular to circular; spores 55  $\mu\text{m}$  in size (Fig. S14.119) [Sample: Peru, Espinar, ID-39361, Paleo-12548, El Descanso Fm., Member C. England Finder: R31-2]

Undetermined 7 (equivalent morphotype: Perinomonoletes “horrible”)

Spore monolete, heteropolar, bilaterally symmetric; laesurae inconspicuous; sclerine 1  $\mu\text{m}$  thick, surface irregular displaying probably a rugulate pattern (perine vestigial?); outline circular; spores 41  $\mu\text{m}$  length x 30  $\mu\text{m}$  wide (Fig. S14.120) [Sample: Peru, Espinar, ID-39721, Paleo-12601, El Descanso Fm., Member C. England Finder: G10-4]

Undetermined 8 (equivalent morphotype: Rugulatriletes “dirty”)

Spore trilete, heteropolar, radially symmetric, apparently rugulate; rugulae irregular; laesurae thin, inconspicuous; sclerine 1.5  $\mu\text{m}$  thick; outline triangular-concave (proximal face); spores 33  $\mu\text{m}$  in size (Fig. S14.121) [Sample: Peru, Espinar, ID-39364, Paleo-12549, El Descanso Fm., Member C. England Finder: F9]

Undetermined 9 (equivalent morphotype: Foveotriletes “mediocre”)

Spore trilete, heteropolar, radially symmetric, reticulate; homobrochate, brochi ample, lumina wide almost circular ca. 35.  $\mu\text{m}$  in diameter, muri thin less than 1  $\mu\text{m}$  wide, undulating; laesurae inconspicuous, as long as proximal face; sclerine coarse, irregular; outline triangular-convex (proximal face); spores 41  $\mu\text{m}$  in size (Fig. S14.122) [Sample: Peru, Espinar, ID-39726, Paleo-12606, El Descanso Fm., Member C. England Finder: M34-3]

Undetermined 10 (equivalent morphotype: Retimonoletes “serratus”)

Spore monolete, heteropolar, bilaterally symmetric, reticulate; homobrochate, brochi ample, lumina almost circular, muri very thin; laesurae inconspicuous; sclerine coarse, 3  $\mu\text{m}$  thick; outline circular; spores 41  $\mu\text{m}$  in size (Fig. S14.123) [Sample: Peru, Espinar, ID-39726, Paleo-12606, El Descanso Fm., Member C. England Finder: R38-3]

Undetermined 11 (equivalent morphotype: Baculatriletes “magnificus”)

Spore trilete, heteropolar, radially symmetric, baculate; baculae dense, ca. 1  $\mu\text{m}$  height, rounded-head; laesurae masked by ornamentation; sclerine inconspicuous; outline triangular-convex (proximal face); spores 22  $\mu\text{m}$  in size (Fig. S14.124) [Sample: Peru, Espinar, ID-39443, Paleo-12550, El Descanso Fm., Member B. England Finder: Q20-1]

Undetermined 12 (equivalent morphotype: Perinotriletes “reticuloides”)

Spore trilete, heteropolar, radially symmetric, spore covered by thin, irregular and reticulate perine, heterobrochate; laesurae as long as proximal face; sclerine inconspicuous; outline triangular-convex (proximal face); spores 42.5  $\mu\text{m}$  in size (Fig. S14.125) [Sample: Peru, Espinar, ID-39443, Paleo-12550, El Descanso Fm., Member B. England Finder: N10-4]

### **Undetermined palynomorphs and associated structures**

Algae (?)

Undetermined 1. Rounded structure having a wall 2  $\mu\text{m}$  thick, resembling a presence of exine and exhibiting projections baculae-shaped, rounded-head, 8  $\mu\text{m}$  length x 1  $\mu\text{m}$  wide. No apertures visible. Structure circular 75  $\mu\text{m}$  in size (Fig. S14.126) [Sample: Peru, Accocunca North, El Descanso Fm., Member B, ID-36569/B47-R17. England Finder: G33-3]

Undetermined 2. Rounded and irregular structure having a wall less than 1  $\mu\text{m}$  thick, resembling a presence of exine. Apparently three apertures present, folded, slightly protuberant, resembling pores annulate. Structure circular 28  $\mu\text{m}$  in size (Fig. S14.127) [Sample: Peru, Accocunca North, El Descanso Fm., Member B, ID-36590/B47-R19. England Finder: F6-4/G6-2]

## Foraminifera

Microforaminiferal linings d'Orbigny 1826 stat. nov. Cavalier-Smith 2017 (Protozoa, Rhizaria, Rhizopodea). Fragment of shell ca. 41  $\mu\text{m}$  in size, having two globose chambers from a probably spiral structure; chambers ca. 23  $\mu\text{m}$  in diameter (Fig. S14.128) [Sample: Peru, Accocunca North, El Descanso Fm., Member B, ID-36569/B47-R17. England Finder: N10-2]

## Scolecodont

Two small and complete jaws of a fossil Polychaete (Annelidae) ca. 32  $\mu\text{m}$  length x 15  $\mu\text{m}$  wide ea. Jaws globose type, serrate at apical margin, having small acute teeth ea.; sometimes isolated without serrate pattern (Fig. S14.129) [Sample: Peru, Espinar, ID-39703, Paleo-12586, El Descanso Fm., Member B. England Finder: K34]

## Fungal Spores

*Asterina* sp. L veill  (Microthyriaceae, Dothidiales) (Hooghiemstra, 1984)

Fruit body shield-shaped, circular, flattened, psilate, dark brown, 83  $\mu\text{m}$  in diameter, displaying ca. 20 elonged, uniform and radially ordered ascomata around a central ostiole (Fig. S15.130) [Sample: Peru, Accocunca North, El Descanso Fm., Member B, ID-36584/B47-R16. England Finder: N37]

*Microthyrium* sp. aff. *M. ciliatum* Gremmen & De Kam (or *Trichothyrina* sp.)

(Microthyriaceae, Dothidiales) (Hooghiemstra, 1984)

Fruit body shield-shaped, circular, flattened, psilate, yellowish to blackish, 160  $\mu\text{m}$  in diameter, circular, hyaline, displaying ca. 50 elonged, uniform and radially ordered ascomata (hyphae) ca. 82 $\mu\text{m}$  length x 8  $\mu\text{m}$  wide around a central ostiole ca. 24  $\mu\text{m}$  in diameter (Fig. S15.131) [Sample: Peru, Espinar, ID-39361, Paleo-12548, El Descanso Fm., Member C. England Finder: F46-1]

*Neurospora* sp. Shear & B.O. Dodge (Sordariaceae) (Hooghiemstra, 1984)

Ascospores slightly circular, 17  $\mu\text{m}$  in diameter, no apertures visible, ornamented, with more or less parallel ridges longitudinally oriented, (Fig. S15.132) [Sample: Peru, Espinar, ID-39361, Paleo-12548, El Descanso Fm., Member C. England Finder: X44]

*Tetraploa* sp. aff. *T. aristata* Berk. & Broome (Massarinaceae)

Conidia ca 88  $\mu\text{m}$  in total length, divided into 4 sections (columns) with 4 cells ea.; body ca. 28  $\mu\text{m}$  length x 15  $\mu\text{m}$  wide; 2 to 4 septate branches coming from main body, ca. 80  $\mu\text{m}$  ea. composed by 5 up to 6 hyaline cells (Fig. S15.133) [Sample: Peru, Espinar, ID-39443, Paleo-12550, El Descanso Fm., Member B. England Finder: R25]

Undetermined 1. Spore? reddish-yellow, no apertures visible, ornamented, reticulate-shaped, irregular; outline circular, 90  $\mu\text{m}$  in size (Fig. S15.134) [Sample: Peru, Accocunca North, El Descanso Fm., Member B, ID-36579/B47-R21. England Finder: R39]

Undetermined 2. Spore? reddish-dark, apparently having 2 apertures pore-shaped, wall psilate, unstratified, 1  $\mu\text{m}$  thick, outline circular, 15  $\mu\text{m}$  in size (Fig. S15.135) [Sample: Peru, Huanu Huanu, El Descanso Fm., Member C, ID-36592/B47-R13. England Finder: O37-1]

Undetermined 3. Probably fungal spore, reddish, pluricellular ca. 12 cells, resembling polyad condition, no apertures visible, wall psilate, layer unstratified, outline circular, 26  $\mu\text{m}$  in size (Fig. S15.136) [Sample: Peru, Huanu Huanu, El Descanso Fm., Member C, ID-36592/B47-R13. England Finder: U31-4/U32-3]

Undetermined 4. Spore? reddish, irregular structure, without visible apertures, wall psilate, unstratified, thin, 1  $\mu\text{m}$  thick, outline circular irregular, 68  $\mu\text{m}$  in size (Fig. S15.137) [Sample: Peru, Huanu Huanu, El Descanso Fm., Member C, ID-36563/B47-R15. England Finder: O18-1]

Undetermined 5. Probably fungal spore (Sordariaceae?), ascospore foraminate, black, displaying dense and geometrically distributed pits, circular, 8  $\mu\text{m}$  in diameter, protruding, surrounded by persistent thickenings ea., resembling annulus condition; outline ellipsoidal, 120

$\mu\text{m}$  length x  $58 \mu\text{m}$  wide (Fig. S15.138) [Sample: Peru, Espinar, ID-39726, Paleo-12606, El Descanso Fm., Member C. England Finder: U24-1]

Undetermined 6. Spore? reddish, ascopore elongated, unicellular, longitudinally striate, wall ca.  $1.5 \mu\text{m}$  thick, ascopore  $24 \mu\text{m}$  length x  $16 \mu\text{m}$  wide (Fig. S15.139) [Sample: Peru, Espinar, ID-39460, Paleo-12573, El Descanso Fm., Member B. England Finder: M18]

Undetermined 7. Spore? yellowish, ascopore circular, displaying two parts resembling two valves of joined, hyaline, wall thin, less than  $1 \mu\text{m}$  thick, folded, irregular; ascopore  $72 \mu\text{m}$  in size (Fig. S15.140) [Sample: Peru, Espinar, ID-40127, Paleo-12609, El Descanso Fm., Member B. England Finder: K37]

#### Amoebae

*Arcella* sp. Ehrenberg aff. *A. discoides* (Arcellidae, Testacea) (Hooghiemstra, 1984)

Structure circular, umbrella-shaped shell with a hole on its center from where finger-like pseudopods emerge, hyaline, pseudopods absent, wall very thin, outline spheroidal,  $72 \mu\text{m}$  in size (Fig. S15.141) [Sample: Peru, Espinar, ID-40127, Paleo-12609, El Descanso Fm., Member B. England Finder: Y8-4]

#### Diatoms

*Aulacoseira* sp. Thwaites (Coscinodiscophyceae, Aulacoseiraceae)

Structure single, bilaterally symmetric, rectangular (valvar view), probably spheroidal (polar view); granulate, granulae longitudinally oriented;  $40 \mu\text{m}$  length x  $20 \mu\text{m}$  wide (Fig. S15.142) [Sample: Peru, Espinar, ID-40132, Paleo-12621, El Descanso Fm., Member C. England Finder: J6]

*Cocconeis* sp. Ehrenberg (Bacillariophyceae, Cocconeidaceae)

Structure elongated, bilaterally symmetric, displaying a continuous and straight raphe ca.  $72 \mu\text{m}$  length x  $1 \mu\text{m}$  wide, rounded ended; frustulate, pennate, having transapical striae, equidistant between them (valvar view); outline elongated  $80 \mu\text{m}$  length x  $20 \mu\text{m}$  wide (Fig. S15.143) [Sample: Peru, Espinar, ID-40132, Paleo-12621, El Descanso Fm., Member C. England Finder: N47]

*Cyclotella* sp. (Kützing) Brébisson (Mediphyceae, Stephanodiscaceae)

Structure single, radially symmetric, centric, cylindrical, central area  $\frac{1}{2}$  valve face, two shadow lines present, radius uniseriate, outline spheroidal, 33  $\mu\text{m}$  in diameter (Fig. S15. 144)

[Sample: Peru, Espinar, ID-40132, Paleo-12621, El Descanso Fm., Member C. England Finder: O35 & M19]

*Eunotia* sp. Ehrenberg (Bacillariophyceae, Eunotiaceae)

Structure elongated, bilaterally symmetric, probably presence of raphe; valve frustulate, pennate, having transapical striae, equidistant between them (pleural view); outline elongated, 65  $\mu\text{m}$  length x 20  $\mu\text{m}$  wide (Fig. S15. 145) [Sample: Peru, Espinar, ID-40132, Paleo-12621, El Descanso Fm.,

Member C. England Finder: D48]

*Pinnularia* sp. Ehrenberg (Bacillariophyceae, Pinnulariaceae)

Structure elongated, bilaterally symmetric, displaying a continuous and straight raphe ca. 72  $\mu\text{m}$  length x 1  $\mu\text{m}$  wide, rounded ended; frustulate, pennate, having transapical striae, equidistant between them (valvar view); outline elongated 80  $\mu\text{m}$  length x 20  $\mu\text{m}$  wide (Fig. S15. 146)

[Sample: Peru, Espinar, ID-40132, Paleo-12621, El Descanso Fm., Member C. England Finder: LR37]

Undetermined 1 (*Cyclotella* sp.? *Aulacoseira* sp.?) (Mediphyceae, Stephanodiscaceae)

Probably polar view of *Aulacoseira* sp. Structure single, radially symmetric, centric, cylindrical, radius uniseriate, outline spheroidal, 28  $\mu\text{m}$  in diameter (Fig. S15. 147) [Sample: Peru,

Espinar, ID-40132, Paleo-12621, El Descanso Fm., Member C. England Finder: N39]

Undetermined 2 (Bacillariophyceae)

Structure single, bilaterally symmetric, rectangular (valvar view), probably spheroidal (polar view); striate (septate), septae oriented across pervalvar axis, ca. 1.5  $\mu\text{m}$  wide ea.; square fragments ca. 28  $\mu\text{m}$  length x 28  $\mu\text{m}$  wide (Fig. S15. 148) [Sample: Peru, Espinar, ID-39703, Paleo-12586, El

Descanso Fm., Member B. England Finder: U39-1]

Undetermined 3 (*Navicula* sp.? Bory de Saint-Vincent) (Bacillariophyceae, Naviculaceae)

Structure elongated, bilaterally symmetric, boat-shaped, displaying a continuous and straight raphe as long as polar length, rounded ended; pennate, having transapical radiate striae,

striae fine, dense, equidistant between them (valvar view); central area large, continuous, resembling an equatorial ring, outline elongated 88  $\mu\text{m}$  length x 22  $\mu\text{m}$  wide (Fig. S15.149)

[Sample: Peru, Espinar, ID-40132, Paleo-12621, El Descanso Fm., Member C. England Finder: H43 & L47-4]

### Phytoliths

Areaceae type. Structure siliceous, spherical, spinulose, hyaline, ca. 20  $\mu\text{m}$  in size (Fig. S15.150) [Sample: Peru, Espinar, ID-39703, Paleo-12586, El Descanso Fm., Member B. England Finder: MS39]

Poaceae type. Structure siliceous, elongated, faceted, hyaline, 52  $\mu\text{m}$  length x 12  $\mu\text{m}$  wide (Fig. S15.151) [Sample: Peru, Espinar, ID-40132, Paleo-12621, El Descanso Fm., Member C. England Finder: M35-3]

### Acari

#### Undetermined 1 (Arthropoda, Chericerata, Acarida)

Small larvae, hexapoda, having small and inconspicuous chelicera; pedipals threr times as losg as main body; legs as long as body, having six segments, coxa sessile; body triangular-globose 200  $\mu\text{m}$  length x 100  $\mu\text{m}$  wide (Fig. S15.152) [Sample: Peru, Espinar, ID-39364, Paleo-12549, El Descanso Fm., Member C. England Finder: Q10]

#### Undetermined 2 (Arthropoda, Chericerata, Acarida)

Small larvae hexapoda, chelicera and pedipals inconspicuous; two first pairs of legs shorts 1/3 as long as body; distal pair of legs as long body; body rounded, ca. 200  $\mu\text{m}$  length x 95  $\mu\text{m}$  wide (Fig. S15.153) [Sample: Peru, Espinar, ID-39467, Paleo-12580, El Descanso Fm., Member b. England Finder: V41]

#### Undetermined 3 (Arthropoda, Chericerata, Acarida)

Nymphal stage, octopoda, having small and inconspicuous quelicera; legas and pedipals thin, short; body globose-rounded ca. 150  $\mu\text{m}$  length x 85  $\mu\text{m}$  wide (Fig. S15.154) [Sample: Peru, Espinar, ID-39706, Paleo-12589, El Descanso Fm., Member B. England Finder: E14-4]

### *Macrofossil descriptions*

Ninety-nine macrofossil compressions and impressions of leaves and fruits were collected from eight localities. From those, 43 samples were described and assigned to a morphotype, 33 were collected from the Member B and 10 from the Member C (**Error! Reference source not found.**). The remaining 23 samples were too fragmented so they could not be described and assigned to a morphotype. Thirteen silica permineralizations of wood were collected from 7 localities, many of them were found in pastures or the edges of small streams. From those 13 samples, 7 were assigned to a morphotype. All the wood localities belonged to the Member B (**Error! Reference source not found.**).

#### **Description of morphotypes from Member B**

Morphotype DSB1

Morphotype: DSB1 (Fig. S16)

Taxonomic name: Tribe Ingeae

Systematic affinity. Order Fabales Bromhead; Family Leguminosae Jussieu; Subfamily Caesalpinioideae DC; Clade: Mimosoid *sensu* LPWG, 2017; Tribe Ingeae *sensu* Lewis and Rico, 2005; Genus and species *incertae sedis*

Morphotype exemplar. STRI-MUSM 39442, comprising a hand specimen and three sections in TS, TLS and RLS.

Locality exemplar. Ituruta Sector, Colpamayo Community, Pichigua District, limit between Canas and Espinar Provinces, Cusco Department, Peru. Locality-ID:110044. 14°37'42.96"S 71°21'53.64"W (WGS84 18N) at 3956 m above sea level.

Other specimens studied. STRI-MUSM 41477, Locality-ID: 110072.

Stratigraphic position and age. Upper Member B, El Descanso Formation, Descanso-Yauri Basin. The age of the locality is late Miocene, between  $12.07 \pm 0.7$  Ma (igneous zircon U-Pb dating) and  $9.1 \pm 0.7$  Ma (Kar et al., 2016).

Repository. Museum of Natural History of the Universidad Nacional Mayor de San Marcos Lima, Peru.

Description. Growth ring boundaries indistinct; vessels diffuse porous, 65% solitary and 32% in short radial multiples of 2–3(–4); solitary vessel outline is oval; perforation plates simple; intervessel pits alternate, and small (mean = 5.5; SD = 0.8; n = 25; range 4–7 $\mu$ m); vessel-parenchyma pits with distinct borders, similar in size and shape to intervessel pits; mean tangential vessel diameter is 169  $\mu$ m (SD = 25.3; n = 55; range 120–230); mean vessel density is 4.8 mm<sup>-2</sup> (SD = 1.5; n = 38; range 2–9); mean vessel length is 178.7  $\mu$ m (SD = 32.4; n = 7; range 133–241); tyloses are present but rare; vascular tracheids were not observed. Fibers are non-septate and thin to thick walled; apotracheal axial parenchyma is diffuse; paratracheal axial parenchyma is abundant vasicentric (70%) and occasionally confluent (30%); when confluent 2–3(–4) vessels are linked; axial parenchyma strands are typically 2 cells high, but sometimes up to 4 cells high. Rays are uniseriate and homocellular; ray height measured in average number of cells is 13 (SD = 6.8; n = 9; 4–23 cells). There are between 4–10 rays per mm (SD = 1.77; n = 17). Prismatic crystals are frequently found in chambered fibers and axial parenchyma cells that form chains of more than 11 chambers.

IAWA features present. 2, 5, 13, 22, 25, 30, 42, 46, 52, 66, 69, 76, 79, 83, 91, 96, 104, 115, 142

Remarks. The fossil morphotype most likely belongs to the family Fabaceae based on the combination of diffuse porous vessel arrangement, vessels that are solitary and grouped in

clusters, simple perforation plates, alternate intervessel pit arrangement, vessels-ray parenchyma pits similar to intervessel pits, homocellular and uniseriate rays, paratracheal axial parenchyma and diffuse apotracheal parenchyma (Wheeler and Baas, 1992). Within Fabaceae this fossil morphotype most likely belongs to the Mimosoid clade due to the presence of indistinct growth rings, diffuse porous wood, diffuse parenchyma, vasicentric and sometimes confluent, paratracheal parenchyma, non-storied structures, axial parenchyma strands are 2 cells high, rays are homocellular, uniseriate and have an average height of 13 cells, and prismatic crystals are frequently found in chambered fibers (Metcalf and Chalk, 1950; Baretta-Kuipers, 1981; Wheeler and Baas, 1992; Evans et al., 2006). Within the mimosoid clade and following Evans et al. (24) we used the combination of non-septate fibers, not banded axial parenchyma, uniseriate rays, and a Neotropical distribution to reduce our search and compare the fossil morphotype with members of the Tribe Mimosae: *Dicrostachys* group, and *Dinizia* group, and the Tribe Ingeae: *Abarema* alliance, *Chloroleucon* alliance, *Inga* alliance, *Pithecellobium* group, *Samanea* alliance, *Enterolobium* and some species of *Acacia*. When comparing this fossil morphotype with the mentioned groups of the Tribe Mimosae, we found that unlike the fossil, the *Dinizia* group has lozenge or winged aliform axial parenchyma (*Dinizia* the only genus of the group, has been recently removed from the mimosoid clade; LPWG, (Legume Phylogeny Working Group, 2017); and the *Dicrostachys* group has vessels that are more frequent and have smaller diameter, and the axial parenchyma is aliform or unilateral. The wood anatomy of the *Acacia* species listed by Evans et al. (2006) show these species also have vessels that are more frequent and have a smaller diameter. The comparison of the fossil morphotype with the Tribe Ingeae showed similarities with various members of the groups *Pithecellobium*, and the *Abarema* and *Inga* alliances. Given that the phylogenetic relationships between these groups and alliances lack of

resolution and there is an overlap in the wood anatomy some of the taxa, we proposed a taxonomic affinity of the fossil morphotype with the entire Tribe Ingeae. In order to perform the paleoclimatic analysis we only included the taxa present in the selected region around the CAP: *Abarema*, *Albizia*, *Calliandra*, *Cedrelinga*, *Cojoba*, *Enterolobium*, *Hydrochorea*, *Inga*, *Pithecellobium*, *Samanea*, *Zapoteca* and *Zygia*.

#### Morphotype DSB2

Morphotype number: DSB2 (Fig. S17)

Taxonomic name: *Andiroxylon sp.*

Systematic affinity. Order Fabales Bromhead, 1838; Family Leguminosae Jussieu; Subfamily Papilionoideae DC; Genus *Andiroxylon* Müller-Stoll & Mädal; species *incertae sedis*

Morphotype exemplar. STRI-MUSM 21147, comprising a hand specimen and three sections in TS, TLS and RLS.

Locality exemplar. San Miguel Community, Pichigua District, Espinar Province, Cusco Department, Peru. Locality-ID:610007. 14°40'46.80"S 71°18'38.10"W (WGS84 18N) at 4036 m above sea level.

Stratigraphic position and age. Upper Member B, El Descanso Formation, Descanso-Yauri Basin. The age of the locality is late Miocene, slightly younger than 10.03±0.2 Ma (igneous zircon U-Pb dating; Fig. S18)

Repository. Museum of Natural History of the Universidad Nacional Mayor de San Marcos Lima, Peru.

Description. Growth ring boundaries indistinct; vessels diffuse porous, 70% solitary and 27% in short radial multiples of 2–3(–4); and 3% are un clusters; solitary vessel outline is oval; perforation plates are simple; intervessel pits are alternate, and have a small to medium size (mean = 6.35; SD = 0.9; n = 19; range 5–8 $\mu$ m); vessel-parenchyma pits with distinct borders, similar in size and shape to intervessel pits; mean tangential vessel diameter is 273  $\mu$ m (SD = 53.3; n = 32; range 159–395; the sample is slightly compressed tangentially so the measurements were taken in the tangential and radial axis to reduce the noise); mean vessel density is 5.3 mm<sup>-2</sup> (SD = 1.9; n = 162; range 2–8); mean vessel length is 254.9  $\mu$ m (SD = 23.2; n = 37; range 218–313); vascular tracheids were not observed. Fibers are thin to thick walled; paratracheal axial parenchyma is confluent to banded, parenchyma bands typically of (6–) 8–10 (–14) cells; numerous vessels are linked in the bands; axial parenchyma strands vary from 3–5 cells high, but sometimes up to 7 cells high. Rays are 2–3 (–4) cells wide; the body ray cells are procumbent with one row of square marginal cells; ray height measured in average number of cells is 8 (SD = 1.1; n = 25; 6–10 cells). There is an average of 12 rays per mm (SD = 1.2; n = 8; range 10–13). All rays and vessel elements are storied.

IAWA features present. 2, 5, 13, 22, 25, 30, 43, 46, 47v, 52, 69, 83, 85, 92, 93v, 97, 104, 115, 118, 120

Remarks. The fossil morphotype most likely belongs to the family Fabaceae based on the combination of diffuse porous vessel arrangement, vessels that are solitary and grouped in clusters, simple perforation plates, alternate intervessel pit arrangement, vessels-ray parenchyma pits similar to intervessel pits, homocellular and uniseriate rays, paratracheal axial parenchyma (Metcalf and Chalk, 1950; Baretta-Kuipers, 1981; Wheeler and Baas, 1992). Within Fabaceae, the presence of storied rays and vessels, non-septate fibers and abundant paratracheal

parenchyma in the fossil, suggest a closer affinity with members of the subfamily Papilionoideae (Baretta-Kuipers, 1981; Wheeler and Baas, 1992). Other characters like the presence of diffuse porous wood, large vessels which are solitary or in radial clusters; confluent parenchyma forming thick tangential bands; short and multiseriate rays are, suggest affinities with the fossil genus *Andiroxylon* (Müller-Stoll and Mädler, 1967; Jud and Dunham, 2017) and also with the extant genera *Andira* (Pennington, 2003) and *Hymenolobium* (Gasson, 2000). In order to perform the paleoclimatic analysis we included *Hymenolobium* and *Andira*.

Tree height estimation. Based on the completeness of the sample (STRI-MUSM 21147) tree height was estimated using the diameter of the log (Fig. S17A). The sample has 75.4 cm of diameter and 614 cm of its length are exposed. Based on the tapering from the base to the top of the log we assumed that the log corresponded to the base of the tree. Using linear regression models that account for the allometric relation between stem diameter and tree –height in modern trees, we estimated the approximate height of this fossil sample (Niklas, 1994; Feldpausch et al., 2012). Four different regression models were used for the calculation, one that uses a global dataset (Niklas, 1994), while the other three used large tropical datasets from: west Amazonia, tropical South America and the pantropical region (Feldpausch et al., 2012). Tree-height estimations for this sample range between 29.8 to 34.6 m, depending on the regression model used.

Morphotype DSB3

Morphotype number: DSB3 (Fig. S19)

Taxonomic name: *Anacardioxylon* sp.

Systematic affinity. Order: Sapindales; Family Anacardiaceae R. Br.; Subfamily Anacardioideae Link; Genus *Anacardioxylon* Felix; species *incertae sedis*

Morphotype exemplar. STRI-MUSM 36598, comprising a hand specimen and three sections in TS, TLS and RLS.

Locality exemplar. San Genaro Community, Pichigua District, Espinar Province, Cusco Department, Peru. Locality-ID: 430160. 14°44'39.12"S 71°18'46.08"W (WGS84 18N) at 4053 m above sea level.

Stratigraphic position and age. Upper Member B, El Descanso Formation, Descanso-Yauri Basin. The age of the locality is late Miocene, approximately 9.1±0.7 Ma (igneous zircon U-Pb dating from San Genaro locality; 2)

Repository. Museum of Natural History of the Universidad Nacional Mayor de San Marcos Lima, Peru.

Description. Growth ring boundaries are distinct; wood is semi-ring-porous to diffuse porous; vessels in radial multiples of 4 or more are common (50%); vessel in clusters are also common (32%); and few solitary vessels (18%); perforation plates are simple; intervessel pits are alternate, and have medium size (mean = 8.36; SD = 0.9; n = 14; range 7–10µm); vessel–parenchyma pits with much reduced borders to apparently simple; mean tangential vessel diameter is 80.1 µm (SD = 48.8; n = 106; range 10–195); mean vessel density is 27 mm<sup>-2</sup> (SD = 5.8; n = 5; range 19–34); mean vessel length is 205.1 µm (SD = 42.2; n = 12; range 150–282); tyloses are present but rare; vascular tracheids might be present. Fibers are thin to thick walled; apotracheal axial parenchyma is sparse or in patches; paratracheal axial parenchyma is scanty. Rays are (3–) 4 (–5) cells wide; and are heterocellular with body ray cells procumbent and one row of square marginal cells; weakly differentiated sheath cells; ray height measured in average

number of cells is 20 (SD = 4.4; n = 16; 11–28 cells). There is an average of 10 rays per mm (SD = 1.4; n = 13; range 7–11). Prismatic crystals are present in marginal ray cells but infrequent.

IAWA features present. 2, 4, 10, 11v, 13, 22, 26, 31, 40v, 41, 42v, 48, 52, 69, 76, 98, 106, 115

Remarks. The combination of semi-ring-porous wood, with vessel in radial multiples of 4, clusters or solitary, alternate intervessel pits, and vessel– parenchyma pits with much reduced borders to apparently simple and scanty paratracheal parenchyma, present in this fossil morphotype, can be also be found in members of the families Araliaceae and Anacardiaceae (InsideWood 2004-onwards). Araliaceae, however, differs from the fossil morphotype in the vessel length, which in the fossil is in average 205  $\mu\text{m}$  (range 150–282), while in Araliaceae is 1050  $\mu\text{m}$  (range 332–1719; Oskolski, 1996). The fossil also lacks helical thickenings and radial canals, characters present in most Araliaceae. In particular the lack of scalariform perforation plates and the presence of vascular tracheids, excludes Neotropical Araliaceae from the comparison (Oskolski, 1996). Anacardiaceae shares with the fossil the characters above in addition to short vessel elements, vasicentric tracheids, simple perforation plates, sparse axial parenchyma, multicellular and heterocellular rays and weakly differentiated sheath cells, and prismatic crystal in marginal ray cells (Terrazas Salgado, 1994). These characters are also consistent with the subfamily Anacardioideae (Terrazas Salgado, 1994; Pell et al., 2011). The diagnosis for the fossil genus *Anacardioxylon* matches the character of the fossil, however, further comparisons are needed to provide a species name.

Interestingly, this sample had preserved dry-wood termite coprolites (Fig. S19I). These structures have been characterized in the past (Labandeira et al., 1997; Garcia Massini and Pujana, 2013; Jud and Dunham, 2017).

In order to perform the paleoclimatic analysis we included all the member of the subfamily Anacardioideae that were present around the CAP: *Anacardium*, *Astronium*, *Camptosperma*, *Campylopetalum*, *Cardenasiodendron*, *Haplorhus*, *Loxopterygium*, *Lithrea*, *Mauria*, *Myracrodruon*, *Ochoterena*, *Orthopterygium*, *Schinopsis*, *Schinus*, *Thyrsodium* and *Toxicodendron*.

Morphotype DSB4

Morphotype number: DSB4 (Fig. S20)

Taxonomic name: Mimosoid

Systematic affinity. Order Fabales Bromhead, 1838; Family Leguminosae Jussieu, 1789; Subfamily Caesalpinioideae DC; Clade Mimosoid; Genus and species: *incertae sedis*

Morphotype exemplar. STRI-MUSM 44454, comprising a hand specimen and three sections in TS, TLS and RLS.

Locality exemplar. Ituruta Sector, Colpamayo Community, Pichigua District, limit between Canas and Espinar Provinces, Cusco Department, Peru. STRI-locality-ID:110083.

14°37'11.71"S 71°22'14.74"W (WGS84 18N) at 4045 m above sea level.

Other specimens studied. STRI-MUSM 39396 (Locality-ID 110042); STRI-MUSM 44451 (Locality-ID 110081); STRI-MUSM 44452 (Locality-ID 110082); STRI-MUSM 41422 (Locality-ID 110066)

Stratigraphic position and age. Upper Member B, El Descanso Formation, Descanso-Yauri Basin. The age of the locality is late Miocene, between  $12.07 \pm 0.7$  Ma (igneous zircon U-Pb dating) and  $9.1 \pm 0.7$  Ma (2).

Repository. Museum of Natural History of the Universidad Nacional Mayor de San Marcos Lima, Peru.

Description. Growth ring boundaries indistinct; vessels diffuse porous, 71% solitary and 29% in short radial multiples of 2–3; solitary vessel outline is oval; perforation plates simple; intervessel pits alternate, and small (mean = 4.6; SD = 0.57; n = 33; range 3.5–5.7  $\mu\text{m}$ ); vessel-parenchyma pits with distinct borders, similar in size and shape to intervessel pits; mean tangential vessel diameter is 192  $\mu\text{m}$  (SD = 24.5; n = 27; range 143–250); mean vessel density is 6.7  $\text{mm}^{-2}$  (SD = 1.9; n = 23; range 3–10); mean vessel length is 254.6  $\mu\text{m}$  (SD = 48.6; n = 5; range 198–321); tyloses are present. Fibers are thin to thick walled, and possibly non-septate; apotracheal axial parenchyma is diffuse; paratracheal axial parenchyma is vasicentric and narrow, with only a 1 to 3 layers of parenchyma cells around the vessel or vessel multiple; axial parenchyma strands are typically 5 to 8 cells high. Rays have 1 to 3 cells width and are homocellular; ray height measured in average number of cells is 20 (SD = 4.5; n = 10; 12–25 cells). There are between 6–10 rays per mm (SD = 1.47; n = 6). Prismatic crystals are frequently found in chambered axial parenchyma cells.

IAWA features present. 2, 5, 13, 22, 25, 30, 42, 47, 52, 69, 79, 83, 93, 97, 104, 115, 142, 143

Remarks. The fossil morphotype most likely belongs to the family Fabaceae based on the combination of diffuse porous vessel arrangement, vessels that are solitary and grouped in clusters, simple perforation plates, alternate intervessel pit arrangement, vessels-ray parenchyma

pits similar to intervessel pits, homocellular and uniseriate rays, paratracheal axial parenchyma and diffuse apotracheal parenchyma (Metcalf and Chalk, 1950; Baretta-Kuipers, 1981; Wheeler and Baas, 1992). Within Fabaceae this fossil morphotype most likely belongs to the Mimosoid clade due to the presence of indistinct growth rings, diffuse porous wood, diffuse parenchyma, vasicentric and sometimes confluent, paratracheal parenchyma, non-storied structures, rays are homocellular, uniseriate and have an average height of 20 cells, and prismatic crystals are frequently found in chambered parenchyma and fibers (Metcalf and Chalk, 1950; Baretta-Kuipers, 1981; Wheeler and Baas, 1992; Evans et al., 2006). Within the mimosoid clade we were not able to conclude a deeper affinity given that we were not certain about the presence of non-septate fiber.

Morphotype DSB5

Morphotype number: DSB5 (Fig. S21)

Taxonomic name: Arecaceae

Systematic affinity. Order Arecales Bromhead. Family Arecaceae Bercht. & J. Presl. Genus and species: *incertae sedis*

Morphotype exemplar. STRI-MUSM 39439 (Locality\_ID 430175)

Other samples studied. STRI-MUSM 41310, 41423, 41424, 41474, 41475 (Locality\_ID 110066)

Stratigraphic position and age. Upper Member B, El Descanso Formation, Descanso-Yauri Basin. The age of these localities is late Miocene, between  $12.07 \pm 0.7$  Ma (igneous zircon U-Pb dating) and  $9.1 \pm 0.7$  Ma (2).

Repository. Museum of Natural History of the Universidad Nacional Mayor de San Marcos  
Lima, Peru.

Description. Leaf fragments are plicate. Leaf size unknown. Two subsets of parallelodromous and closely spaced veins. These subsets are recognized by their width, and independently of their order the spacing ranges from 0.32 mm to 0.9 mm. The second subset appears from 1 time in between a pair of first subsets. The first subset constitutes the majority of veins. Veins that cross the subsets at oblique angles.

Remarks. Read and Hickey (1972) provided a list of characters to identify palm leaves from fossil fragments. Leaves from the DSB11 morphotype present some of these characters like fragments of plicate leaves with two subsets of parallelodromous veins and fine perpendicular veins that cross the subsets at oblique angles. However, given that the specimens found were only small fragments the observation of some the other characters (like the presence of a uniform midvein bounded on either side by two orders of parallel veins) necessary to identify with certainty palm leaves is not possible.

Description of morphotypes from Member C

Morphotype DSC1

Morphotype number: DSC1 (Fig. S22A)

Taxonomic name: *Ribes sp.*

Systematic affinity. Order Saxifragales Bercht. & J. Presl. Family Grossulariaceae DC.

Genus: *Ribes* L. Species: *incertae sedis*

Morphotype exemplar. STRI-MUSM 44870 (Locality\_ID 430156)

Other samples studied. STRI-MUSM 44873 (Locality\_ID 430156)

Stratigraphic position and age. Member C, El Descanso Formation, Descanso-Yauri Basin.

The age of this locality is Pliocene, between  $4.8 \pm 1.1$  Ma and  $3.9 \pm 0.1$  Ma (detrital zircon U-Pb dating; S2).

Repository. Museum of Natural History of the Universidad Nacional Mayor de San Marcos Lima, Peru.

Description. Leaf attachment petiolate; blade attachment marginal; laminar size notophyll; length is approximately 3.5 cm and width is 4.9 cm; laminar L:W ratio is 0.7:1; laminar shape is ovate; leaf basally and medially symmetrical; leaf palmately lobed; margin crenate. Lobe apices have an obtuse angle and the shape is straight. Base angle is reflex and shape is cordate. Primary vein framework palinactinodromous. Number of basal veins is 3. Agrophic veins simple. Major secondaries vein framework is craspedodromous and arising at low angles. Major secondary vein spacing gradually increasing proximally, smoothly increasing proximally; attachment decurrent. Interior secondaries present. Minor secondary course craspedodromous. Marginal secondary present. Intersecondary veins present, with a proximal course parallel to major secondaries, a length <50% of subjacent secondary, a distal course basiflexed, not joining subjacent secondary at right angles, occurring at < 1 per intercostal area. Intercostal tertiary veins irregular reticulated. Epimedial tertiaries reticulate. Quaternary vein fabric irregular reticulated. Areolation moderately developed. Freely ending veinlets possibly with one or two dichotomous branches. Marginal veins looped. Tooth spacing irregular, with two orders of teeth; 6 teeth/cm;

sinus shape angular. Tooth shapes cv/cv and st/st. Principal vein present; terminates on proximal flank of tooth; accessory vein looped, rosoid teeth type.

Remarks. Based on the leaf characteristics of extant *Ribes* summarized by Hermsen (2005) we concluded that the fossil morphotype DSC3 has taxonomic affinities with this extant genus because they share the presence of notophyll, crenate, tri-lobed leaves with cordate bases, palinactinodromous venation, secondary veins craspedodromous, rosoid teeth with a cv/cv shape.

Morphotype DSC2

Morphotype number: DSC2 (Fig. S22B)

Taxonomic name: *Berberis* sp.

Systematic affinity. Order Ranunculales Juss. ex Bercht. & J. Presl. Family Berberidaceae Juss. Genus: *Berberis* L. Species: *incertae sedis*.

Morphotype exemplar. STRI-MUSM 41428 (Locality\_ID 490011)

The age of this locality is Pliocene, between  $4.8 \pm 1.1$  Ma and  $3.9 \pm 0.1$  Ma (detrital zircon U-Pb dating; S2).

Repository. Museum of Natural History of the Universidad Nacional Mayor de San Marcos Lima, Peru.

Description. Blade attachment marginal. Laminar size microphyll with a length 2.59 cm and a width of 1.7 cm. Laminar L:W ratio is 1.5:1. Laminar shape elliptic to obovate. Leaf basally and medially symmetrical. Margin unlobed and dentate. Apex angle obtuse and shape convex. Base angle acute and shape concave. Primary vein framework pinnate. Number of basal veins is one. Major secondary vein framework are festooned semicraspedodromous, this principal lateral veins form angular arcs. Major secondary vein spacing decreasing proximally; major secondary angle to midvein smoothly increasing proximally; major secondary attachment to midvein is

excurrent. Intercostal tertiary veins irregular reticulated; intercostal tertiary vein angle variability is inconsistent; epimedial tertiaries reticulate. Exterior tertiary course terminating at the margin. Tooth spacing irregular and developed from the half towards the apex of the leaf; one order of teeth; 2 teeth/cm; sinus shape rounded; tooth shapes st/st; principal vein present; terminates on proximal flank of tooth or at the apex of the tooth.

Remarks. The morphotype was described based on one specimen. *Berberis* is the only genus of the family Berberidaceae distributed in South America. Based on the leaf characteristics of extant *Berberis* summarized by Ramírez and Cevallos-Ferriz (2000) we concluded that the fossil morphotype DSC2 has taxonomic affinities with this extant genus because they share the presence of microphyll, dentate elliptic leaves, pinnate primary venation and festooned semicraspedodromous secondary veins with angular archs, teeth with a st/st shape. Morphotype DSC2 is very similar to *Berberis saxicola* Lechl. a species that grows around the CAP region.

Morphotype DSC3

Morphotype number: DSC3 (Fig. S22C)

Taxonomic name: *Berberis* sp.

Systematic affinity. Order Ranunculales Juss. ex Bercht. & J. Presl. Family Berberidaceae Juss. Genus *Berberis* L. Species: *incertae sedis*.

Morphotype exemplar. STRI-MUSM 44871 (Locality\_ID 430156)

Other samples studied. STRI-MUSM 44872 and 44875 (Locality\_ID 430156) and STRI-MUSM 39380 (Locality\_ID 490011)

The age of this locality is Pliocene, between  $4.8 \pm 1.1$  Ma and  $3.9 \pm 0.1$  Ma (detrital zircon U-Pb dating; S2).

Repository. Museum of Natural History of the Universidad Nacional Mayor de San Marcos  
Lima, Peru.

Description. Blade attachment marginal. Lamina size nanophyll. Lamina L:W ratio 2.2:1. Lamina shape obovate. Leaf basally and medially symmetrical. Tridentate. Apex angle acute and shape straight. Base angle acute and shape decurrent. Primary vein framework pinnate. Number of basal vein 1. Major secondary vein framework festooned semicraspedodromous; major secondaries start branching at 1/3 of the leaf (from the base). Higher veins are not observed. Tooth spacing irregular, with one order of teeth; only three teeth are present at the apex of the leaf. Principal vein is probably present and terminating at the apex of the tooth.

Remarks. As mentioned above, *Berberis* is the only genus of the family Berberidaceae distributed in South America. Around 169 species of *Berberis* are found in South America (Adhikari et al., 2015), so there is variability in the leaf architecture of this genus. This morphotype is different from DSC2 (also related to *Berberis*) because of its smaller lamina size and obovate shape, and number of teeth. Based on the leaf characteristics of extant *Berberis* summarized by Ramírez and Cevallos-Ferriz (2000) we concluded that the fossil morphotype DSC4 has taxonomic affinities with this extant genus *Berberis* because they share the presence of nanophyll, dentate obovate leaves, with pinnate primary venation and festooned semicraspedodromous secondary veins with angular arches; 3 teeth are only present and are located in the apex of the leaf and they have a st/st shape. Morphotype DSC4 is very similar to *Berberis humbertiana* J.F. Macbr. a species that grows near the CAP region.

Morphotype DSC4

Morphotype number: DSC4 (Fig. S22D)

Taxonomic name: *Polylepis* sp.

Systematic affinity. Order Rosales Bercht. & J. Presl. Family Rosaceae Juss. Genus:

*Polylepis* L. Species: *incertae sedis*.

Morphotype exemplar. STRI-MUSM 44894 (Locality\_ID 430156)

Other samples studied. STRI-MUSM 44895–908 (Locality\_ID: 430156) and STRI-MUSM 44909–916 (Locality\_ID: 110037)

The age of this locality is Pliocene, between  $4.8 \pm 1.1$  Ma and  $3.9 \pm 0.1$  Ma (detrital zircon U-Pb dating; S2).

Repository. Museum of Natural History of the Universidad Nacional Mayor de San Marcos Lima, Peru.

Description. Leaf (or leaflet, see comments) attachment is petiolate. Blade attachment marginal. Laminar size nanophyll with an average length of 8.9 mm and width 3.82 mm. Laminar L:W ratio is 2.3:1. Laminar shape obovate. Leaf basally and medially asymmetrical. Margin unlobed and crenate to dentate. Apex angle obtuse and shape emarginated occasionally mucronate. Base angle acute and shape straight. Primary vein framework pinnate; veins separated from  $30-40^\circ$ . Number of basal veins is 2. Major secondaries vein framework festooned semicraspedodromous and sometimes semicraspedodromous. Major secondary vein spacing decreasing proximally, with more or less a regular secondary angle; attachment basally decurrent and excurrent towards the apex. Marginal secondary present, intercostal tertiary veins opposite percurrent obtuse to midvein. Vein angle decreasing exmedially. Quaternary vein fabric alternate percurrent. Areolation good development. Freely ending vein lets mostly one branched, with not visible termination. Margin dentate to crenate. Tooth spacing irregular, with one orders of teeth; sinus shape angular. Tooth shapes cv/st. Principal vein present and terminates on sinus; accessory vein looped.

Remarks. Based on the leaf characteristics of extant *Polylepis* summarized by Simpson (1979) we concluded that the fossil morphotype DSC1 has taxonomic affinities with this extant genus because they share the presence of nanophyll leaflets, crenate to dentate, leaves, with asymmetric bases, emarginated or straight and sometimes mucronate apices, pinnate primary venation and festooned semicraspedodromous and sometimes craspedodromous secondary veins, teeth with a cv/st shape.

Morphotype DSC5

Morphotype number: DSC5 (Fig. S22E)

Taxonomic name. *Polystichum* sp.

Systematic affinity. Order Polypodiales Link. Family Dryopteridaceae Herter. Genus: *Polystichum* Roth. Species: *incertae sedis*.

Morphotype exemplar. STRI-MUSM 43483 (Locality\_ID 430156)

The age of this locality is Pliocene, between  $4.8 \pm 1.1$  Ma and  $3.9 \pm 0.1$  Ma (detrital zircon U-Pb dating; S2).

Repository. Museum of Natural History of the Universidad Nacional Mayor de San Marcos Lima, Peru.

Description. Detached pinnate fragment, segments (pinnae or pinnulae) alternate, sterile. Raquis grooved slightly geniculate at the alternate insertion of segments attached at acute angles. Segments (pinnulae) oblong, base cuneate with an acroscopic deltate auricle, segment-apex acuminate-acute, margin acroscopically slightly serrate and entire basiscopically, venation free, 1–2 furcate between the midrib and the margin of the lamina. (Aliaga et al., *in prep*).

Morphotype DSC6

Morphotype number: DSC6 (Fig. S22F)

Taxonomic name: Juncaceae

Systematic affinity. Order Poales Small. Family Poaceae Durande. Genus and species:  
*incertae sedis*.

Morphotype exemplar. STRI-MUSM 41411 (Locality\_ID: 110060)

The age of this locality is Pliocene, between  $4.8 \pm 1.1$  Ma and  $3.9 \pm 0.1$  Ma (detrital zircon U-Pb dating; S2).

Repository. Museum of Natural History of the Universidad Nacional Mayor de San Marcos Lima, Peru.

Description. Inflorescence composed from at least four fruits (visible in the front), but possibly six or seven (number of pedicels visible). The fruits are possibly developed of an umbel inflorescence. The pedicels have an average length of 5.4 mm. The individual fruits have an average length of 3.57 mm and width of 1.2 mm. The fruits are possibly capsules, which are ovoid in shape and surrounded by tepals that are slightly shorter than the length of the fruit, around 3.15 mm. Three tepals are visible in each fruit, so there are possibly 6 in total, they have an acuminate apex. Two or three bracts are visible in the front of each fruit and have an approximate length of 1.2 mm.

Remarks. Neotropical Juncaceae have variable inflorescence types, within which racemose types like umbels are found in some groups. Fruits of neotropical Juncaceae are capsules of 1.5 to 5 mm in length, that can be ovoid and with a prominent beak (Balslev, 1996) like those present in the DSC13 morphotype. The presence of sepal-like structures and bracts around the pedicellate fruits, is also a characteristic of Juncaceae fruits. In addition, the leaf-like structure

and possible stem associated to the DSC13 infructescence, with parallelodromous venation, can support the similarities with Juncaceae.

Morphotype DSC7

Morphotype number: DSC7 (Fig. S22G)

Taxonomic name. *Equisetum* sp.

Systematic affinity. Order Equisetales DC. ex Bercht. & J. Presl. Family Equisetaceae

Michx. ex DC. Genus: *Equisetum* L. Species: *incertae sedis*

Morphotype exemplar: STRI-MUSM 39326 (Locality\_ID 110040)

Other samples studied: STRI-MUSM 39437 (Locality\_ID 490011)

The age of this locality is Pliocene, between  $4.8 \pm 1.1$  Ma and  $3.9 \pm 0.1$  Ma (detrital zircon U-Pb dating; Kar et al., 2016).

Repository. Museum of Natural History of the Universidad Nacional Mayor de San Marcos Lima, Peru.

Description. Aerial axes grooved and ridged longitudinally; axes are approximately 4.5 mm in diameter in one specimen and 11 mm in the second specimen, internodal lengths are short and vary between 2 to 5 mm in one specimen and around 6 mm in the other specimen. Scars of branches are whorled and seen in at some nodes. Leaves are only seen in one specimen, are borne at the nodes, are around 3 mm long, have attenuate apices, at least 14 were counted in one side of the specimen, are fused into a collar; the collar is approximately 2 mm long.

Remarks. *Equisetum* is plant with a particular unique morphology. The morphotype DSC12 share with the extant genus *Equisetum* the presence of stems longitudinally ribbed, and leaves

that are whorled and laterally fused at the base and free at the apexes, forming a sheath-like structure at the nodes.

### *Paleoclimatic analyses*

The original fossil pollen dataset consisted of 66 samples (50 from Member B and 16 from Member C) described in terms of 66 taxa (23 and 43 identified at family and genus level, respectively; Table S4 and Table S5), 48 of them represented in the modern pollen dataset. By applying the criteria for selecting samples for the analyses, the fossil palynology dataset was reduced to 38 samples that contained 47 taxa (34 and 4 samples from members B and C, respectively; Fig. S23). Thus, the modern palynology library contained the environmental distribution of 47 taxa (Data S1), which served as the basis for making estimations of precipitation and temperature for 38 samples (Table S6).

The four and seven macrofossil morphotypes found in Members B and C were represented by seven and 29 distributions of modern taxa (Table S7). Thus, the modern vegetation library was composed of 36 taxa (Data S2) that served as the basis for estimating the environmental space of the two analyzed stratigraphic members (Fig. S18). Macrofossil estimates yielded a median elevation of 260 m for member B (interquartile range between 50 and 470 m), and 3600 m for member C (interquartile range between 3500 and 3950 m). Macrofossil-based precipitation estimates were 1720 mm for member B and 927 mm for member C (interquartile range between 1413 and 2062 mm for Member B, and 711 and 1148 mm for Member C).

Correction based on global temperatures resulted in average displacements of the elevation estimates by ~650 and 440 m for members B and C, respectively (Fig. S24). For Member B, corrected modal elevation was 2300 and 900 m based on pollen and macrofossil evidence, respectively (median pollen-based estimate 2580 and IQR between 1900 and 3300 m; median

macrofossil-based estimate 910 and IQR between 700 and 1120 m). Pollen and macrofossil estimation of elevation for Member C were more consistent reaching modes of 3980 and 4030 m, respectively (median pollen-based estimate 3360 and IQR between 3580 and 3840 m; median macrofossil-based estimate 3990 and IQR between 3580 and 4380 m) (Fig. S25).

Sensitivity of the estimates  $\Delta y/\Delta x$  to the mixture proportion ( $\lambda_2$  and  $\lambda_1$ ) was very high for the mixture of elevation for member B (Fig. S26A), indicating lack of convergence of pollen and macrofossil estimates (Fig. S26). Differently, elevation estimates for Member B and Modern and precipitation in all cases were robust, showing low variability along the mixture proportion (Fig. S26). Mixtures of macrofossils and pollen estimates for precipitation in all cases and for elevation of member C and Modern declined monotonically as a function of  $\lambda_1$  (lower estimates as the proportion of pollen increased, Fig. S26), and therefore the final estimate was based on mixing the PDFs using  $\lambda_2 = \lambda_1 = 0.5$  (Fig. S27G,H). Given their high sensitivity to the mixture proportion, elevation estimates for Member B showed an increasing trend as  $\lambda_1$  increased with an inflection point at  $\lambda_1 = 0.615$  (Fig. S26A), and thus it was considered the optimum value (Fig. S27G). The final estimates of environmental space showed a trend that progressed in time towards ascending elevation and decreasing precipitation (Fig. S27). However, changes from Miocene to Pliocene were far more apparent than changes from Pliocene to Holocene (Fig. S28).

### ***Palynological analyses and comparison with modern ecosystems***

*Family abundance.* The fossil palynological record from the Descanso-Yauri Basin showed that the most abundant families (>50 counts) for the Member B were Podocarpaceae, Cyatheaceae, Poaceae, Polygonaceae, Amaranthaceae, Polypodiaceae, Asteraceae, Chloranthaceae, Malvaceae, Lycopodiaceae, Araceae, Rosaceae, Solanaceae, and

Caryophyllaceae. For the Pliocene Member C, only Poaceae and Cyatheaceae had more than 50 counts.

*Plant habit.* A comparison of the plant habit between Members B and C was done using a generalized linear model with two multiple dependent variables and a quasi-binomial distribution in R. The model accounts for additional variance attributed to differences in sample sizes between the members and quality of the samples. We only found significant differences in the abundance of arboreal taxa between Members B and C ( $p = 0.0495^*$ ). Shrub, herb and fern counts were relatively similar between both Members ( $p > 0.05$ ) (Fig. S29). A second comparison was done between modern data from the Altiplano region, and the palynological record from Member C. This comparison was aiming to evaluate if the proportion of angiosperm and fern taxa was similar between the Pliocene and modern ecosystems. We compared the relative abundance of angiosperms and ferns of samples of the Member C against a quaternary sample from the Espinar region, and modern puna records from herbaria (GBIF.org). Our comparison showed that the quaternary sample is representative of the modern puna ecosystem (elevation range = 3400 and 4700 m), and also that ferns were far more abundant in the Pliocene Member C than in modern Puna ecosystems (Fig. S30).

*Comparison of floristic composition.* Using the floristic composition inferred from the fossil palynological data and a modern pollen dataset (Fig. S31), we made a comparison to estimate quantitatively similarities with floras from different elevation ranges. First, we defined natural altitudinal ranges based on similarities between modern sites across the altitudinal gradient. The modern dataset contained 300 sites from South America that spanned elevations between 180 and 4700 m (Fig. S31). We used the Chao Dissimilarity Index (CDI) as a measure of dissimilarity between the modern sites, where 0 is the least dissimilar and 1 the most dissimilar.

To define the natural altitudinal ranges, we created datasets for sites present in intervals of 250 m of elevation. These intervals were overlapped by 50 m. Then we estimated the CDI for the comparison between each interval of a 250 m of elevation with the one immediately above. We then use a probability density function to plot the calculated CDI for each interval (Fig. S32A). The resultant plot was used to define visually ranges that were more similar. We defined four ranges: lowlands from 0 to 1200 m, lower montane from 1200 to 2400 m, upper montane from 2400 to 3400 m, and puna from 3400 to 4700 m (Fig. S32).

Subsequently, we compared independently the palynological record from Members B and C (samples > 50 counts) with all the 250 m intervals across the entire altitudinal gradient and plotted the probability density using the *polygon* function in R from the Graphics package (Fig. S32C,D). Based on the observed pattern, in which the Member B was more similar to montane ecosystems, and the Member C was more similar to puna ecosystems we made an additional analysis. We compared the Member B with the two natural altitudinal ranges defined before: the lower montane (1200 to 2400 m), and the upper montane (2400 to 3400 m); and the Member C with the puna from (3400 to 4700 m). We found that the modern montane forests are highly heterogeneous, and that the palynoflora from the Member B is not strictly similar to one from a montane forest (Fig. 3A,B). Instead we found that the palynoflora from the Member C is highly overlapped with those from the puna (Fig 3C)

## SUPPLEMENTARY REFERENCES

- Adhikari, B., R. Milne, R. T. Pennington, T. Särkinen, and C. A. Pendry. 2015. Systematics and biogeography of *Berberis* s.l. inferred from nuclear ITS and chloroplast *ndhF* gene sequences. *Taxon* 64: 39–48.
- Balslev, H. 1996. Juncaceae. *Flora Neotropica* 68: 1–167.
- Baretta-Kuipers, T. 1981. Wood anatomy of Leguminosae: its relevance to taxonomy. *Advances in legume systematics*. 2., 677–705. The Royal Botanic Garden, Kew, United Kingdom.
- Black, L. P., S. L. Kamo, C. M. Allen, D. W. Davis, J. N. Aleinikoff, J. W. Valley, R. Mundil, et al. 2004. Improved <sup>206</sup>Pb/<sup>238</sup>U microprobe geochronology by the monitoring of a trace-element-related matrix effect; SHRIMP, ID-TIMS, ELA-ICP-MS and oxygen isotope documentation for a series of zircon standards. *Chemical Geology* 205: 115–140.
- Boonchai, N. 2012. Systematic affinities and paleoenvironment of Eocene petrified woods from southwestern Wyoming, USA. Jilin University, Changchun, China.
- Cerpa, L., and P. Meza. 2001. Las cuencas neogenas del sur del Perú: la cuenca Descanso–Yauri (Mioceno). Evolución sedimentológica y tectónica. Universidad Nacional de San Antonio Abad del Cusco, Cusco, Perú.
- Chao, A., R. L. Chazdon, R. K. Colwell, and T.-J. Shen. 2005. A new statistical approach for assessing similarity of species composition with incidence and abundance data. *Ecology Letters* 8: 148–159.
- Ellis, B., D. C. Daly, L. J. Hickey, J. V. Mitchell, K. R. Johnson, P. Wilf, and S. L. Wing. 2009. *Manual of Leaf Architecture*. Cornell University Press, Ithaca, NY.
- Evans, J. A., P. E. Gasson, and G. P. Lewis. 2006. Wood anatomy of the Mimosoideae. *IAWA Journal* 5.
- Feldpausch, T. R., J. Lloyd, S. L. Lewis, R. J. W. Brienen, M. Gloor, A. Monteagudo Mendoza, G. Lopez-Gonzalez, et al. 2012. Tree height integrated into pantropical forest biomass estimates. *Biogeosciences* 9: 3381–3403.
- Fick, S. E., and R. J. Hijmans. 2017. WorldClim 2: new 1-km spatial resolution climate surfaces for global land areas: new climate surfaces for global land areas. *International Journal of Climatology* 37: 4302–4315.
- Garcia Massini, J. L., and R. R. Pujana. 2013. Silicified Termite Coprolites in Mesquite-Like Wood from the Miocene of La Rioja, Argentina. *International Journal of Plant Sciences* 174: 585–591.
- Gasson, P. E. 2000. Does wood anatomy support tribal and generic classification in papilionoid Leguminosae. *Advances in Legume Systematics* 9, 201–215. The Royal Botanic Garden, Kew, United Kingdom.

- GBIF.org. 2018. GBIF: Global Biodiversity Information Facility. Website <https://www.gbif.org/> [accessed 28 February 2019].
- Gehrels, G. E., V. A. Valencia, and J. Ruiz. 2008. Enhanced precision, accuracy, efficiency, and spatial resolution of U-Pb ages by laser ablation–multicollector–inductively coupled plasma–mass spectrometry. *Geochemistry, Geophysics, Geosystems* 9: 1–13.
- Graham, A. 2010. Late Cretaceous and Cenozoic history of Latin American vegetation and terrestrial environments. Missouri Botanical Garden Press.
- Hansen, J., M. Sato, G. Russell, and P. Kharecha. 2013. Climate sensitivity, sea level and atmospheric carbon dioxide. *Philosophical Transactions of the Royal Society A: Mathematical, Physical and Engineering Sciences* 371: 20120294–20120294.
- Hermesen, E. J. 2005. The fossil record of Iteaceae and Grossulariaceae in the Cretaceous and Tertiary of the United States and Canada. Cornell University, Ithaca, New York, USA.
- IAWA, C. 1989. IAWA list of microscopic features for hardwood identification. *IAWA Bulletin n. s.*: 219–332.
- Ibanez-Mejia, M., A. Pullen, J. Arenstein, G. E. Gehrels, J. Valley, M. N. Ducea, A. R. Mora, et al. 2015. Unraveling crustal growth and reworking processes in complex zircons from orogenic lower-crust: The Proterozoic Putumayo Orogen of Amazonia. *Precambrian Research* 267: 285–310.
- Jud, N. A., and J. I. Dunham. 2017. Fossil woods from the Cenozoic of Panama (Azucero Peninsula) reveal an ancient neotropical rainforest. *IAWA Journal* 38: 366–S2.
- Kar, N., C. N. Garzzone, C. Jaramillo, T. Shanahan, V. Carlotto, A. Pullen, F. Moreno, et al. 2016. Rapid regional surface uplift of the northern Altiplano plateau revealed by multiproxy paleoclimate reconstruction. *Earth and Planetary Science Letters* 447: 33–47.
- Labandeira, C. C., T. L. Phillips, and R. A. Norton. 1997. Oribatid Mites and the Decomposition of Plant Tissues in Paleozoic Coal-Swamp Forests. *PALAIOS* 12: 319–353.
- Legume Phylogeny Working Group. 2017. A new subfamily classification of the Leguminosae based on a taxonomically comprehensive phylogeny – The Legume Phylogeny Working Group (LPWG). *Taxon* 66: 44–77.
- Lewis, G. P., B. D. Schrire, B. Mackinder, and M. Lock. 2005. Legumes of the world. Royal Botanic Gardens, Kew, Richmond, U.K.
- Maitner, B. S., B. Boyle, N. Casler, R. Condit, J. Donoghue, S. M. Durán, D. Guaderrama, et al. 2017. The bien r package: A tool to access the Botanical Information and Ecology Network (BIEN) database. *Methods in Ecology and Evolution*: 1–7.
- Melo, A. 2017. CommEcol: Community Ecology Analyses. R package version 1.6.5.

- Metcalf, C. R., and L. Chalk. 1950. *Anatomy of the Dicotyledons*. Oxford University Press, United Kingdom.
- Müller-Stoll, W. R., and E. Mädler. 1967. Die fossilen Leguminosen-Hölzer. Eine Revision der mit Leguminosen verglichenen fossilen Hölzer und Beschreibung alterer und neuer Arten. *Palaeontographica Abteilung B* 119: 95–174.
- Niklas, K. J. 1994. Predicting the Height of Fossil Plant Remains: An Allometric Approach to an Old Problem. *American Journal of Botany* 81: 1235.
- Oskolski, A. A. 1996. A survey of the wood anatomy of the Araliaceae. Recent advances in wood anatomy, 99–119. Rotorua.
- Paces, J. B., and J. D. Miller. 1993. Precise U-Pb ages of Duluth Complex and related mafic intrusions, northeastern Minnesota: Geochronological insights to physical, petrogenetic, paleomagnetic, and tectonomagmatic processes associated with the 1.1 Ga Midcontinent Rift System. *Journal of Geophysical Research: Solid Earth* 98: 13997–14013.
- Peel, D., and G. J. McLachlan. 2000. Robust mixture modelling using the t distribution. *Statistics and Computing* 10: 339–348.
- Pell, S. K., J. D. Mitchell, A. J. Miller, and T. A. Lobova. 2011. Anacardiaceae. In K. Kubitzki [ed.], *Flowering Plants. Eudicots: Sapindales, Cucurbitales, Myrtaceae*, 7–50. Springer Berlin Heidelberg, Berlin, Heidelberg.
- Pennington, R. T. 2003. Monograph of *Andira* (Leguminosae-Papilionoideae). *Systematic Botany Monographs* 64: 1–143.
- Peppe, D. J., L. J. Hickey, I. M. Miller, and W. A. Green. 2008. A Morphotype Catalogue, Floristic Analysis and Stratigraphic Description of the Aspen Shale Flora (Cretaceous–Albian) of Southwestern Wyoming. *Bulletin of the Peabody Museum of Natural History* 49: 181–208.
- Pullen, A., M. Ibáñez-Mejía, G. E. Gehrels, D. Giesler, and M. Pecha. 2018. Optimization of a Laser Ablation-Single Collector-Inductively Coupled Plasma-Mass Spectrometer (Thermo Element 2) for Accurate, Precise, and Efficient Zircon U-Th-Pb Geochronology. *Geochemistry, Geophysics, Geosystems* 19: 3689–3705.
- Ramírez, J. L., and S. R. S. Cevallos-Ferriz. 2000. Leaves of Berberidaceae (*Berberis* and *Mahonia*) from Oligocene sediments, near Tepexi de Rodríguez, Puebla. *Review of Palaeobotany and Palynology* 110: 247–257.
- Read, R. W., and L. J. Hickey. 1972. A Revised Classification of Fossil Palm and Palm-like Leaves. *Taxon* 21: 129.
- Simpson, B. B. 1979. A Revision of the Genus *Polylepis* (Rosaceae: Sanguisorbeae). *Smithsonian Contributions to Botany*: 1–62.

- Stacey, J. S., and J. D. Kramers. 1975. Approximation of terrestrial lead isotope evolution by a two-stage model. *Earth and Planetary Science Letters* 26: 207–221.
- Terrazas Salgado, T. 1994. Wood anatomy of the Anacardiaceae: Ecological and phylogenetic interpretation. Ph.D. The University of North Carolina at Chapel Hill, United States -- North Carolina.
- Vélez, M. I., C. Jaramillo, A. Salazar-Ríos, X. Benito, S. Fritz, P. Tapia, D. Lubiniecki, et al. 2018. Aquatic ecosystems in a newly formed ecospace: Early Pliocene lakes in the Central Andean Altiplano. *Palaeogeography, Palaeoclimatology, Palaeoecology* 490: 218–226.
- Wand, M. P., and M. C. Jones. 1994. Kernel smoothing. Chapman and Hall/CRC.
- Wheeler, E. A. 2011. InsideWood — a web resource for hardwood anatomy. *IAWA Journal*: 199–211.
- Wheeler, E. A., and P. Baas. 1992. Fossil wood of the Leguminosae: a case study in xylem evolution and ecological anatomy. *Advances in legume systematics*. 4. The fossil record., 281–302. The Royal Botanic Garden, Kew, United Kingdom.
- Wood, G. D., A. M. Gabriel, and J. C. Lawson. 1996. Palynological techniques e processing and microscopy. *Palynology: principles and applications*, 29–50. *Palynology: principles and applications*, Dallas, TX. USA.

## SUPPLEMENTARY FIGURES

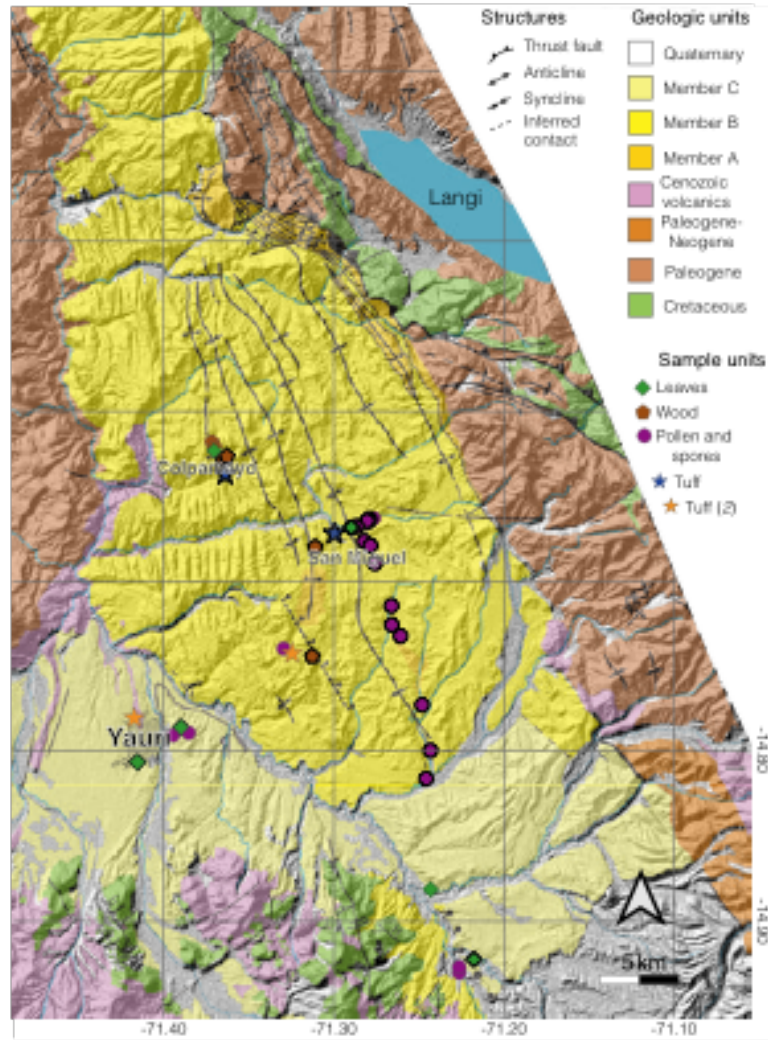


**Fig. S1. Geological map of the Descanso-Yauri Basin.**

Geologic map for the Descanso-Yauri Basin, showing where the samples were collected (modified from 2).

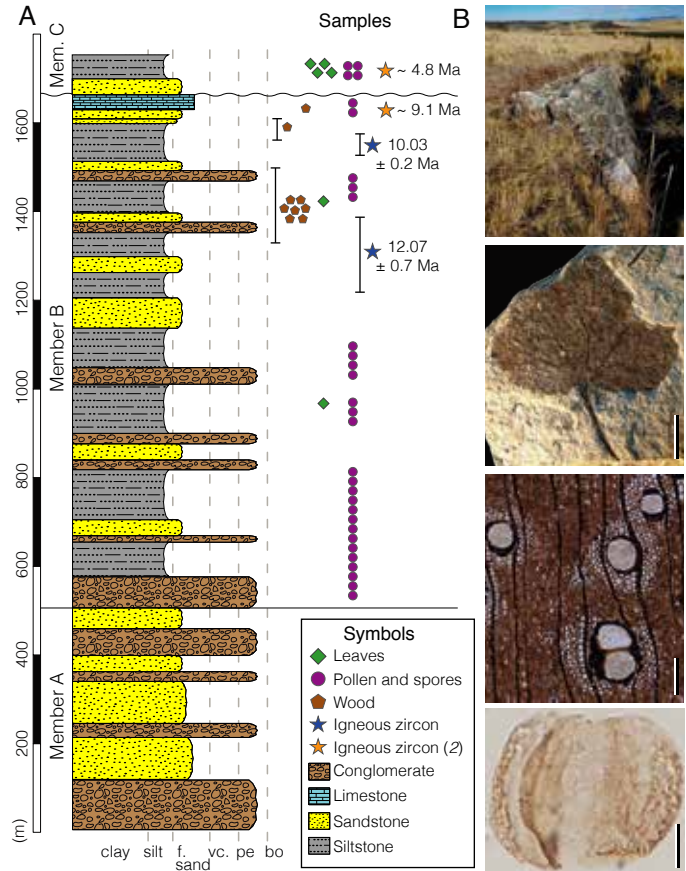


**Fig. S2. Geological setting of the Descanso-Yauri Basin.**

Geological setting of the Descanso-Yauri Basin. (A). Stratigraphic column for El Descanso Formation, including Members A, B and C (modified from Kar et al. 2016). Bars next to the samples correspond to the uncertainty in the stratigraphic depth for the sample or group of samples. Undulating line represents the unconformity between Members B and C. (B) Photographs of some of the macro- and microfossils collected for this study. From top to bottom: Fossil log with 7 m of length; *Ribes* leaf (scale = 10 mm); legume fossil wood anatomy (scale = 1 mm); *Podocarpus* pollen (scale = 10  $\mu$ m).

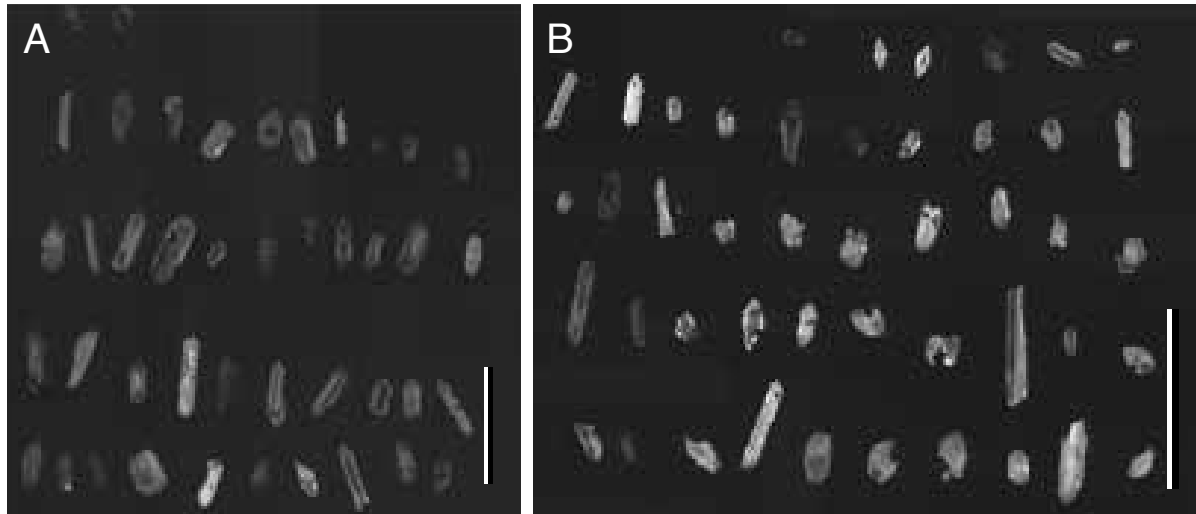


**Fig. S3. Cathodoluminescence images of zircons**

Cathodoluminescence images of zircons from tuffaceous horizons showing internal oscillatory-zoned textures **A.** Colpamayo region sample STRI-MUSM 44449. **B.** San Miguel region sample STRI-MUSM 44448 are characterized by internal oscillatory-zoned textures

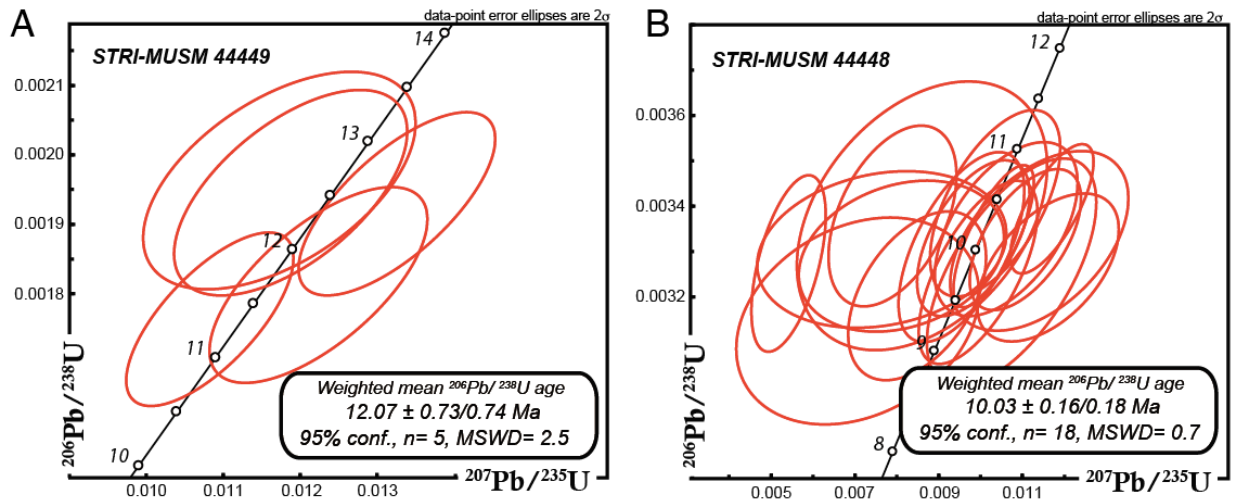


**Fig. S4. Wetherill concordia diagrams.**

Wetherill concordia diagrams. Uncertainties in the reported  $^{206}\text{Pb}/^{238}\text{U}$  weighted means for each sample are in the form  $\pm X/Y \text{ Ma}$ , where the first uncertainty level ‘X’ only represents analytical uncertainty and the second term ‘Y’ includes propagation of the reproducibility of the zircon reference materials measured during the same analytical session. **A.** Colpamayo region sample STRI-MUSM 44449. **B.** San Miguel region sample STRI-MUSM 44448 are characterized by internal oscillatory-zoned textures.

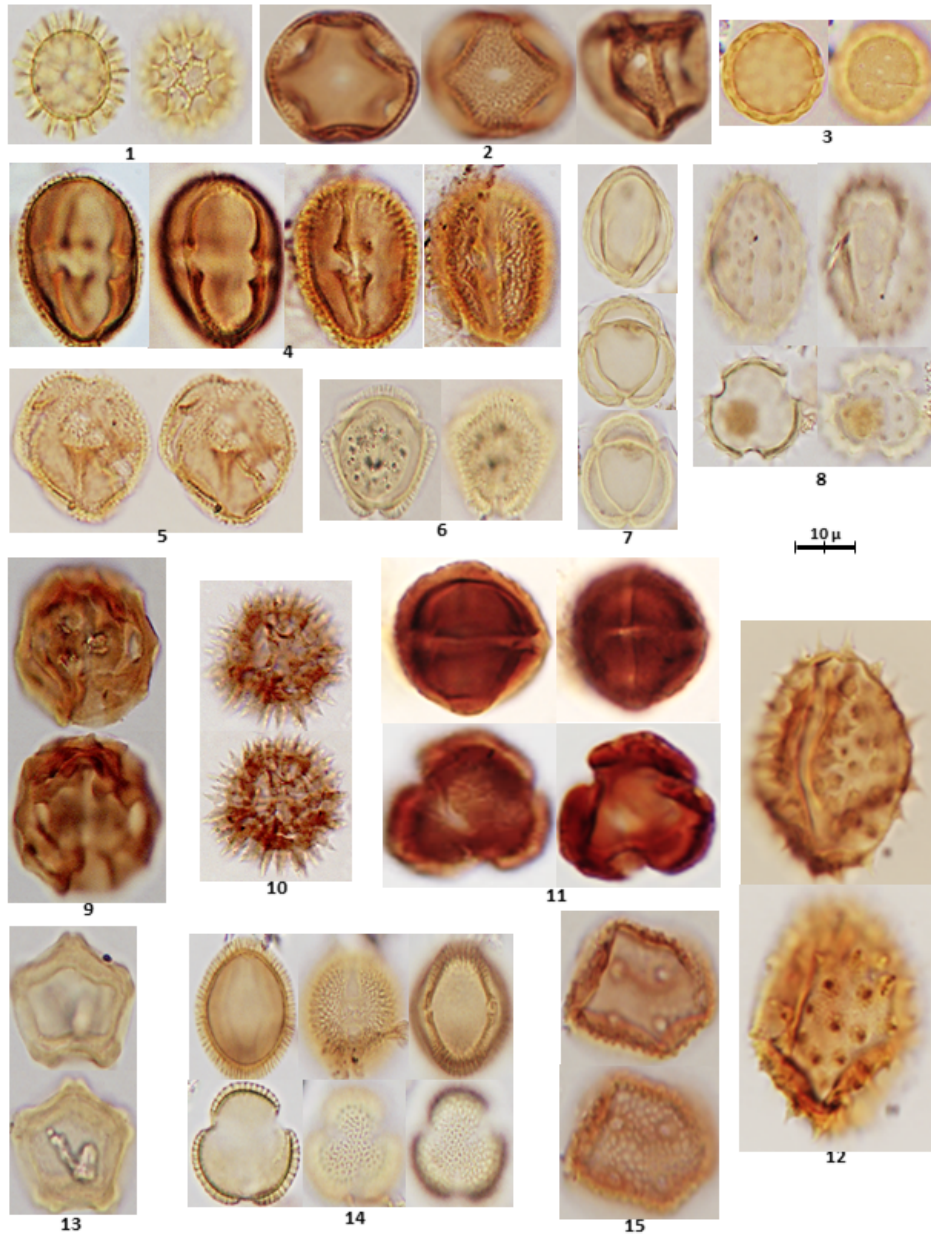


**Fig. S5. Micrographs of palynomorphs.**

Amaranthaceae: *Amaranthus* sp.1 (1); *Amaranthus* sp.2 (2); *Chenopodium* sp. (3).  
 Anacardiaceae: *Anacardium* sp. (4); *Schinus* sp. (5). Araliaceae: *Schefflera* sp. (6). Asteraceae:  
*Ambrosia* sp. (7); *Baccharis* sp. (8); *Barnadesia* sp. (9); *Hypochoeris* sp. (10); *Mutisia* sp. (11);  
 Undetermined (12). Betulaceae: *Alnus* sp. (13). Brassicaceae: *Brassica* sp. (14). Buxaceae:  
*Styloceras* sp. (15) (x1000)

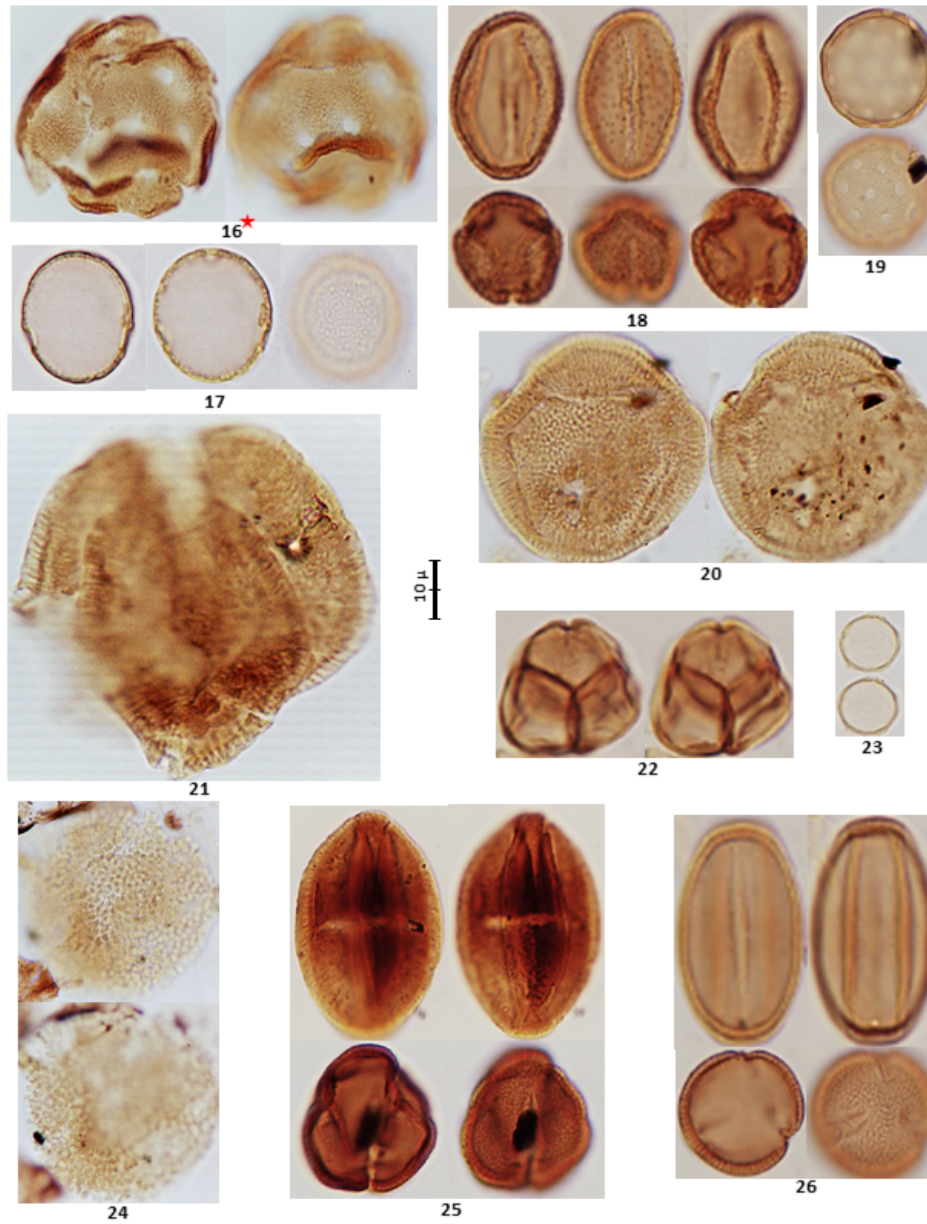


**Fig. S6. Micrographs of palynomorphs.**

Cactaceae: *Opuntia* sp. (16). Cannabaceae: *Celtis* sp. (17). Caprifoliaceae: *Valeriana* sp. (18).  
 Caryophyllaceae: *Arenaria* sp. (19). Convolvulaceae: *Evolvulus* sp. (20); *Iseia* sp. (21).  
 Ericaceae: *Gaultheria* sp. (22). Euphorbiaceae: *Acalypha* sp. (23); *Croton* sp. (24); *Sapium* sp.  
 (25); *Tetrorchidium* sp. (26) (x1000) (★)=50% reduced

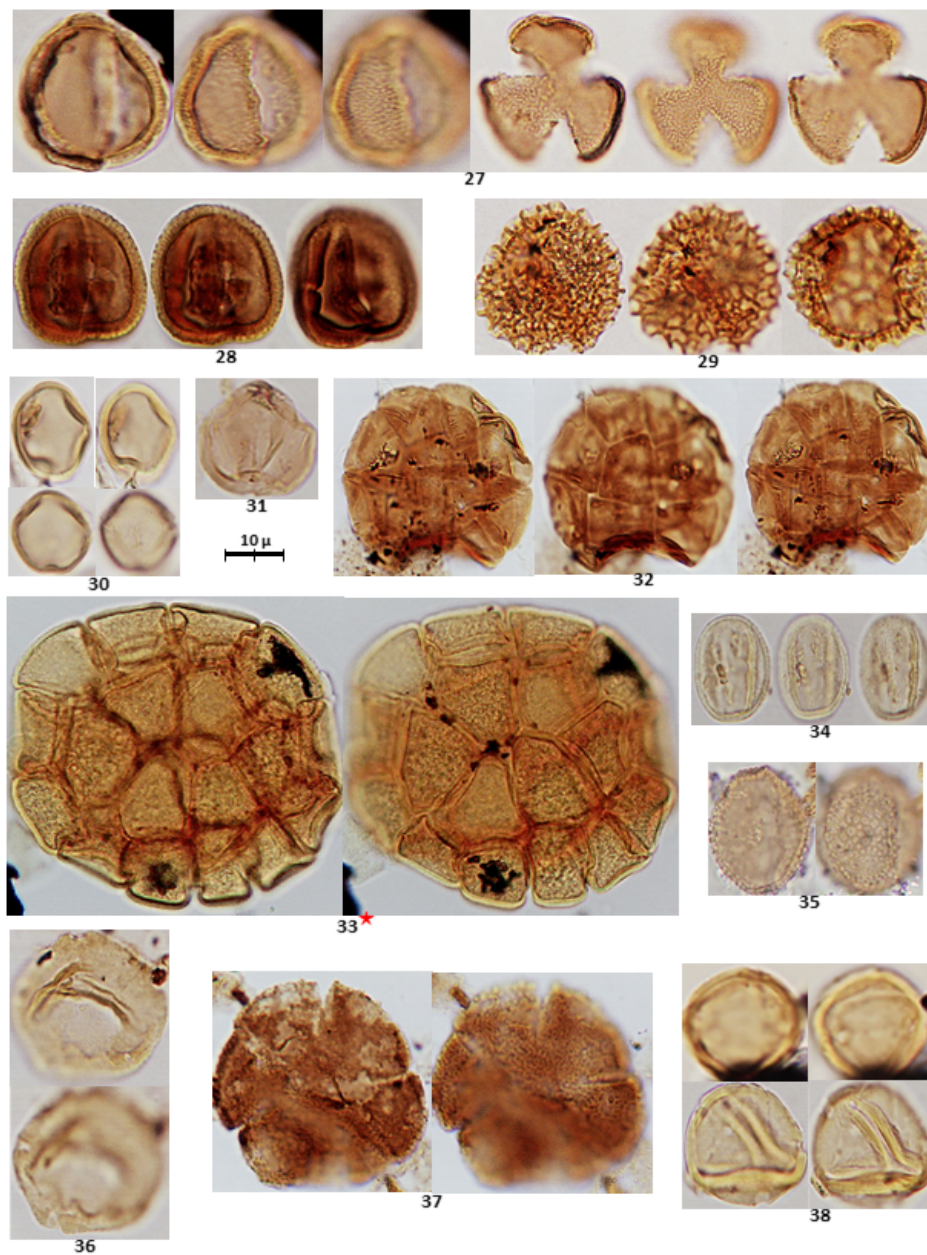


**Fig. S7. Micrographs of palynomorphs.**

Euphorbiaceae: Unknown sp.1 (27); Unknown sp.2 (28). Fabaceae-Caesalpinioideae: *Jacqueshuberia* sp. (29). Fabaceae-Faboideae: *Trifolium* sp. (30); Unknown (31). Fabaceae-Mimosoideae: *Acacia* sp. (32); *Inga* sp. (33). Fagaceae: *Quercus* sp. (34). Hypericaceae: *Vismia* sp. (35). Juglandaceae: *Juglans* sp. (36). Lamiaceae: *Hyptis* sp. (37). Malpighiaceae: *Tetrapteryx* sp. (38) (x1000) (★)=50% reduced

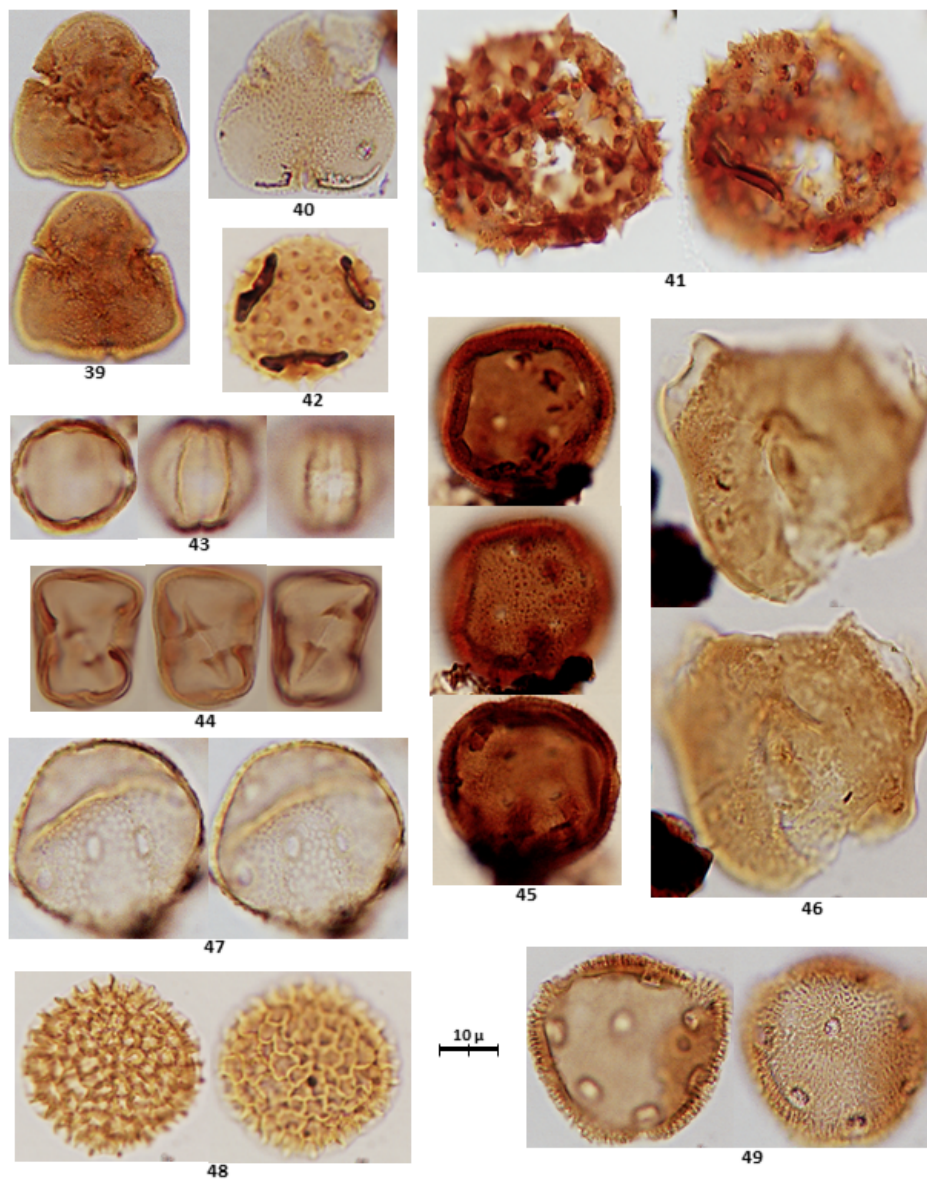


**Fig. S8. Micrographs of palynomorphs.**

Malvaceae-Bombacoideae: *Pseudobombax* sp. (39). Malvaceae-Grewioideae: *Mortoni dendron* sp. (40). Malvaceae-Malvoideae: *Acaulimalva* sp. (41). Malvaceae: Unknown (42). Melastomataceae/Combretaceae: Unknown (43). Meliaceae: *Trichilia* sp. (44). Nyctaginaceae: *Mirabilis* sp. (45). Onagraceae: *Fuchsia* sp. (46). Papaveraceae: *Bocconia* sp. (47). Polygonaceae: *Polygonum* sp. (48). Portulacaceae (Montiaceae): *Calandrinia* sp. (49) (x1000)

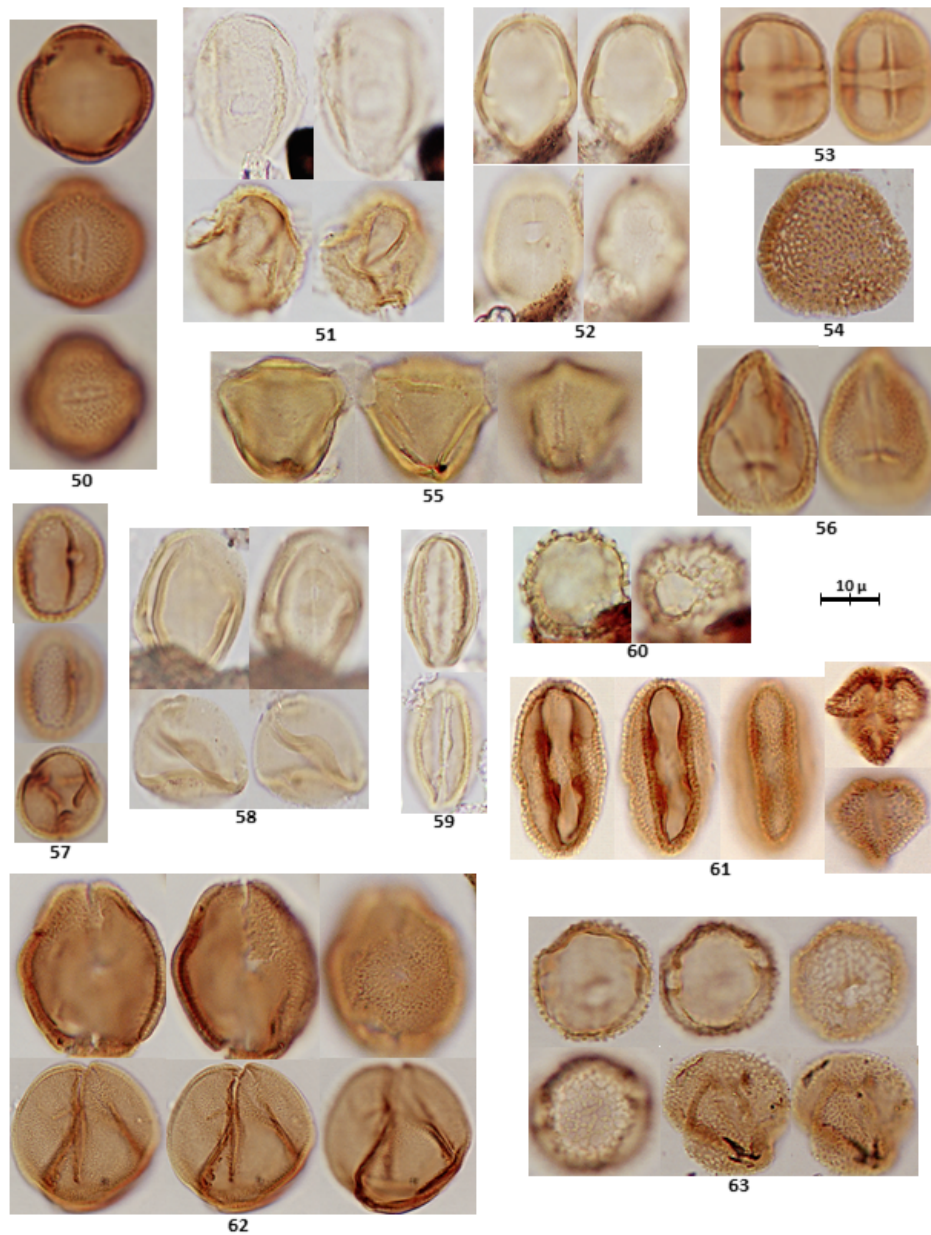


**Fig. S9. Micrographs of palynomorphs.**

Primulaceae: *Myrsine* sp. (50). Rosaceae: *Polylepis* sp. (51). Sapotaceae: Unknown (52). Solanaceae: *Solanum* sp. (53). Thymelaeaceae: *Daphnopsis* sp. (54). Vochysiaceae: *Vochysia* sp. (55). ANGIOSPERMAE-Eudicotyledoneae: Unknown 1 (56); Unknown 2 (57); Unknown 3 (58); Unknown 4 (59); Unknown 5 (60); Unknown 6 (61); Unknown 7 (62); Unknown 8 (63). (x1000)

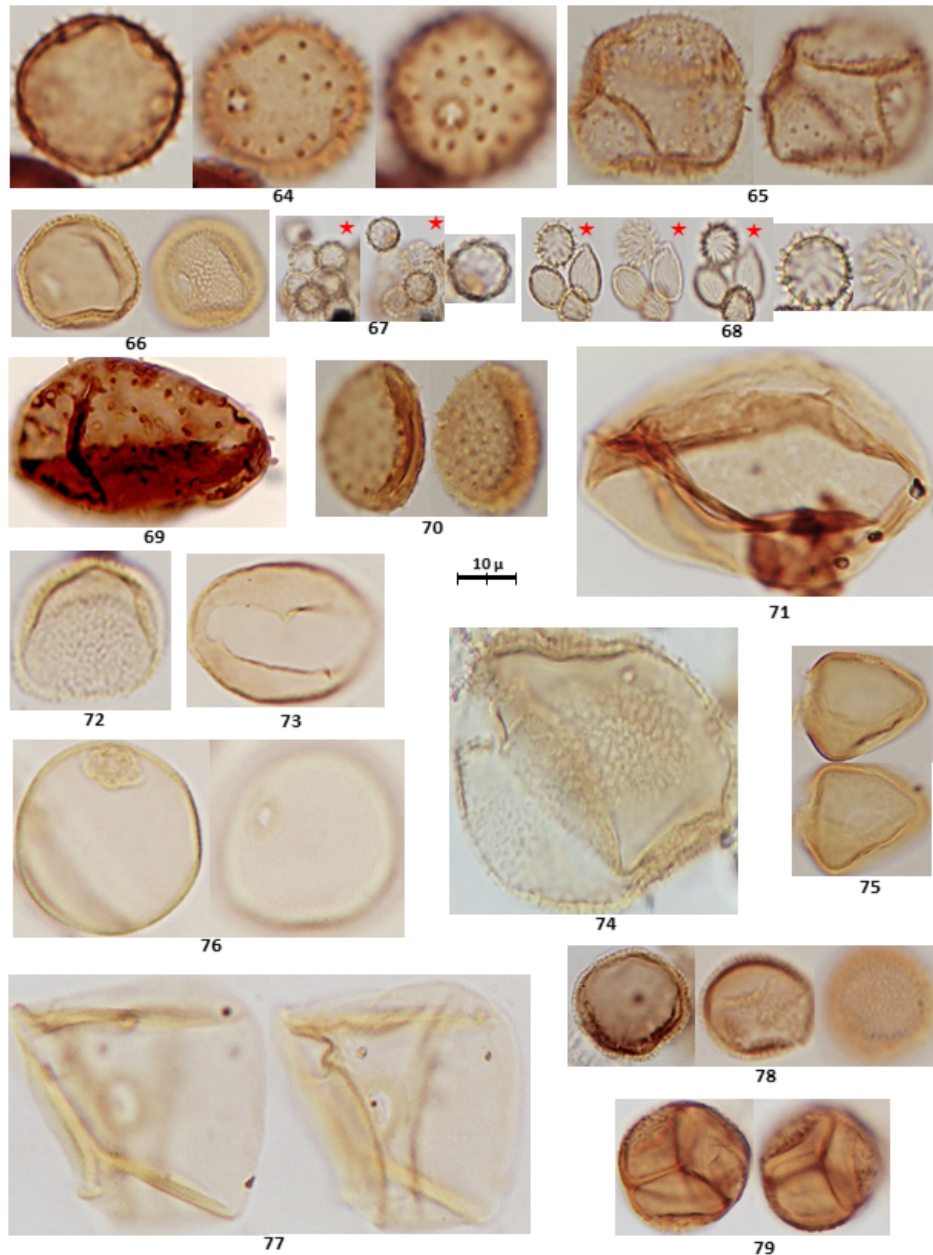


**Fig. S10. Micrographs of palynomorphs.**

ANGIOSPERMAE-Monocotyledoneae. Alismataceae: *Echinodorus* sp. (64); *Sagittaria* sp. (65).  
 Araceae: *Anthurium* sp.1 (66); *Anthurium* sp.2 (67); *Spatyphyllum* sp. (68). Arecaceae:  
*Lepidocarium* sp. (69); *Socratea* sp. (70); Unknown 1 (71); Unknown 2 (72); Unknown 3 (73).  
 Bromeliaceae: *Tillandsia* sp. (74). Cyperaceae: *Cyperus* sp. (75). Poaceae: *Calamagrostis* sp.  
 (76); *Hordeum* sp. (77). ANGIOSPERMAE-Basals. Chloranthaceae: *Hedyosmum* sp. (78).  
 Winteraceae: *Drimys* sp. (79). (x1000) (★)=50% reduced; ⋅=Cluster and isolated grain.

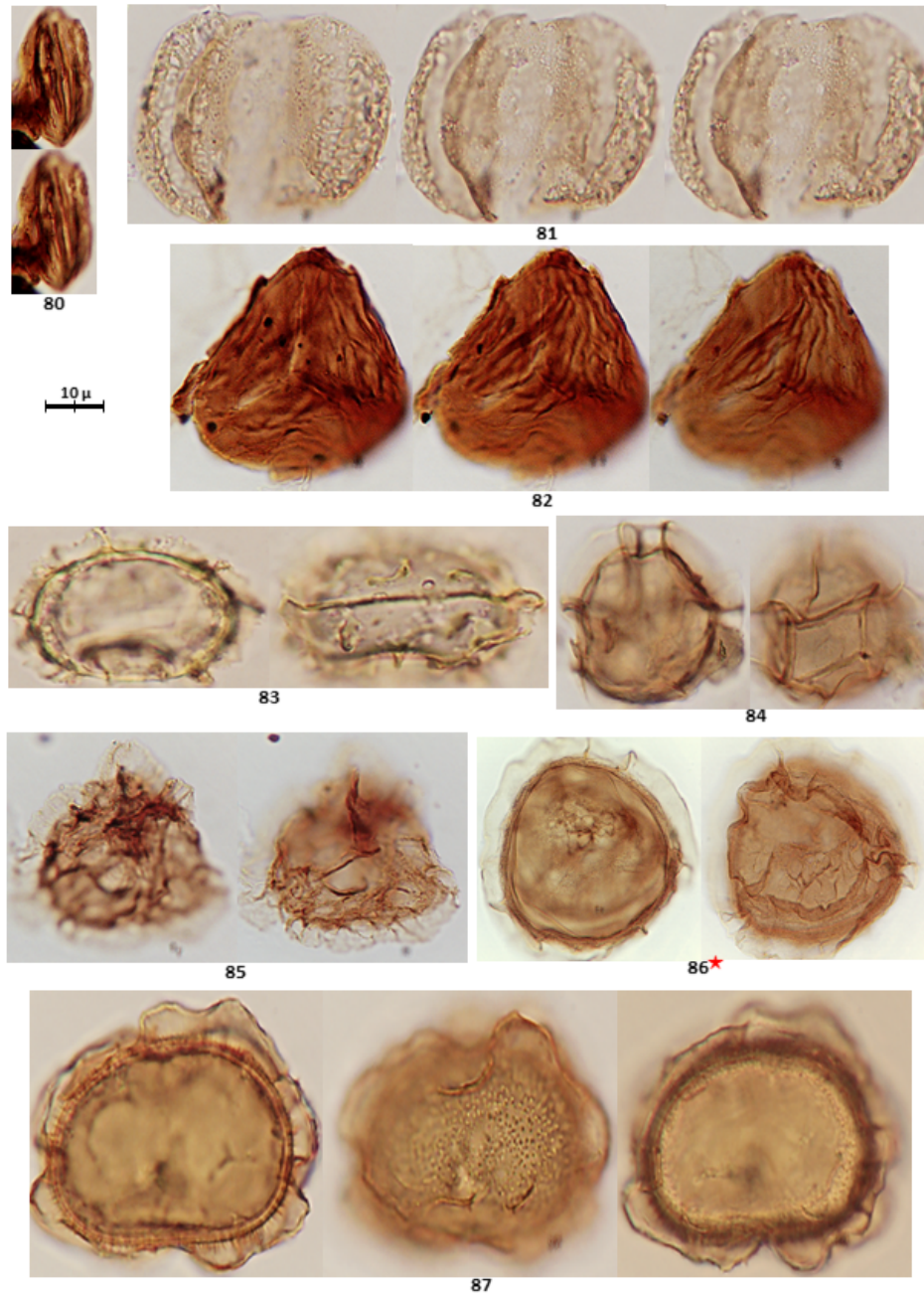


**Fig. S11. Micrographs of palynomorphs.**

GNETOPHYTA. Ephedraceae: *Ephedra* sp. (80). PINOPHYTA. Podocarpaceae: *Podocarpus* sp. (81). TRACHAEOPHYTA. Anemiaceae: *Anemia* sp. (82). Aspleniaceae: *Asplenium* sp.1 (83); *Asplenium* sp.2 (84); *Asplenium* sp.3 (85); *Asplenium* sp.4 (86). Blechnaceae: *Blechnum* sp. (87) (x1000) (★)=50% reduced

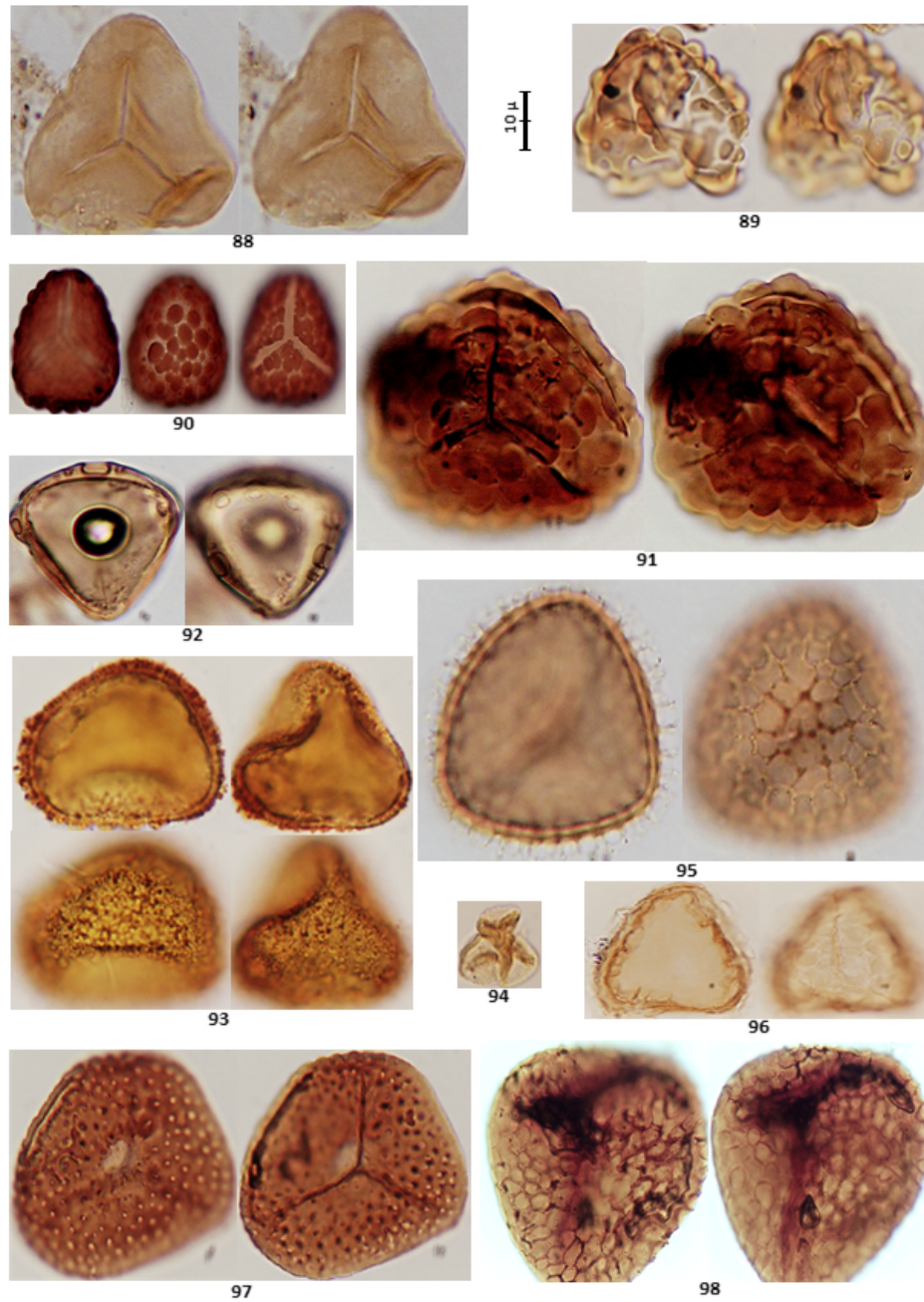


**Fig. S12. Micrographs of palynomorphs.**

Cyatheaceae: *Cyathea* sp.1 (88); *Cyathea* sp. 2 (89); *Cyathea* sp.3 (90); *Cyathea* sp. 4 (91); *Hemitelia* sp. (92). Dennstaedtiaceae: *Hypolepis* sp. (93). Hymenophyllaceae: *Hymenophyllum* sp. (94). Lycopodiaceae: *Lycopodium* sp.1 (95); *Lycopodium* sp.2 (96); *Lycopodium* sp.3 (97); *Lycopodium* sp.4 (98) (x1000)

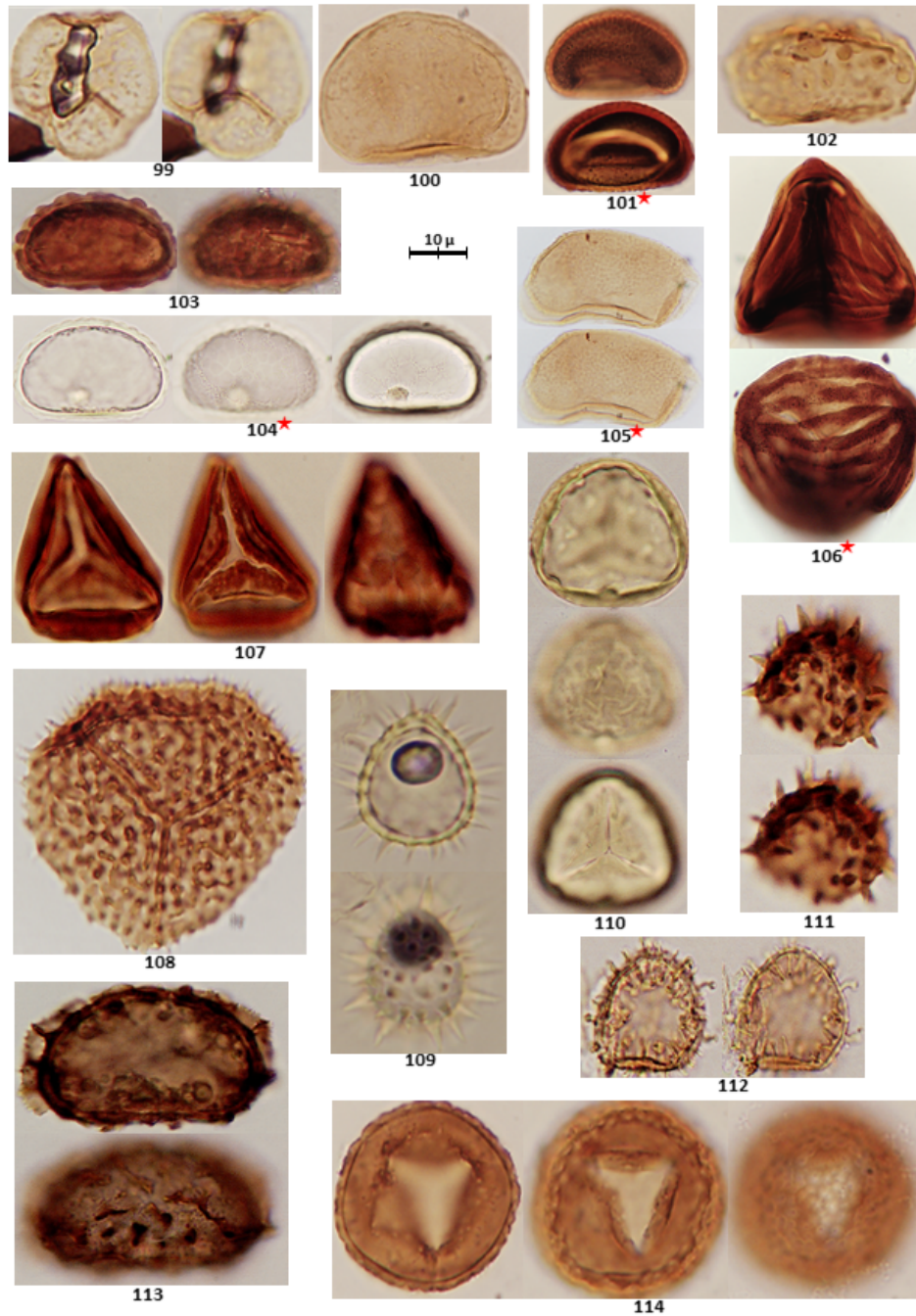


**Fig. S13. Micrographs of palynomorphs.**

Polypodiaceae: *Grammitis* sp. (99); *Polypodium* sp.1 (100); *Polypodium* sp.2 (101); *Polypodium* sp.3 (102); *Polypodium* sp.4 (103); *Polypodium* sp.5 (104); *Polypodium* sp.6 (105). Pteridaceae: *Ceratopteris* sp. (106); *Jamesonia* sp. (107). Selaginellaceae: *Selaginella* sp.1 (108); *Selaginella* sp.2 (109); *Selaginella* sp.3 (110); *Selaginella* sp.4 (111); *Selaginella* sp.5 (112).

Thelypteridaceae: *Thelypteris* sp. (113). TRACHAEOPHYTA: Unknown sp.1 (114) (x1000)

(★)=50% reduced.

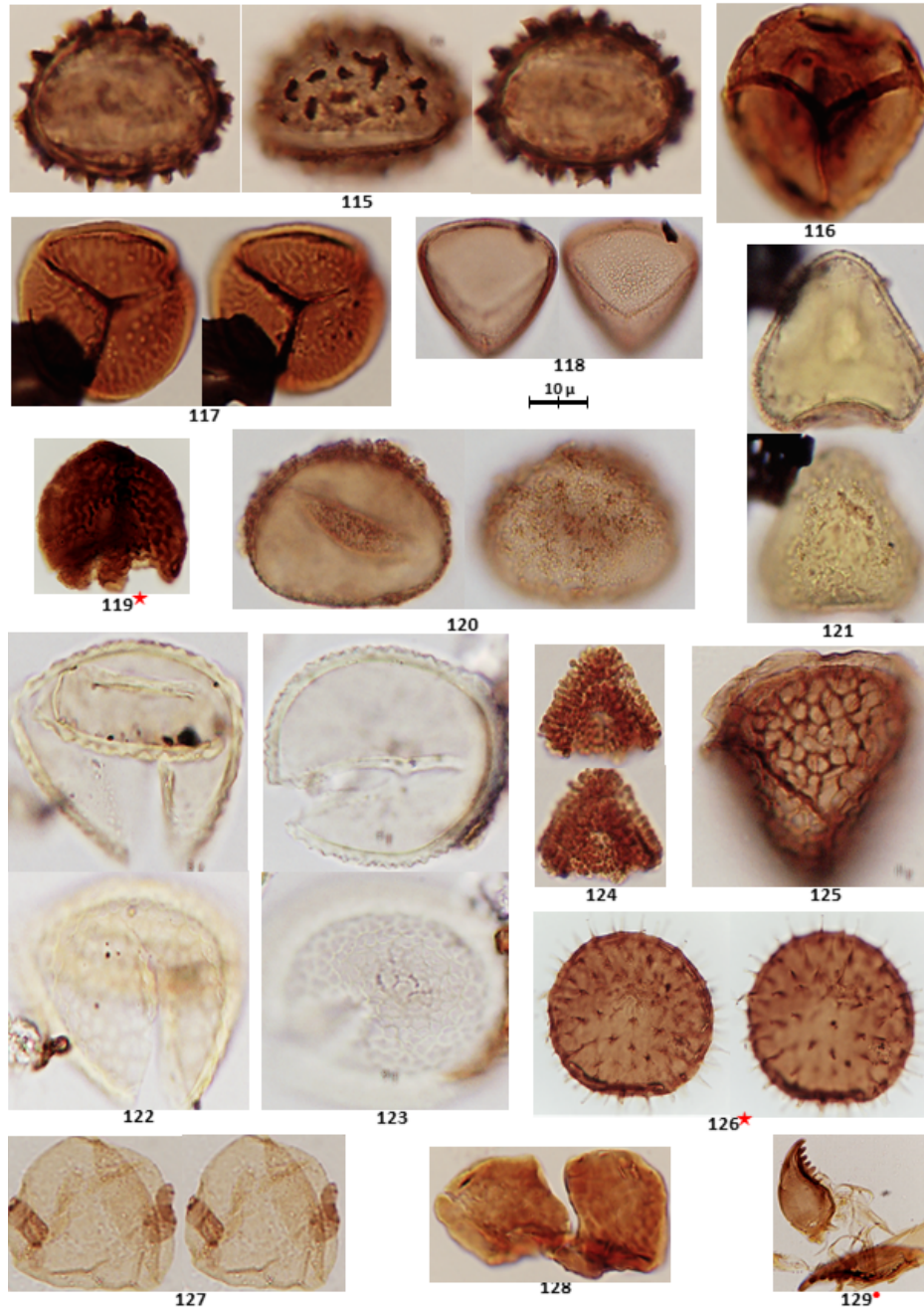


**Fig. S14. Micrographs of palynomorphs.**

TRACHAEOPHYTA: Unknown sp.2 (115); Unknown sp.3 (116); Unknown sp.4 (117); Unknown sp.5 (118); Unknown sp.6 (119); Unknown sp.7 (120); Unknown sp.8 (121); Unknown sp.9 (122); Unknown sp.10 (123); Unknown sp.11 (124); Unknown sp.12 (125). UNDETERMINED PALYNOMORPHS AND ASSOCIATED ORGANISMS. Algae 1(?) (126), Algae 2(?) (127), Microforam lining (128); Scolecodont (129<sup>\*</sup>) (x1000) (★)=50% reduced (⊛)=Not in scale

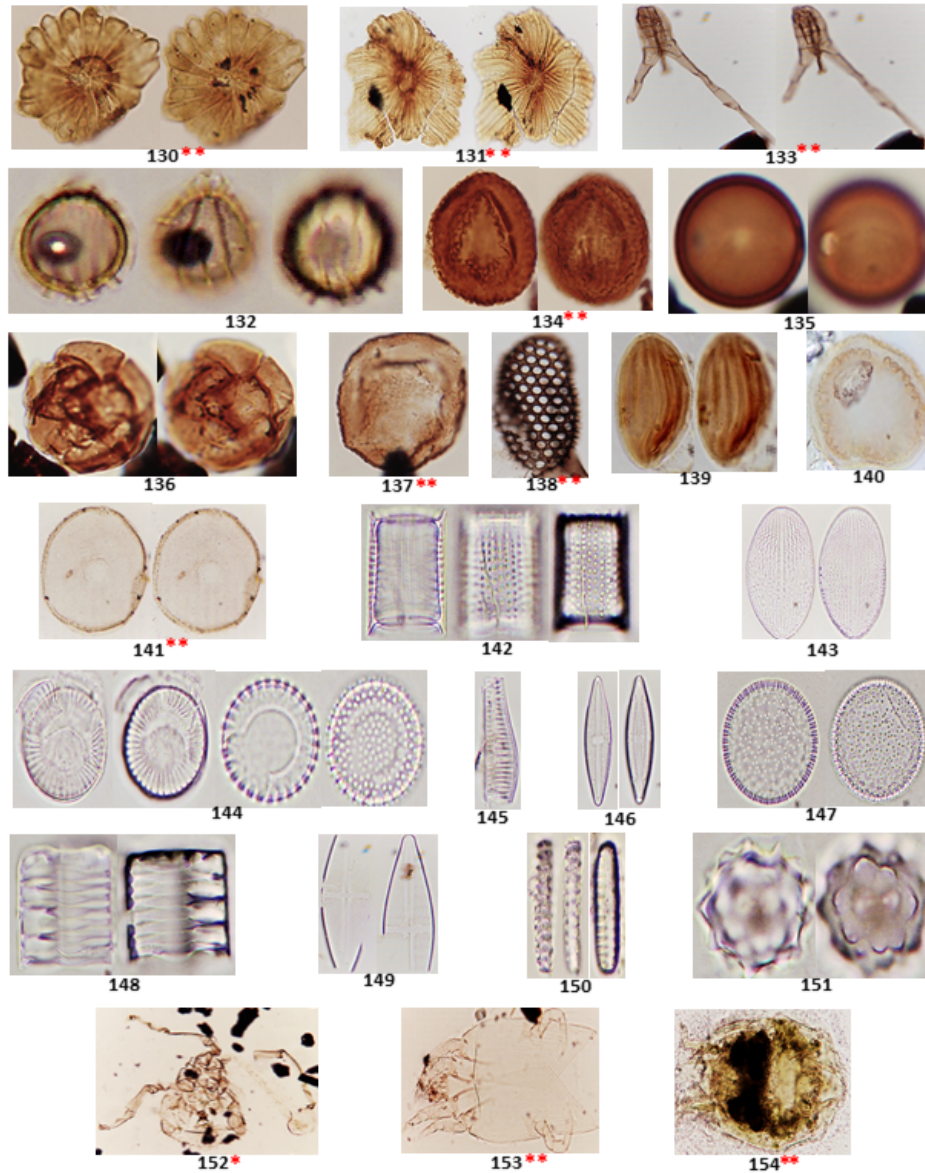


**Fig. S15. Micrographs of palynomorphs.**

UNDETERMINED PALYNOMORPHS AND ASSOCIATED ORGANISMS. Fungal Spores: *Asterina* sp. (130); *Microthyrium* sp. (131); *Neurospora* sp. (132); *Tetraploa* sp. (133); Unknown 1 (134); Unknown 2 (135); Unknown 3 (136); Unknown 4 (137); Unknown 5 (138); Unknown 6 (139); Unknown 7 (140). Amoebae: *Arcella* sp. (141). Diatoms: *Aulacoseira* sp. (142); *Cocconeis* sp. (143); *Cycotella* sp. (144); *Eunotia* sp. (145); *Pinularia* sp. (146); Unknown 1 (147); Unknown 2 (148); Unknown 3 (149) Phytoliths: Arecaceae type (150); Poaceae type (151). Acari: Unknown 1 (152); Unknown 2 (153); Unknown 3 (154) (x1000) (\*= x200) (\*\*= x400) (all pictures in this plate are not in scale).

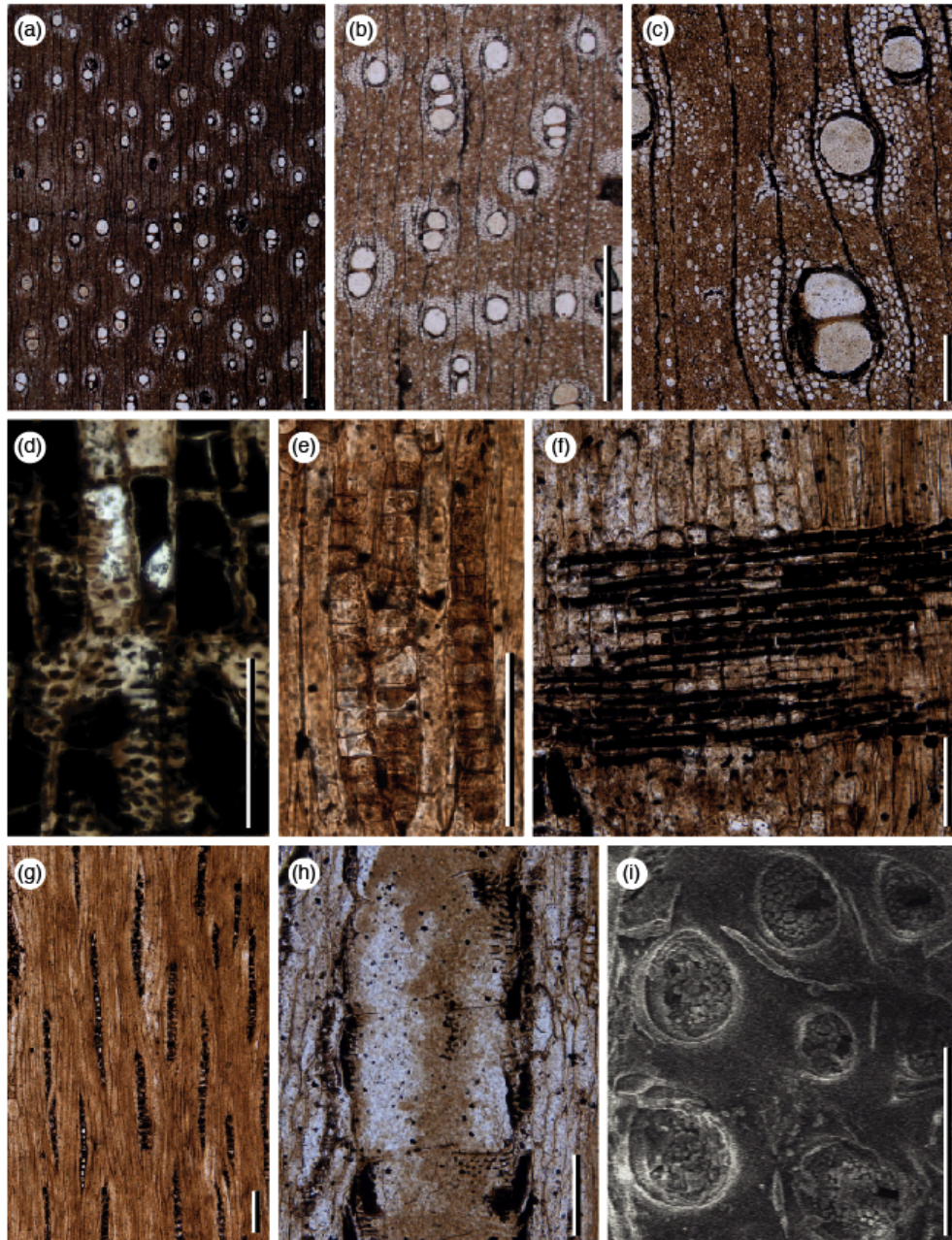


**Fig. S16. Wood anatomy DSB1.**

Wood anatomy DSB1 (Tribe Ingeae affinity; STRI-MUSM 39442). (a) Diffuse porous wood with vessels solitary and in short radial multiples with indistinct growth rings; TS; scale bar = 1000  $\mu\text{m}$ . (b) Vasicentric and confluent axial parenchyma; TS; scale bar = 1000  $\mu\text{m}$ . (c) Diffuse axial parenchyma; TS; scale bar = 20  $\mu\text{m}$ . (d) Vessel-parenchyma pitting similar to intervessel pits; RLS; scale bar = 20  $\mu\text{m}$ . (e) Prismatic crystals in chambered axial parenchyma; TLS. (f) Homocellular rays; RLS. (g) Uniseriate rays; TLS. (h) Short vessel elements with simple perforation plates; RLS. (i) Intervessel pits; SEM; scale bar = 10  $\mu\text{m}$ . (d-h) scale bars = 100  $\mu\text{m}$ .

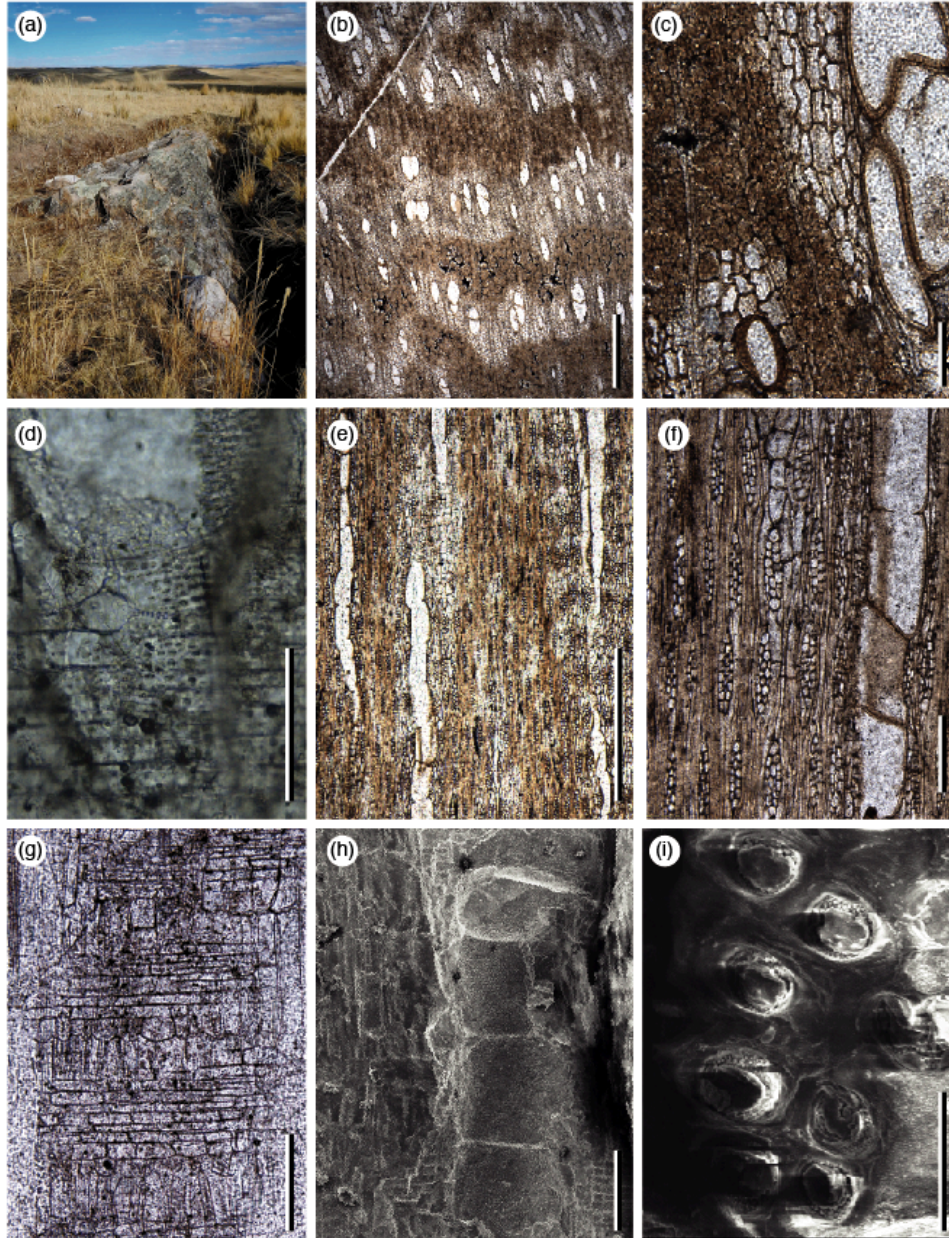


**Fig. S17. Wood anatomy DSB2.**

Wood anatomy and *in situ* photograph of DSB2 (*Andiroxylon* affinity; STRI-MUSM 21147). (a) Landscape photograph of the locality showing the sample *in situ* (b) Diffuse porous wood with vessels solitary and in short radial multiples with indistinct growth rings and confluent axial parenchyma; TS; scale bar = 1000 µm. (c) Fibers are thin to thick walled; TS; scale bar = 100 µm. (d) Vessel-parenchyma pitting similar to intervessel pits; RLS; scale bar = 100 µm. (e) Rays and vessel elements storied; TLS; scale bar = 1000 µm. (f) Multiseriate rays; TLS; scale bar = 200 µm. (g) Heterocellular rays; RLS; scale bar = 200 µm. (h) Short vessel elements with simple perforation plates; SEM; scale bar = 200 µm. (i) Intervessel pits; SEM; scale bar = 10 µm.

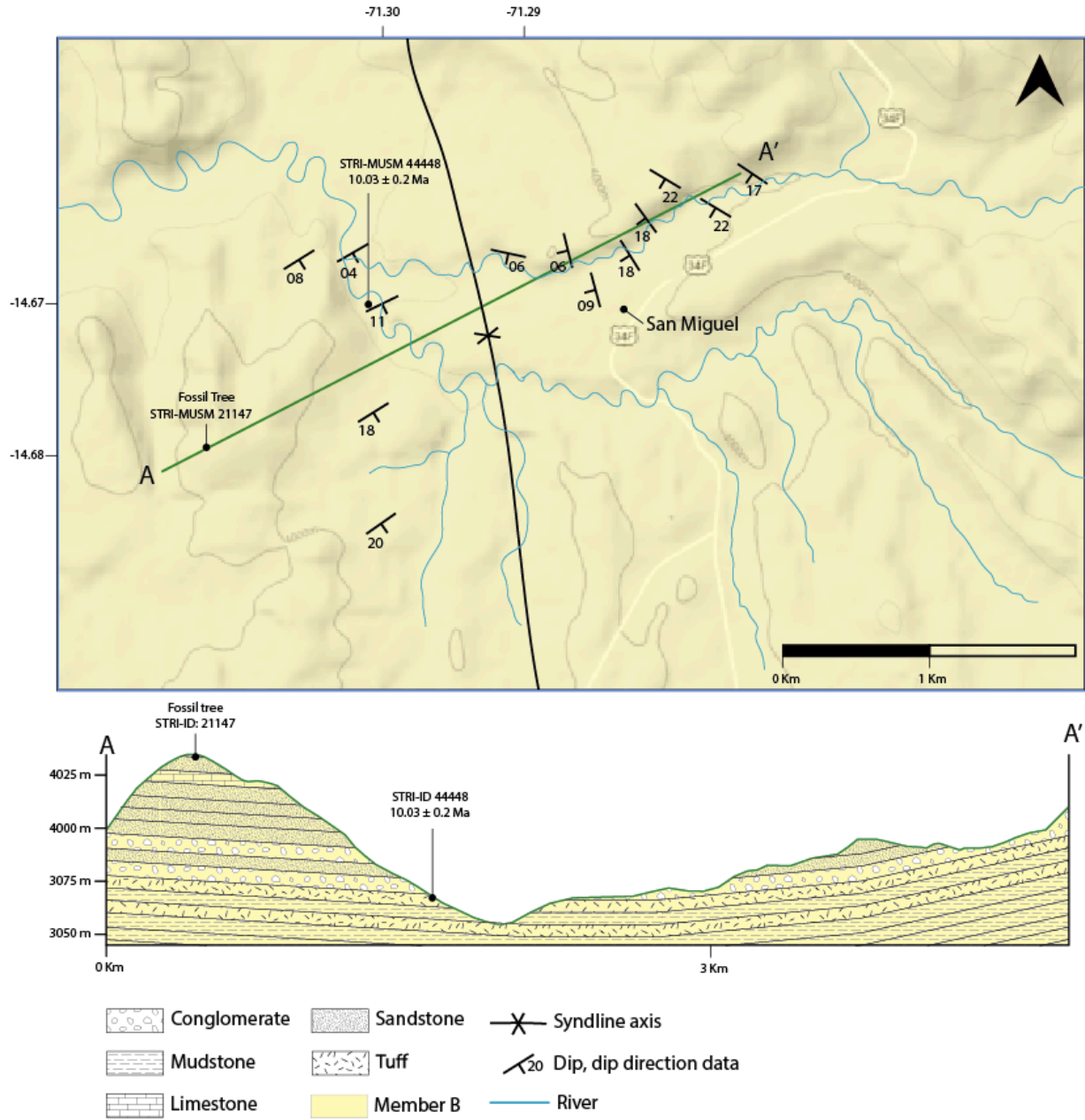


**Fig. S18. Topographic map and structural section, from the San Miguel region.**

Topographic map and structural section, from the San Miguel region (Member B) where the tuff (STRI-MUSM 44448) and the fossil log sample were collected (STRI-MUSM 21147). The green line represents the drawn cross section

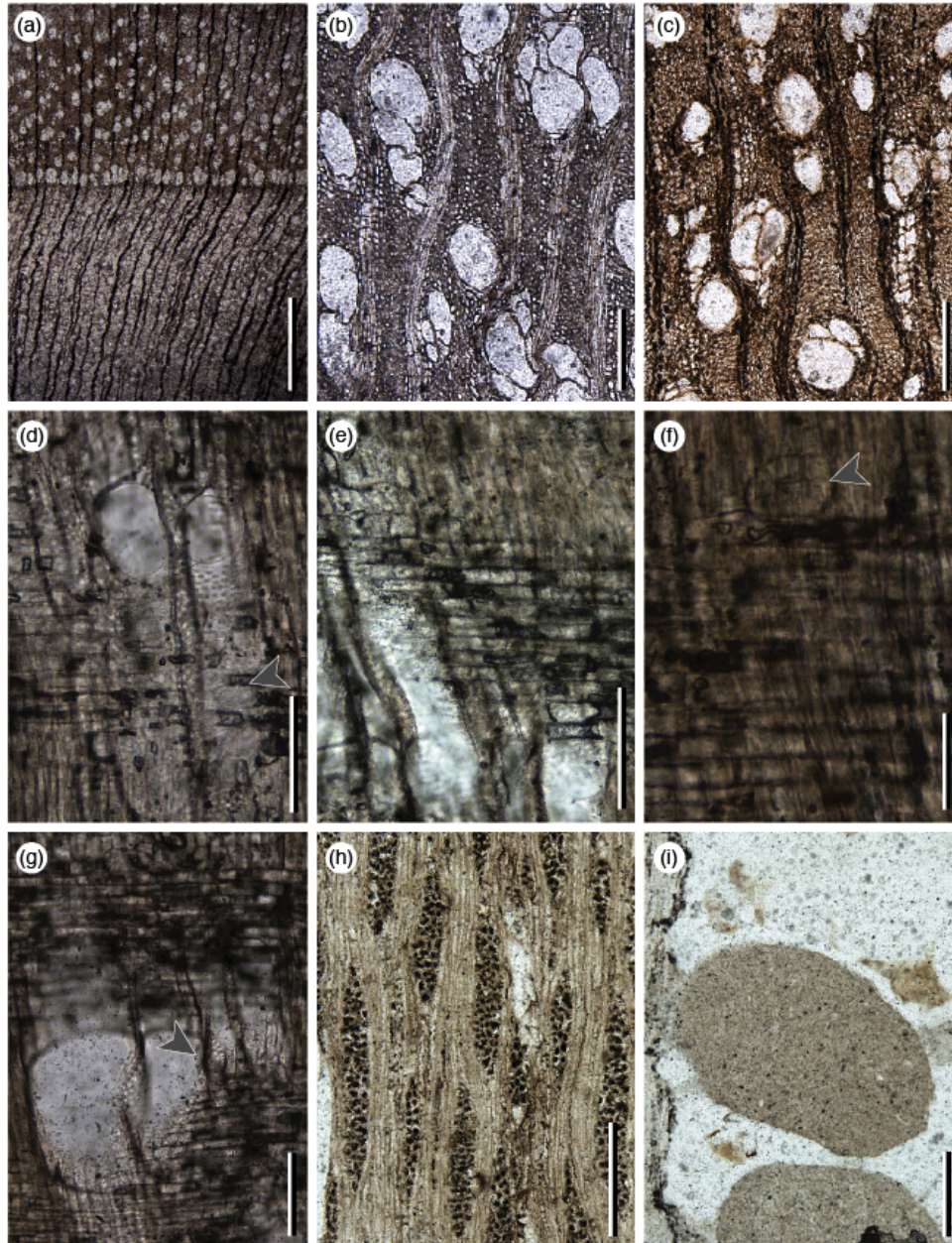


**Fig. S19. Wood anatomy DSB3.**

Wood anatomy DSB3 (*Anacardioxylon* affinity; STRI-MUSM 36598). (a) Semi-ring porous wood with distinct growth rings to diffuse porous; TS; scale bar = 1000  $\mu\text{m}$ . (b,c) Vessels are in radial multiples, clusters or solitary; TS; scale bars = 200  $\mu\text{m}$ . (d) Simple perforations plates. Arrow shows vessel–parenchyma pits with much reduced borders to apparently simple; RLS; scale bar = 100  $\mu\text{m}$ . (e) Heterocellular rays; RLS; scale bar = 100  $\mu\text{m}$ . (f) Arrow shows a prismatic crystal in a marginal ray cell; RLS; scale bar = 50  $\mu\text{m}$ . (g) Very narrow vessel elements; RLS; scale bar = 100  $\mu\text{m}$ . (h) Multiseriate rays; TLS; scale bar = 200  $\mu\text{m}$ . (i) Dry-wood termite coprolites; TLS; scale bar = 200  $\mu\text{m}$ .

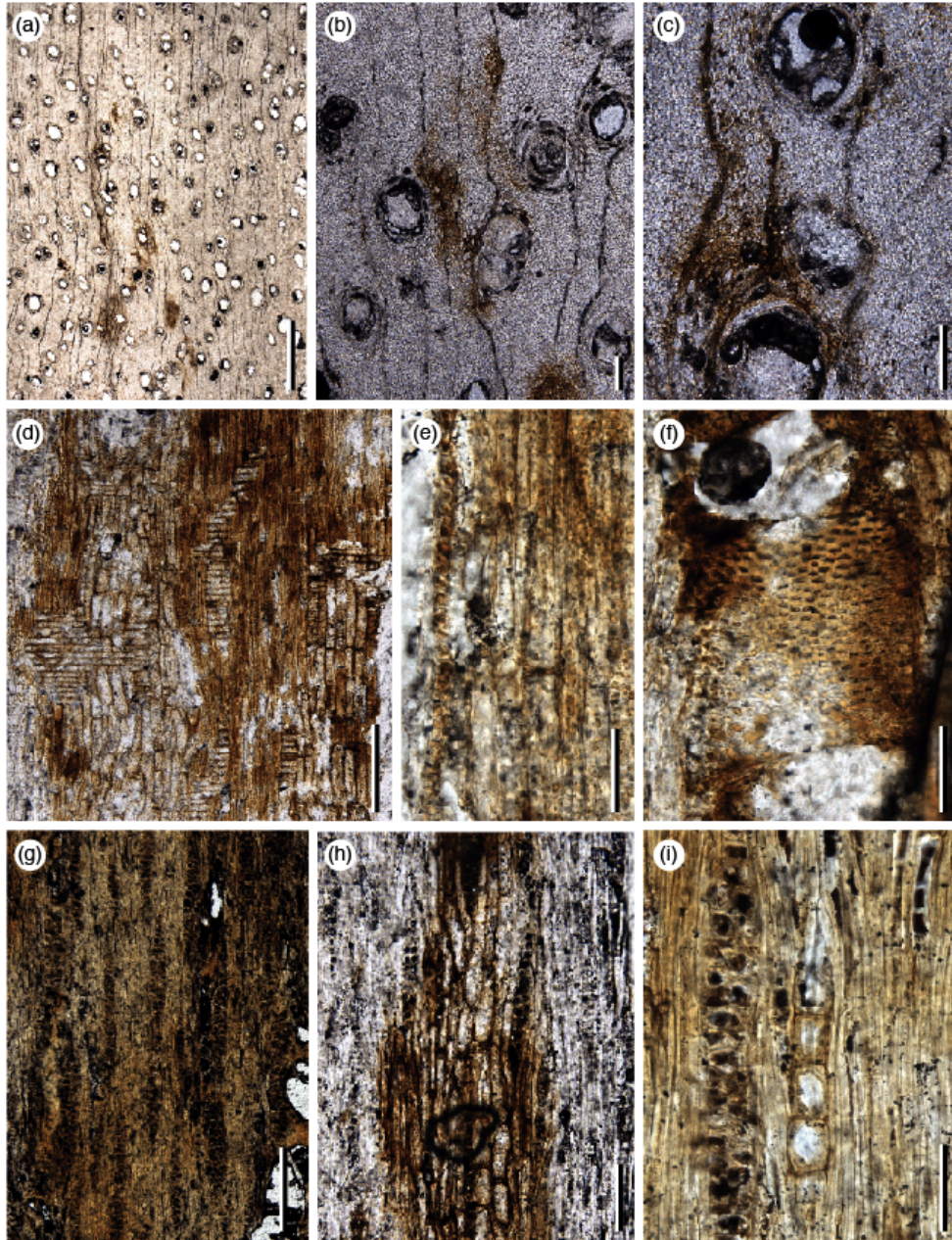


**Fig. S20. Wood anatomy DSB4.**

Wood anatomy DSB4 (Tribe Ingeae affinity; STRI-MUSM 44454). (a) Diffuse porous wood with mostly vessels solitary and indistinct growth rings; TS; scale bar = 1000  $\mu\text{m}$ . (b,c) Vasicentric axial parenchyma; TS; scale bars = 100  $\mu\text{m}$ . (d) Homocellular rays; RLS; scale bar = 200  $\mu\text{m}$ . (e) Prismatic crystals in chambered fibers; RLS; scale bar = 50  $\mu\text{m}$ . (f) Short vessel elements with simple perforation plates; RLS; scale bar = 50  $\mu\text{m}$ . (g) Multiseriate rays; TLS; scale bar = 100 $\mu\text{m}$ . (h) Axial parenchyma strands with 5 to 8 cells high; TLS; scale bar = 100 $\mu\text{m}$ . (i) Prismatic crystals in chambered axial parenchyma; scale bar = 50  $\mu\text{m}$ .

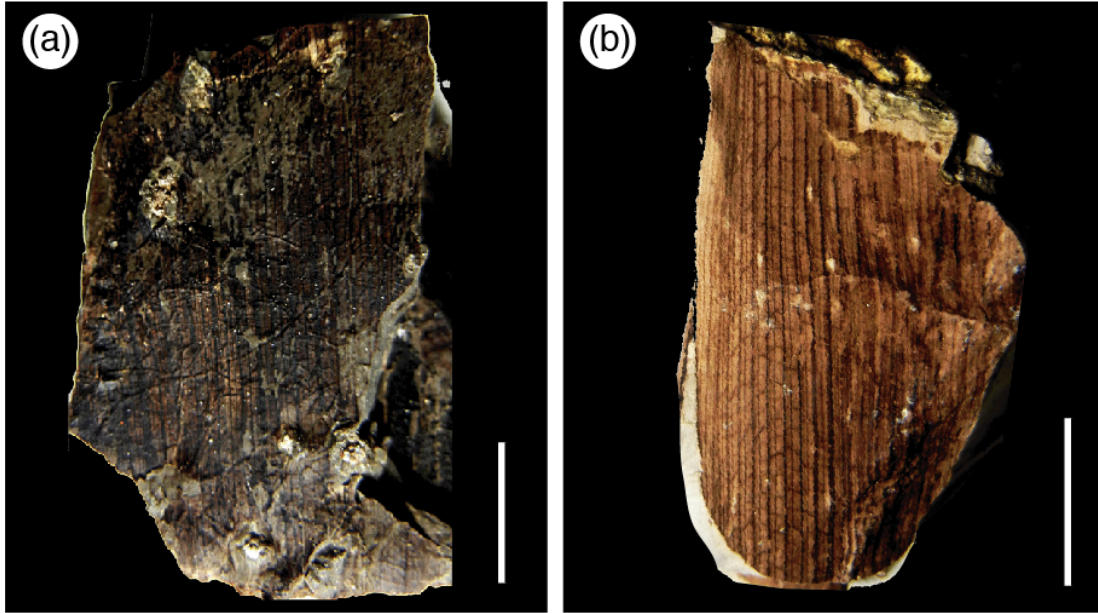


**Fig. S21. Leaf fragments DSB5.**

Leaf fragments DSB5 (Arecaceae affinity) showing fine venation details. Scale bars = 0.5 cm.  
(a) STRI-MUSM 39439. (b) STRI-MUSM 41424

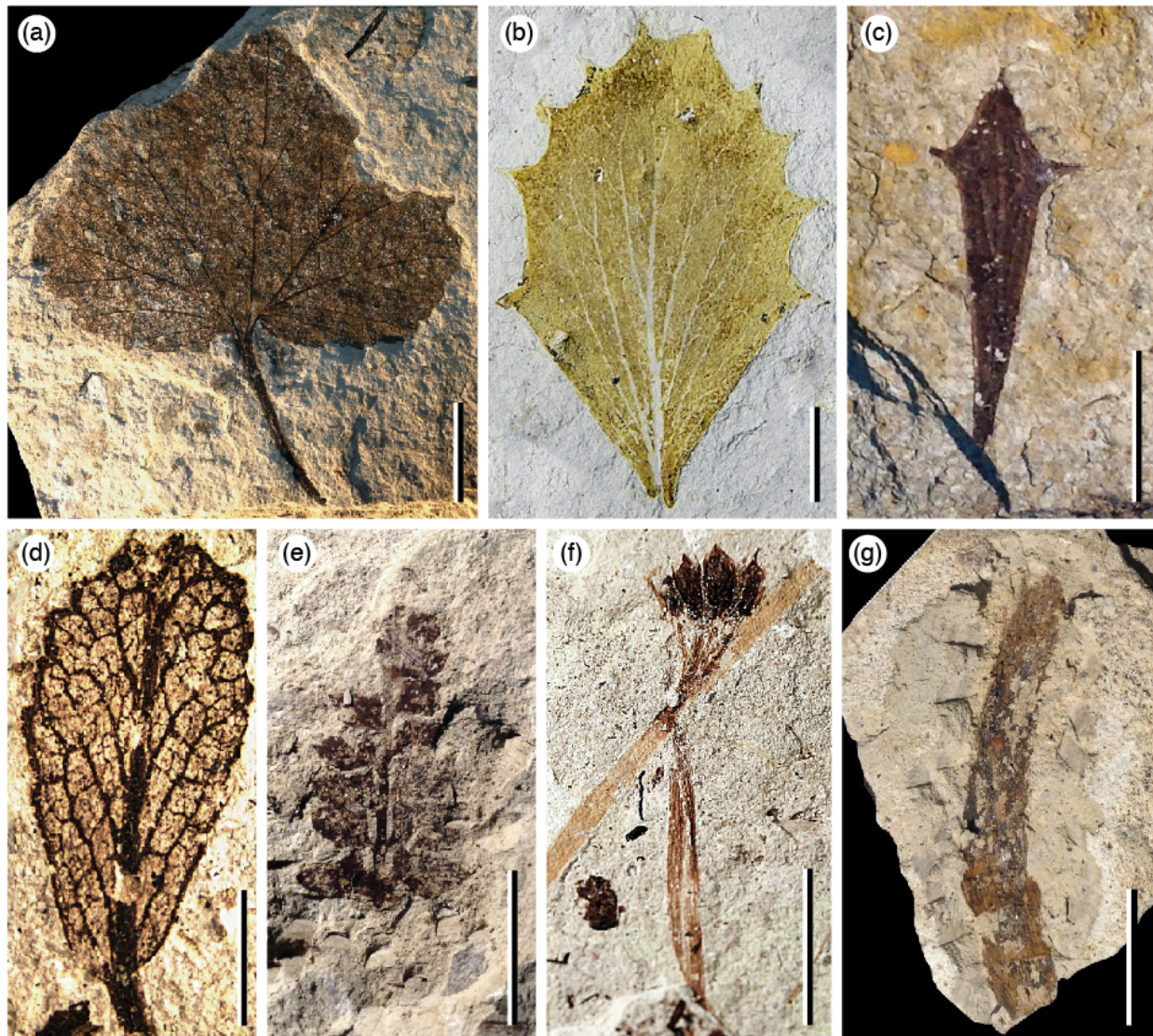


**Fig. S22. Macrofossil compressions and impressions from Member C.**

Macrofossil compressions and impressions of leaves and fruits. (a) Leaf DSC1 (*Ribes* affinity; STRI-MUSM 44870). Scale bar = 1 cm. (b) Leaf DSC2 (*Berberis* affinity; STRI-MUSM 41428). Scale bar = 0.5 cm. (c) Leaf DSC3 (*Berberis* affinity; STRI-MUSM 44871). Scale bar = 0.5 cm. (d) Leaf DSC4 (*Polylepis* affinity; STRI-MUSM 44894). Scale bar = 0.25 cm. (e) Branch DSC5 (*Polystichum* affinity; STRI-MUSM 43483). Scale bar = 1 cm. (f) Infructescence DSC6 (Juncaceae affinity; STRI-MUSM 41411). Scale bar = 0.5 cm. (g) Stem DSC7 (*Equisetum* affinity; STRI-MUSM 39326). Scale bar = 1 cm.

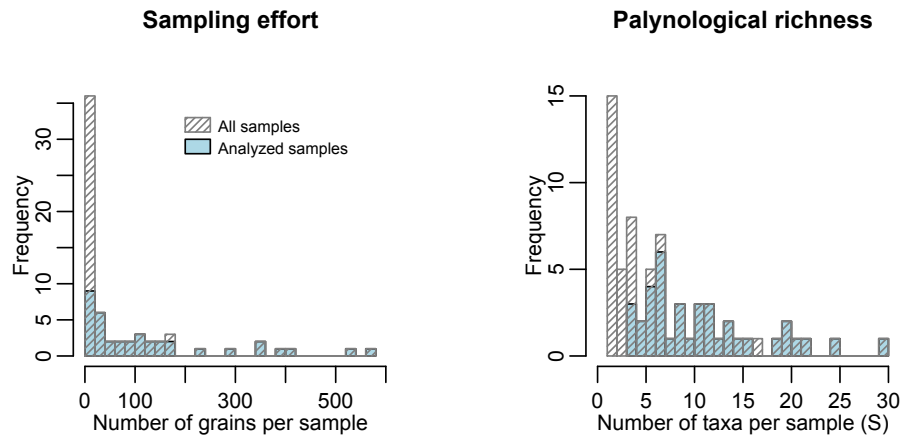


**Fig. S23. Palynological counts and number of taxa.**

Comparison of palynological counts (left) and number of taxa (right) present in all the fossil pollen samples and samples selected for quantitative estimations of elevation and precipitation.

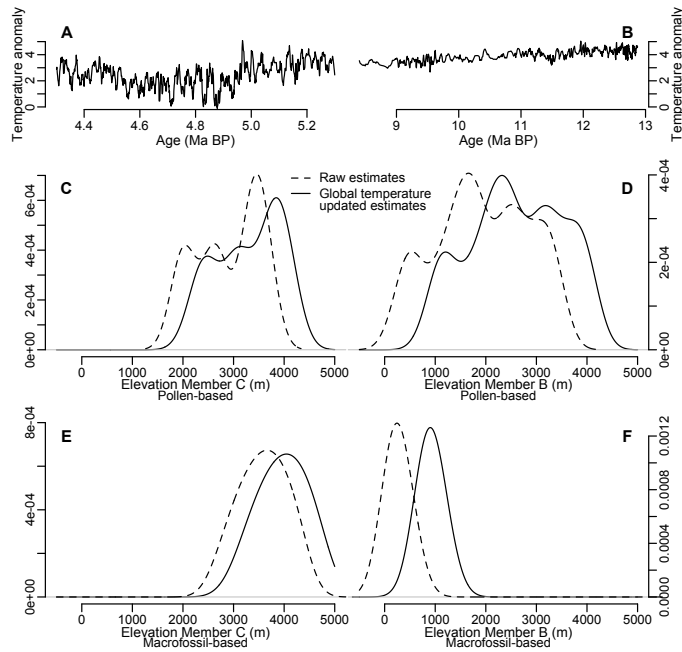


**Fig. S24. Correction of temperature estimates by global temperature anomaly.**

Correction of temperature estimates by global temperature anomaly through the periods encompassed by the sampled time intervals. Global temperature anomalies for stratigraphic members C (A) and B (B) (data from Hansen et al. 2013). Probability density distributions of raw (dashed lines) and updated estimates (solid line) for: C. Pollen-based Member C; D. Pollen-based Member B; E. Macrofossil-based Member C; F. Pollen-based Member B.

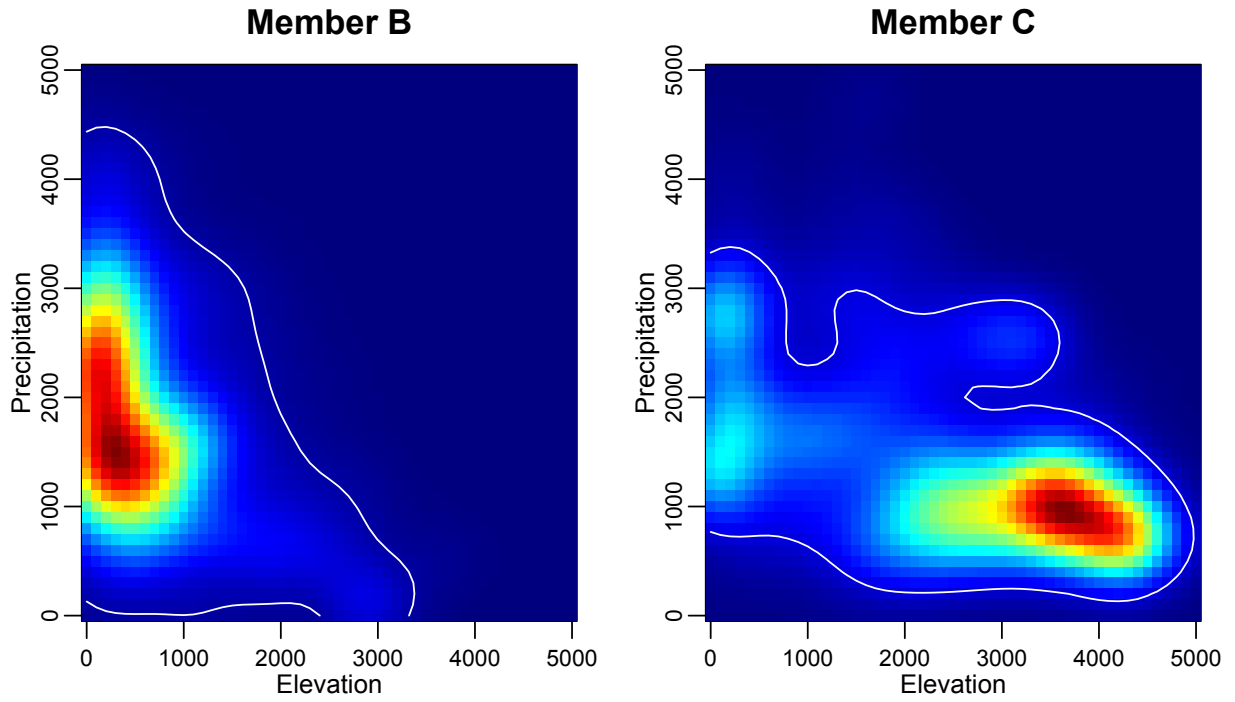


**Fig. S25. Probability density for environmental space.**

Probability density for elevation and precipitation for the Miocene Member B and the Pliocene Member C.

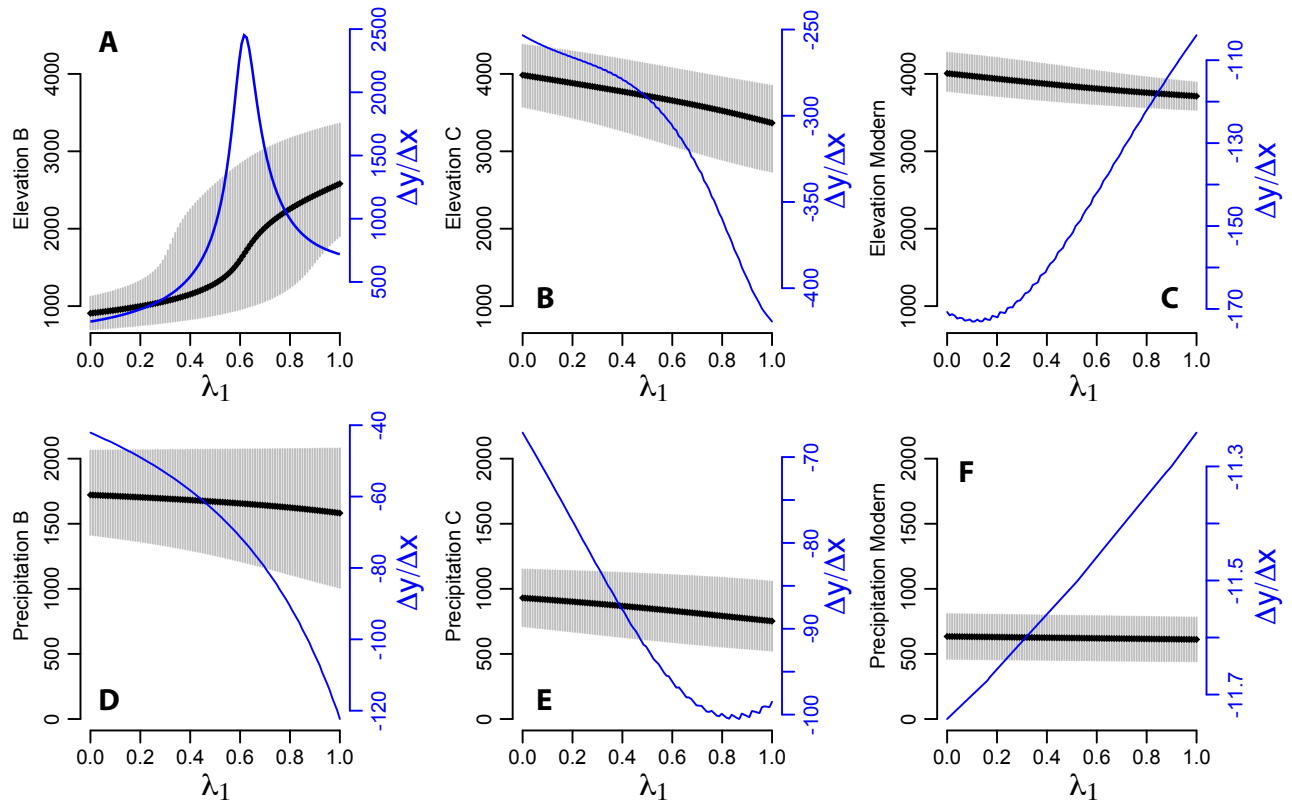


**Fig. S26. Elevation and precipitation estimates under the mixture model.**

Elevation (A to C) and precipitation estimates (D to F) as a function of microfossil representation factor in the mixture model ( $\lambda_1$ ; first derivative in blue). Estimate median shown by the black line with interquartile range represented by gray shadows.

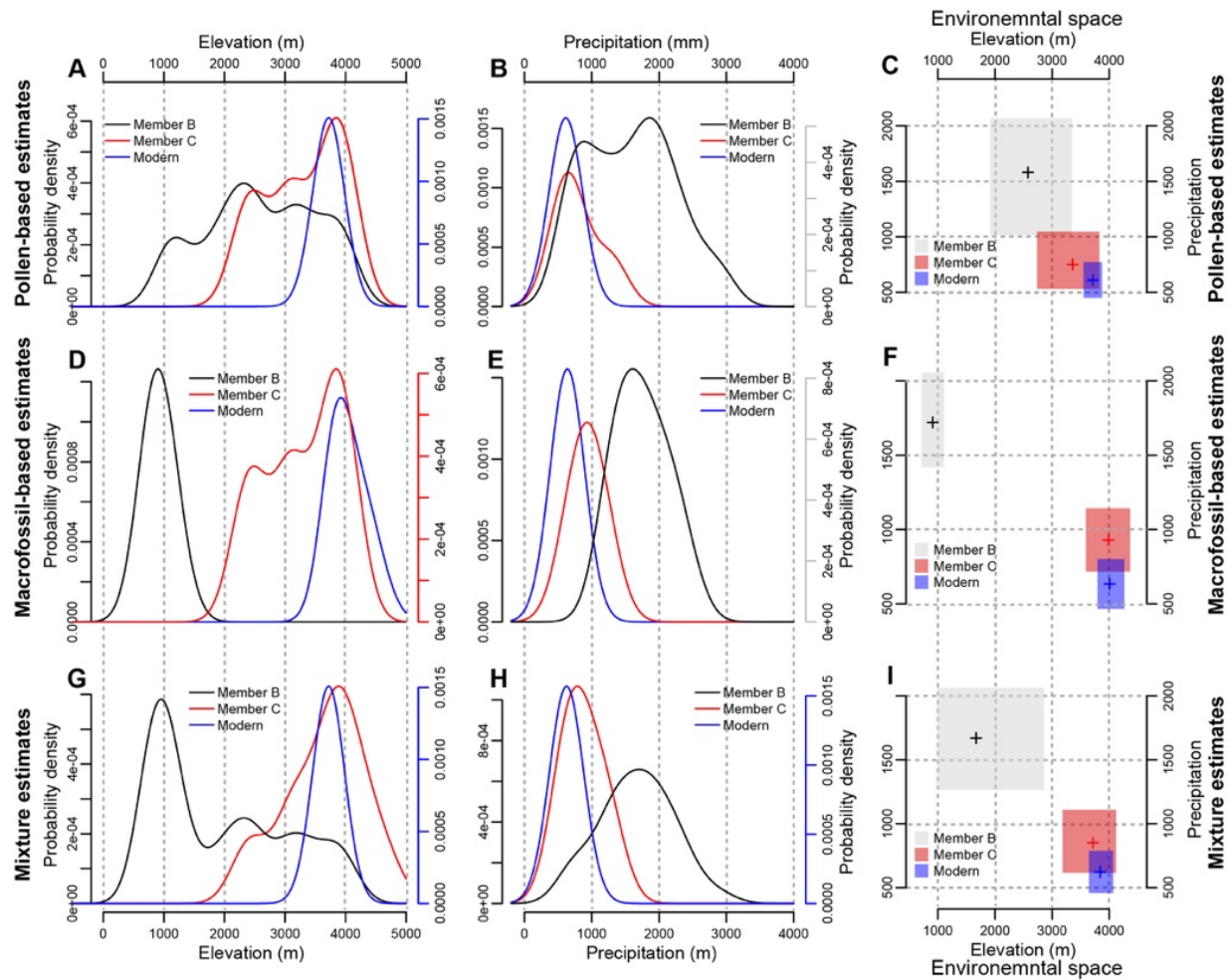


**Fig. S27. Marginal probability density distributions for elevation and precipitation.** Marginal probability density distributions for elevation and precipitation estimated for members A and B based on pollen (A and B) and macrofossil (D and E) data, and a micro- and macrofossils mixture model (G and H). The resulting environmental space produced by the combination of elevation and precipitation using each approach is shown in panels C (microfossils), F (macrofossils), and I (Mixture model).

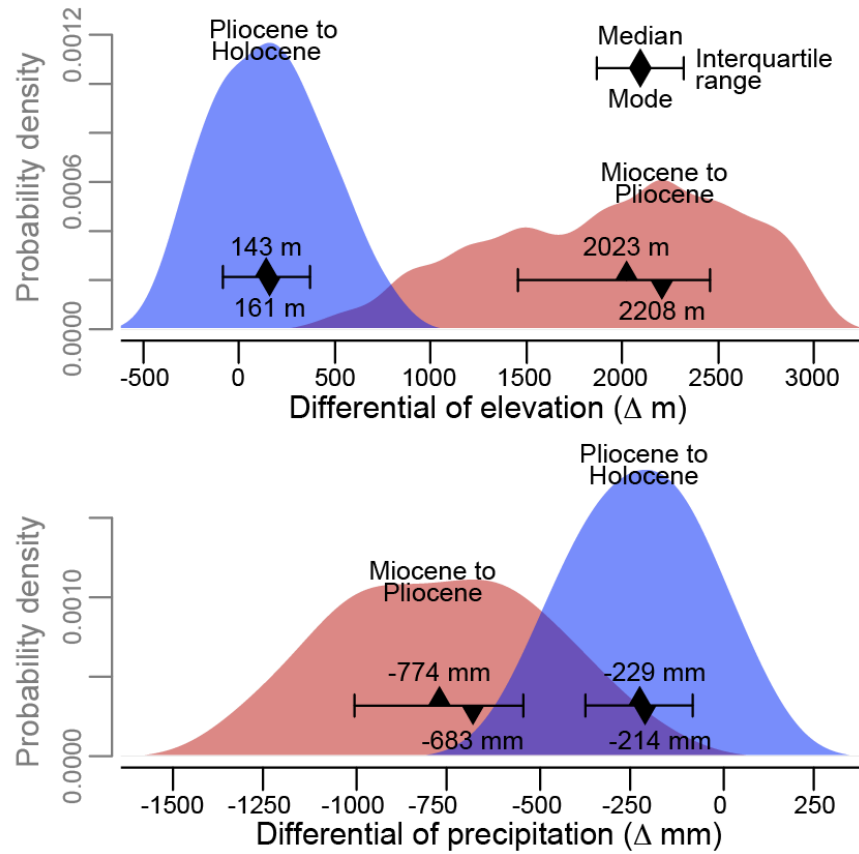


**Fig. S28. Credible distribution of elevation and precipitation.**

Credible distribution of elevation and precipitation changes from the late Miocene to the early Pliocene, and from the Early Pliocene to the Holocene at Espinar, Peruvian Andean highlands.

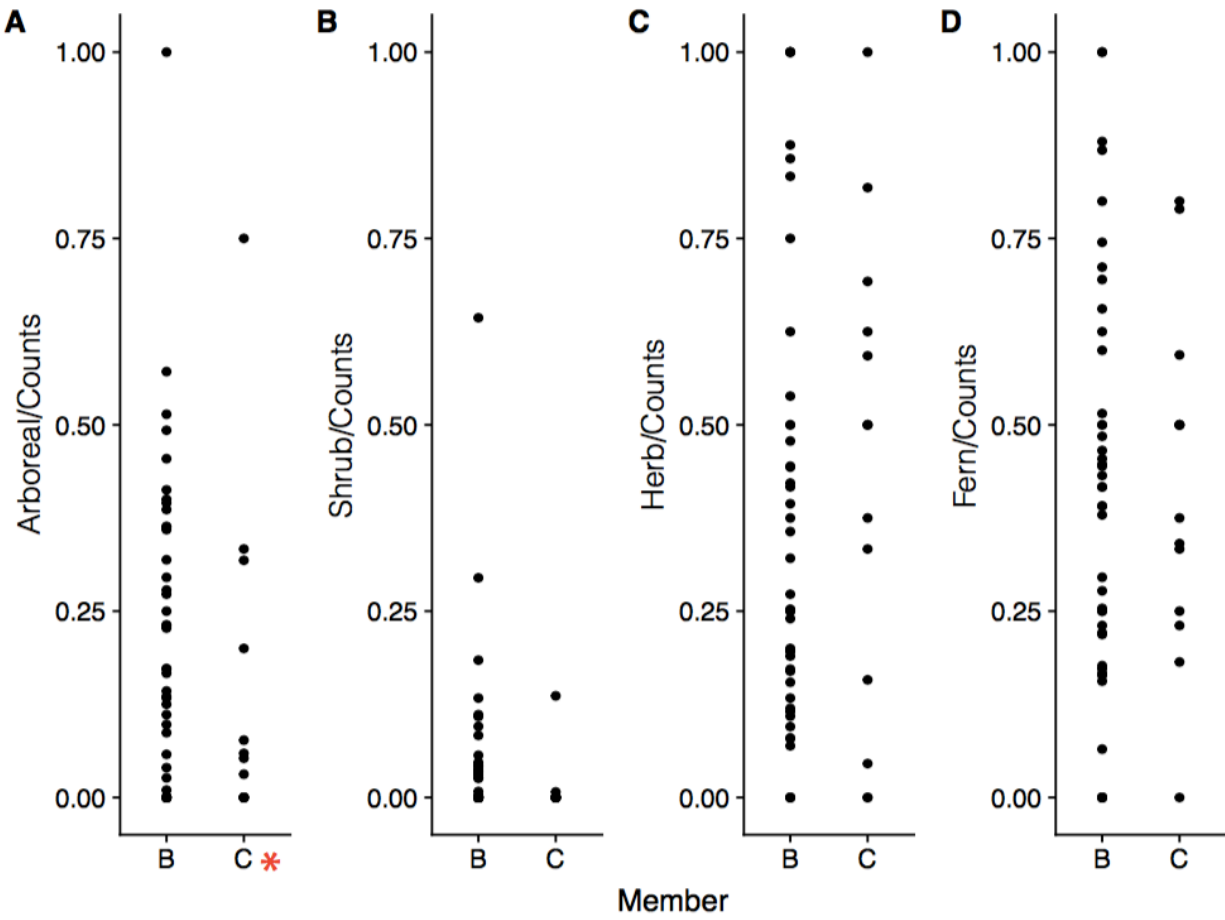


**Fig. S29. Generalized linear model comparison for plant habit.**

Generalized linear model comparing the plant habit between Members B and C. A. Arboreal. B. Shrub. C. Herb. D. Fern. The red asterisk indicates significant differences.

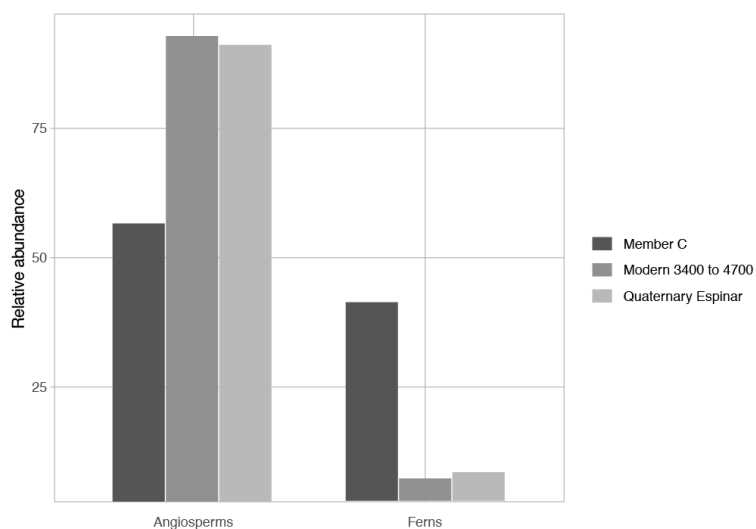


**Fig. S30. Comparison of the relative abundance of angiosperm and fern taxa.** Comparison of the relative abundance of angiosperm and fern taxa estimated from the palynoflora from the Member C, a quaternary sample from Espinar, and modern Altiplano records from GBIF.org

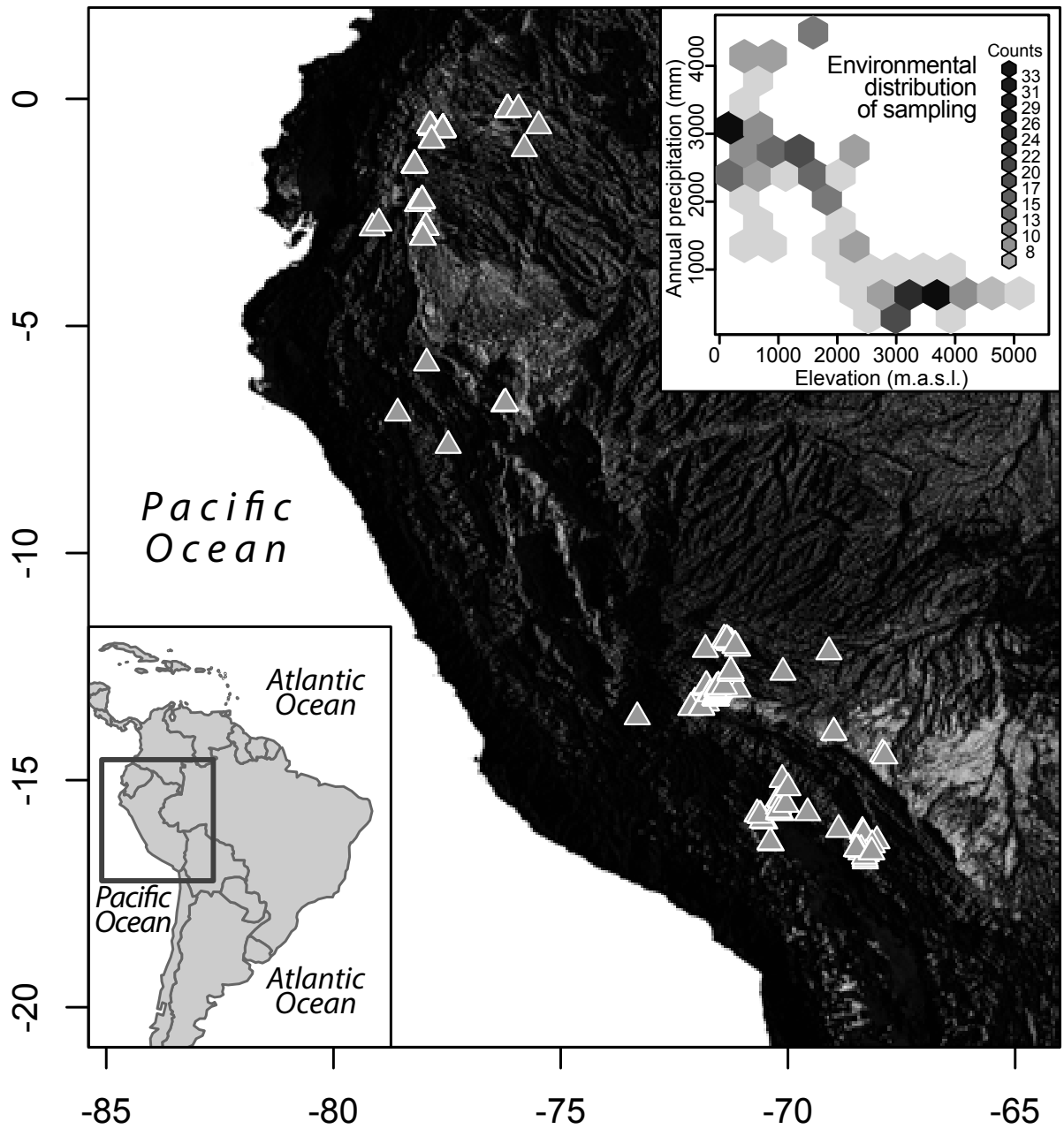


**Fig. S31 Modern palynological dataset.**

Modern palynological dataset, showing the geographic location of the sites and the environmental distribution of the sites (elevation and mean annual precipitation).

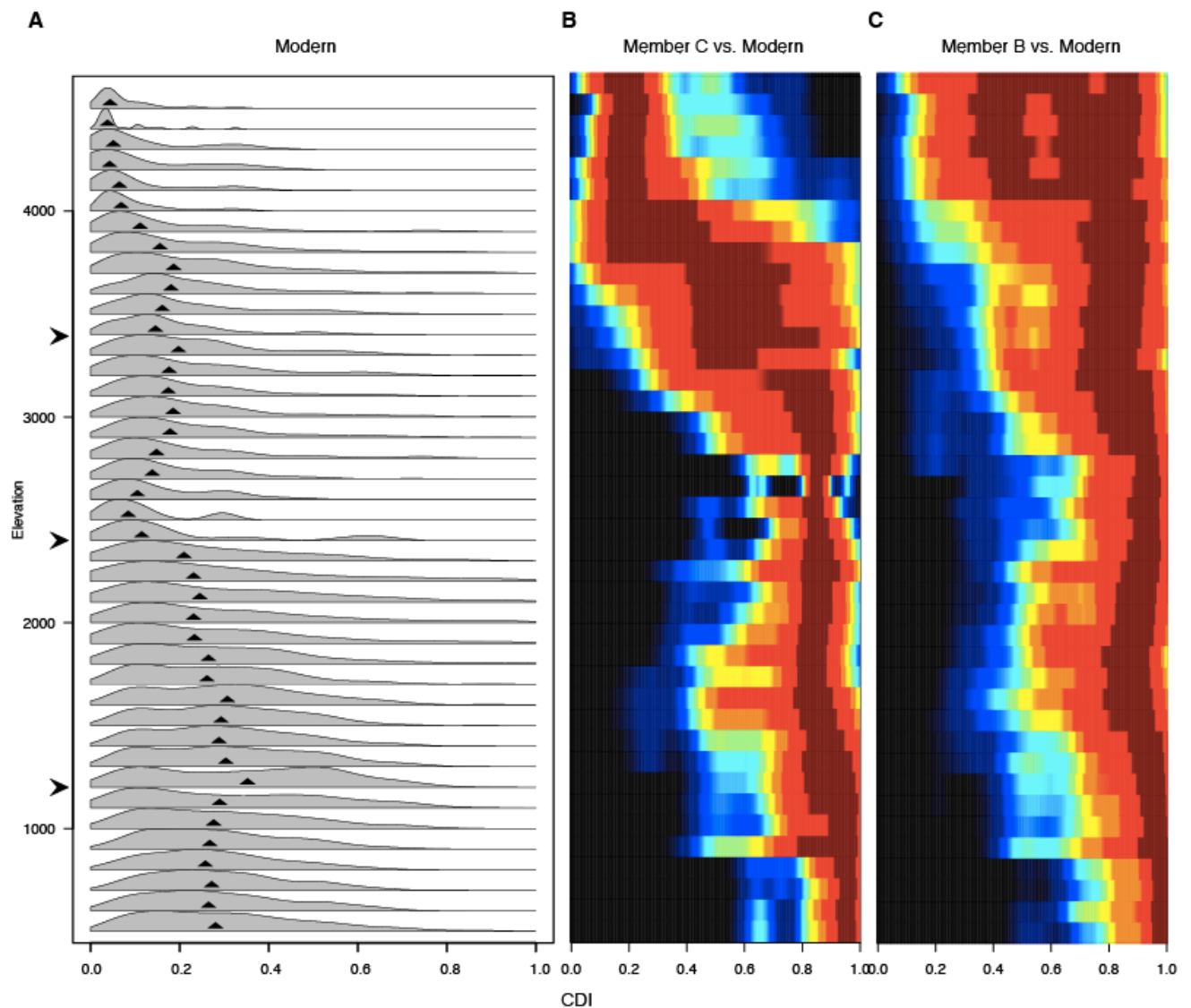


**Fig. S32. Palynoflora composition along an altitudinal gradient.**

Chao Dissimilarity Index (CDI) to evaluate similarities in the palynoflora composition along an altitudinal gradient. In the CDI 0 is the least dissimilar and 1 the most dissimilar A. Probability density plots for overlapped intervals of 250 m. Wider plots represent more dissimilar samples, and narrower plots represent more similar samples. The triangles inside each plot represent the median. Black arrows in the y axis represent the breaks to propose altitudinal ranges: 0–1200 m, 1200 – 2400 m, 2400 – 3400 m, and 3400 – 4700 m. B. Probability density of Member C palynoflora compared with modern intervals along the entire gradient. C. Probability density of Member B palynoflora compared with modern intervals along the entire gradient. Dark red indicates higher probability, and dark blue lower probability.

**Table S1. U-Pb geochronological analyses.**

Data from U-Pb geochronological analyses for two samples. STRI 44449 was collected in the Colpamayo region at 14.6371°S and 71.36393°W at 3923 m of elevation and STRI 44448 was collected in the San Miguel region at 14.67194°S and 71.29971°W at 3957 m of elevation.

Analysis	Isotope ratios										Apparent ages (Ma)								
	U (ppm)	206Pb 204Pb	U/Th	206Pb* 207Pb*	± (%)	207Pb* 235U*	± (%)	206Pb* 238U	± (%)	error corr.	206Pb* 238U*	± (Ma)	207Pb* 235U	± (Ma)	206Pb* 207Pb*	± (Ma)	Best age (Ma)	± (Ma)	Conc (%)
<b>STRI-44449</b>																			
z01	188	10957	0.7	22.5881	4.2	0.0119	5.2	0.0019	3.1	0.60	12.5	0.4	12.0	0.6	NA	NA	12.5	0.4	NA
z02	600	33867	2.5	21.3656	1.6	0.0260	3.3	0.0040	2.9	0.87	25.9	0.7	26.1	0.8	39.3	38.9	25.9	0.7	NA
z03	101	643	0.9	40.2937	4.6	0.0098	5.8	0.0029	3.6	0.61	18.5	0.7	9.9	0.6	NA	NA	18.5	0.7	NA
z04	183	10729	1.2	22.4469	3.3	0.0381	4.0	0.0062	2.2	0.56	39.9	0.9	38.0	1.5	NA	NA	39.9	0.9	NA
z05	724	7634	1.5	21.1549	2.4	0.0181	3.4	0.0028	2.4	0.70	17.9	0.4	18.3	0.6	62.9	58.3	17.9	0.4	NA
z06	727	26852	3.2	21.3777	1.6	0.0178	2.9	0.0028	2.5	0.84	17.8	0.4	17.9	0.5	37.9	38.4	17.8	0.4	NA
z07	71	959	1.0	38.3708	4.8	0.0124	6.5	0.0034	4.3	0.66	22.2	0.9	12.5	0.8	NA	NA	22.2	0.9	NA
z08	383	22387	2.1	21.4429	1.5	0.0408	3.4	0.0063	3.1	0.90	40.8	1.3	40.6	1.4	30.6	35.4	40.8	1.3	NA
z09	474	6034	1.4	20.9058	4.0	0.0136	5.0	0.0021	3.0	0.60	13.3	0.4	13.7	0.7	91.0	93.9	13.3	0.4	NA
z10	357	13243	0.8	20.6172	2.8	0.0173	4.3	0.0026	3.3	0.77	16.6	0.5	17.4	0.7	123.9	65.0	16.6	0.5	NA
z11	324	15786	3.7	20.9631	2.9	0.0218	4.4	0.0033	3.3	0.74	21.3	0.7	21.9	0.9	84.5	69.8	21.3	0.7	NA
z12	370	6653	1.1	21.9302	3.2	0.0216	4.3	0.0034	3.0	0.69	22.1	0.7	21.7	0.9	NA	NA	22.1	0.7	NA
z13	73	102622	2.2	20.1809	4.0	0.0436	5.1	0.0084	3.3	0.63	41.0	1.3	43.3	2.2	174.0	92.8	41.0	1.3	NA
z15	639	34424	5.4	18.8460	1.0	0.1495	2.6	0.0204	2.4	0.92	130.4	3.1	141.5	3.4	331.5	23.3	130.4	3.1	NA
z16	244	5936	1.1	19.7087	3.5	0.0225	4.6	0.0032	2.9	0.64	20.7	0.6	22.6	1.0	229.0	81.8	20.7	0.6	NA
z17	87	11560	1.9	21.3628	4.3	0.0411	4.9	0.0064	2.3	0.47	41.0	0.9	40.9	2.0	39.6	103.7	41.0	0.9	NA
z21	544	5134	0.9	22.4587	2.9	0.0108	4.1	0.0018	2.9	0.71	11.4	0.3	10.9	0.4	NA	NA	11.4	0.3	NA
z22	826	34582	1.1	20.0709	2.8	0.0133	3.9	0.0019	2.8	0.71	12.4	0.3	13.4	0.5	186.7	64.7	12.4	0.3	NA
z23	744	106302	3.2	21.2953	2.6	0.0169	3.6	0.0026	2.5	0.69	16.8	0.4	17.0	0.6	47.1	62.3	16.8	0.4	NA
z24	587	40547	0.7	21.4411	1.7	0.0391	3.9	0.0061	3.5	0.90	39.1	1.3	38.9	1.5	30.8	41.0	39.1	1.3	NA
z25	100	1849	1.8	24.6950	4.1	0.0240	5.2	0.0043	3.2	0.62	27.7	0.9	24.1	1.2	NA	NA	27.7	0.9	NA
z26	229	12646	0.9	18.6411	3.6	0.0185	5.0	0.0022	3.4	0.68	14.3	0.5	16.6	0.8	356.2	81.8	14.3	0.5	NA
z27	139	30339	1.4	21.7329	4.3	0.0211	5.6	0.0033	3.5	0.63	21.4	0.7	21.2	1.2	NA	NA	21.4	0.7	NA
z28	118	3138	0.9	23.0060	7.2	0.0163	8.4	0.0027	4.4	0.52	17.5	0.8	16.4	1.4	NA	NA	17.5	0.8	NA
z29	153	2265	1.3	26.5886	3.8	0.0169	5.4	0.0033	3.8	0.71	21.0	0.8	17.1	0.9	NA	NA	21.0	0.8	NA
z30	140	2126	1.4	23.0765	5.2	0.0117	6.2	0.0020	3.3	0.53	12.6	0.4	11.8	0.7	NA	NA	12.6	0.4	NA
z31	281	17161	1.0	20.4268	3.5	0.0122	4.7	0.0018	3.2	0.67	11.7	0.4	12.3	0.6	145.8	82.1	11.7	0.4	NA
z34	111	1475	0.5	5.6325	29.9	0.0592	30.8	0.0024	7.6	0.25	15.6	1.2	58.4	17.5	2630.0	509.9	15.6	1.2	NA
z35	133	3231	1.6	21.1590	3.2	0.0397	4.3	0.0061	2.9	0.68	39.2	1.1	39.5	1.7	62.5	75.8	39.2	1.1	NA
																	130.4		
<b>STRI-44448</b>																			
z01	229	9391	0.7	20.4234	4.4	0.0168	6.1	0.0025	4.2	0.70	16.0	0.7	16.9	1.0	146.1	102.5	16.0	0.7	NA
z02	175	82028	2.4	21.6361	5.0	0.0103	6.1	0.0016	3.6	0.59	10.5	0.4	10.5	0.6	9.1	119.3	10.5	0.4	NA
z03	445	2450	0.3	7.1598	18.9	0.0331	19.2	0.0017	3.7	0.19	11.1	0.4	33.1	6.3	2223.1	330.3	11.1	0.4	NA
z04	186	914	1.0	28.1482	16.1	0.0071	16.7	0.0014	4.5	0.27	9.3	0.4	7.1	1.2	NA	NA	9.3	0.4	NA
z05	299	11290	0.8	11.3046	13.1	0.0201	13.4	0.0016	2.9	0.22	10.6	0.3	20.2	2.7	1392.5	252.4	10.6	0.3	NA
z06	321	12034	0.8	19.5301	4.0	0.0111	4.9	0.0016	2.8	0.58	10.1	0.3	11.2	0.5	250.0	92.1	10.1	0.3	NA
z07	688	12775	0.7	14.0938	5.0	0.0161	5.8	0.0016	3.0	0.52	10.6	0.3	16.2	0.9	956.0	102.1	10.6	0.3	NA
z08	216	4046	1.2	20.5814	5.6	0.0106	6.6	0.0016	3.5	0.53	10.2	0.4	10.7	0.7	128.0	131.2	10.2	0.4	NA
z09	699	162024	1.7	19.0327	2.4	0.0117	3.5	0.0016	2.5	0.73	10.4	0.3	11.8	0.4	309.0	54.2	10.4	0.3	NA
z10	230	1673	0.9	26.2179	11.9	0.0081	12.3	0.0015	3.1	0.25	9.9	0.3	8.2	1.0	NA	NA	9.9	0.3	NA
z11	277	5848	0.9	22.0280	4.6	0.0098	5.6	0.0016	3.1	0.56	10.1	0.3	9.9	0.6	NA	NA	10.1	0.3	NA
z12	95	4670	1.7	19.4797	6.1	0.0107	7.7	0.0015	4.7	0.61	9.8	0.5	10.8	0.8	255.9	139.5	9.8	0.5	NA
z13	180	877	1.3	28.0052	7.1	0.0079	7.9	0.0016	3.5	0.45	10.3	0.4	8.0	0.6	NA	NA	10.3	0.4	NA
z14	322	4603	1.1	21.0458	4.4	0.0099	5.8	0.0015	3.8	0.65	9.8	0.4	10.0	0.6	75.2	105.0	9.8	0.4	NA
z15	136	3176	1.3	18.9353	6.7	0.0114	7.6	0.0016	3.6	0.47	10.1	0.4	11.5	0.9	320.7	152.5	10.1	0.4	NA
z16	52	6306	1.4	17.9957	6.9	0.0229	8.0	0.0030	4.2	0.52	19.2	0.8	23.0	1.8	435.2	153.4	19.2	0.8	NA
z17	472	12919	0.8	16.5177	5.4	0.0147	6.1	0.0018	2.8	0.45	11.3	0.3	14.8	0.9	623.0	116.7	11.3	0.3	NA
z18	290	20165	0.8	20.4566	2.9	0.0228	4.7	0.0034	3.7	0.78	21.7	0.8	22.8	1.1	142.3	69.2	21.7	0.8	NA
z19	175	379228	1.4	16.6105	1.1	0.7692	3.3	0.0927	3.1	0.95	671.5	16.9	579.3	14.4	610.8	22.9	571.5	16.9	93.6
z20	142	1150	1.1	38.9677	5.6	0.0054	6.7	0.0015	3.6	0.54	9.9	0.4	5.5	0.4	NA	NA	9.9	0.4	NA
z21	1215	38248	0.5	20.9886	1.8	0.0170	3.7	0.0026	3.3	0.87	16.7	0.5	17.2	0.6	81.7	43.5	16.7	0.5	NA
z22	251	68642	1.0	18.1122	5.1	0.0116	6.0	0.0015	3.1	0.51	9.8	0.3	11.7	0.7	420.8	114.0	9.8	0.3	NA
z23	121	2667	1.1	4.5644	34.8	0.0560	35.0	0.0019	4.0	0.11	12.0	0.5	55.4	18.9	2974.0	581.6	12.0	0.5	NA
z24	184	3354	1.6	24.0686	7.1	0.0085	7.9	0.0015	3.6	0.45	9.5	0.3	8.6	0.7	NA	NA	9.5	0.3	NA
z25	462	4657	0.6	5.3598	17.0	0.0452	17.2	0.0018	3.0	0.17	11.3	0.3	44.9	7.6	2712.2	282.0	11.3	0.3	NA
z26	220	9305	0.7	22.0487	3.4	0.0222	4.8	0.0035	3.4	0.71	22.8	0.8	22.3	1.1	NA	NA	22.8	0.8	NA
z27	98	1575	1.0	25.7202	13.2	0.0086	14.2	0.0016	5.3	0.37	10.3	0.5	8.7	1.2	NA	NA	10.3	0.5	NA
z28	721	16696	1.8	21.0337	2.5	0.0103	3.8	0.0016	2.8	0.75	10.1	0.3	10.4	0.4	76.6	80.1	10.1	0.3	NA
z29	189	1427	1.2	28.0092	15.6	0.0076	15.9	0.0016	3.2	0.20	10.0	0.3	7.7	1.2	NA	NA	10.		

**Table S2. Palynological samples.**

Palynological samples. Information from the 75 palynological samples studied from Member B and C and two quaternary samples collected from a swamp.

STRI ID	Member	Section	Segment	Depth (m)	Cumulative depth (m)	Palynomorphs	Morphotypes/sample
39443	B	San Miguel	Segment A	4.2	504.2	389	19
39444	B	San Miguel	Segment A	4.3	504.3	7	4
39445	B	San Miguel	Segment A	11	511	0	0
39446	B	San Miguel	Segment A	12.5	512.5	4	2
39447	B	San Miguel	Segment A	14	514	4	3
39449	B	San Miguel	Segment B	6.5	544.5	290	23
39450	B	San Miguel	Segment B	9.5	547.5	59	8
39451	B	San Miguel	Segment B	10.5	548.5	0	0
39452	B	San Miguel	Segment B	15.5	553.5	130	22
39453	B	San Miguel	Segment B	25.3	563.3	8	4
39454	B	San Miguel	Segment B	29	567	1	1
39455	B	San Miguel	Segment B	33	571	8	4
39456	B	San Miguel	Segment B	33.3	571.3	118	16
39457	B	San Miguel	Segment B	48	586	155	14
39458	B	San Miguel	Segment B	48.1	586.1	408	29
39460	B	San Miguel	Segment C	39	631	527	39
39459	B	San Miguel	Segment C	48	640	53	11
39461	B	San Miguel	Segment E	6.5	679.5	100	13
39463	B	San Miguel	Segment E	51.1	724.1	0	0
39464	B	San Miguel	Segment E	51.2	724.2	6	2
39465	B	San Miguel	Segment E	53.5	726.5	5	3
39467	B	San Miguel	Segment E	81	754	6	3
39466	B	San Miguel	Segment E	81.05	754.05	1	1
39468	B	San Miguel	Segment E	81.1	754.1	0	0
39698	B	San Miguel	Segment F	3	903	1	1
39699	B	San Miguel	Segment F	5	905	9	4
39701	B	San Miguel	Segment F	9	909	12	7
39700	B	San Miguel	Segment F	13	913	1	1
39702	B	San Miguel	Segment F	20	920	38	6
39703	B	San Miguel	Segment F	24	924	24	10
39706	B	San Miguel	Segment G	1	941	12	7
39704	B	San Miguel	Segment G	1.5	941.5	14	7
36583	B	San Miguel	Segment G	9.5	949.5	88	11
39705	B	San Miguel	Segment G	10	950	571	13
39713	B	San Miguel	Segment H	3	1038	102	9
39714	B	San Miguel	Segment H	5	1040	11	6

39715	B	San Miguel	Segment I	2	1050	25	7
39716	B	San Miguel	Segment I	4	1052	1	1
40128	B	Top B		18	1398	1	1
36566	B	Accocunca N		21	1401	162	21
36590	B	Accocunca N		21.3	1401.3	66	10
36589	B	Accocunca N		22	1402	178	23
36569	B	Accocunca N		22.45	1402.45	407	30
36569_S2	B	Accocunca N		22.46	1402.46	352	26
36584	B	Accocunca N		26	1406	147	15
36591	B	Accocunca N		28	1408	18	10
36579	B	Accocunca N		29	1409	225	28
39718	B	San Miguel	Segment Q	4.6	1422.6	0	0
39719	B	San Miguel	Segment Q	22	1440	8	3
40130	B	Top B	Close Top		1600	0	0
39717	B	San Miguel	Segment R	5	1630	1	1
36582	B	Checca		0	1380	70	11
36587	B	Checca		15	1395	102	12
39710	B?	Palpatamayo	Esperanza		?	12	6
39709	B?	Palpatamayo	Esperanza		?	5	2
39708	B?	Palpatamayo	Esperanza		?	22	7
39707	B?	Palpatamayo	Esperanza		?	0	0
<b>Total B</b>						<b>4964</b>	<b>113</b>
40131	C	Cerro Pucara	Dump Pit	1.8	1601.8	5	3
40132	C	Cerro Pucara	Dump Pit	1.9	1601.9	2	2
39721	C	Cerro Pucara	Close Top	23	1623	11	4
39722	C	Cerro Pucara	Close Top	27	1627	3	3
39723	C	Cerro Pucara	Close Top	48	1648	8	3
39724	C	Cerro Pucara	Close Top	52	1652	1	1
39725	C	Cerro Pucara	Close Top	56	1656	0	0
36573	C	Huanu Huanu		1.6	1601.6	22	10
39364	C	Huanu Huanu	MIV	3	1603	32	11
36563	C	Huanu Huanu		3.2	1603.2	8	4
39361	C	Huanu Huanu	MIV	3.2	1603.2	19	9
36594	C	Huanu Huanu		3.3	1603.3	14	7
36592	C	Huanu Huanu		10.2	1610.2	6	4
40125	C	Huanu Huanu	Meter 11	11	1611	2	2
40126	C	Huanu Huanu	Meter 11	11.1	1611.1	0	0
40127	C	Huanu Huanu	Meter 11	11.2	1611.2	139	19
<b>Total C</b>						<b>272</b>	<b>47</b>
39726	Q	Swamp	Organic			179	20
40129	Q	Swamp	Organic			13	4
<b>Total Q</b>						<b>192</b>	<b>23</b>

**Table S3. Macrofossil samples.**

Macrofossil samples. Stratigraphic information associated with for the morphotypes described and number of samples per morphotype per locality by Member.

Affinity	Organ	Morphotype number	Taxon	Member B					Member C					
				430175	110066	110083 a,b,c,d	110044	610007	430160	430156	490011	110037	110040	110060
Stratigraphic depth (m)				950	1350-1500	1350-1500	1350-1500	~1550-1600	~1600	~1700-1800	~1700-1750	~1750-1800	~1700-1800	~1700-1800
DIC	Wood	DSB1	Ingeae			1	1							
DIC	Wood	DSB2	<i>Andiroxylon</i>					1						
DIC	Wood	DSB3	<i>Anacardioxylon</i>						1					
DIC	Wood	DSB4	Mimosoid		1	4								
MON	Leaf	DSB5	Arecaceae	5	5									
DIC	Leaf	DSC1	<i>Ribes</i> sp.							2				
DIC	Leaf	DSC2	<i>Berberis</i> sp.								1			
DIC	Leaf	DSC3	<i>Berberis</i> sp.							3	1			
DIC	Leaf	DSC4	<i>Polylepis</i> sp.							15		8		
FER	Leaf	DSC5	<i>Polystichum</i> sp.							1				
MON	Fertile	DSC6	Juncaceae											1
FER	Stem	DSC7	<i>Equisetum</i> sp.								1		1	

**Table S4. Fossil pollen taxa identified at family level.**

Fossil pollen taxa identified at family level and their representation in the modern pollen dataset.

<b>Fossil taxon</b>	<b>Represented in modern</b>	<b>Fossil taxon</b>	<b>Represented in modern</b>	<b>Fossil taxon</b>	<b>Represented in modern</b>
Alismataceae	*	Brassicaceae	*	Malpighiaceae	*
Amaranthaceae	*	Caryophyllaceae	*	Malvaceae	*
Anacardiaceae	*	Chenopodiaceae	*	Poaceae	*
Araceae	*	Cyperaceae	*	Polygonaceae	*
Araliaceae	*	Convolvulaceae	*	Portulacaceae	*
Arecaceae	*	Ericaceae	*	Lamiaceae	*
Asteraceae	*	Euphorbiaceae	*	Solanaceae	*
Bombacaceae	*	Fabaceae (Papil)	*		

**Table S5. Fossil pollen taxa identified at genus level.**

Fossil pollen taxa identified at genus level and their representation in the modern pollen dataset

Fossil taxon	Represented in modern	Fossil taxon	Represented in modern	Fossil taxon	Represented in modern
<i>Acacia</i>	*	<i>Ephedra</i>	*	<i>Opuntia</i>	
<i>Acalypha</i>	*	<i>Fuchsia</i>	*	<i>Podocarpus</i>	*
<i>Alnus</i>	*	<i>Grammitis</i>		<i>Polylepis</i>	*
<i>Ambrosia</i>	*	<i>Hedyosmum</i>	*	<i>Polypodium</i>	
<i>Anemia</i>		<i>Hemitelia</i>		<i>Quercus</i>	*
<i>Asplenium</i>		<i>Hymenophyllum</i>		<i>Selaginella</i>	
<i>Baccharis_Senecio</i>	*	<i>Hypolepys</i>		<i>Styloceras</i>	
<i>Blechnum</i>		<i>Inga</i>	*	<i>Thelypteris</i>	
<i>Bocconia</i>	*	<i>Iseia</i>	*	<i>Tillandsia</i>	*
<i>Celtis</i>	*	<i>Jamesonia</i>		<i>Trichilia</i>	*
<i>Ceratopteris</i>		<i>Juglans</i>	*	Unknown	
<i>Croton</i>	*	<i>Mirabilis</i>		<i>Valeriana</i>	*
<i>Cyathea</i>		<i>Mutisia</i>	*	<i>Vismia</i>	*
<i>Daphnopsis</i>	*	<i>Myrsine</i>	*	<i>Vochysia</i>	*
<i>Drymis</i>					

**Table S6. Elevation and precipitation estimates.**  
Elevation and precipitation estimates for palynological samples

Sample	Elevation (m)				Precipitation (mm)			
	Mean	Med.	Quantile 0.25	Quantile 0.75	Mean	Median	Quantile0.25	Quantile 0.75
C_7	3334	3300	3000	3700	540	500	300	700
C_8	2638	3100	2700	3500	773	700	500	1000
C_9	3584	3600	3225	3900	622	600	400	800
C_14	2012	1800	600	3600	1288	1300	700	1700
B_4.2	2726	3100	1700	3500	1050	700	500	1400
B_44.5	1440	1200	700	1700	1956	2400	1325	2700
B_47.5	3402	3400	3100	3700	639	600	400	800
B_53.5	1435	1150	800	1500	1777	1600	1325	2500
B_63.3	2283	3000	400	3300	859	800	600	1100
B_71.3	2418	1850	1400	3500	1501	2000	600	2400
B_86	1116	1100	900	1400	2080	2300	1500	2600
B_86.1	3185	3300	3000	3600	734	700	500	900
B_131	2400	3000	1400	3500	1275	900	600	2300
B_140	1456	700	325	3275	1132	1200	700	1500
B_179.5	1659	1500	700	2900	2281	2400	800	2875
B_409	1395	1100	400	1775	1689	1450	900	2600
B_420	551	300	100	400	2225	2050	1300	2800
B_424	1072	600	300	1475	1842	1500	1200	2775
B_441	518	500	200	700	2862	2800	2600	3100
B_441.5	402	400	200	600	1944	1600	1300	2800
B_449.5	3255	3400	3000	3800	763	650	400	800
B_450	2477	3200	525	3600	811	700	500	1200
B_538	3110	3200	2900	3600	628	600	425	800
B_540	600	500	225	900	2933	2900	2700	3100
B_550	1851	1800	1600	2100	2215	2500	2200	2700
B_901	2903	3300	1500	3700	1212	800	500	2400
B_901.3	945	500	200	1100	2531	2800	2500	3100
B_902	2674	3000	1800	3500	1382	800	500	2400
B_902.45	2674	3250	1300	3700	1105	800	500	1475
B_902.46	2272	1700	1200	3500	1628	1500	600	2600
B_906	1785	1400	1000	2925	1910	2350	925	2700
B_908	3071	3400	3000	3800	748	700	500	900
B_909	1846	1400	500	3500	1820	2300	800	2700
B_940	250	200	100	400	2508	1800	1400	3900
B_1	1575	750	400	3300	2074	2700	700	3000
B_3	1862	1700	425	3300	1672	850	600	2900
B_4	3417	3500	3100	3900	718	600	400	800
B_5	1905	1100	500	3575	1356	1300	700	1700

**Table S7. Taxa present in the macrofossil record.**

Taxa present in the macrofossil record and modern taxa associated with the estimation

Member	Taxon	Modern associates used for building PDF <sub>macro</sub>
C	<i>Polylepis</i> sp.	<i>Polylepis</i> sp.
	<i>Berberis</i> sp.	<i>Berberis</i> sp.
	<i>Ribes</i> sp.	<i>Ribes</i> sp.
	<i>Berberis</i> sp.	<i>Berberis</i> sp.
	<i>Polystichum</i> sp.	<i>Polystichum</i> sp.
	<i>Equisetum</i> sp.	<i>Equisetum</i> sp.
	Juncaceae	Juncaceae
B	Arecaceae	Arecaceae
	Ingeae	<i>Abarema</i> , <i>Albizia</i> , <i>Calliandra</i> , <i>Cedrelinga</i> , <i>Cojoba</i> , <i>Enterolobium</i> , <i>Hydrochorea</i> , <i>Inga</i> , <i>Pithecellobium</i> , <i>Samanea</i> , <i>Zapoteca</i> , and <i>Zygia</i>
	<i>Andiroxylon</i>	<i>Hymenolobium</i> , and <i>Andira</i>
	<i>Anacardioxylon</i>	<i>Anacardium</i> , <i>Astronium</i> , <i>Camptosperma</i> , <i>Cardenasiodendron</i> , <i>Haplorhus</i> , <i>Loxopterygium</i> , <i>Lithrea</i> , <i>Mauria</i> , <i>Myracrodruon</i> , <i>Ochoterena</i> , <i>Orthopterygium</i> , <i>Schinopsis</i> , <i>Schinus</i> , <i>Thyrsodium</i> , and <i>Toxicodendron</i>

## **CHAPTER 2**

### **THE PALEOBOTANICAL RECORD FROM THE MIDDLE TO LATE EOCENE ESMERALDAS FORMATION FROM COLOMBIA**

CAMILA MARTÍNEZ

#### **ABSTRACT**

An important step in the evolution of our modern glacial climate state occurred during the Middle Eocene to Early Oligocene, when the global temperature cooled, and the first Antarctic ice sheet appeared. This dramatic climate change caused a significant global turnover in marine and terrestrial biotas, however, more evidence from tropical regions is still needed to document these changes at low latitudes. A new macroflora from the Esmeraldas Formation of Colombia provides plant fossil evidence to understand some of the biotic changes that could have occurred in tropical regions. The Esmeraldas Flora has been collected from two localities and has more than seven hundred specimens that include compressions and impressions of leaves mostly, but also seeds, fruits and seldom flowers. Detailed stratigraphic data shows that the Flora was deposited in floodplains of braided and meandering rivers. Chemostratigraphic and palynological analyses indicate that the Esmeraldas Flora has a late Eocene age. A total of 35 leaf morphotypes were described from both localities. Quantitative paleoclimatic analyses based on leaf fossil material from the Esmeraldas Formation suggest drier conditions during deposition compared to present conditions. Morphologic analyses of fertile material together with comparisons with

modern taxa, suggest the presence of families like Fabaceae, Menispermaceae, Passifloraceae, Salviniaceae, Solanaceae, and possibly Cyperaceae. The evidence presented here suggests that the Esmeraldas Flora could represent the earliest record of a seasonally dry forest in tropical regions.

## INTRODUCTION

An important step in the evolution of our modern glacial climate state occurred during the middle Eocene to Early Oligocene, when the global temperature cooled, and the terrestrial climate became drier and more seasonal (Berggren and Prothero, 1992). Major changes in ocean circulation and global climate occurred during this time, causing significant turnovers in marine and terrestrial biotas (Berggren and Prothero, 1992). Specifically, during the late Paleocene to the Early Eocene, the warmest climatic episode of the Cenozoic era occurred (Berggren et al., 1998), and subsequently, during the Middle Eocene to Early Oligocene, the global temperature cooled, and the first Antarctic ice sheet appeared (Berggren and Prothero, 1992; Zachos et al., 2008). Studies focused on the impact of climate change on terrestrial environments have been mainly concentrated in high-latitudes, and little is known about tropical ecosystems during this period. For a long time, hypotheses suggested that the tropics did not warm during global warming intervals (e.g. Late Cretaceous: D'hondt and Arthur 1996). However, more recent data from tropical sea surface and deep-sea paleotemperatures, indicate that during the early Paleogene, tropical temperatures were also higher than modern values (Jaramillo and Cárdenas, 2013), contrary to those previous hypotheses. However, despite the increasing paleotemperature evidence from tropical regions, the temperature gradient between the poles and lower latitudes during global warming events is still not well understood. As a consequence, relevant questions related to how the climate in the tropics has changed through geologic time remain wide open.

The plant fossil record provides significant evidence for estimating the climate in past terrestrial environments and therefore its detailed study would be fundamental for reconstructing past ecosystems. Here, I describe a new macroflora from the Middle to Late Eocene Esmeraldas Formation of Colombia. These new records represent a body of plant fossil evidence that provides a unique opportunity to study biotic changes caused by the global cooling and increasing aridity that characterized the Late Eocene to Early Oligocene interval in this tropical region. The discovery of this new flora from the Esmeraldas Formation is relevant because it is the first Eocene flora reported from the Neotropical Region (Tropical America) that can be used for quantitative climate estimation methods. This formation and the Flora provides information about the depositional environment, the type of ecosystem, and climate conditions for the Middle to Late Eocene in low latitudes.

Numerous methods have been proposed to estimate climatic conditions based on the leaf physiognomic characters of various floras. Most classical methods include leaf margin analysis and leaf area analysis for estimating paleotemperature and paleoprecipitation, respectively (Wilf, 1997; Wilf et al., 1998). Others use multivariate analyses, like CLAMP, that include multiple categorical leaf traits to estimate climate based on canonical correspondence analyses (Wolfe, 1993, 1995; Spicer, 2016). More recently, methods that use digital information from leaf physiognomy have also been proposed (Peppe et al., 2011). Whereas all these methods are calibrated based on modern datasets from different sites distributed around the globe, it has been discovered that the inclusion or exclusion of some sites leads to different results. Some studies using these methods and aiming to estimate climate for tropical or South American sites have been calibrated using more regional datasets (Gregory-Wodzicki et al., 1998; Jacobs and Herendeen, 2004; Hinojosa et al., 2011).

The Eocene macrofossil record from tropical South America has been poorly studied, and it consists of a few scattered records. Most of these studies have not been executed with standard methods for performing leaf physiognomic paleoclimatic analyses. One of the most studied Eocene areas is the Fonseca Formation in Brazil. In this formation, there are seldom records of macrofossil leaves and fruits, but there is not an overall reconstruction of the paleoecosystem nor quantitative paleoclimatological analyses (Berry, 1935; Duarte, 1958; Lima and Salard-Cheboldaef, 1981; Mello et al., 2000; Fanton et al., 2012). Other Eocene Neotropical records come from the Upper Eocene Bucaro Formation of Panama (Herrera et al., 2012). These records are well preserved and described, and its taxonomic affinities suggest similarities with extant rainforest ecosystems, however, there are not large leaf collections from this Formation and therefore leaf physiognomic analyses have not been performed. New descriptions of leaf and fertile material from the Middle to Late Eocene Esmeraldas Formation provide an important and unusual opportunity to reconstruct the floristic composition and the type of ecosystem during this time.

Among the types of past ecosystems described in the Neotropics, are pre-Eocene tropical rainforest ecosystems and there is compelling evidence to confirm their presence (Wing et al., 2009). Neotropical evidence of seasonally dry tropical forests (SDTF), however, is very scarce. Graham and Dilcher (1995) reviewed the Cenozoic record of northern Latin America and the southern United States and concluded that SDTF did not become widespread in this area until the Miocene or Pliocene. The macrofossil record from the Miocene Loja, Cuenca and Nabón Basins of Ecuador provides the only such evidence from the contemporary tropics that documents the presence of an SDTF (Burnham, 1995; Burnham and Carranco, 2004). The evidence used to support the presence of this ecosystem is based mainly on the taxonomic affinities of fossil taxa,

whose modern relatives (*Tipuana* and *Loxopterygium*), have today a restricted distribution to SDTF (Burnham, 1995; Burnham and Carranco, 2004).

The aim of this study is to describe the new Esmeraldas Flora from the Middle to Late Eocene of Colombia, within a stratigraphic framework, that allows the use of different proxies including taxonomic identifications, leaf physiognomy paleoclimatic analyses, cuticle analyses, bulk organic carbon-isotopic analyses and stratigraphic information, to reconstruct the parameters characterizing this past ecosystem.

### ***Geologic setting***

The Middle Magdalena Valley Basin (MMVB) is located in the northwestern part of South America, and preserves a large reserve of information about the northern Andean tectonic history. The MMVB today lies between the Central and the Eastern Cordilleras in Colombia and is part of a large foreland basin system (Gómez et al., 2005). The MMVB had two stages, the first one was a rifting phase that spanned the Mesozoic, while the second one was a foreland system that began in the late Cretaceous and continued throughout the Cenozoic. This foreland stage of the MMVB can be divided into two major substages. In the first substage, the MMVB was integrated with the Llanos Basin, and had a continuous deposition across the future Eastern Cordillera, and occurred between the Late Cretaceous to Early Eocene (Cooper et al., 1995; Nie et al., 2010, 2012). The second substage started in the middle Eocene, when the Eastern Cordillera began its uplift and became a topographic barrier that unlinked the MMVB from the Llanos Basin (Cooper et al., 1995; Nie et al., 2010, 2012). Between the first and the second substages, there is an unconformity, the MMVU, whose development was related to the uplift and quiescence of the Central Cordillera (Gómez et al., 2005).

The rocks examined and faunal collection sites occur in the Nuevo Mundo Syncline, which is located in the northern part of the MMVB, in the western flank of the Eastern Cordillera, where there is a complete Cenozoic stratigraphic column exposed (~7000 m of thickness) (Caballero et al., 2010). Within the section, the La Paz, Esmeraldas and Mugrosa Formations were examined for this study. The location and Middle to Late Eocene age of the Esmeraldas Formation represent a key interval in the evolution of the foreland basin system of the MMVB. The studied site is located in the eastern flank of the Nuevo Mundo Syncline, in the area surrounding the Hidrosogamoso dam, near the road that leads from Bucaramanga to Barrancabermeja (Fig. 1).

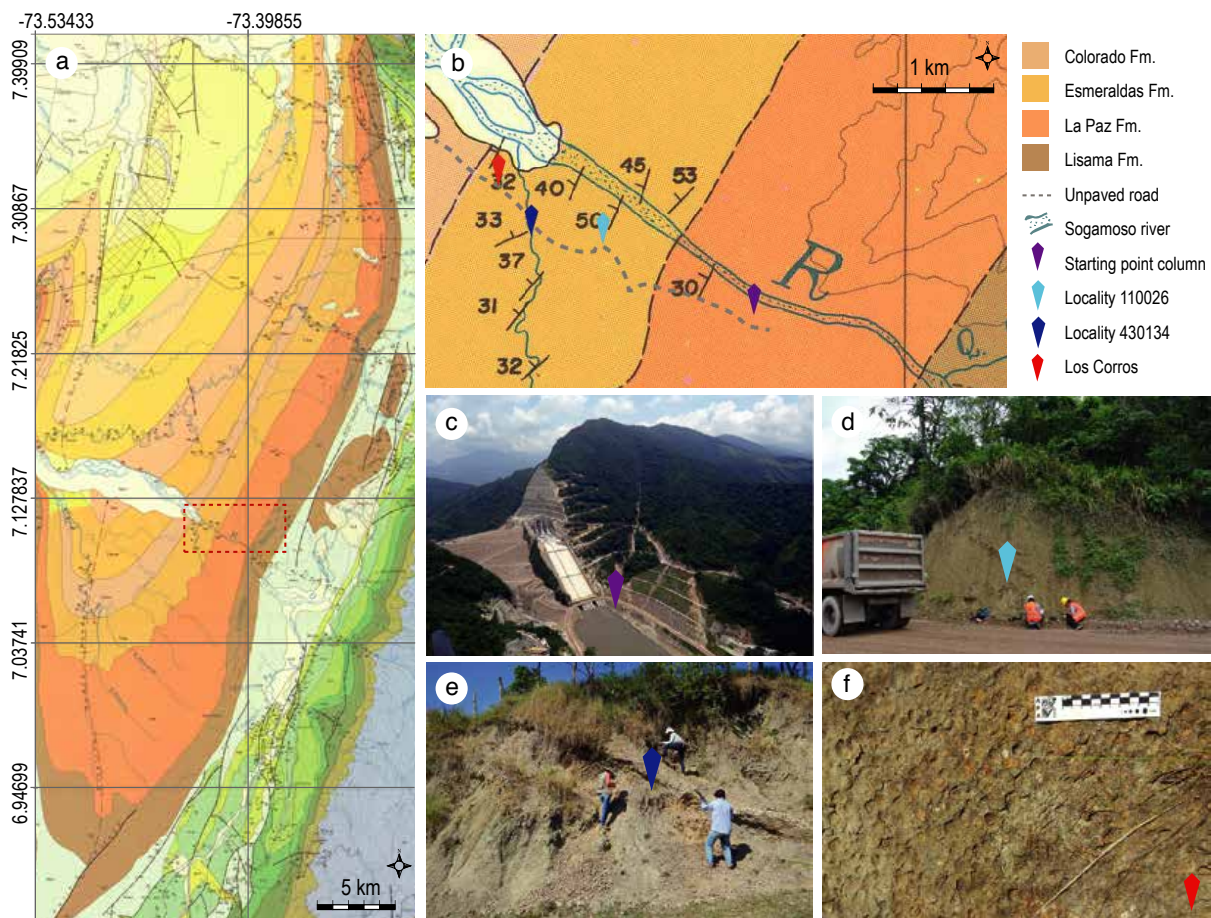


**Fig. 1. Location of fossil plant outcrops.**

**a)** Geologic map modified from Ward et al. (1977) showing the Nuevo Mundo Syncline. **b)** Zoomed area from the red rectangle showing the main localities and formations. **c)** Base of the column, specifically shown with purple diamond in La Paz Formation. Colored diamonds on map are keyed to same color diamonds on photos c, d, e, f. **d)** Locality 110026. **e)** Locality 430134. **f)** Sample from Los Corros Horizon.

Various biostratigraphic studies have focused on strata exposed in the Nuevo Mundo Syncline, but there is a slight disagreement about the ages of the formations studied here. The age of the La Paz Formation is proposed to be Early to Middle Eocene (Pardo-Trujillo et al., 2003; Caballero, 2010). The reported age of the Esmeraldas Formation ranges from late Early Eocene to Late Eocene based on a detailed palynological analysis (Rodríguez-Forero et al., 2012). The Corros Fossil Horizon, is located towards the uppermost part of the Esmeraldas Formation and corresponds to the boundary unit between the Eocene and the Oligocene. This horizon is recognized by the presence of freshwater bivalves and gastropods in shales and fine-grained mudstone beds (Pilsbry and Olsson, 1935; Nuttall, 1990; Gómez et al., 2005). The age of the Mugrosa Formation is estimated as Oligocene (Caballero, 2010). The overlap in the age estimations for the La Paz Formation and the Esmeraldas Formation can be clarified with the use of independent calibration methods.

It has been demonstrated that bulk organic-carbon isotopes ( $\delta^{13}\text{C}_{\text{TOM}}$ ) are a powerful tool for chemostratigraphic correlations in tropical terrestrial environments (Arens and Jahren, 2000; Hesselbo et al., 2003; Carvajal-Ortiz et al., 2009). These correlations use perturbations of the carbon cycle that have been widely recorded and dated within marine sedimentary sequences and terrestrial stable carbon isotopes variations measured from organic matter (Carvajal-Ortiz et al., 2009). The correlation between stable isotopes of carbon ( $\delta^{13}\text{C}$ ) from marine and terrestrial sequences has been previously used as a chronostratigraphic tool (Arens and Jahren, 2000; Hesselbo et al., 2003; Carvajal-Ortiz et al., 2009). Despite that the carbon composition of

terrestrial organic matter can be affected by microbial and plant fractionation, and different depositional environments, Carvajal-Ortiz et al. (2009) showed that there is not a significant correlation between these parameters and therefore  $\delta^{13}\text{C}_{\text{TOM}}$  could be used for chronostratigraphic purposes. The correlation proposed by Carvajal-Ortiz et al. (2009) provides evidence for the utility of the methods in Cenozoic tropical regions, since they correlate the  $\delta^{13}\text{C}_{\text{carbonate}}$  curve from Zachos et al. (2001) and a Paleocene-Eocene terrestrial  $\delta^{13}\text{C}_{\text{TOM}}$  sequence from northern Colombia, deposited under fluvial and deltaic conditions.

A more expanded correlation, from the Llanos Basin and the Llanos Foothills, also from Colombia, that include, Paleocene, Eocene and Oligocene data has also been proposed (Jaramillo *pers. comm.*; Fig. 2). The depositional environment of the Llanos composite section is mainly fluvial, however, a marine incursion reported by Santos et al. (2008) is known to have reached the central Llanos region during the Late Eocene. Although a marine incursion could affect the  $\delta^{13}\text{C}$  signature in an analysis of bulk organic matter, in the Llanos area the terrestrial influence was stronger than the marine. The presence of dinoflagellates indicating marine conditions in the Llanos composite section does not exceed 27% in terms of diversity of marine vs. terrestrial palynomorphs Santos et al. (2008), and does not exceed 5% in terms of abundance in the total organic matter (Jaramillo *pers. comm.*). As a result, the carbon signature from  $\delta^{13}\text{C}_{\text{TOM}}$  curve from the Llanos Composite section is not significantly affected by this marine incursion and can be correlated with the Zachos et al. (2001)  $\delta^{13}\text{C}_{\text{carbonate}}$  curve. The Llanos Composite section can also be used as reference material for a proposed chronostratigraphic correlation for the section of the Nuevo Mundo Syncline studied here.

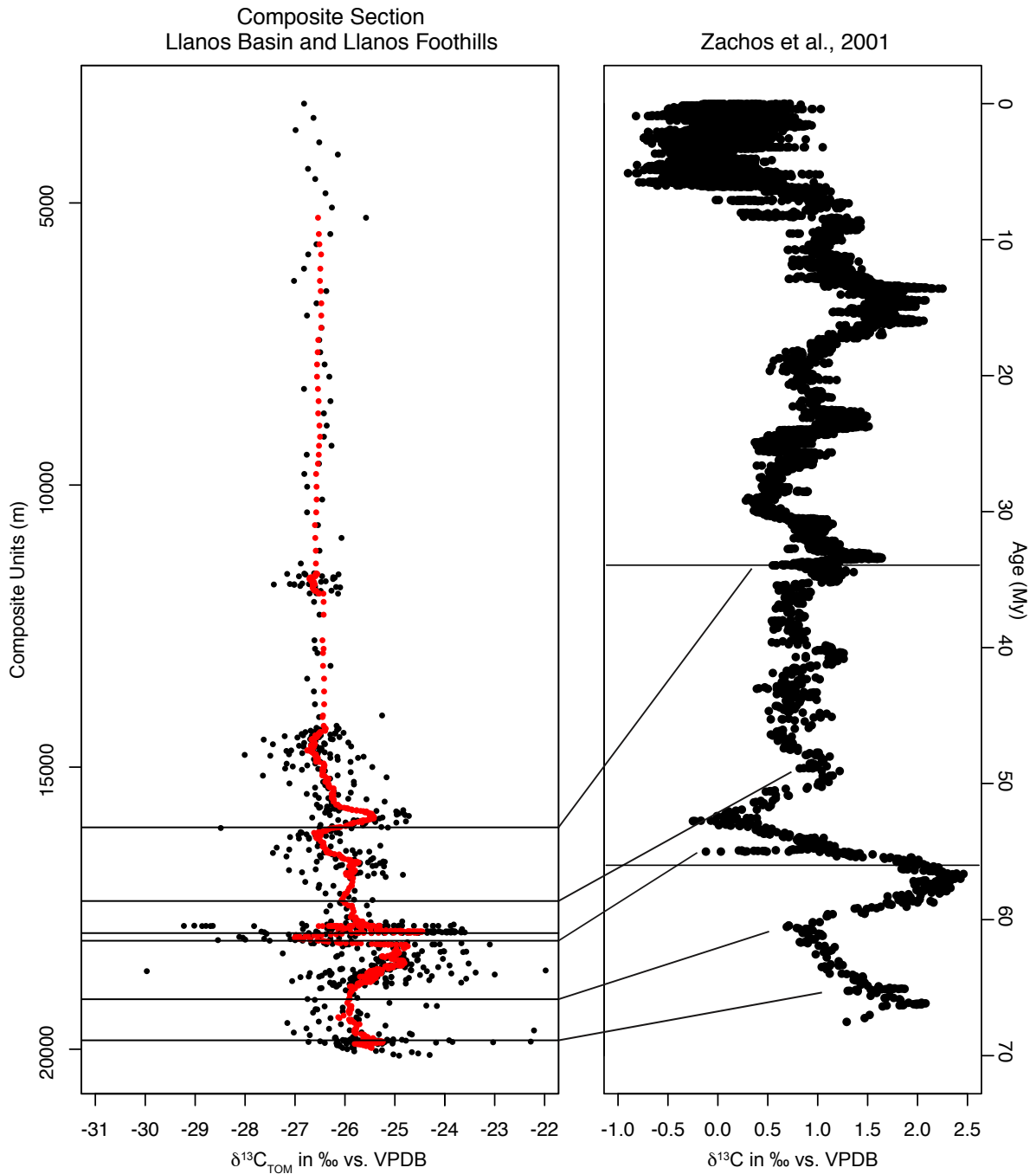


**Fig. 2. Chronostratigraphic correlation Llanos section**

Chronostratigraphic correlation between the  $\delta^{13}\text{C}_{\text{TOM}}$  isotopic composition of bulk terrestrial organic matter from a composite Section of the Llanos Basin and Llanos Foothills of Colombia and the Zachos et al. curve of  $\delta^{13}\text{C}$  carbonate (Zachos et al., 2001; Jaramillo *pers. comm.*). Horizontal lines in the Zachos curve represent the time range of the Eocene Epoch.

The depositional environment from the Esmeraldas Formation has been interpreted in different ways. Caballero et al. (2010) proposed that the eastern flank of the Esmeraldas Formation was deposited in estuarine environments with high marine influence, while the western flank was more fluvial and lacustrine. However, Gómez et al. (2005) suggested that the Esmeraldas Formation did not have marine influence and instead, they described that it was deposited in alluvial plains with minor drainage channel deposits. A marine incursion has been reported during the Late Eocene in north-western South America, reaching the Eastern Cordillera and the Central-Eastern Llanos Foothills (Santos et al., 2008). However, the palynological evidence presented earlier by Forero-Rodríguez et al. (2012) and facies analyses by Gómez et al. (2005) suggest that the Esmeraldas Formation did not undergo marine influence. New evidence from the macro and microfossil record from this study would be key to improving interpretations of the depositional environment.

## METHODS

***Fieldwork.*** The region was first explored in 2013, thanks to a paleontological salvage project led by the Smithsonian Tropical Research Institute, the Colombian Geological Survey and Isagen (power generation company). The region was explored with the collaboration of a group of 30 paleontologists and geologists from different institutions that were in the field for different time periods throughout approximately 5 months. I visited the region again in 2015 with three undergraduate volunteers, to increase the macrofossil collection of the floras from the Esmeraldas localities.

***Stratigraphic section.*** A stratigraphic section was measured starting from the dam's gate and going in a northwest direction (Fig. 1), along a dirt road that was built for the construction of the dam and was not flooded, nor covered by cement after the completion of the dam's

construction. The road leads from the gate to a rubble deposit of Isagen named Miramar approximately 1.5 km away. The stratigraphic section was measured with a Jacob's staff where there was exposure of the rocks. A wooden staff was placed as a mark every 150 cm. Covered intervals were measured with GPS data and structural data measured with a geologic compass. Lithological descriptions and classifications were done following Miall (1996). The interpretation of the depositional environment was based on Reineck and Singh (1980), Caballero (2010) and Caballero et al. (2010). The stratigraphic data was digitalized using the SDAR software (Stratigraphic Data Analysis in R). SDAR software is developed in the R language (R Development Core Team 2013) and combined with a MySQL database designed to store stratigraphic data, and to graphically represent stratigraphic, sedimentological, and paleontological data (Ortiz et al., 2015).

***Collection of samples.*** We collected samples of approximately 200 g of rock every 50 cm along the entire section (1147 samples in total). The samples were collected soon after Isagen did the road cuts for the dam's construction. In addition, pits of approximately 20 cm of depth were dug with a pick axe to collect each rock sample and decrease the risk of contamination. Later, the samples were subsampled for palynological and isotopic analyses. A total of 83 samples were processed for palynology and  $\delta^{13}\text{C}_{\text{TOM}}$  isotopic analysis.

Each specimen was observed using a Zeiss StemI SV8 Stereo Microscope and photographed with a Nikon D200 camera with varied low-angle lighting. Sediment was carefully removed using an air scribe to expose possible attachments and the maximum number of features. All the fossil material was studied at the Geosciences laboratory of the Universidad de los Andes, in Bogotá, Colombia and stored at the Paleontological Museum of the Colombian Geological

Survey in Bogotá, Colombia, and the Mapuka Museum located at the Universidad del Norte in Barranquilla, Colombia.

**Leaf morphotyping.** Fossil leaves were organized and described by morphotypes following the method proposed by Peppe et al. (2008). Each morphotype has a two-letter prefix (IP) based on the formation name plus a number starting from one. The description of each morphotype was done following the terminology of Ellis et al. (2009).

**Cuticles.** Cuticles were separated from the rock and prepared following (Kouwenberg et al., 2007). When possible, a paintbrush was used for separation; when this was not possible a polyester overlay was used to remove the cuticle from the rock. The preparation of the samples for observation in the microscope included various steps with HCL and HF treatments. The observation of the samples was done using a transmitted light Olympus BX60 microscope and a fluorescence Olympus BX-FLA microscope. The photomicrograph? images were then used to take measurements using ImageJ software. After treatment with HCL, the cuticles were sent for  $\delta^{13}\text{C}$  analysis to the Cornell Isotope Laboratory (see details of the procedure below).

**Paleoclimatic analyses.** The paleoclimate from the Esmeraldas Formation was estimated using leaf margin and leaf area analyses. The analyses were done independently for each locality (430134 and 110026). Once the leaf morphotypes were created, only those that corresponded to dicots were selected for the analyses. Leaf margin type (toothed vs. entire) was described for each morphotype and then a proportion of leaves with entire margin ( $pE$ ) was estimated for each locality. Leaf size was estimated following Ellis et al. (2009) terminology and was measured for all of the leaves in each morphotype. A leaf size template was drawn in an acetate sheet to facilitate the measurement of incomplete specimens. The leaf size categories used for the analysis were leptophyll (<25 mm<sup>2</sup>), nanophyll (25 – 225 mm<sup>2</sup>), microphyll (225 – 2025 mm<sup>2</sup>),

notophyll (2015 – 4500 mm<sup>2</sup>) and mesophyll (4500 – 18225 mm<sup>2</sup>) (Webb, 1959). The quantification of leaf area was done following Wilf et al. (1998). The number of leaves in each leaf size category was counted for each morphotype, then a relative proportion ( $p_i$ ) was calculated based on the total number of leaves in each morphotype. The mean for each leaf size category was calculated and then multiplied by the mean natural log areas of the leaf size categories ( $a_i$ ) (2.12, 4.32, 6.51, 8.01, 9.11 correspond to the five categories listed above). Subsequently, these resultant values were added to calculate the mean natural log of leaf size ( $\Sigma a_i p_i$ ) for each locality.

Paleotemperature was calculated for each locality using the estimated  $pE$  value and three simple regression models. These models used three different calibration datasets: Tropical Africa and Bolivia (Kowalski and Dilcher, 2003), worldwide (Wilf, 1997), and Tropical South America (Hinojosa et al., 2011). Paleoprecipitation was calculated for each locality using the estimated  $\Sigma a_i p_i$  value and two simple regression models. These models used two different calibration datasets: Worldwide (Wilf et al., 1998) and Tropical Africa and Bolivia (Jacobs and Herendeen, 2004).

### ***$\delta^{13}C$ isotopic analysis from bulk organic matter.***

Aiming to obtain a better age estimation for this section, rock samples were processed for  $\delta^{13}C$  from bulk organic matter ( $\delta^{13}C_{TOM}$ ) for chronostratigraphic purposes. Samples were processed at the Cornell Stable Isotope Laboratory. Approximately 20 g of rock were ground using a Pfeiffer Vacuum machine. All the equipment used for grinding was cleaned each time using Kimtech wipes with isopropanol to avoid contamination. Samples were then treated with multiple treatments of 1N HCl to remove carbonate and then rinsed three times with distilled water to remove chloride. Between 0.1 and 11.0 mg of carbonate-free sample was loaded into tin

sample capsules and placed in a NA2500 elemental analyzer. Combustion gases were carried in a helium stream through a Conflo II interface to a Thermo Delta V isotope ratio mass spectrometer. All carbon isotope results are expressed in standard delta notation relative to VPDB. To ensure the accuracy and precision of the instrument an in-house standard was analyzed after every 10 samples. The ability of the instrument to accurately measure the results of the samples was quantified using a chemical Methionine standard. Based on the results of the samples, delta values obtained between the amplitudes of 300 mV and 15000 mV for  $\delta^{13}\text{C}$  error was 0.26 ‰. Isotope corrections were performed using two-point normalization of  $\delta^{13}\text{C}$  data using two additional in-house standards (CBT and KCRN).

## RESULTS

### *Stratigraphic section*

The stratigraphic section includes the upper part of La Paz Formation, full extent of Esmeraldas Formation, and base of the Mugrosa Formation, with thickness of 1371 meters (Fig. 3 and Fig. S1). The palynological analyses are being currently undertaken by Jhonatan Martínez-Murcia at the Universidad de Caldas, Manizales, Colombia.

The strata from the uppermost La Paz Formation is dominated by thick sandstone beds that reach up to 20 m, that correspond to channel deposits interbedded with mudstone and conglomerate beds, with erosive contacts. The beds are parallel to the paleo-horizontal except the thick sandstone channel deposits that terminate laterally. Cross stratification is observed in sandstone beds. The Esmeraldas Formation, in contrast, is dominated by mudstone, muddy-sandstones beds, and siltstones, although sandstone beds are also present but are less frequent and have lesser thickness. Some parts of the Esmeraldas Formation (around 650 m of

stratigraphic height) are characterized by the presence of root traces that are expressed by color variation and material variation, and are ubiquitous in varicolored mudstone and muddy sandstone beds. Carbonate nodules were also observed in beds with root traces. Bed contacts are mostly non-erosive, except the upper surfaces of mudstones overlain directly by sandstone beds, which are slightly erosive. The Formation is also characterized by the presence of beds fining upwards from sandstones to mudstones, and thick beds of muddy sandstone with poor lamination. Plant remains were found in various horizons above 650 m of stratigraphic height, however, only two localities were found to have material with good preservation. The Corros Horizon is located at the top of the Esmeraldas Formation and is characterized by the presence of abundant mollusks and fish remains. Immediately overlying the Esmeraldas Formation is the Mugrosa Formation which is dominated by siltstone, sandstone and claystone beds.

The depositional environment along the section decrease in energy from the base to the top. The top of the La Paz formation was deposited in environments with high velocity water flow, like braided rivers, inferred from the presence of thick sandstone beds with cross stratification and conglomerates. The Esmeraldas Formation was deposited in lower energy environments compared with La Paz Formation. These fluvial conditions correspond to floodplains associated to channels of meandering rivers. The plant macrofossils were collected from two localities from the Esmeraldas Formation. The locality 110026 was found at 7°6'25.20"N, 73°25'22.84"W at 211 m of elevation and at a stratigraphic height of 660 m. Locality 430134 was found at 7°06'30.24"N, 73°25'45.12"W at 177 m of elevation and at a stratigraphic height of 880 m. The depositional environment for both localities is very similar (as interpreted above for the Formation). Nevertheless, there is subtle difference in the energy levels between these two localities: locality 110026 displays slightly higher energy compared to locality 431034. Locality

110026 is dominated by muddy-sandstones and channels (Fig. 3). Locality 430134 is 220 stratigraphic meters above locality 110026 and is dominated by siltstones (Fig. 3). See details of lithological interpretations and the depositional environments of each locality in Chapters 3 and 4 of this dissertation.

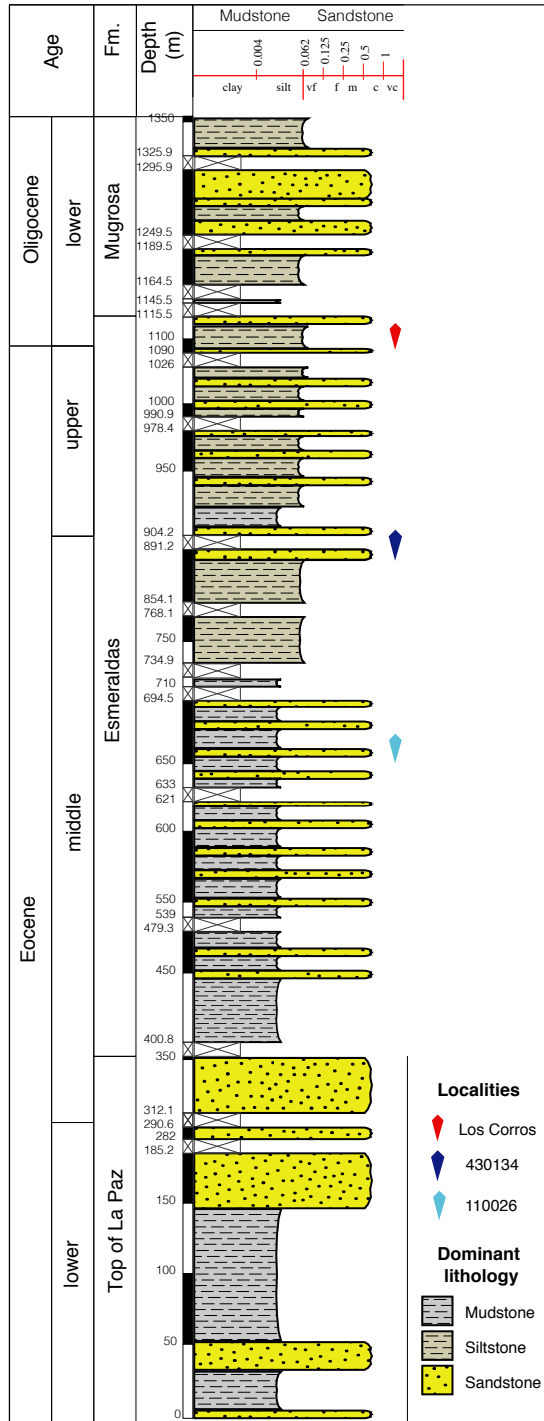


**Fig. 3. Stratigraphic section**

Stratigraphic section for the top of La Paz Formation, the Esmeraldas Formation and the base of the Mugrosa Formation. The authors of this column are: Andrés Cárdenas, Camila Martínez, Federico Moreno and Sebastian Gómez (See supplementary figure for higher resolution of the stratigraphic column).

### *$\delta^{13}\text{C}$ isotopic analysis from bulk organic matter.*

Results from the  $\delta^{13}\text{C}$  analyses of 76 samples of bulk organic matter, at approximately 10 m stratigraphic intervals are shown in Table S1. Values obtained for each run for in-house standards for normalization correction and precision purposes are shown in Table S2. Each sample analyzed has its correspondent stratigraphic height, weight, the amplitude of the sample  $\text{CO}_2$  peak in mV, the recalculated percent of carbon, and the  $\delta^{13}\text{C}_{\text{TOM}}$  ‰ vs. Vienna Pee Dee Belemnite (VPDB). The vertical succession of  $\delta^{13}\text{C}_{\text{TOM}}$  values has been compared to the Llanos Composite of  $\delta^{13}\text{C}_{\text{TOM}}$  values, to establish a correlation of the La Paz, Esmeraldas and Mugrosa formations to the Eocene and early Oligocene (Fig. 4).

Values for  $\delta^{13}\text{C}_{\text{TOM}}$  for the 76 samples analyzed range from - 28.83 to - 22.52‰. The most negative values (< - 28 ‰) were recorded for the upper most part of the section, the more positive values (> - 24 ‰) were recorded at the base, the middle and the top of the section (Fig. 4). Towards the base of the section, along the first 200 stratigraphic meters, in La Paz Formation, strong oscillations in the isotopic values, from - 27 to - 23‰, occur over short stratigraphic distances. This pattern is associated to the values from the lower Eocene (Figure 4). This range could possibly span the Paleocene Eocene Thermal Maximum (PETM), however, more samples along this interval are needed to confirm this hypothesis. Samples from the Esmeraldas Formation (stratigraphic height between 400 and 1115 m) have values that also range for - 27 to - 23‰. However, the values change across a thickness exceeding 200 m, producing a broad pattern, which is similar to a peak that is also observed in the Llanos section (Figure 4) and the Zachos curve (Fig. 2) in the middle Eocene around 40 to 44 Ma. This correlation indicates that much of the Esmeraldas Formation is coetaneous with the Mid-Eocene Climatic Optimum. The sample from the Corros Horizon has a strong negative value of - 27.31‰, a value that is similar

to the one recorded for the Llanos section in the boundary between the Eocene and the Oligocene. Samples from the Mugrosa Fm. (stratigraphic height between 1145 and 1350 m) oscillated between - 23 to - 28.8‰ over a short stratigraphic distance. This pattern is relatively similar to early Oligocene patterns observed in the Zachos curve and the Llanos section (Figs. 2, 4), although the Nuevo Mundo negative values are more extreme than in the Llanos Composite section.”

Flora 110026 occurs within the interval of less depleted of  $\delta^{13}\text{C}$  values for organic carbon (- 25 to - 23‰), whereas Flora 430134 occurs in an interval with consistently greater depletion of  $^{13}\text{C}$  (- 26 to - 25‰). The  $\delta^{13}\text{C}_{\text{TOM}}$  stratigraphy and its correlation to the Los Llanos section indicate that the age of Flora 430134 is approximately 36 to 39 Ma and Flora 110026 is 41 to 45 Ma (Fig. 4).

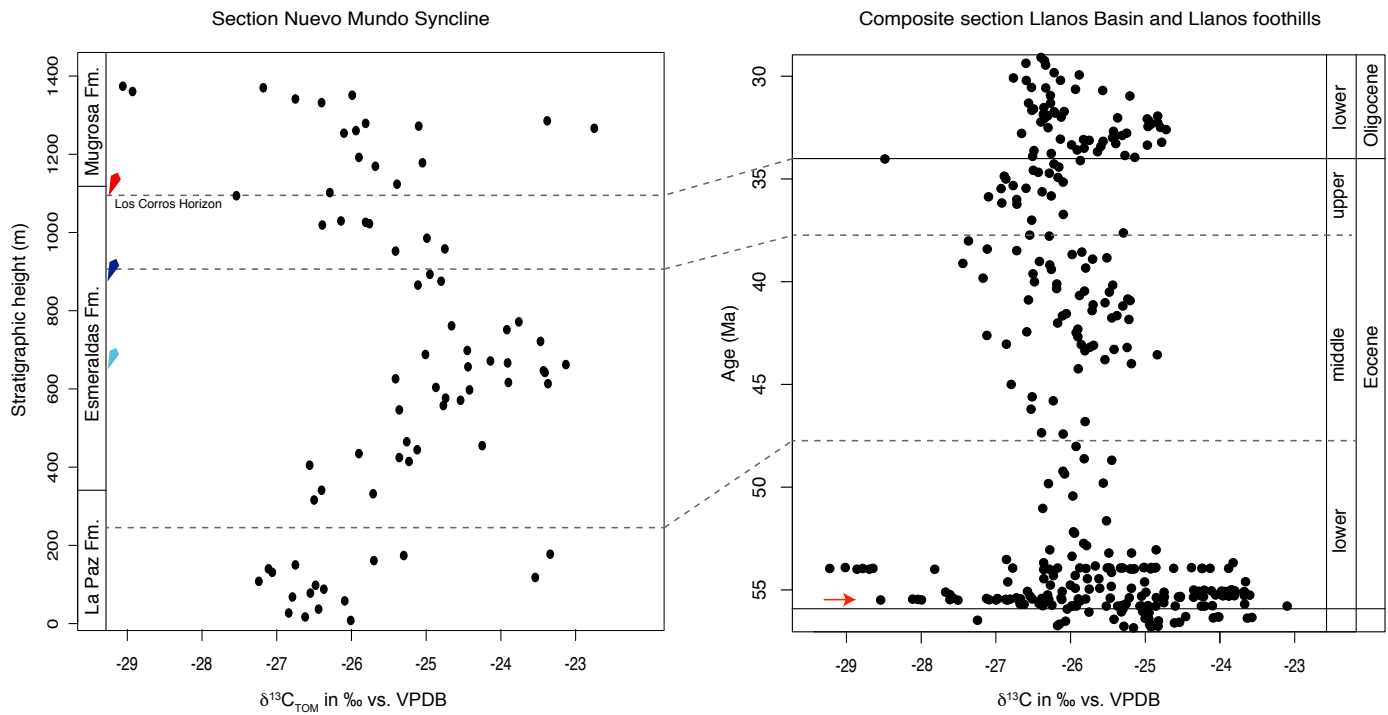


**Fig. 4. Chronostratigraphic correlation Nuevo Mundo Syncline**

Chronostratigraphic correlation of the  $\delta^{13}\text{C}$  isotopic composition of bulk terrestrial organic matter from the Nuevo Mundo Syncline ( $\delta^{13}\text{C}_{\text{TOM}}$ , left panel, this study) and the Composite

Llanos and Llanos foothills section (Jaramillo *pers. comm.*). Red arrow indicates the Paleocene-Eocene Thermal Maximum. The dashed line indicates the end of the first part of the Early Eocene Climatic Optimum. The dark blue diamond corresponds to Flora 430134, and light blue corresponds to Flora 110026 (Table S1).

### ***Macrofossil collection and morphotyping***

Most of the 714 macrofossil specimens consist of compressions and impressions of angiosperm leaves, some with cuticles preserved, but the collection also included seeds, fruits and flowers. The locality 430134 has more abundant fossil material and also fossils with better preservation compared to fossils from locality 110026. In locality 430134, a total of 488 macrofossils were collected. In addition, 237 were included for measurements and identified to morphotype for the census analysis. Of the fossils collected from locality 430134, 421 specimens were impressions or compressions of fossil leaves, that were split into 25 morphotypes, while 67 were of fertile material (seeds, fruits or flower fragments), from which 7 morphotypes were recognized. In locality 110026, a total of 226 macrofossils were collected. Of the fossils collected at this locality, 131 specimens are impressions or compressions of fossil leaves, that were split into 9 morphotypes, while 61 represent fertile material (seeds, fruits or flower fragments) from which 4 morphotypes were recognized.

### ***Description of morphotypes***

#### **Leaves**

#### **Dicot Angiosperms**

#### **Morphotype ES1**

#### **Figure 5a**

Locality: 430134

Morphotype exemplar: 44962

Other specimens studied: 35521, 35557, 35662, 44962, 44961, 44963, 44960, 44958, 44959, 44965

Description: The leaf attachment is petiolate. The blade attachment is marginal. The laminar size is microphyll; the laminar L:W ratio is between 1.5:1 to 2:1; the laminar shape is elliptic to slightly ovate with medial and basal symmetry. The lamina is unlobed and untoothed. The apex angle is acute; the base angle is obtuse; the base shape is convex. Primary venation is pinnate. Major secondaries are eucamptodromous becoming brochidodromous distally, the spacing is gradually increasing proximally, with a uniform angle and a excurrent attachment. The minor secondary course simple is brochidodromous. The intercostal tertiary veins are opposite percurrent and perpendicular to the midvein. The epimedial tertiaries are opposite percurrent, and have a proximal course perpendicular to midvein; its distal course is parallel to intercostal tertiaries. Exterior tertiary course is looped. Quaternary vein fabric is alternate percurrent. Areolation moderate development.

### **Morphotype ES2**

#### **Figure 5b**

Locality: 430134

Morphotype exemplar: 45096

Other specimens studied: 45096, 45097, 45107

Description: The leaf attachment is petiolate. The blade attachment is marginal. The laminar size is microphyll; the laminar L:W ratio is 1:1; the laminar shape is elliptic, with medial and basal symmetry. The lamina is unlobed and untoothed. The base angle is reflexed; the base shape

is cordate. Primary venation is basal acrodromous with 9 basal veins; the agrophic veins are compound. Major secondaries are festooned brochidodromous, interior secondaries are present. The minor secondary course is simple brochidodromous. The intercostal tertiary veins are mixed percurrent and perpendicular to the midvein. The epimedial tertiaries are opposite percurrent, and have a proximal course acute to midvein, its distal course parallel to intercostal tertiary. Exterior tertiary course is looped. Quaternary vein fabric is irregular reticulate. Quinary vein fabric irregular reticulate. Areolation is moderately developed. Freely ending veinlets are mostly one branched, with tracheoid idioblast termination. Marginal ultimate venation is looped.

### **Morphotype ES3**

#### **Figure 5c**

Locality: 430134

Morphotype exemplar: 44983

Other specimens studied: 35618, 35654, 35654, 35654, 44966, 44967, 44968, 44969, 44970, 44971, 44972, 44973, 44974, 44975, 44976, 44977, 44978, 44979, 44980, 44981, 44982, 44983

Description: The leaf attachment is petiolate. The blade attachment is marginal. The laminar size is microphyll; the laminar L:W ratio is 1.8:1 between 6:1; the laminar shape is elliptic, with medial and basal symmetry. The lamina is unlobed and untoothed. The base angle is obtuse and the shape is rounded to concavo-convex. Primary venation is basal acrodromous with 5 to 7 basal veins; the agrophic veins are simple. Interior secondaries are present. The minor secondary course is simple brochidodromous. The intercostal tertiary veins are straight opposite percurrent, perpendicular to the midvein, with a vein angle increasing exmedially. The epimedial tertiaries are opposite percurrent, and have a proximal course perpendicular to the midvein, its distal

course is parallel to intercostal tertiary. Quaternary vein fabric is mixed percurrent. Quaternary vein fabric probably regular reticulate. Areolation is well developed.

### **Morphotype ES5**

#### **Figure 5d**

Locality: 430134

Morphotype exemplar: 36165

Other specimens studied: 36165

Description: The leaf attachment is petiolate. The blade attachment is marginal. The laminar size is nanophyll; the laminar L:W ratio is 1:1; the laminar shape is ovate, with medial and basal symmetry. The lamina is unlobed and untoothed. The apex angle is obtuse and the shape is rounded. The base angle is reflex and the shape is cordate. Primary venation is pinnate; the agrophic veins are simple. Major secondaries are simple brochidodromous, with irregular spacing and uniform angle. The minor secondary course is simple brochidodromous with a proximal course perpendicular to midvein. Intersecondary veins are weak, with lengths shorter than 50% of subjacent secondary; these are basiflexed and do not join subjacent secondaries at right angles, and they do not occur at all the intercostal areas. The intercostal tertiary veins are mixed percurrent and perpendicular to the midvein.

### **Morphotype ES6**

#### **Figure 5e**

Locality: 430134

Morphotype exemplar: 45196

Other specimens studied: 35662, 35662, 35669, 45192, 45193, 45194, 45195, 45196, 45197, 45198, 45199

Description: The laminar size is microphyll. The laminar L:W ratio is 1:1; the laminar shape is ovate, with medial symmetry. The lamina is unlobed and untoothed. Primary venation is actinodromous; the agrophic veins are compound. Major secondaries are festooned brochidodromous. Marginal secondary vein is strong. The intercostal tertiary veins are mixed percurrent. Quaternary vein fabric is alternate percurrent.

### **Morphotype ES9**

#### **Figure 5f**

Locality: 430134

Morphotype exemplar: 45094

Other specimens studied: 35366, 35549, 35661, 45088, 45089, 45090, 45091, 45092, 45093, 45094

Description: The laminar size is microphyll; the laminar L:W ratio is probably 2:1; the laminar shape is possibly ovate, with medial symmetry. The lamina is unlobed and untoothed. The apex angle is reflex and the shape is emarginated. Primary venation is pinnate. Major secondaries are festooned brochidodromous. Intersecondary veins are strong, parallel to major secondaries, with lengths shorter than 50% of subjacent secondary; these are reticulating distally, and they do not occur at all the intercostal areas. The intercostal tertiary veins are irregular reticulate, with an inconsistent vein angle. The epimedial tertiaries are reticulate. Quaternary vein fabric is regular reticulate.

## Morphotype ES11

### Figure 5g, h and 6

Locality: 430134 and 110026

Morphotype exemplar: 35549

Other specimens studied: 35148, 35195, 35210, 35229, 35258, 35274, 35367, 35521, 35549, 35549, 35557, 35557, 35557, 35618, 35618, 35624, 35659, 35661, 35661, 35661, 35669, 35669, 36330, 45206, 45207, 45208, 45209, 45210, 45211, 45212, 45213, 45214, 45216, 45217, 45218, 45219, 45220, 45220, 45221, 45222, 45223, 45224, 45225, 45226, 45227, 45229, 45230, 45231, 45232, 45233, 45234, 45235

Description: The leaf attachment is petiolate. The blade attachment is marginal. The petiole is very thick. The laminar size is microphyll to notophyll; the laminar L:W ratio is between 2:1 and 3:1; the laminar shape is elliptic, with medial and basal symmetry. The lamina is unlobed and untoothed. The base angle is acute and the shape is decurrent. Primary venation is pinnate with 3 basal veins. Major secondaries are eucamptodromous becoming brochidodromous distally. The minor secondary course is simple brochidodromous. Intersecondary veins are parallel to major secondaries, with lengths shorter than 50% of subjacent secondaries; these are basiflexed and do not join subjacent secondaries at right angles, and they do not occur at all the intercostal areas. The intercostal tertiary veins are mixed percurrent, obtuse to the midvein, with a consistent vein angle. The epimedial tertiaries are mixed percurrent, and have a proximal course parallel to subjacent secondaries, its distal course is basiflexed to intercostal tertiary. Quaternary vein fabric is alternate percurrent. Quinary vein fabric is reticulate. Areolation is well developed.

*Cuticle.* All the 31 cuticle specimens collected, prepared and observed under the microscope, are possibly from the same morphotype. Although most of the fragments were loosened, some of them were larger and with enough characters preserved to associate it to morphotype ES11 (Fig. 6). Despite the high quantity of samples and the different attempts to clean them using various methods that include hydrochloric acid, hydrofluoric acid, and sodium peroxide, I was not able to observe epidermal features using light microscopy (LM) and boundaries between cells were not clear under epifluorescence (EF), therefore the description of the material could not be completed and nor was their sufficient data for stomatal counts and stomatal indexes.

The specimens have thick epicuticular waxes. The inferred adaxial side has only observable stomata on top of the midvein and in association with secondary veins. The inferred abaxial side has the stomata evenly distributed on the lamina, however, they are hard to observe due to the presence of the epicuticular waxes. A few of the observed stomata had perpendicular striations. The only measurement taken was the pore length of stomata which was measured from nine stomata, the mean was 28.3  $\mu\text{m}$ , the standard deviation was 3.44  $\mu\text{m}$ , the minimum value was 23.3 $\mu\text{m}$  and the maximum value was 34.1  $\mu\text{m}$ .

The  $\delta^{13}\text{C}$  isotopic signature measured in 12 specimens shows uniform values. The mean  $\delta^{13}\text{C}$  isotopic signature was -27.5‰, the standard deviation was 0.802, the minimum value was -28.26‰, and the maximum value was -25.68‰. The percentage of carbon content in the samples was relatively high in all the samples, although there was some variation, the mean was 35.7%, the standard deviation was 15.7, the minimum value was 9.49%, and the maximum value was 57.82%.

### **Morphotype ES13**

#### **Figure 5i**

Locality: 430134

Morphotype exemplar: 36153

Other specimens studied: 35368, 35669, 36153, 45078, 45079, 45080, 45081, 45082, 45083, 45084, 45085, 45086, 45087

Description: The leaf attachment is petiolate. The blade attachment is marginal. The laminar size is microphyll; the laminar L:W ratio is 1.1:1; the laminar shape is ovate, with medial and basal symmetry. The lamina is unlobed and untoothed. The base angle is obtuse and the shape is rounded. Primary venation is suprabasal actinodromous with 5 basal veins; the agrophic veins are simple. Major secondaries are simple brochidodromous. Interior secondaries are present. The minor secondary course is simple brochidodromous. The intercostal tertiary veins are mixed percurrent, acute to the midvein.

### **Morphotype ES15**

#### **Figure 5j**

Locality: 430134

Morphotype exemplar: 45018

Other specimens studied: 35521, 35549, 35553, 35553, 35622, 35624, 35662, 35662, 35662, 35662, 35662, 35667, 35669, 45018, 45019, 45020, 45021, 45022, 45023, 45024, 45025, 45026, 45027, 45028, 45029, 45030, 45031, 45032, 45033, 45034, 45035, 45036, 45037, 45038, 45039, 45040, 45041, 45042, 45043, 45044, 45045, 45046, 45047, 45048, 45049, 45050, 45051, 45052,

45053, 45054, 45055, 45056, 45057, 45058, 45059, 45060, 45061, 45062, 45063, 45064, 45065, 45066, 45067, 45068, 45069, 45070, 45071, 45072, 45073, 45074, 45075, 45076, 45077

Description: The leaf attachment is petiolate. The blade attachment is marginal. The laminar size is nanophyll to microphyll; the laminar L:W ratio is 2:1; the laminar shape is elliptic, with medial and basal symmetry. The lamina is unlobed and untoothed. The apex angle is acute and the shape is acuminate. The base angle is acute and the shape is cuneate to rounded. Primary venation is pinnate, with 3 basal veins. Major secondaries are eucamptodromous becoming brochidodromous distally. The minor secondary course is simple brochidodromous. Perimarginal veins are marginal secondary proximally. Intersecondary veins are parallel to major secondaries, with lengths shorter than 50% of subjacent secondary, these reticulate distally, and they do not occur at all the intercostal areas. The intercostal tertiary veins are mixed percurrent, obtuse to the midvein, with an obtuse vein angle. The epimedial tertiaries are opposite percurrent, and have a proximal course acute to the midvein, its distal course is basiflexed to intercostal tertiary. Quaternary vein fabric is mixed percurrent. Quinary vein fabric is reticulate. Areolation is moderate in development. Freely ending veinlets are mostly one branched, with simple termination. Marginal ultimate venation is looped.

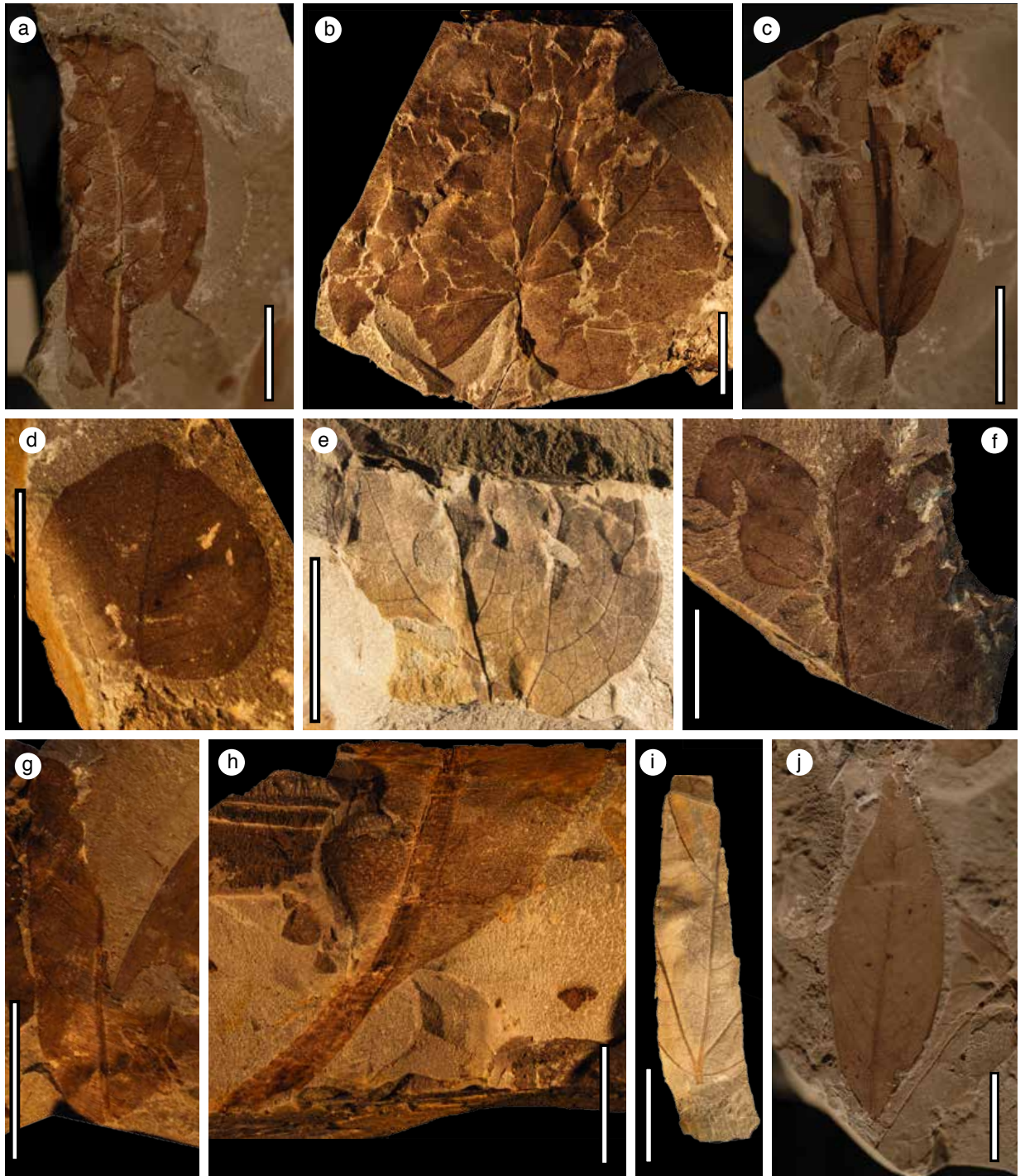


**Fig. 5. Fossil leaf morphotype exemplars**

Fossil leaf morphotype exemplars from the Esmeraldas Formations. **a.** ES-1, STRI-ID-44962, **b.** ES-2, STRI-ID-45096. **c.** ES-3, STRI-ID-44983. **d.** ES-5, STRI-ID-36165. **e.** ES-6, STRI-ID-44196. **f.** ES-9, STRI-ID-45094. **g.** ES-11, STRI-ID-35549. **h.** ES-11, STRI-ID-35521. **i.** ES-13, STRI-ID-36153. **j.** ES-15, STRI-ID-45018. All scales = 1 cm.

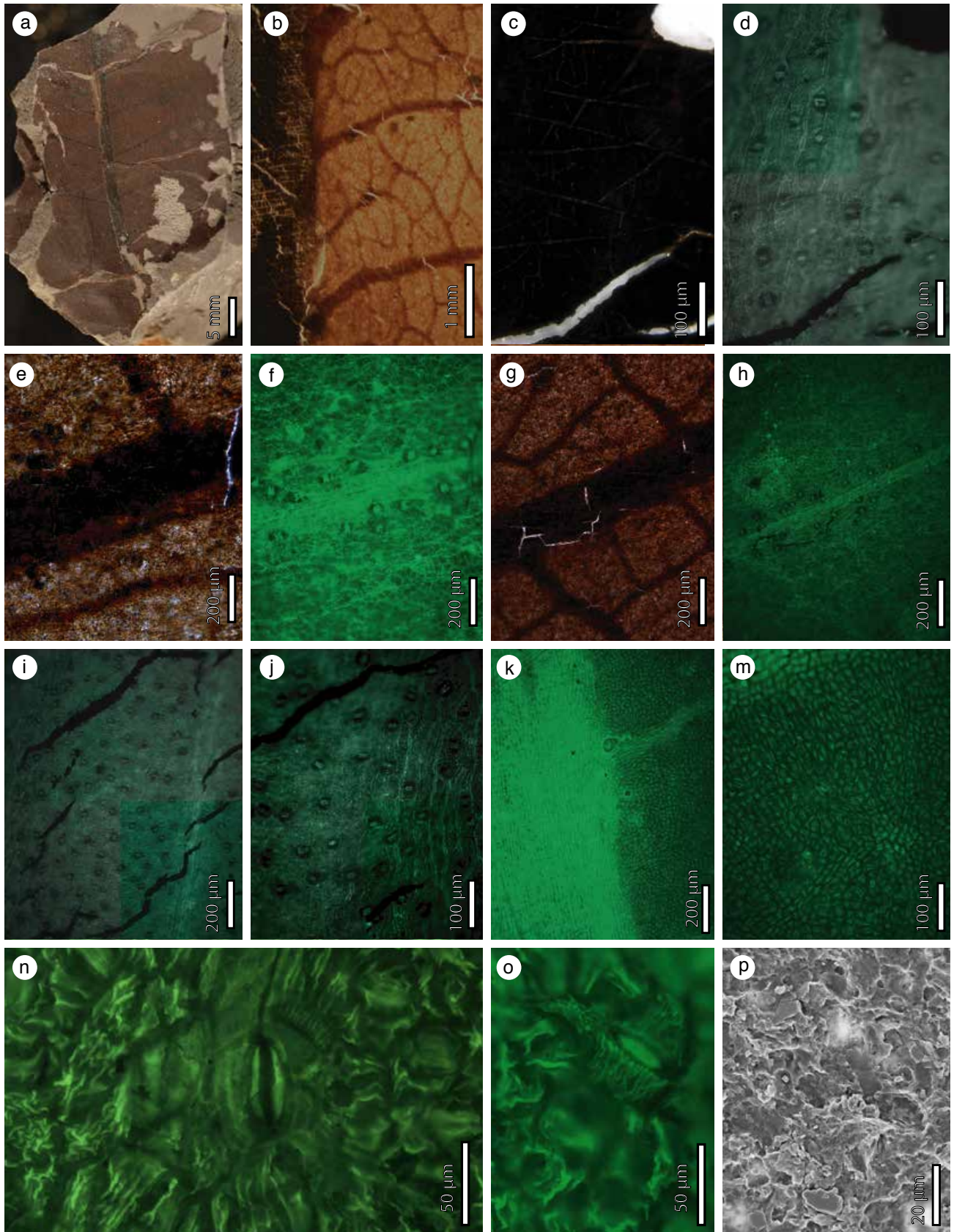


### **Fig. 6. Micrographs of cuticles**

Micrographs of cuticles from morphotype ES11. **a.** Macrophotograph of specimen on the rock showing cuticle preservation. **b.** Micrograph of cuticle removed from the rock showing the midvein and attachment of the secondary veins. **c.** Light microscopy (LM) photograph of a fraction of the midvein. **d.** Epifluorescence microscopy (EF) photograph the stomata present on top of the same fraction of the midvein shown in image *c.* **e.** (LM) photograph of a fraction of a secondary vein. **f.** (EF) photograph the stomata present along the sides of the same fraction of the secondary vein shown in image *e.* **g.** (LM) photograph of another fraction of a secondary vein. **h.** (EF) photograph the stomata present along the sides of the same fraction of the secondary vein shown in image *g.* **i.** Stomata present on the midvein. **j.** Stomata present on the midvein. **b-j.** Inferred adaxial side. **k.** Midvein and lamina epidermal cells. **m.** Epidermal cells from lamina and minor veins. **n.** Close-up of a stoma, showing epicuticular waxes. **o.** Close-up of a stoma, showing epicuticular waxes and perpendicular striations on the stoma. **p.** SEM photograph showing possibly epicuticular waxes. **k-p.** Inferred abaxial side of the leaf. All photographs were taken from sample STRI-ID-45224.

### **Morphotype ES20**

#### **Figure 7a**

Locality: 430134

Morphotype exemplar: 45003

Other specimens studied: 44997, 45016, 44992, 44992, 44992, 44992, 44995, 44995, 44995, 45012, 45013, 44994, 45010, 45015, 45003, 45001, 44999, 45000, 45017, 45008, 45009, 44998, 45004, 45014, 44996, 35667, 35667, 36165, 35661, 35652, 35658, 35557, 36165, 45006, 45007, 45005, 35557, 45002, 44993, 45011

Description: The leaf attachment is petiolate. The blade attachment is marginal. The laminar size is nanophyll to microphyll; the laminar L:W ratio is 1.7:1; the laminar shape is elliptic, with medial and basal symmetry. The lamina is unlobed and untoothed. The apex is angle is acute and the shape is acuminate. The base angle is obtuse and the shape is convex to straight-cuneate.

Primary venation is pinnate with 3 basal veins. Major secondaries are festooned

brochidodromous. The minor secondary course is simple brochidodromous, major secondary

spacing is regular with a uniform and decurrent attachment. Intersecondary veins are parallel to

major secondaries, with lengths shorter than 50% of subjacent secondary; these are basiflexed and do not join subjacent secondaries at right angles, and they do not occur at all the intercostal areas. The intercostal tertiary veins are alternate percurrent, acute to the midvein, with a vein angle increasing exmedially. The epimedial tertiaries are alternate percurrent, and have a proximal course parallel to subjacent secondary, its distal course is basiflexed, and have an exterior tertiary course looped. Quaternary vein fabric is alternate percurrent. Quinary vein fabric is reticulate. Areolation is well developed. Freely ending veinlets, two or more with dichotomous branching, with tracheoid idioblasts termination.

### **Morphotype ES21**

#### **Figure 7b**

Locality: 430134

Morphotype exemplar: 45114

Other specimens studied: 45107, 45109, 45106, 45105, 45104, 45112, 45114, 45110, 45111, 45108, 45113, 45448

Description: The leaf attachment is petiolate. The blade attachment is submarginal. The laminar size is microphyll; the laminar L:W ratio is 2:1; the laminar shape is elliptic, with medial and basal symmetry. The lamina is unlobed and untoothed. The base angle is reflex and the shape is auriculate. Primary venation is pinnate with 5 basal veins; the agrophic veins are simple. Major secondaries are festooned brochidodromous. The minor secondary course is simple brochidodromous. The intercostal tertiary veins are opposite to mixed percurrent, obtuse to the midvein, with a consistent vein angle. The epimedial tertiaries are opposite percurrent, and have a proximal and distal course parallel to intercostal tertiary. Quaternary vein fabric is mixed percurrent. Quinary vein fabric is possibly reticulate. Areolation is moderately developed.

## **Morphotype ES22**

### **Figure 7c**

Locality: 430134

Morphotype exemplar: 45127

Other specimens studied: 35364, 36161, 35667, 35669, 45119, 45129, 45122, 45124, 45123, 45117, 45115, 45125, 35624, 45116, 45121, 45127, 45118, 45128, 45120, 45126

Description: The blade attachment is marginal. The laminar size is nanophyll to microphyll; the laminar L:W ratio is 1:1; the laminar shape is elliptic, with medial and basal symmetry. The lamina is unlobed and untoothed. The apex is acute and the shape is acuminate. The base angle is obtuse and the shape is rounded. Primary venation is pinnate with 5 basal veins. Major secondaries are simple brochidodromous. The minor secondary course is simple brochidodromous. The intercostal tertiary veins are exmedially ramified. The epimedial tertiaries are ramified, and have a proximal course parallel to subjacent secondary. Quaternary vein fabric is irregular reticulate. Areolation is poorly developed.

## **Morphotype ES23**

### **Figure 7d**

Locality: 430134

Morphotype exemplar: 45189

Other specimens studied: 35661, 45190, 35669, 45191, 45189

Description: The blade attachment is marginal. The laminar size is microphyll; the laminar L:W ratio is 1.3:1; the laminar shape is elliptic, with medial and basal symmetry. The lamina is unlobed and untoothed. The apex is obtuse and the shape is rounded. The base angle is obtuse

and the shape is rounded. Primary venation is pinnate. Major secondaries are simple brochidodromous. Intersecondary veins are parallel to major secondaries, with lengths shorter than 50% of subjacent secondary; these are basiflexed and do not join subjacent secondaries at right angles, and they do not occur at all the intercostal areas. The intercostal tertiary veins are mixed percurrent, obtuse to the midvein, with a consistent vein angle. The epimedial tertiaries are opposite percurrent, and have a proximal course perpendicular to the midvein, its distal course is basiflexed. Quaternary vein fabric is mixed percurrent. Quinary vein fabric is irregular reticulate. Areolation is well developed. Freely ending veinlets are mostly one branched, with tracheoid idioblasts termination.

### **Morphotype ES24**

#### **Figure 7e**

Locality: 430134

Morphotype exemplar: 44951

Other specimens studied: 44951, 44952, 44955, 44953, 44956, 44954

Description: The lamina size is microphyll; the lamina L:W ratio is 3:1; the lamina shape is elliptic, with medial symmetry. The lamina is unlobed and untoothed. The surface has red glands. Primary venation is pinnate. Major secondaries are festooned brochidodromous with spacing gradually increasing proximally, with uniform secondary angle and a decurrent attachment. The minor secondary course is simple brochidodromous. The intercostal tertiary veins are mixed percurrent, obtuse to the midvein, with an inconsistent vein angle. The epimedial tertiaries are opposite percurrent, and have a proximal course parallel to subjacent secondary to the midvein, its distal course is basiflexed. Quaternary vein fabric is alternate percurrent.

Quaternary vein fabric is reticulate. Areolation is moderately developed. Freely ending veinlets are mostly unbranched, with simple termination.

### **Morphotype ES26**

#### **Figure 7f**

Locality: 430134

Morphotype exemplar: 45166

Other specimens studied: 45166

Description: The leaf attachment is petiolate. The blade attachment is marginal. The laminar size is microphyll; the laminar L:W ratio is 1.5:1; the laminar shape is elliptic, with medial and basal symmetry. The lamina is unlobed and toothed. The base angle is obtuse and the shape is obtuse. Primary venation is pinnate. Major secondaries are craspedodromous with irregular spacing and decurrent attachment. Marginal secondary vein present. The minor secondary course is craspedodromous. The intercostal tertiary veins are sinuous opposite percurrent, obtuse to the midvein, with consistent vein angles. Quaternary vein fabric is mixed percurrent.

Tooth spacing regular, with one teeth order; 1 to 1.5 teeth per cm; with rounded sinus shape. Tooth has a convex/convex shape, and a spherulate apex shape; principal vein is probably present.

### **Morphotype ES28**

#### **Figure 7g**

Locality: 430134

Morphotype exemplar: 35662

Other specimens studied: 35662, 45183, 45184, 45188, 45187, 45186, 35360, 36102, 36102, 45182, 45178, 45180, 45179, 45181, 45185

Description: The leaf attachment is petiolate. The blade attachment is marginal. The laminar size is microphyll; the laminar L:W ratio is 2:1; the laminar shape is oblong, with medial and basal symmetry. The lamina is unlobed and untoothed. The base angle is acute and the shape is concavo-convex. Primary venation is pinnate. Major secondaries are festooned brochidodromous. The minor secondary course is simple brochidodromous. Intersecondary veins are parallel to major secondaries, with lengths longer than 50% of subjacent secondary, and there is more than one per intercostal areas. The intercostal tertiary veins are irregular reticulate. The epimedial tertiaries are reticulate, and have a proximal course acute to the midvein. Exterior tertiary course is looped. Quaternary vein fabric is irregular reticulate.

### **Morphotype ES29**

#### **Figure 7h**

Locality: 430134

Morphotype exemplar: 35624

Other specimens studied: 45135, 35549, 35624, 45134, 45131, 45130, 45136, 45133, 45132, 45137

Description: The laminar size is microphyll; the laminar L:W ratio is >4:1; the laminar shape is linear, with medial symmetry. The lamina is unlobed and untoothed. Primary venation is pinnate. Major secondaries are eucamptodromous. The minor secondary course is simple brochidodromous. The intercostal tertiary veins are alternate percurrent, obtuse to the midvein.

The epimedial tertiaries are reticulate, and have a proximal course parallel to subjacent secondary veins and a distal course basiflexed. Quaternary vein fabric is irregular reticulate.

### **Morphotype ES30**

#### **Figure 7i**

Locality: 430134

Morphotype exemplar: 44991

Other specimens studied: 44989, 35661, 44986, 35654, 35654, 44984, 44991, 44990, 44987, 44988, 44985, 35556

Description: The leaf attachment is petiolate. The blade attachment is marginal. The laminar size is microphyll; the laminar L:W ratio is 1.7:1; the laminar shape is elliptic, with medial and basal symmetry. The lamina is unlobed and untoothed. The base angle is obtuse and the shape is decurrent to convex. Primary venation is pinnate, with 4 basal veins. Major secondaries are eucamptodromous, with irregular spacing and uniform angle and decurrent attachment. Intersecondary veins are parallel to major secondaries, with lengths shorter than 50% of subjacent secondary; these are basiflexed and do not join subjacent secondaries at right angles, and they do not occur at all the intercostal areas. The intercostal tertiary veins are alternate percurrent, acute to the midvein, with a vein angle increasing exmedially. The epimedial tertiaries are alternate percurrent, and have a proximal course parallel to subjacent secondary, and a distal course is parallel to intercostal tertiary. Quaternary vein fabric is possibly alternate percurrent.

### **Morphotype ES31**

#### **Figure 7j**

Locality: 430134

Morphotype exemplar: 45138

Other specimens studied: 35622, 35652, 35658, 35658, 35661, 45138, 45139, 45140, 45141, 45142, 45143, 45144, 45145, 45146

Description: The leaf attachment is petiolate. The blade attachment is marginal. The laminar size is nanophyll to microphyll; the laminar L:W ratio is 1.5:1; the laminar shape is ovate, with medial and basal symmetry. The lamina is unlobed and untoothed. The apex is acute and the shape is straight. The base angle is obtuse and the shape is rounded. Primary venation is pinnate with 3 basal veins. Major secondaries are festooned brochidodromous, with irregular spacing, uniform angle and excurrent attachment. The minor secondary course is craspedodromous. Intersecondary veins are parallel to major secondaries, with lengths longer than 50% of subjacent secondary; these are reticulating exmedially, and there is one per intercostal area. The intercostal tertiary veins are mixed percurrent, obtuse to the midvein, with a consistent vein angle. The epimedial tertiaries are opposite percurrent, and have a proximal course parallel to subjacent secondaries, its distal course is basiflexed; exterior tertiary course is looped. Quaternary vein fabric is irregular reticulate.

### **Morphotype ES32**

#### **Figure 7k**

Locality: 430134

Morphotype exemplar: 45149

Other specimens studied: 45148, 45147, 45149, 35651, 35651, 45150

Description: The leaf or leaflet attachment is petiolate. The blade attachment is marginal. The laminar size is leptophyll; the laminar L:W ratio is 2:1; the laminar shape is elliptic, with medial and basal symmetry. The lamina is unlobed and untoothed. The apex is obtuse and the shape is rounded. The base angle is obtuse and the shape is rounded. Primary venation is pinnate. Major secondaries are festooned brochidodromous. The minor secondary course is simple brochidodromous. Intersecondary veins are parallel to major secondaries, with lengths longer than 50% of subjacent secondary; these are basiflexed and do not join subjacent secondaries at right angles, and they do not occur at all the intercostal areas. The intercostal tertiary veins are exmedially ramified. The epimedial tertiaries are ramified, and have a proximal course acute to the midvein.

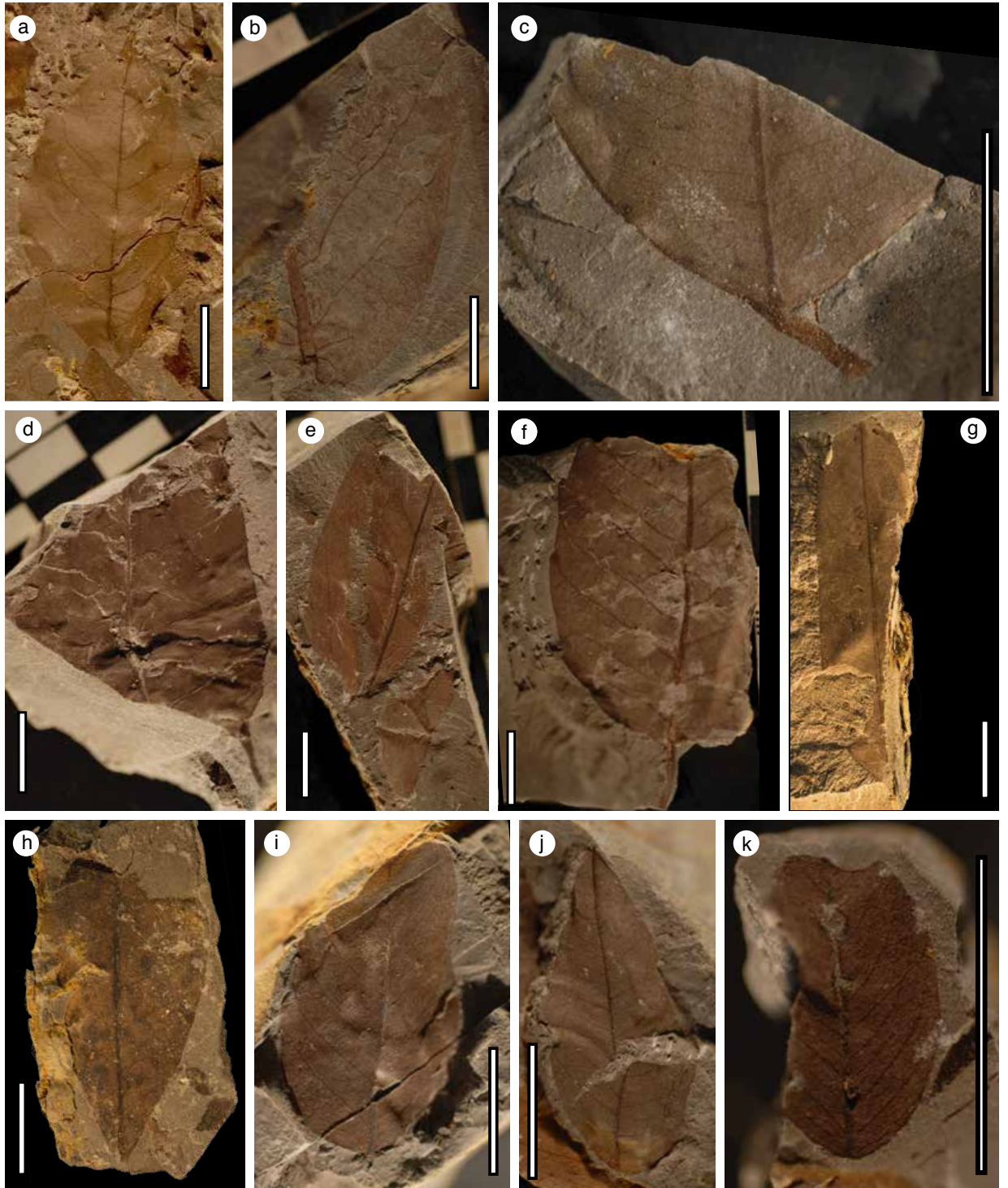


**Fig. 7. Fossil leaf morphotype exemplars**

Fossil leaf morphotype exemplars from the Esmeraldas Formations. **a.** ES-20, STRI-ID-45003, **b.** ES-21, STRI-ID-45114. **c.** ES-22, STRI-ID-45127. **d.** ES-23, STRI-ID-45189. **e.** ES-24, STRI-ID-44951. **f.** ES-26, STRI-ID-45166. **g.** ES-28, STRI-ID-35662. **h.** ES-29, STRI-ID-

35624. **i.** ES-30, STRI-ID-44991. **j.** ES-31, STRI-ID-45138. **j.** ES-32, STRI-ID-45149. All scales = 1 cm.

### **Morphotype ES33**

#### **Figure 8a**

Locality: 430134

Morphotype exemplar:

Other specimens studied: 35549, 36102, 45151, 45152, 45152, 45153, 45154, 45155, 45156, 45157, 45158

Description: The blade attachment is marginal. The laminar size is leptophyll to nanophyll; the laminar L:W ratio is 3:1; the laminar shape is oblong, with medial symmetry and basal asymmetry. The lamina is unlobed and untoothed. The apex is obtuse and the shape is rounded. The base angle is obtuse and the shape is rounded to slightly cordate. Primary venation is pinnate. Major secondaries are festooned brochidodromous. The intercostal tertiary veins are irregularly reticulate.

### **Morphotype ES34**

#### **Figure 8b**

Locality: 430134

Morphotype exemplar:

Other specimens studied: 35553, 45159, 45160, 45161, 45162, 45163, 45164, 45165

Description: The leaf attachment is petiolate. The blade attachment is marginal. The laminar size is nanophyll; the laminar L:W ratio is 2:1; the laminar shape is elliptic, with medial and basal symmetry. The lamina is unlobed and untoothed. The base angle is obtuse to reflex and the

shape is rounded to cordate. Primary venation is pinnate. Major secondaries are festooned brochidodromous with a wavy course. The intercostal tertiary veins are irregular reticulate.

### **Morphotype ES35**

#### **Figure 8c**

Locality: 430134

Morphotype exemplar:

Other specimens studied: 35557, 35624, 45170, 45171, 45172, 45173

Description: The laminar shape is possibly elliptic or oblong, with medial symmetry. The lamina is unlobed and untoothed. Primary venation is pinnate. Major secondaries are simple brochidodromous. The intercostal tertiary veins are sinuous opposite percurrent, obtuse to the midvein. Quaternary vein fabric is alternate percurrent.

### **Morphotype ES36**

#### **Figure 8d**

Locality: 430134

Morphotype exemplar:

Other specimens studied: 45167, 45168, 45169

Description: The laminar shape is possibly elliptic or oblong; the lamina has medial symmetry, is unlobed and toothed. The laminar size is possibly notophyll. Primary venation is pinnate. Major secondaries are semicraspedodromous, with decurrent attachment. The intercostal tertiary veins are sinuous opposite percurrent, obtuse to the midvein. Quaternary vein fabric is alternate percurrent.

Tooth spacing is regular, with one teeth order; 7 to 8 teeth/cm; sinus shape rounded. Tooth shape is convex to straight at the proximal flank, and straight to concave at the distal flank.

### **Morphotype ES37**

#### **Figure 8e**

Locality: 430134

Morphotype exemplar:

Other specimens studied: 45099, 45100, 45101, 45102, 45103

Description: The laminar shape is ovate, with medial symmetry. The lamina is unlobed and toothed. The laminar size is microphyll; the laminar L:W ratio is 1–2:1. The apex angle is acute. Primary venation is pinnate. Major secondaries are semicraspedodromous with an acute angle. The intercostal tertiary veins are alternate percurrent, and are obtuse to the midvein. Quaternary vein fabric is alternate percurrent.

Tooth spacing is regular, with one tooth order; there are approximately 12 teeth/cm; sinus shape angular. The tooth shape is convex/convex cv/cv.

### **Morphotype ES41**

#### **Figure 8f**

Locality: 110026

Morphotype exemplar:

Other specimens studied: 45237, 45289

Description: The leaf is possibly compound and the following description might represent a leaflet. The lamina attachment is petiolate. The petiole is thick possibly pulvinate. The blade

attachment is marginal. The laminar size is nanophyll; the laminar L:W ratio is 2.7:1; the laminar shape is elliptic, with medial and basal asymmetry. The lamina is unlobed and untoothed. The apex angle is acute with a straight shape. The base angle is obtuse and the shape is rounded. Primary venation is pinnate. Major secondaries are brochidodromous.

### **Morphotype ES42**

#### **Figure 8g**

Locality: 110026

Morphotype exemplar:

Other specimens studied: 45236

Description: The leaf is compound. The leaflet laminar size is nanophyll; the laminar L:W ratio is 2.4:1; the laminar shape is elliptic, with medial symmetry. The lamina is unlobed and untoothed. The apex angle is reflexed and the shape is emarginate. The base shape is possibly rounded. Primary venation is pinnate. Major secondaries are brochidodromous. Marginal vein is present and conspicuous. Intersecondary veins are parallel to subjacent secondaries, with lengths longer than 50% of subjacent secondary; these join subjacent secondaries, and they do not occur at all the intercostal areas. The intercostal tertiary veins are possibly alternate percurrent.

### **Morphotype ES43**

#### **Figure 8h**

Locality: 110026

Morphotype exemplar:

Other specimens studied: 35106, 35160, 35205, 35216, 35225, 35234, 35269, 35270, 35275, 36084, 36085, 36085, 36088, 36088, 36089, 45238, 45239, 45240, 45266, 45267, 45268, 45269,

45270, 45271, 45272, 45273, 45274, 45275, 45276, 45277, 45278, 45279, 45280, 45281, 45282, 45284, 45285, 45286, 45287

Description: The leaf attachment is petiolate. The blade attachment is marginal. The laminar size is notophyll to mesophyll; the laminar L:W ratio is 1.5:1; the laminar shape is ovate, with medial and basal symmetry. The lamina is unlobed and toothed. The apex angle is acute and the shape is straight. The base angle is reflex and the shape is cordate. Primary venation is actinodromous with more than three basal veins; the agrophic veins are compound. Major secondaries are semicraspedodromous. Interior secondaries are present. The minor secondary course is semicraspedodromous. The intercostal tertiary veins are mostly opposite percurrent, perpendicular to the midvein. Quaternary vein fabric is alternate percurrent.

Tooth spacing slightly irregular, with one tooth order; around seven teeth per cm; sinus shape is angular. Tooth shape is straight/straight.

### **Morphotype ES44**

#### **Figure 8i**

Locality: 110026

Morphotype exemplar:

Other specimens studied: 35272, 36084, 36089, 45247, 45248, 45249

Description: The leaf attachment is petiolate. The blade attachment is marginal. The laminar size is microphyll and mesophyll; the laminar L:W ratio is 1.7:1; the laminar shape is ovate, with medial and basal symmetry. The lamina is unlobed and untoothed. The base angle is obtuse and the shape is rounded. Primary venation is actinodromous with three strong basal veins; the agrophic veins are simple. Major secondaries are simple brochidodromous. Interior secondaries

are present. The minor secondary course is simple brochidodromous. The intercostal tertiary veins are opposite percurrent, acute to perpendicular to the midvein. The epimedial tertiaries are opposite percurrent, and have a proximal course acute to the midvein, its distal course is parallel to intercostal tertiary. Quaternary vein fabric is alternate percurrent.

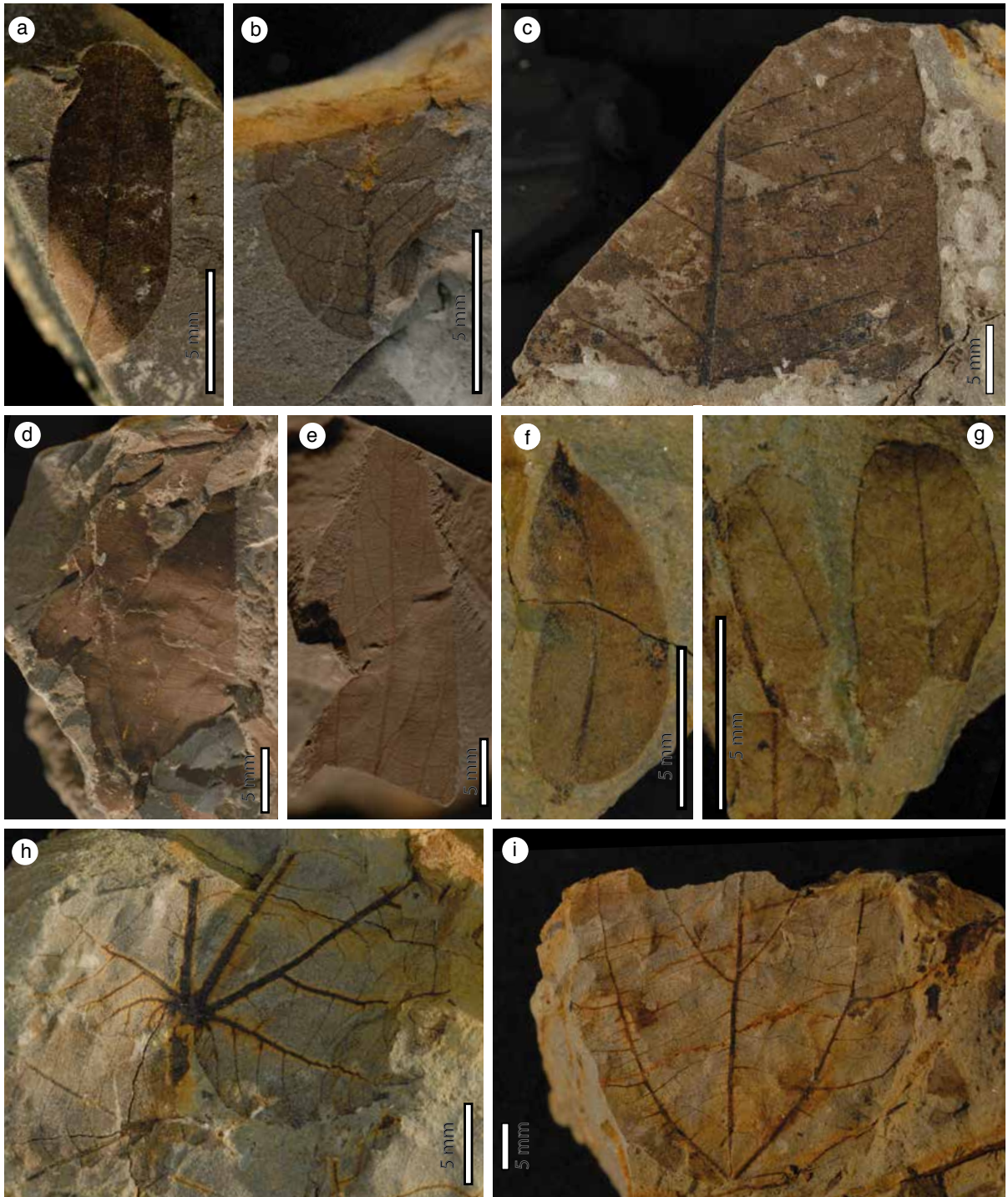


**Fig. 8. Fossil leaf morphotype exemplars**

Fossil leaf morphotype exemplars from the Esmeraldas Formations. **a.** ES33, STRI-ID-45156, **b.** ES34, STRI-ID-45162. **c.** ES35, STRI-ID-45170. **d.** ES36, STRI-ID-45167. **e.** ES37, STRI-ID-45101. **f.** ES41, STRI-ID-45237. **g.** ES42, STRI-ID-45236. **h.** ES43, STRI-ID-35269. **i.** ES44, STRI-ID-35272. All scales = 0.5 cm.

## **Morphotype ES45**

### **Figure 9a**

Locality: 110026

Morphotype exemplar:

Other specimens studied: 35159, 35209, 36088, 45241, 45242, 45243, 45245, 45246, 45288

Description: The blade attachment is marginal. The laminar size is notophyll; the laminar L:W ratio is 1.8:1; the laminar shape is ovate, with medial and basal symmetry. The lamina is unlobed and toothed. The apex angle is acute and the shape is possibly straight. The base angle is obtuse and the shape is possibly rounded. Primary venation is actinodromous with three major basal veins; the agrophic veins are compound. Major secondaries are brochidodromous. Interior secondaries are present. The minor secondary course is craspedodromous. The intercostal tertiary veins are opposite percurrent, perpendicular to the midvein. The epimedial tertiaries are opposite percurrent. Quaternary vein fabric is alternate percurrent.

Tooth spacing regular, with one tooth order; around 10 teeth/cm; sinus shape rounded. Tooth shapes; and flexuous/straight. Principal vein present; terminates present tooth apex.

## **Morphotype ES46**

### **Figure 9b**

Locality: 110026

Morphotype exemplar:

Other specimens studied: 35096, 45252, 45253, 45254

Description: The leaf attachment is petiolate. The blade attachment is marginal. The laminar size is microphyll; the laminar L:W ratio is 1.8:1; the laminar shape is elliptic, with medial and basal symmetry. The lamina is unlobed and untoothed. The apex angle is reflex and the shape is emarginate. The base angle is obtuse and the shape is rounded. Primary venation is pinnate. Major secondaries are brochidodromous. Intersecondary veins are present, with lengths shorter than 50% of subjacent secondary. The intercostal tertiary veins are possibly reticulated.

### **Morphotype ES47**

#### **Figure 9c**

Locality: 110026

Morphotype exemplar:

Other specimens studied: 35260, 35271, 35400, 45250, 45251

Description: The blade attachment is marginal. The laminar size is microphyll to mesophyll; the laminar L:W ratio is 2.1:1; the laminar shape is ovate, with medial and basal symmetry. The lamina is unlobed and untoothed. The apex angle is acute. The base angle is acute. Primary venation is pinnate. Major secondaries are brochidodromous and have a decurrent attachment. Intersecondary veins are parallel to subjacent secondaries, with lengths shorter than 50% of subjacent secondary; these are reticulating, and they do not occur at all the intercostal areas. The intercostal tertiary veins are alternate percurrent, obtuse to the midvein. The epimedial tertiaries are alternate percurrent. Quaternary vein fabric is alternate percurrent.

### **Morphotype ES48**

#### **Figure 9d**

Locality: 110026

Morphotype exemplar:

Other specimens studied: 35203, 35204, 35220, 35223, 35227, 35267, 35280, 35403, 45228, 45257, 45258, 45259, 45260, 45261, 45262, 45264, 45265, 45290, 45291, 45292, 45303, 45304

Description: The leaf attachment is petiolate, possibly pulvinate. The blade attachment is marginal. The laminar size is microphyll; the laminar L:W ratio is 2.1:1; the laminar shape is elliptic, with basal asymmetry. The lamina is unlobed and untoothed. The apex angle is reflex and the shape is emarginate. The base angle is obtuse and the shape is rounded. Primary venation is pinnate. Major secondaries are festooned brochidodromous. Intersecondary veins are parallel to subjacent secondaries, with lengths longer than 50% of subjacent secondary; these are reticulating distally, and they do not occur at all the intercostal areas. The intercostal tertiary veins are alternate percurrent.

### **Monocots**

At least four monocot morphotypes were recognized, however, due to the high degree of incompleteness of these specimens they were not described but they are illustrated in Fig. 9e–h. They are recognized as monocots because they have parallelodromous and closely spaced veins.

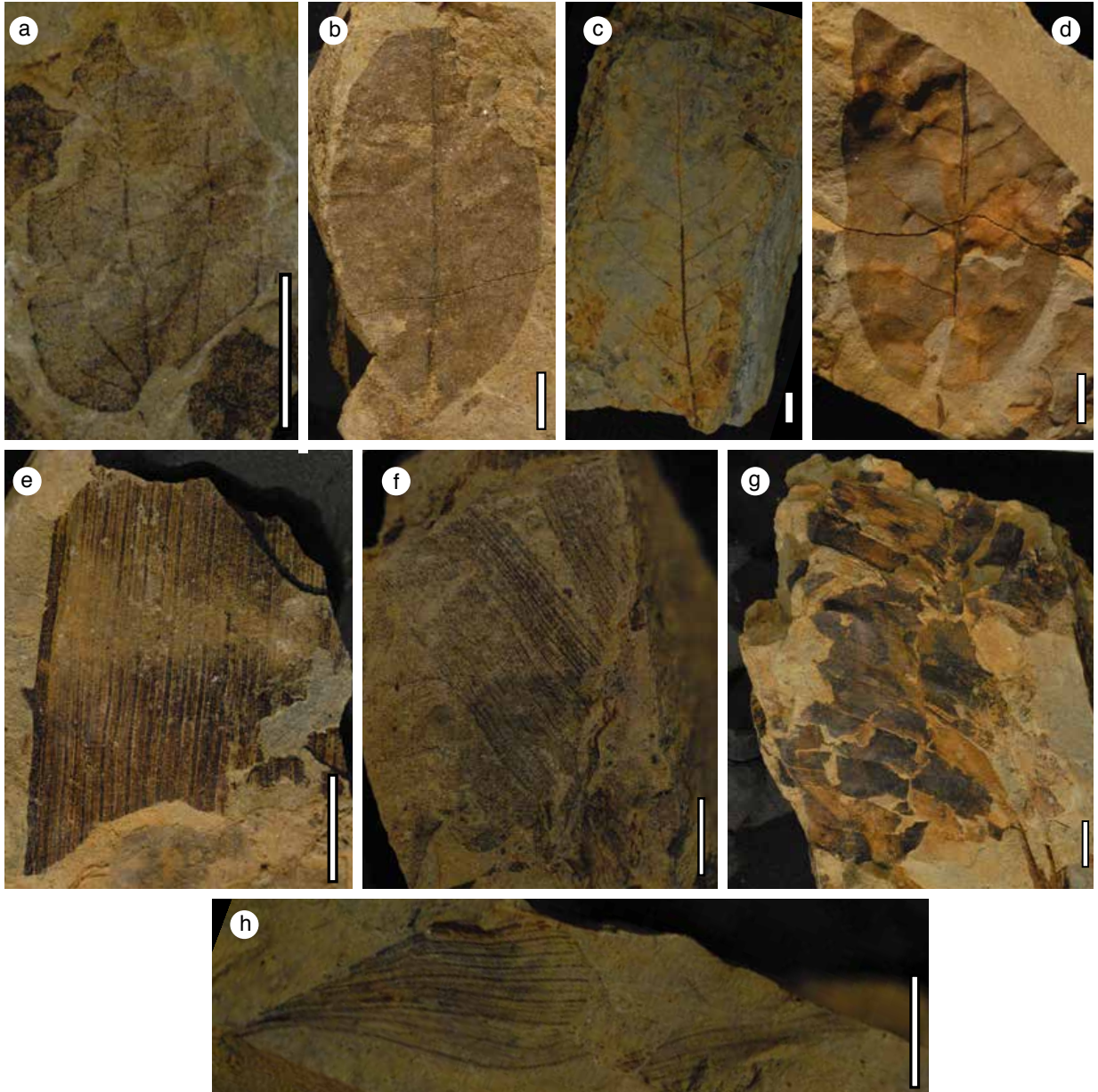


**Fig. 9. Fossil leaf morphotype exemplars**

Fossil leaf morphotype exemplars from the Esmeraldas Formations and monocot morphotypes. **a.** ES45, STRI-ID-45156, **b.** ES46, STRI-ID-45162. **c.** ES47, STRI-ID-45170. **d.** ES48, STRI-ID-45167. **e–h.** monocot morphotypes. All scales = 0.5 cm.

## Ferns

### Morphotype ES49

#### Figure 10

*Salvinia* sp.

Systematic affinity. Class Filicopsida; Order Salviniiales; Family Salviniaceae; Genus *Salvinia*; Species *incertae sedis*.

Locality: 430134

Morphotype exemplar: 35515

Other specimens studied: 35660, 36164

Description: These fossils consist on detached floating leaf compressions. Shape of floating leaves varies between oblong and ovate; width is 6.2 mm and length is 7 mm (only one specimen was found complete), base of lamina is cordate and apex is rounded (Fig. 10). Primary vein narrows distally. Floating leaves have 28 secondary veins, which are alternate, have straight courses, and remain parallel to each other from base to apex (Fig. 10). Angle between primary and secondary veins increases towards base of lamina; proximal secondary veins have an angle between  $110^{\circ}$  and  $80^{\circ}$ ; middle secondary veins have an angle between  $60^{\circ}$  to  $50^{\circ}$  and distal secondary veins between  $50^{\circ}$  to  $38^{\circ}$  (Fig. 10). Areoles have hexagonal shape in outline; its width ranges from 0.4 mm to 0.7 mm, and its length  $\sim$  0.2 mm to 0.4 mm. Usually, there is 1 tubercle per areole is 1, but sometimes there are 2 (Fig. 10). Tubercles are arranged in parallel rows that follow orientation of secondary veins. See details and comparisons in Pérez et al. (2017)

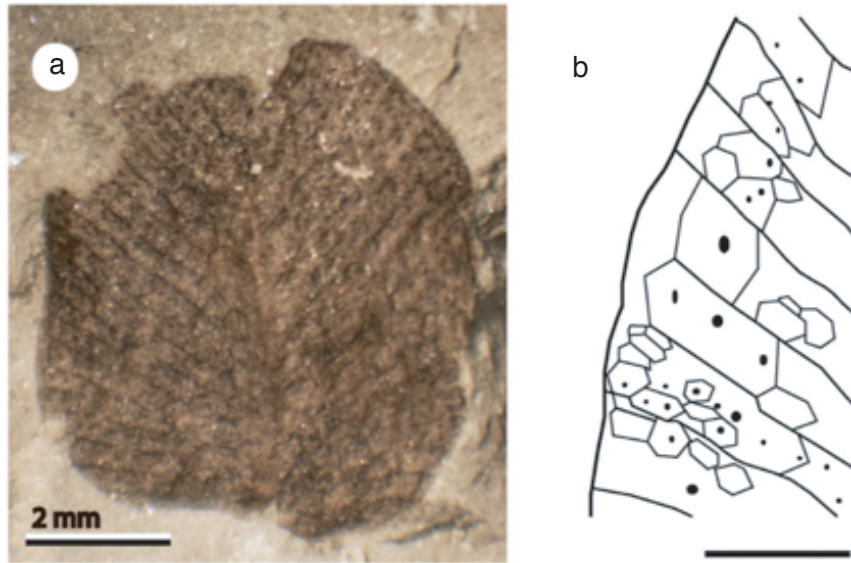


**Fig. 10. Morphotype ES49.**

Morphotype ES49. Macrofossil of *Salvinia* sp. 1 from the Esmeraldas Formation. STRI-35515. **a.** Floating leaf showing primary and secondary veins. STRI-35515. **b.** Drawing showing hexagonal areolas with one, two or three tubercles inside. STRI-35515.

## Reproductive structures

### Dicot Angiosperms

#### Morphotype ES50

#### Figure 11

Systematic affinity. Class Magnoliopsida; Order, Family, Genus and species *incertae sedis*.

Locality: 430134

Morphotype exemplar: 35554

Description: This morphotype is known from one specimen. The flowers have radial symmetry and have a diameter of 6.2 mm (from a top view). The perianth is well differentiated into calyx and corolla. The calyx is formed of five quincuncially arranged distinct sepals. From its insertion to its tip, the sepals measure between 1.9 and 2.2 (mean 2.1 mm) of length and

between 1.4 and 1.8 (mean 1.6 mm) of width. The calyx cells are isodiametric. The corolla is not preserved completely, but the bases of the petals are evident and these alternate with the sepals. The floral disc is 2.14 mm of diameter.

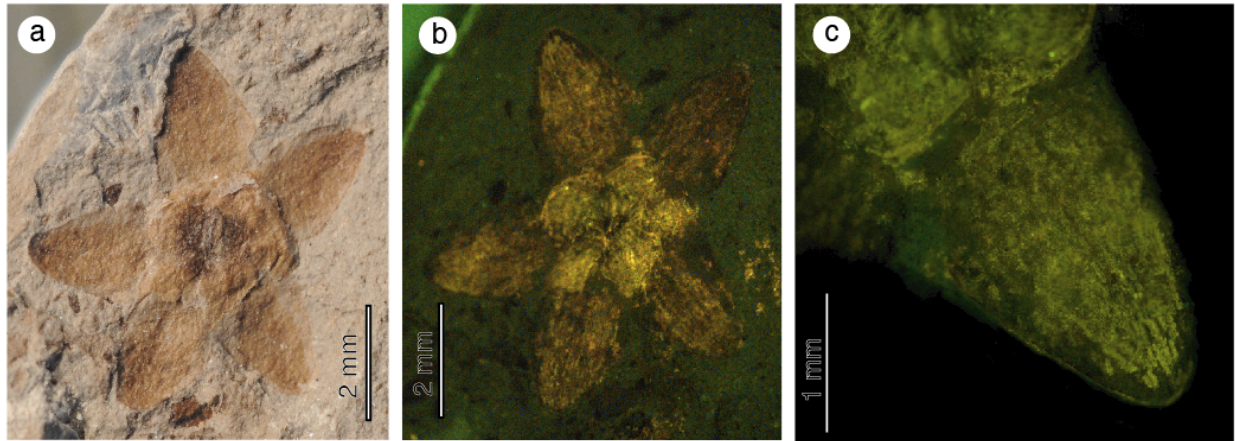


**Fig. 11. Morphotype ES50.** Flower compression STRI-ID-35554. **a.** Macro-photograph. **b.** Stereoscopic epifluorescence photograph. **c.** Sepal close-up.

### Morphotype ES51

#### Figure 12

Systematic affinity. Class Magnoliopsida; Order, Family, Genus and species *incertae sedis*.

Locality: 430134

Morphotype exemplar: 46599

Other specimens studied: 46600

Description: This morphotype is known from two specimens found in the same piece of rock, together with sample 36163. The flowers have radial symmetry. The differentiation between calyx and corolla could not be clearly determined, but it is probable (due to the location of the whorl) that the parts observed correspond to petals. The corolla is formed of five valvate distinct petals. The corolla is one whorled gamopetalous and campanulate; from the base of the

flower to the base of the petal lobes the corolla measures 2.6 mm and its width is 2.02 mm; the lobes are valvate and measure between 1.2 and 1.8 (mean 1.4 mm) in length and 0.7 and 0.9 (mean 0.8 mm) in width. From its insertion to its tip, the petals measure between 1.2 and 1.8 (mean 1.4 mm) of length and between 0.7 and 0.9 (mean 0.8 mm) of width. The corolla cells are isodiametric. There are 5 stamens and during anthesis, the stamens are exerted with respect to the perianth. The anthers are between 0.5 and 0.6 (mean 0.56 mm) in length and between 0.31 and 0.37 (mean 0.34 mm) in width.

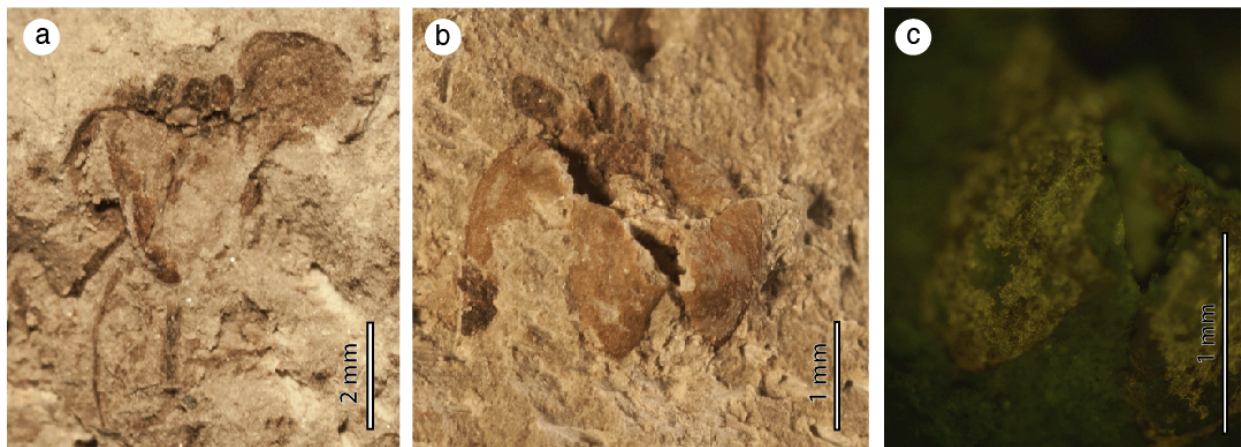


**Fig. 12. Morphotype ES51.**

Morphotype ES51. Flower compressions. **a.** Macro-photograph STRI-ID-46600. **b.** Macro-photograph STRI-ID-46599. **c.** Stereoscopic epifluorescence photograph petal close-up STRI-ID-46599.

### Morphotype ES52

#### Figure 13

*Stephania palaeosudamericana?*

Systematic affinity. Class Magnoliopsida; Order Ranunculales, Family Menispermaceae,

Genus *Stephania*; Species cf. *Stephania palaeosudamericana*

Locality: 110026

Morphotype exemplar: 43991

Description: The description was based on one specimen. Endocarp has in length 9.6 mm and in width 6.7 mm. The styler scar is inferred to be basal, based on the shape of the endocarp. Endocarp curvature is dorsoventral with a crescent and obovate shape. One limb is possibly broader and has also a broader dorsal ridge. The condyle is not preserved but based on the inferred basal styler scar, the condyle is deduced to be planar and compressed bilaterally. Ridging of the endocarp is only observed to be transverse. Endocarp wall is 1.2 mm in thickness (measured from the locule cast to the middle proximal side of the endocarp) and woody, based on its coaly preservation. The endocarp has a perforation that is complete, obovate and is 3.8 mm in length and 2.6 mm wide. The endocarp has conspicuous intrusive ribs within the locule that deforms the seed (>15 intrusive ribs). The funicular vascular supply possibly enters the locule ventrally. Endosperm is present and smooth.

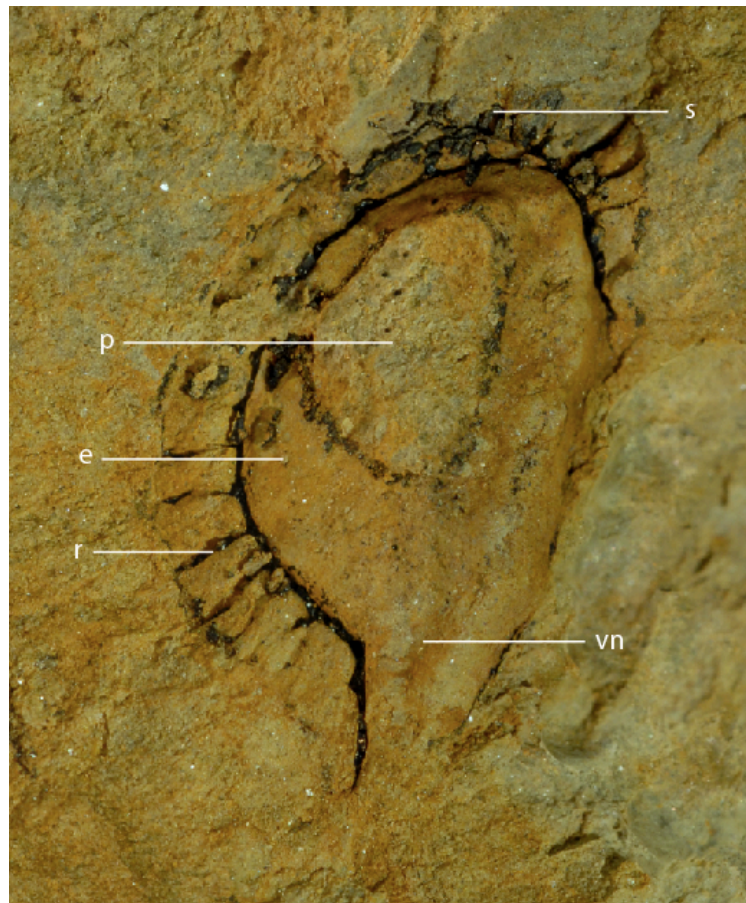


**Fig. 13. Morphotype ES52.**

Morphotype ES52. Endocarp compression STRI-ID-43991. e: endosperm; p: perforation; r: ribs; s: spines; vn: ventral notch

Notes: The Menispermaceae seed is described following the terminology Wefferling et al., (2013). Two methods were used for the identification of the seeds. As a first approximation, we used the key for fruit and seed characters of Menispermaceae (Wefferling et al., 2013). Further comparisons were done based on the matrices compiled by Herrera et al. (2011) and Wefferling et al. (2013).

Systematic affinity with *Stephania palaeosudamericana*: The results from the first analysis done following the key of Wefferling et al. (2013) suggested a systematic affinity with the SPACC clade, which includes the genera: *Stephania*, *Perichasma*, *Antizoma*, *Cyclea* and *Cissampelos*. The affinity with this clade is supported by the presence of an endocarp with dorsoventral curvature, dorsal ridging, condyle, endosperm, a locule with hippocrepiform shape, and a ventral vascular trace. Further comparisons within the SPACC clade were done using the character matrices included in Wefferling et al. (2013) and Herrera et al. (2011) studies. The fossil described here differs from *Perichasma* and *Antizoma* by the presence of only longitudinal ridging, which in this fossil is observed to be only transverse. The new fossil also differs from *Antizoma* and *Cyclea* by the presence ribs, which are conspicuous in the fossil. *Cissampelos* is also different because it has endocarps that are often imperforate, and also has two lateral and dorsal crests, which are not present in the fossil.

None of the characters described allowed the separation of the new fossil described here from the extant genus *Stephania* and the fossil species *Stephania paleosudamericana*. *Stephania paleosudamericana* (Herrera et al., 2011) only differs from our description by characters related to the size, including the total size, the perforation size, the wall thickness and the number of

ribs. We consider that these size-related characters can be highly affected by the developmental stage of the endocarps, the preservation of the fossils and possible intraspecific variation, and therefore are not sufficient grounds to name a new fossil species. If further collections from the Esmeraldas Formation reveal that there are more differences between this Eocene record and the Paleocene *S. paleosudamericana* fossil, a new species or morphogenus should be named.

### **Morphotype ES53**

#### **Figure 14**

Solanaceae

Systematic affinity. Class Magnoliopsida; Order Solanales, Family Solanaceae, Tribe Physalinae; Genus and species *incertae sedis*

Locality: 430134

Morphotype exemplar: 36163

Description: The morphotype was described based on one specimen of a compressed fruit with a preserved surrounding calyx. Pedicel preserved in the specimen had 5.22 mm in length, and a width of 0.6 mm. The estimated pedicel L:W ratio is higher than 8:1. Calyx basally is not invaginated, highly inflated and completely surrounds the berry, is five-lobed, partly open at apex, length by width 10.8 mm by 8.5 mm (1.3:1). Calyx lobes are equally sized, sinuses angular and incised one-sixth the total calyx length, tips acute triangular. Venation has one robust primary meridional vein per lobe, terminating at the lobed apex and alternating with secondary veins. Secondary veins emerge from the base, are visually distinct from the primaries and other vein orders, and bifurcate close to the lobe sinuses (Fig. 14c). Intersecondary veins arising near the base, visually distinct from secondaries and tertiaries, dichotomizing into the random,

irregular reticulum of tertiary through at least fourth order veins that fill most of the vein field. Berry is oval, flattened and coalified from fossilization, length by width 6.2 mm by 3.2 mm filling the half width of the calyx; seeds not preserved.

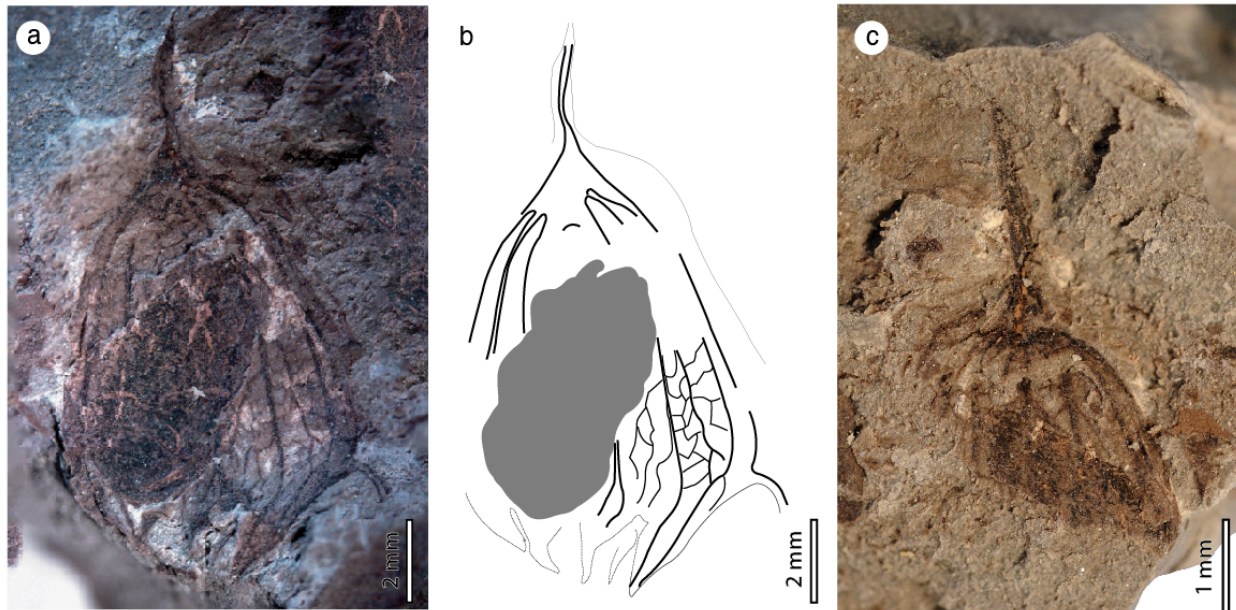


**Fig. 14. Morphotype ES53.**

Morphotype ES53. Fruit compression STRI-ID-36163. **a.** Stack photograph. **b.** Sketch showing venation details of the calyx. **c.** Counterpart.

Notes: The fossil was described based on the terminology described by Wilf et al. (2017)

Phylogenetic analysis: Following the same parameters, procedure and analysis performed by Wilf et al. (2017). The analysis included 110 modern taxa with accrescent calyx from the Solanaceae family. The results suggest that this fossil has a taxonomic affinity with the Tribe Physalinae, however is outside core group of *Physalis* (Fig. 15). Characters that differ between the fossil *Physalis infinemundi* are the pedicel length and width, its ratio L:W and more importantly the lack of invagination of the base of the accrescent calyx.



*Deviacer?*

Systematic affinity. Class Magnoliopsida; Order, Family, Genus and species *incertae sedis*

Locality: 430134

Morphotype exemplar: 35663

Other specimens studied: 44918, 44919, 44920, 44921, 44922, 44923, 35663

Description: The fossil specimens represent a fruit with a single proximal locule and a distal wing. The description was based on 7 specimens. The fruit has an average length of 17.6 mm from the pedicel attachment to the wing tip. Three specimens were found to be complete, so direct measurements of total length were done on these specimens and ranged between 15 to 23 mm. The broadest point of the fruit is located in the wing area and is on average 8 mm in width; there was a strong variability found in the wing width, with values that ranged between 6–11 mm. The ratio of the fruit length and width is 2:1. The wing is between 8 to 16 mm in length from the distal margin of the locule to the distal margin of the wing, and is between 6 to 11 mm in width at its broadest point. The locule is oval in shape, and has a length of 6 mm and a width 2.4 mm. The total length and width ratio is 4.5. The fruit has a faintly preserved style remnant located at end of the locule and beginning of the wing (Fig. 16a,b). The fruit has a constriction at the proximal side of the locule that could represent the attachment to the calyx (Fig. 16b). The locule has dense parallel venation (Fig. 16a). The boundary between the locule and the wing is transitional and then there is not a clear demarcation line between the two. The wing has dense parallel major venation with stronger veins investing the backbone of the wing and terminating at the distal side of the wing. Towards the distal side of the wing the veins are more spread and diminish in thickness. The primary veins have dichotomous branching. The minor venation is parallel. The fossils have a smooth margin along the wing.

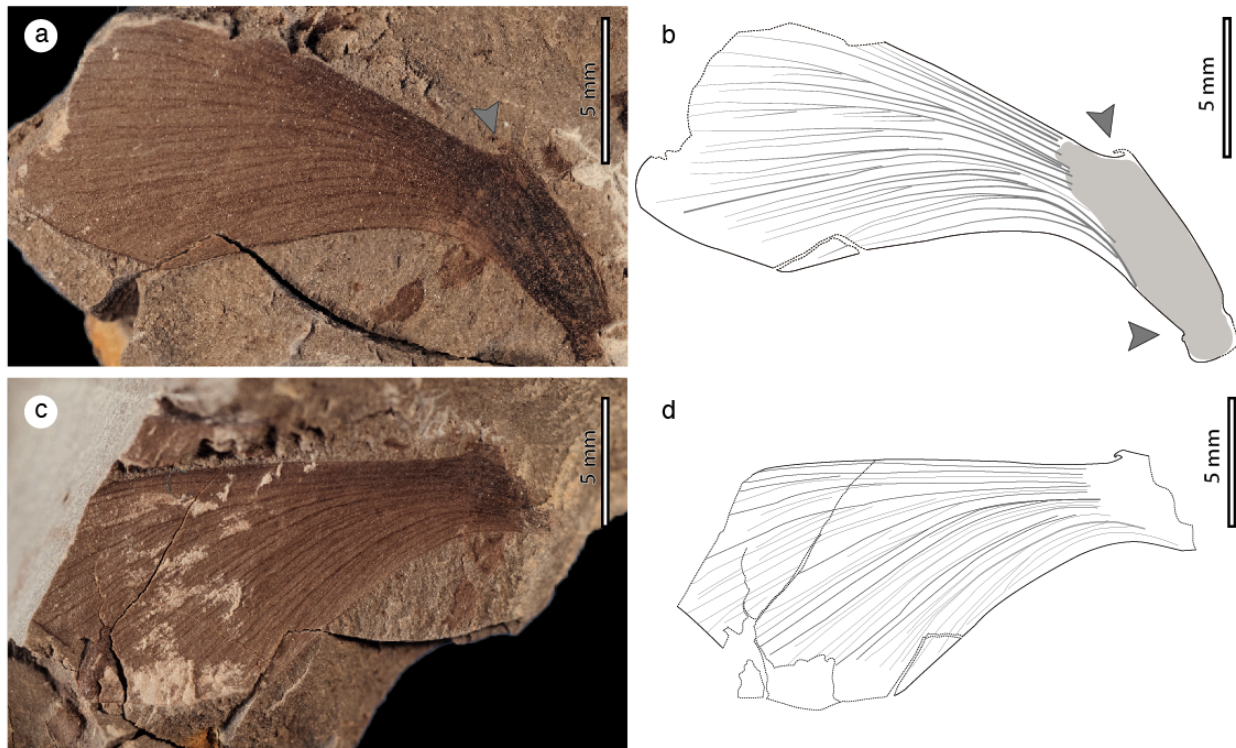


**Fig. 16. Morphotype ES54.**

Morphotype ES54. Samara compression STRI-ID-35663. **a.** Macro-photograph of the fruit. **b.** Sketch showing venation details. Upper arrow shows the presence of a faint style remnant. Lower arrow shows a constriction that could represent the attachment to the calyx **c.** Macro-photograph of the counterpart. **d.** Sketch showing venation details of the counterpart.

**Morphotype ES55**

**Figure 17a**

Legume pod 1

Systematic affinity. Class Magnoliopsida, Order Fabales, Family Fabaceae, Genus and species *incertae sedis*

Locality: 430134

Morphotype exemplar: 44942

Other specimens studied: 35065, 35146, 35178, 35206, 36085, 45293, 45294, 45295, 45296

Description: This morphotype was described based on fruit fragments because the specimens were not complete. The valve had a width of 18.2 mm and a length larger than 33.8 mm. The outline is smooth. Constrictions were not observed. At least three possible grooves run transversely across the valve at near right angles to the main vein. The style remnant is located towards the middle of the valve and has a length of 0.8 mm and a width of 1.54 mm.

### **Morphotype ES56**

#### **Figure 17b**

Legume pod 2

Systematic affinity. Class Magnoliopsida, Order Fabales, Family Fabaceae, Genus and species *incertae sedis*

Locality: 430134

Morphotype exemplar: 44940

Other specimens studied: 35065, 35146, 35178, 35206, 36085, 45293, 45294, 45295, 45296

Description: This morphotype was described based on fruit fragments because the specimens were not complete. The valve had a width of 11.6 mm and a length larger than 16 mm. The outline is smooth. Constrictions were not observed. A thick vein encircles the valve. External to this vein on one side of the valve there is a narrow keel (up to 1.1 mm wide). At least five possible grooves run transversely across the valve at near right angles to the main vein. The style remnant is located towards one axis of the valve and has a length of 1.2 mm and a width of 0.48 mm.

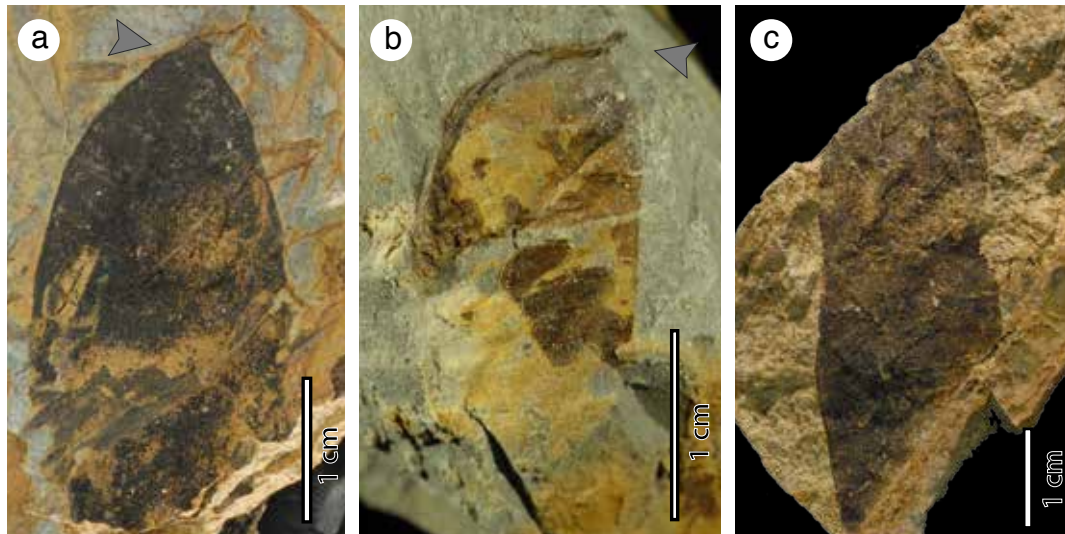


**Fig. 17. Legume pods.**

Legume pods. **a.** ES55, STRI-ID-44942. **b.** ES56, STRI-ID-44940. **c.** Possible legume pod, not described.

## Monocot Angiosperms

### Morphotype ES57

#### Figure 18

Cyperaceae? Achene

Systematic affinity. Class Liliopsida; Order Poales; Family cf. Cyperaceae Genus and species *incertae sedis*

Locality: 430134

Morphotype exemplar: 44948

Other specimens studied: 35441, 35551, 35656, 35665, 35671, 36085, 36152, 44944, 44945, 44946, 44947

Description: This achene morphotype is described based on 12 specimens. The holotype has 3D preservation, therefore most of the description is based on this specimen. The description was done following Jiménez-Mejías and Martinetto (2013) terminology. The fruit shape is elliptic, with a length and width of 1.3 and 1.42 mm, respectively; the L:W ratio is 1.1:1. What is interpreted as the callus remnant has a width of 0.27 mm. The base is winged, the wing has a length of 1.12 mm and a width of 0.62 mm. The pericarp is thin and has a thickness of 0.02 mm. The seed coat has transverse ridges with polygonal shape. The tubercle is very thick and covers approximately the entire apical part of the seed, has a width of 1.30 mm and a thickness of 0.64 mm. The achene is inflated. The two structures coming out from the tubercle are interpreted here as possible style or stigma remnants. In most of the specimens two asymmetrical appendages were observed, only a few had one. In the holotype one appendage was 4.2 mm in length and 0.8 in width, the other had the same width and a length of 1.8 mm.

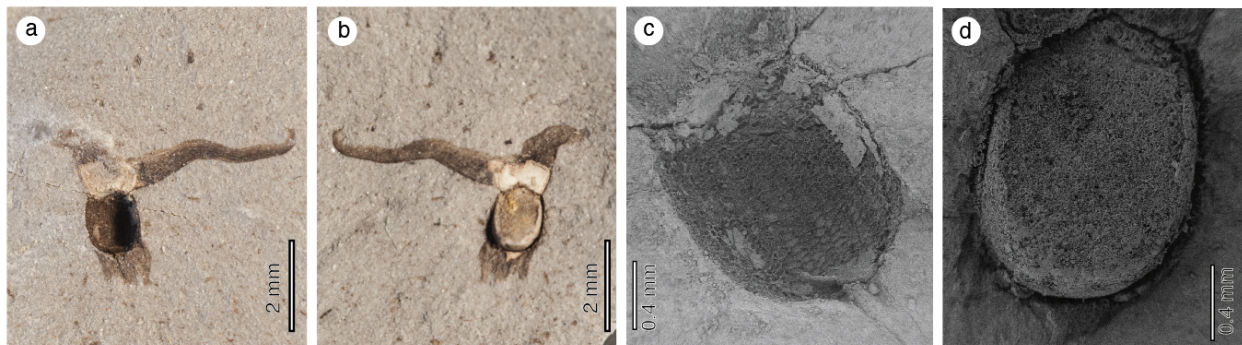


**Fig. 18. Morphotype ES57. ‘**

Morphotype ES57. Fruit compression STRI-ID-44948. **a.** Macro-photograph of the fruit. **b.** Macro-photograph of the fruit counterpart. **c.** SEM photograph showing the seed coat with transverse ridges with polygonal shape. **d.** SEM photograph for the counterpart.

Notes: This fossil morphotype shares with achenes from the Cyperaceae family; the presence of a seed with elliptical shape, a seed-coat with transverse ridges, and a thick tubercle.

The affinity is however uncertain, because none of the extant specimens observed have similar appendages to those borne from the tubercle as observed in the holotype.

***Paleoclimatic analyses***

*Leaf area estimation*— Leaf size classes, the proportion of each leaf class in each locality, and values used to estimate the mean natural log of the leaf area (*MlnA*) for each locality and are shown in Table 1. Although there are fewer morphotypes described for locality 110026 compared to locality 430134 (9 vs. 26) the proportion of leaf size categories is relatively similar. Microphyll leaf class size is the most abundant in both localities (Table 1). Smaller leaf size classes such as leptophyll and nanophyll are slightly more abundant in locality 431034, while larger leaf size classes such as notophyll and mesophyll are slightly more abundant in locality 110026 compared with locality 431034 (Table 1). These differences are however, not significant and therefore it can be inferred that both localities have a relatively similar distribution of leaf sizes. The *MlnA* was slightly higher for locality 110026 compared with locality 430134 (Table 1).

Leaf economic traits (Royer et al., 2007) and digital leaf physiognomy methods (Royer et al., 2005; Peppe et al., 2011) could not be performed because most of the leaves from this flora did not have petioles preserved and the preservation did not occur in one plane, instead most leaves were undulated and fragmented due to the lack of lamination of the rocks in which they were preserved.

Size class	Size class ranges (cm <sup>2</sup> )	<i>p<sub>i</sub></i>		<i>a<sub>i</sub></i>	<i>MlnA (a<sub>i</sub>p<sub>i</sub>)</i>	
		110026 (N=9)	430134 (N=26)		110026	430134
Leptophyll	≤0.25	0	0.027497	2.12	0	0.058293
Nanophyll	0.25–2.25	0.207801	0.260943	4.32	0.897702	1.127274
Microphyll	2.25–20.25	0.449733	0.547944	6.51	2.927767	3.567117

Notophyll	20.25–45.00	0.207594	0.125153	8.01	1.662834	1.002481
Mesophyll	45.00–182.25	0.134869	0	9.11	1.228663	0
$\Sigma a_i p_i$					6.716968	5.755167

**Table 1. Mean leaf area estimation.**

$MlnA$  is the average leaf area of all dicot species calculated according to Wilf et al. (1998), where  $MlnA = \Sigma a_i p_i$ , where  $a_i$  corresponds to the seven means of the natural log areas of the size classes (Wilf, 1998), and  $p_i$  corresponds to the proportion of species in each of the size classes.

*Leaf margin estimation*— For locality 110026, seven out of nine morphotypes have entire margins. Therefore,  $pE$  for this locality was 0.7778. For locality 430134, 22 out of 26 morphotypes have entire margins, therefore  $pE$  for this locality was 0.8461.

*Leaf area and margin analyses* — Table 2 shows leaf area paleoprecipitation and leaf margin paleotemperature estimates. The precipitation for stratigraphically higher locality (430134), with more diverse and abundant leaves, was lower than for the other locality (110026). The estimated mean annual precipitation varies from 50 cm (430134) to 104 cm (110026). The equation based on tropical reference data only (Jacobs and Herendeen, 2004) gave higher precipitation estimates. For all the reference equations, the estimates of mean annual temperature range between 22° to 27° C. Temperature estimates are slightly lower (1 °C to 2 °C) for the stratigraphically lower locality (110026). The two reference equations whose databases focus on tropical South America (Kowalski & Dilcher, 2003; Hinojosa et al., 2010) yield temperature estimates that differ from one another by approximately 3 °C (Table 2).

Analysis	Method	Data	Equation	SE	Localities	
					430134	110026
Leaf Area	Jacobs and Herendeen, 2004	Tropical Africa and Bolivia (N=42)	$0.309MlnA + 2.566$	$SE = SE(\log Y) * e^{(o - \log Y)}$	77 cm ± 40	104 cm ± 48

	Wilf et al., 1998	Worldwide (N=42)	0.548 <i>MlnA</i> + 0.768	<i>lnMAP</i> +/- 0.359	50 cm (35–72)	85 cm (60–122)
<b>Leaf Margin</b>	Wilf, 1997	Worldwide (N=42, excluding extreme cold)	24.4 <i>pE</i> + 3.25	3.6	23.9 °C	22.2 °C
	Kowalski and Dilcher, 2003	Bolivia (N=12)	31.6 <i>pE</i> – 0.059	3.6	26.7 °C	24.5 °C
	Hinojosa et al., 2010	Tropical South America (N=44)	23.42 <i>pE</i> + 3.6	3.5	23.4 °C	21.8 °C

**Table 2. Results of leaf margin and leaf area analysis**

Results of leaf margin and leaf area analyses for quantitative estimation of paleotemperature and paleoprecipitation. *MlnA* is the mean leaf area of all dicot species and was calculated above for each locality. *pE* is the proportion of dicot leaf morphotypes with entire margins calculated above for each locality. SE corresponds to the standard error.

## DISCUSSION

The flora from the Esmeraldas Formation is the first Eocene macroflora from the Neotropical region to be used in paleoecologic analyses. This flora provides important evidence in reconstructing the vegetation, biogeographic patterns, and climate of the Middle to Late Eocene of this region. Herein, I bring together stratigraphic information, carbon isotope analyses, descriptions of vegetative and fertile material, and paleoclimatic analyses based on leaf physiognomic characteristics, with the goal of reconstructing the paleoenvironment of the Esmeraldas Formation. All the evidence presented here suggests that this flora is highly similar to a contemporary seasonally dry tropical forest ecosystem.

*Stratigraphy.* The exposition of rock along a section that enclosed the Paleogene interval of the Nuevo Mundo Syncline due to the construction of the Hidrosogamoso dam allowed us to measure and collect freshly exposed rocks samples along a continuous section of 1350 m stratigraphic height. Our section included the top of the La Paz Formation, the Esmeraldas

Formation, and the base of the Mugrosa Formation. The lithologic and stratigraphic information gathered here, together with our  $\delta^{13}\text{C}_{\text{TOM}}$  chronostratigraphic analyses, provide sufficient evidence to propose age estimations to more accurately define the depositional environments for these Formations. The lithology, the bed geometry, the bounding contacts and the bed sorting described for the Esmeraldas Formation, provide evidence to infer a depositional environment of floodplains associated to river channels. Features like root traces, soil carbonate nodules, and formation of paleosols could indicate a paleoclimate that experienced rainfall seasonality. The Esmeraldas Formation is a unit of approximately 750 m in thickness, that spans the Middle to Late Eocene.

*Evaluation of marine influence hypothesis.* Both of the macroflora localities studied here were located in the eastern flank of the Esmeraldas Formation in the Nuevo Mundo Syncline (Fig. 1). Caballero et al. (2010) proposed that the eastern flank of the Esmeraldas Formation in the Nuevo Mundo Syncline was deposited in transitional fluvial to estuarine environments under marine influence, while the western flank was fluvial and lacustrine. Gómez et al. (2005) suggested that the Esmeraldas Formation did not have marine influence and was deposited in alluvial plains with minor drainage channel deposits. A marine incursion has been documented during the Middle to Late Eocene in northwestern South America, reaching the Eastern Cordillera and the Central-Eastern Llanos Foothills (Santos et al., 2008). However, the palynological evidence presented earlier by Forero-Rodríguez et al. (2012), and preliminary palynological analysis for samples from this section (Martínez-Murcia *pers. comm.*), found a complete absence of marine palynomorphs. Forero-Rodríguez et al. (2012) describe the depositional environment of the Esmeraldas Formation to be fluvial with a development of a short-lived lacustrine system in the Late Eocene associated that corresponded to Los Corros

Horizon. These palynological evidence together with facies analysis by Gómez et al. (2005), suggest that the Esmeraldas Formation did not form under marine influence. In addition, evidence of the presence of the aquatic fern *Salvinia* towards the top of the Esmeraldas Formations provides information about the lack of salinity of the water bodies in which the microfossil flora was deposited (Locality 430134). *Salvinia* today inhabits calm freshwater bodies such as lakes and ponds (Collinson, 2002) and is intolerant of salinity over 5 psu (Collinson et al., 2013). The presence of *Salvinia* fossils in the Esmeraldas Formation therefore indicates that the paleoenvironment for this locality was not under marine influence.

*$\delta^{13}\text{C}$  analysis from bulk organic matter ( $\delta^{13}\text{C}_{\text{TOM}}$ )*. The geochemical chronostratigraphic analysis based on the  $\delta^{13}\text{C}$  signature from bulk organic matter showed that this method can be used as a complementary dating tool for terrestrial ecosystems. The strong signature shown by the measurements of  $\delta^{13}\text{C}_{\text{TOM}}$  allowed the correlation with a composite northern South America section previously studied and age calibrated with the  $\delta^{13}\text{C}_{\text{carbonate}}$  curve from Zachos et al. (2001). The correlation confirmed the preliminary dating analyses based on palynological evidence from this study and the one from Forero-Rodríguez et al. (2012), and also confirmed that the Corros Horizon marks the boundary between the Eocene and the Oligocene (Pilsbry and Olsson, 1935). Additionally, this analysis provides evidence to propose a slight change in the age of La Paz Formation and the maximum age of the Middle Magdalena Valley Unconformity. The isotopic chronostratigraphic correlation suggests that the top of La Paz Formation is Early Eocene, and therefore the Middle Magdalena Valley Unconformity does not span the Early Eocene in the Nuevo Mundo Syncline. It is possible that the La Paz Formation spans the Early Eocene Climatic Optimum and possibly the Paleocene-Eocene Thermal Maximum. More samples from the base of this section (top of La Paz Formation and the base of Esmeraldas

Formation: stratigraphic height between 0 and 500 m) are currently under analysis; these new data will potentially generate more resolution of the  $\delta^{13}\text{C}_{\text{TOM}}$  towards the base of the section and will improve the correlation with the climatic events from the Early Eocene.

*Cuticles.* Although the cuticle material collected here was difficult to interpret, it contained valuable information regarding stomatal patterns that are not common or widely observed and explored in angiosperms. The stomatal pattern observed in the adaxial cuticle of the ES11 morphotype described here is rarely discovered. The only case in which this pattern has been observed, at least to my knowledge, was to evaluate the taxonomic significance of stomatal distribution patterns in Leguminosae (Leelavathi et al., 1980). Stomata distributed on the midvein and secondary veins in the adaxial side of the leaf has been reported in the legume genus *Pithecellobium* (Leelavathi et al., 1980). Stomata confined to the midvein in the adaxial side was observed in the genera *Albizia*, *Delonix*, *Cassia* and *Abrus* (Leelavathi et al., 1980). They, however, did not report the exact pattern observed in the fossil cuticle from the ES11 morphotype, which has stomata on the midvein and on either side of the secondary veins. The four genera that share these similar stomatal patterns are today distributed mainly in seasonally dry tropical forests, dry tropical woodlands and thorn scrub ecosystems. The leaf architecture of the four legume genera mentioned above is not similar to the leaf architecture of ES11, therefore, a taxonomic association with these groups is not proposed.

In addition to the stomatal patterns, the presence of thick epicuticular waxes can also give taxonomic information for future identification of this morphotype. The thick epicuticular waxes can be inferred to inform paleoecological inferences, since in modern flora epicuticular waxes are more commonly found under water-limiting conditions with high light intensity and temperatures (Jenks and Ashworth, 1999). Modern tropical dry ecosystems could therefore be

characterized by a higher proportion of plants with abundant epicuticular waxes. Difficulties in the interpretation of the stomatal anatomy could possibly be due to the lack of definitions of the cells caused by the presence of the epicuticular waxes, papillae and sunken stomata, however, I am not certain of the last two characters. The fact that only one cuticular morphotype was found despite a high number of samples could result from taphonomic circumstances, if the preservation of this morphotype was favored, perhaps because these thick epicuticular waxes were more resistant to decay (Eglinton and Hamilton, 1967). A more detailed exploration and description of the cuticular material is needed to improve the current interpretations and taxonomic affinities.

*Paleoclimate.* The aim of the paleoclimatic analyses for this study was to generate a first approximation to the paleoclimate of the locality and to explore the application of quantitative paleoclimate methods to this fossil material. The sampling effort for this flora is not enough to obtain robust estimations. For example, floras containing less than 10 morphotypes can have more than 5°C of error in the temperature estimates (Wilf 1997), therefore the paleoclimatic analyses done here with the 9 morphotypes described from the stratigraphically lower locality (110026) are not robust, and were performed only as an exploratory analysis. Both localities involved difficult conditions needed to create a deep quarry and to perform a more standard collecting method to complete a wider census process. One of the localities was located on private property, that we were not allowed to modify drastically, and the other one was next to a private road, that had heavy traffic and no shoulders to provide sufficient space or conditions needed to successfully create a deep quarry. The lack of lamination of the rocks from which the fossils were collected also did not facilitate the extraction of blocks of rock. I did not use digital physiognomy methods (Peppe et al., 2011) for this flora because the lack of lamination and

lithology promoted the preservations of leaves with deep undulations and tridimensionality that would have created noise in a photography-based estimation of area. These characteristics of the rock caused a high number of samples to be fragmented, reducing the number of samples for analysis.

Despite these unfavorable conditions, I was able to conduct exploratory analysis and to conclude that the paleoclimatic conditions estimated for the Esmeraldas Formation were warm and relatively dry. The two fossil localities are not combined in a paleoclimate interval because their stratigraphic separation by approximately 200 m corresponds to an interval of 1 to 10 million years. The greater abundance of samples for the stratigraphically higher locality (430134), compared to the lower locality (110026), results in higher confidence in the 430134 result. The mean annual temperature (MAT) estimated for locality 430134 ranged between 23 and 27 °C depending on the calibration dataset method used for the regression models. The lower MAT values were obtained for the model based on 44 sites from Tropical South America, while the highest MAT values were obtained for the model based on 12 sites from Bolivia. Due to the restricted distribution and small number of sites used for the model that provided the highest estimation, I consider that this value could be biased and consider that the lower MAT value obtained from the Hinojosa et al. (2010) model is more robust. The mean annual paleo-precipitation (MAP) ranged between 50 to 77 cm, also depending on the calibration dataset used for the regression models. The lower MAP value was obtained for the model based on worldwide data, while the highest MAT value was obtained for the model based on tropical South American and African data. Because both models use the same number of sites for calibration, I consider that the estimation based only on tropical sites could provide a more accurate estimation for the

430134 Esmeraldas flora. The estimation for the 110026 locality was for paleo-MAT slightly lower and for paleo-MAP slightly higher by approximately 2 °C and 30 cm, respectively.

How the differing paleoclimate estimates of the two horizons should be interpreted is uncertain. One possibility is that the difference of depositional environments between the two horizons, with higher energy fluvial conditions interpreted for locality 110026, would lead to different taphonomic conditions. Alternatively, during the time period of 5 to 9 Ma between the deposition of the 110026 and the 431034 localities, the climatic conditions could likely have changed. In addition, the more positive values recorded in the  $\delta^{13}C_{TOM}$  for the stratigraphically lower locality (110026; peak near -23‰), compared with values around -25‰ for the stratigraphically higher locality (430134) could be related with climatic differences. In particular the Mid-Eocene Climatic Optimum, which is coetaneous with the  $\delta^{13}C_{TOM}$  peak, could be responsible for these isotopic differences. If so, one would expect that conditions were hotter during the time of the lower Flora (110026). However, our paleo-botanical results show the opposite pattern for paleo-MAT values, with locality 110026 registering approximately 2 °C cooler conditions than for the younger Flora. However, as mentioned before more samples are needed to obtain more robust estimations for this locality.”

Today this region has a MAP of 185.9 cm and a MAT of 26.3°C (based on values for 2012 and 2013) (ISAGÉN, 2014). Therefore, the modern temperature is relatively similar to those Middle to Late Eocene conditions, and yet the estimated precipitation is drastically different, being almost two or three times higher today. Climatic conditions in current environments in Colombia similar to those estimated for the Esmeraldas Formation are found today in the Caribbean region, inter-Andean valleys near the Cauca and Magdalena rivers, and in the north-Andean region in Santander and Norte de Santander (IDEAM, 2015). The type of ecosystem that

today dominates these regions is the seasonally dry tropical forest (SDTF; Pizano et al., 2014). The SDTF is a lowland ecosystem that is characterized by heavy rain seasonality and a high concentration of endemic (restricted to a certain area) species, particularly adapted to long and dry periods (Pizano et al., 2014).

SDTF ecosystems can be defined in terms of temperature, precipitation, and floristic composition. These modern parameters include a wide gradient of temperature and precipitation that can provide suitable conditions for a diverse array of vegetation formations (Graham and Dilcher, 1995; Pennington et al., 2006). The MAT is defined as higher than 17 °C, the MAP is between 50 and 180 cm, and more than 5–6 months receive less than 10 cm of rainfall (Holdridge, 1967; Graham and Dilcher, 1995; Pennington et al., 2006). The MAT and MAP estimations for the Esmeraldas Formation are within the parameters used to define SDTF. Therefore, it is possible this paleoflora would correspond to a SDTF.

The low precipitation estimated for the Esmeraldas Formation is in contrast to Paleocene tropical regimes like the one reported in the Cerrejón Formation located in the northernmost peninsula of South America, in the Guajira Department, Colombia. The Cerrejón Formation represents the earliest record of an American tropical rainforest, in which temperatures of approximately 28 °C were comparable to the estimate for Esmeraldas Formation. However, the Cerrejón Formation mean annual precipitation was considerably higher, with values around 324 cm (Wing et al., 2009). Comparisons with Floras from the Claiborne Flora from Tennessee, USA, show more similar precipitation conditions despite the large differences in latitude. The early Eocene Wilcox Flora is often described as tropical dry forest and is hypothesized as representing a pronounced drying trend from the Paleocene into at least the Middle Eocene

(Wolfe, 1978). This same trend towards drier conditions in the localities represented by the Esmeraldas Flora is suggested by the analysis, discussed here, of new multifaceted evidence.

#### *Taxonomic affinities*

In terms of the taxonomic affinities of the Esmeraldas flora, the occurrence of samara fruits from the Dalbergieae clade within the legumes (Martínez, 2018), multiple morphotypes of leaflets and fruits from the legume family, and the possible presence of the fossil genus *Deviacer*, each suggests that the possible ecosystem which they inhabited was a SDTF. In addition, the other taxa identified in the flora, Solanaceae, Menispermaceae, Salviniaceae (Pérez-Consuegra et al., 2017) and Passifloraceae (Martínez, 2017) are taxa that, although not exclusively distributed in SDTF, are found today in SDTFs in Colombia (Pizano et al., 2014). Future formal descriptions and naming of this fossil material would provide evidence to address inferences about the evolutionary and biogeographic patterns of these families.

All the evidence presented here suggests that the Esmeraldas Flora shares similarities with a SDTF. The macroflora from the Esmeraldas Formation could represent the earliest evidence of a possible SDTF. This has important implications in the understanding of SDTFs, since all the available records until today, suggest that this ecosystem appeared during the Miocene in the Neotropical region (Graham and Dilcher, 1995; Pennington et al., 2009). Future evidence from the palynological record from the Esmeraldas Formation, currently under analysis, will provide more data to test the hypothesis that the Esmeraldas Flora represents the earliest record of a seasonally dry tropical forest. Seasonally dry tropical forests are today economically important and diverse ecosystems with fertile soils that are very suitable for agriculture. Many crops like corn, tomato, beans and peanuts were domesticated within such ecosystems. Given that these taxa have adaptations to survive long dry seasons, understanding the subsequent evolution of

SDTFs might help us anticipate additional implications of our current anthropogenic climate change.

The new paleoclimatic and paleoenvironmental estimates inferred from the Esmeraldas Flora suggest that the global cooling and increasing aridity that characterized the Late Eocene to Early Oligocene interval in temperate regions (Berggren and Prothero, 1992) could have also extended to tropical regions. In the Tropics, the reduced precipitation may have given origin to tropical dry forests, or ecosystems more adapted to rain seasonality. Understanding the climate in the past is a key part of climate modeling into the future, given that it provides information about how the Earth behaved under very different conditions. Paleoclimate parameters can be used to test climate models. Climate models that are calibrated to paleoclimate states are suitable to be used to predict scenarios that can help preview the consequences for our current climate change and guide our policy makers.

### ***Conclusions***

The coupled study of the plant macrofossil record from the Esmeraldas Formation and the stratigraphic record of a section of the Nuevo Mundo Syncline allowed the paleoenvironmental reconstruction of the Esmeraldas Formation. The stratigraphic information and chronostratigraphic isotopic analyses indicate that La Paz Formation has an Early Eocene age, the Esmeraldas Formation is Middle to Late Eocene, and Los Corros Horizon is the limit between the Eocene and the Oligocene. The morphological and anatomical comparative study of the plant macrofossil record from the Esmeraldas Formation allowed the identification of six extant families: Fabaceae, Menispermaceae, Solanaceae, Passifloraceae, Salviniaceae and possibly Cyperaceae. The leaf physiognomy paleoclimatic analyses indicate that the Esmeraldas Flora lived under warm temperatures and seasonal rainfall. The Esmeraldas Flora suggests that

the Middle to Late Eocene tropics had more seasonal conditions than today, like modern temperate regions. All the evidence presented here is indicating that the Esmeraldas Flora represents the earliest evidence of a seasonally dry tropical forest.

## REFERENCES

- Arens, N. C., and A. H. Jahren. 2000. Carbon Isotope Excursion in Atmospheric CO<sub>2</sub> at the Cretaceous-Tertiary Boundary: Evidence from Terrestrial Sediments. *PALAIOS* 15: 314–322.
- Berggren, W. A., S. Lucas, and M.-P. Aubry. 1998. Late Paleocene-early Eocene climatic and biotic evolution: An overview. Late Paleocene-Early Eocene Climatic and Biotic Events in the Marine and Terrestrial Records., 1–17. Columbia University Press, New York, USA.
- Berggren, W. A., and D. R. Prothero. 1992. Eocene-oligocene: climatic and biotic evolution: an overview. Eocene-Oligocene climatic and biotic evolution, 1–28. Princeton University Press, USA.
- Berry, E. W. 1935. Tertiary Plants from Brazil. *Proceedings of the American Philosophical Society* 75: 565–590.
- Burnham, R. J. 1995. A New Species of Winged Fruit from the Miocene of Ecuador: *Tipuana ecuatoriana* (Leguminosae). *American Journal of Botany* 82: 1599–1607.
- Burnham, R. J., and N. L. Carranco. 2004. Miocene winged fruits of *Loxopterygium* (Anacardiaceae) from the Ecuadorian Andes. *American journal of Botany* 91: 1767–1773.
- Caballero, V. M. 2010. Evolución tectono-sedimentaria del Sinclinal de Nuevo Mundo, cuenca sedimentaria Valle Medio del Magdalena Colombia, durante el Oligoceno - Mioceno. Universidad Industrial de Santander, Bucaramanga, Colombia.
- Caballero, V., M. Parra, M. Bohorquez, and A. Roberto. 2010. Levantamiento de la Cordillera Oriental de Colombia durante el Eoceno tardío - Oligoceno temprano: proveniencia sedimentaria en el Sinclinal de Nuevo Mundo, Cuenca Valle Medio del Magdalena. *Boletín de Geología* 32: 45–77.
- Carvajal-Ortiz, H., G. Mora, and C. Jaramillo. 2009. A molecular evaluation of bulk organic carbon-isotope chemostratigraphy for terrestrial correlations: An example from two Paleocene–Eocene tropical sequences. *Palaeogeography, Palaeoclimatology, Palaeoecology* 277: 173–183.
- Collinson, M. E. 2002. The ecology of Cainozoic ferns. *Review of Palaeobotany and Palynology* 119: 51–68.

- Collinson, M. E., S. Y. Smith, J. H. A. van Konijnenburg-van Cittert, D. J. Batten, J. van der Burgh, J. Barke, and F. Marone. 2013. New Observations and Synthesis of Paleogene Heterosporous Water Ferns. *International Journal of Plant Sciences* 174: 350–363.
- Cooper, M. A., F. T. Addison, R. Alvarez, M. Coral, R. H. Graham, A. B. Hayward, S. Howe, et al. 1995. Basin Development and Tectonic History of the Llanos Basin, Eastern Cordillera, and Middle Magdalena Valley, Colombia. *AAPG Bulletin* 79: 1421–1442.
- D'hondt, S., and M. A. Arthur. 1996. Late Cretaceous oceans and the cool tropic paradox. *Science* 271: 1838–1841.
- Duarte, L. 1958. Annonaceae fósseis da Bacia Terciária de Fonseca, Minas Gerais, DNPM, Div. *Boletim Geologico y Minero* 178: 1–27.
- Eglinton, G., and R. J. Hamilton. 1967. Leaf Epicuticular Waxes. *Science* 156: 1322–1335.
- Ellis, B., D. C. Daly, L. J. Hickey, J. V. Mitchell, K. R. Johnson, P. Wilf, and S. L. Wing. 2009. *Manual of Leaf Architecture*. Cornell University Press, Ithaca, NY.
- Fanton, J. C. M., F. Ricardi-Branco, and A. M. Silva. 2012. *Terminalia palaeopubescens* sp. nov. (Combretaceae) da Formação Fonseca (Eoceno/Oligoceno) de Minas Gerais, Brasil: Morfologia Foliar, Fungos Epifílicos Associados e Paleoclima. *Ameghiniana* 49: 273–288.
- Gómez, E., T. E. Jordan, R. W. Allmendinger, K. Hegarty, and S. Kelley. 2005. Syntectonic Cenozoic sedimentation in the northern middle Magdalena Valley Basin of Colombia and implications for exhumation of the Northern Andes. *Geological Society of America Bulletin* 117: 547.
- Graham, A., and D. Dilcher. 1995. The Cenozoic record of tropical dry forest in northern Latin America and the southern United States. Seasonally dry tropical forests, 124–145. Cambridge University Press, Cambridge, UK.
- Gregory-Wodzicki, K. M., W. McIntosh, and K. Velásquez. 1998. Climatic and tectonic implications of the late Miocene Jakokkota flora, Bolivian Altiplano. *Journal of South American Earth Sciences* 11: 533–560.
- Herrera, F., S. R. Manchester, S. B. Hoot, K. M. Wefferling, M. R. Carvalho, and C. Jaramillo. 2011. Phytogeographic implications of fossil endocarps of Menispermaceae from the Paleocene of Colombia. *American Journal of Botany* 98: 2004–2017.
- Herrera, F., S. R. Manchester, and C. Jaramillo. 2012. Permineralized fruits from the late Eocene of Panama give clues of the composition of forests established early in the uplift of Central America. *Review of Palaeobotany and Palynology* 175: 10–24.
- Hesselbo, S. P., H. S. Morgans-Bell, J. C. McElwain, P. M. Rees, S. A. Robinson, and C. E. Ross. 2003. Carbon-Cycle Perturbation in the Middle Jurassic and Accompanying Changes in the Terrestrial Paleoenvironment. *The Journal of Geology* 111: 259–276.

- Hinojosa, L. F., F. Pérez, A. Gaxiola, and I. Sandoval. 2011. Historical and phylogenetic constraints on the incidence of entire leaf margins: insights from a new South American model: South American leaf margin analysis. *Global Ecology and Biogeography* 20: 380–390.
- Holdridge, L. R. 1967. Life zone ecology. Rev. ed. Tropical Science Center, San José, Costa Rica.
- ISAGÉN. 2014. Boletín Microclimático.
- Jacobs, B. F., and P. S. Herendeen. 2004. Eocene dry climate and woodland vegetation in tropical Africa reconstructed from fossil leaves from northern Tanzania. *Palaeogeography, Palaeoclimatology, Palaeoecology* 213: 115–123.
- Jaramillo, C., and A. Cárdenas. 2013. Global Warming and Neotropical Rainforests: A Historical Perspective. *Annual Review of Earth and Planetary Sciences* 41: 741–766.
- Jenks, M. A., and E. N. Ashworth. 1999. Plant epicuticular waxes: function, production, and genetics. *Horticultural reviews* 23: 1–68.
- Jiménez-Mejías, P., and E. Martinetto. 2013. Toward an accurate taxonomic interpretation of *Carex* fossil fruits (Cyperaceae): A case study in section *Phacocystis* in the Western Palearctic. *American Journal of Botany* 100: 1580–1603.
- Kouwenberg, L. L. R., R. R. Hines, and J. C. McElwain. 2007. A new transfer technique to extract and process thin and fragmented fossil cuticle using polyester overlays. *Review of Palaeobotany and Palynology* 145: 243–248.
- Kowalski, E. A., and D. L. Dilcher. 2003. Warmer paleotemperatures for terrestrial ecosystems. *Proceedings of the National Academy of Sciences* 100: 167–170.
- Leelavathi, P., N. Ramayya, and M. Prabhakar. 1980. Foliar stomatal distribution patterns in Leguminosae and their taxonomic significance. *Phytomorphology* 30: 195–204.
- Lima, M. R. de, and M. Salard-Cheboldaeff. 1981. Palynologie des bassins de Gandarela et Fonseca (eocene de l'état de Minas Gerais, Bresil). *Boletim IG* 12: 33–53.
- Martínez, C. 2018. Dalbergieae (Fabaceae) Samara Fruits from the Late Eocene of Colombia. *International Journal of Plant Sciences* 179: 541–553.
- Martínez, C. 2017. Passifloraceae seeds from the late Eocene of Colombia. *American Journal of Botany* 104: 1857–1866.
- Mello, C. L., L. G. Sant'Anna, and L. P. Bergqvist. 2000. The palaeontological site of Fonseca, Minas Gerais state, Brazil (fossil plants of the Tertiary of Brazil). *Sítios geológicos e paleontológicos do Brasil [online]*.

- Miall, A. 1996. *The Geology of Fluvial Deposits: Sedimentary Facies, Basin Analysis*. Springer, Berlin, Germany.
- Nie, J., B. K. Horton, A. Mora, J. E. Saylor, T. B. Housh, J. Rubiano, and J. Naranjo. 2010. Tracking exhumation of Andean ranges bounding the Middle Magdalena Valley Basin, Colombia. *Geology* 38: 451–454.
- Nie, J., B. K. Horton, J. E. Saylor, A. Mora, M. Mange, C. N. Garziona, A. Basu, et al. 2012. Integrated provenance analysis of a convergent retroarc foreland system: U–Pb ages, heavy minerals, Nd isotopes, and sandstone compositions of the Middle Magdalena Valley basin, northern Andes, Colombia. *Earth-Science Reviews* 110: 111–126.
- Nuttall, C. P. 1990. A review of the Tertiary non-marine molluscan faunas of the Pebasian and other inland basins of north-western South America. *British museum (Natural history)*.
- Ortiz, J., C. Moreno, A. Cardenas, and C. Jaramillo. 2015. SDAR 1.0 a New Quantitative Toolkit for Analyze Stratigraphic Data. 2790.
- Pardo-Trujillo, A., C. A. Jaramillo, and F. E. Oboh-Ikuenobe. 2003. Paleogene Palynostratigraphy of the Eastern Middle Magdalena Valley, Colombia. *Palynology* 27: 155–178.
- Pennington, R. T., M. Lavin, and A. Oliveira-Filho. 2009. Woody plant diversity, evolution, and ecology in the tropics: perspectives from seasonally dry tropical forests. *Annual Review of Ecology, Evolution, and Systematics* 40: 437–457.
- Pennington, R. T., J. A. Ratter, and G. P. Lewis. 2006. *Neotropical savannas and seasonally dry forests: plant diversity, biogeography, and conservation*. CRC Press, Boca Raton, Florida, USA.
- Peppe, D. J., L. J. Hickey, I. M. Miller, and W. A. Green. 2008. A Morphotype Catalogue, Floristic Analysis and Stratigraphic Description of the Aspen Shale Flora (Cretaceous–Albian) of Southwestern Wyoming. *Bulletin of the Peabody Museum of Natural History* 49: 181–208.
- Peppe, D. J., D. L. Royer, B. Cariglino, S. Y. Oliver, S. Newman, E. Leight, G. Enikolopov, et al. 2011. Sensitivity of leaf size and shape to climate: global patterns and paleoclimatic applications. *New Phytologist* 190: 724–739.
- Pérez-Consuegra, N., A. Cuervo-Gómez, C. Martínez, C. Montes, F. Herrera, S. Madriñán, and C. Jaramillo. 2017. Paleogene *Salvinia* (Salviniaceae) from Colombia and their paleobiogeographic implications. *Review of Palaeobotany and Palynology* 246: 85–108.
- Pilsbry, H. A., and A. A. Olsson. 1935. Tertiary fresh-water mollusks of the Magdalena embayment, Colombia. *Proceedings of the Academy of Natural Sciences of Philadelphia* 87: 7–39.

- Pizano, C., M. Cabrera, and H. García. 2014. Bosque seco tropical en Colombia; generalidades y contexto. Instituto de Investigación de Recursos Biológicos Alexander von Humboldt, Bogotá DC.
- Reineck, H.-E., and I. B. Singh. 1980. Depositional sedimentary environments: With reference to terrigenous clastics. Springer-Verlag, Berlin, Germany.
- Rodríguez-Forero, G., F. E. Oboh-Ikuenobe, C. Jaramillo-Munoz, M. J. Rueda-Serrano, and E. Cadena-Rueda. 2012. Palynology of the Eocene Esmeraldas Formation, Middle Magdalena Valley Basin, Colombia. *Palynology* 36: 96–111.
- Royer, D. L., L. Sack, P. Wilf, C. H. Lusk, G. J. Jordan, Ü. Niinemets, I. J. Wright, et al. 2007. Fossil Leaf Economics Quantified: Calibration, Eocene Case Study, and Implications. *Paleobiology* 33: 574–589.
- Royer, D. L., P. Wilf, D. A. Janesko, E. A. Kowalski, and D. L. Dilcher. 2005. Correlations of climate and plant ecology to leaf size and shape: potential proxies for the fossil record. *American Journal of Botany* 92: 1141–1151.
- Santos, C., C. Jaramillo, G. Bayona, M. Rueda, and V. Torres. 2008. Late Eocene marine incursion in north-western South America. *Palaeogeography, Palaeoclimatology, Palaeoecology* 264: 140–146.
- Spicer, R. A. 2016. CLAMP, climate leaf analysis multivariate program. *The Open University*. Website <http://clamp.ibcas.ac.cn/> [accessed 11 March 2019].
- Ward, D. E., R. Goldsmith, A. Jimeno, J. Cruz, H. Restrepo, and E. Gómez. 1977. Geologic map of the Bucaramanga Quadrangle (H-12), Colombia.
- Webb, L. J. 1959. A Physiognomic Classification of Australian Rain Forests. *Journal of Ecology* 47: 551–570.
- Wefferling, K. M., S. B. Hoot, and S. S. Neves. 2013. Phylogeny and fruit evolution in Menispermaceae. *American Journal of Botany* 100: 883–905.
- Wilf, P. 1997. When are Leaves Good Thermometers? A New Case for Leaf Margin Analysis. *Paleobiology* 23: 373–390.
- Wilf, P., M. R. Carvalho, M. A. Gandolfo, and N. R. Cúneo. 2017. Eocene lantern fruits from Gondwanan Patagonia and the early origins of Solanaceae. *Science* 355: 71–75.
- Wilf, P., S. L. Wing, D. R. Greenwood, and C. L. Greenwood. 1998. Using fossil leaves as paleoprecipitation indicators: An Eocene example. *Geology* 26: 203.
- Wing, S. L., F. Herrera, C. A. Jaramillo, C. Gómez-Navarro, P. Wilf, and C. C. Labandeira. 2009. Late Paleocene fossils from the Cerrejón Formation, Colombia, are the earliest record of Neotropical rainforest. *Proceedings of the National Academy of Sciences* 106: 18627–18632.

- Wolfe, J. A. 1993. A Method of Obtaining Climatic Parameters from Leaf Assemblages. U.S. Government Printing Office.
- Wolfe, J. A. 1978. A paleobotanical interpretation of Tertiary climates in the Northern Hemisphere: Data from fossil plants make it possible to reconstruct Tertiary climatic changes, which may be correlated with changes in the inclination of the earth's rotational axis. *American Scientist* 66: 694–703.
- Wolfe, J. A. 1995. Paleoclimatic Estimates from Tertiary Leaf Assemblages. *Annual Review of Earth and Planetary Sciences* 23: 119–142.
- Zachos, J. C., G. R. Dickens, and R. E. Zeebe. 2008. An early Cenozoic perspective on greenhouse warming and carbon-cycle dynamics. *Nature* 451: 279–283.
- Zachos, J., M. Pagani, L. Sloan, E. Thomas, and K. Billups. 2001. Trends, Rhythms, and Aberrations in Global Climate 65 Ma to Present. *Science* 292: 686–693.

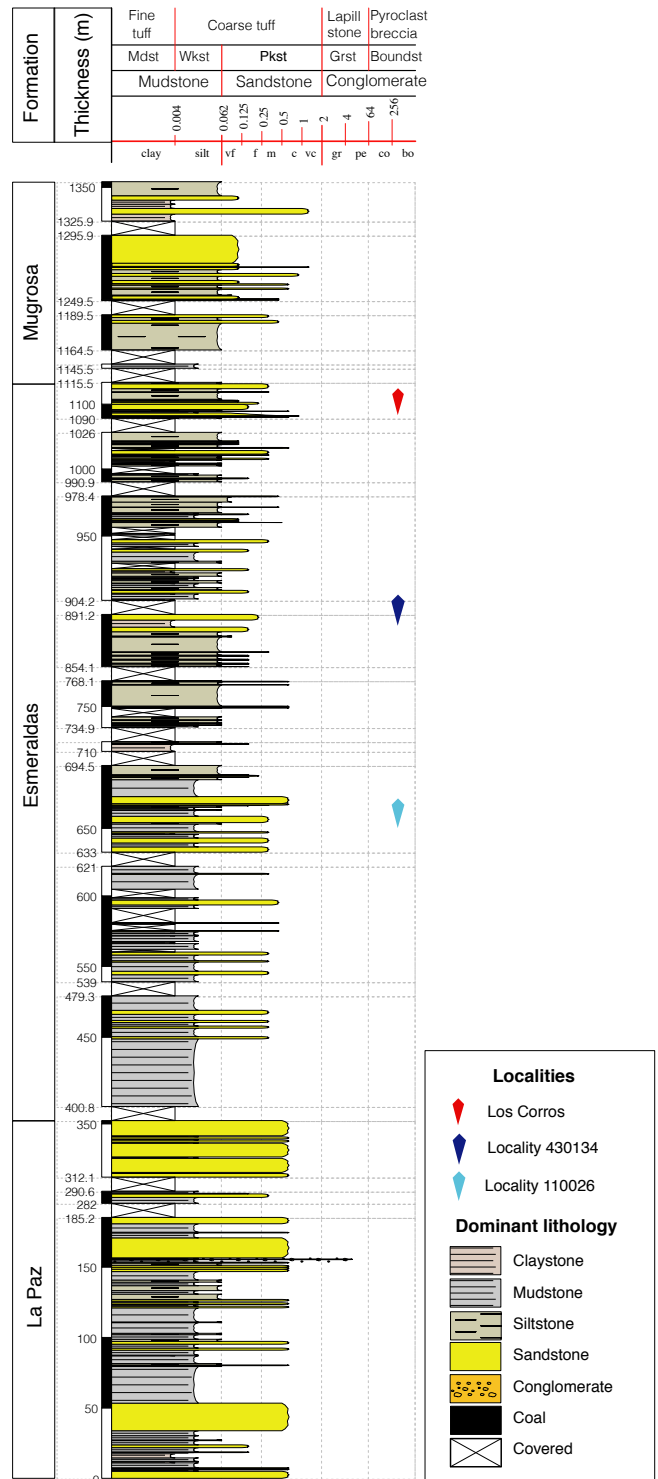


**Fig. S1. Stratigraphic section for the Paleogene of the Nuevo Mundo Syncline**  
 Stratigraphic section for the Paleogene of the Nuevo Mundo Syncline, including the top of La Paz Formation, the Esmeraldas Formation and the base of the Mugrosa Formation.

<b>Run 1</b>					
Strat. height (m)	Sample ID	Weight (mg)	CO <sub>2</sub> Amp (mV)	%C	$\delta^{13}\text{C}_{\text{TOM}}$ vs. VPDB
4	1	39.91	366	0.10	-25.78
13	2	40.12	247	0.07	-26.39
23	3	39.92	352	0.10	-26.61
33	4	40.06	246	0.07	-26.21
54	5	39.86	324	0.10	-25.86
64	6	40.14	303	0.09	-26.56
74	7	40	324	0.09	-26.32
84	8	40.08	273	0.08	-26.14
94	9	40.1	243	0.07	-26.25
104	10	39.93	208	0.06	-27.01
114	11	39.94	456	0.13	-23.31
127	12	40.11	305	0.09	-26.83
136	13	40.08	251	0.07	-26.88
146	14	39.88	239	0.07	-26.52
157	15	39.89	278	0.10	-25.47
170	16	40.03	167	0.07	-25.07
173.5	17	40.07	207	0.11	-23.11
312	18	40.03	4,404	2.47	-26.27
328	19	40.11	1,585	0.82	-25.48
337	20	40.05	2,450	0.90	-26.17
<b>Run 2</b>					
401	21	40.09	347	0.09	-26.33
410.5	22	39.87	614	0.16	-25.00
420.5	23	40.13	843	0.22	-25.13
430.5	24	39.97	550	0.14	-25.67
440.5	25	39.92	845	0.24	-24.89
451	26	40.12	383	0.10	-24.02
461	27	39.9	780	0.21	-25.03
542.5	28	40.09	1,050	0.28	-25.13
553.5	29	39.96	335	0.10	-24.54
567	30	39.86	507	0.14	-24.31
572.5	31	40.09	537	0.16	-24.51
593.5	33	40.12	411	0.12	-24.19
600	34	40.1	1,134	0.30	-24.64
609.5	35	39.86	656	0.18	-23.14
612.5	36	40.15	313	0.09	-23.67

622	37	39.91	459	0.12	-25.18
638	38	39.93	248	0.07	-23.18
642.5	39	40.12	262	0.08	-23.20
<b>Run 3</b>					
652.5	40	40	345	0.10	-24.21
662.5	41	40.11	966	0.27	-23.68
658.2	42	39.97	372	0.12	-22.90
667.53	43	40.15	413	0.11	-23.91
717.7	44	40.04	424	0.12	-23.24
747.5	46	40.09	301	0.09	-23.69
757.5	47	40.14	464	0.14	-24.43
767.5	48	40.08	498	0.15	-23.53
861.5	49	40.042	922	0.25	-24.88
871.5	50	39.928	501	0.14	-24.57
889	52	40.046	337	0.10	-24.72
948.5	53	39.979	358	0.11	-25.18
954	54	39.989	398	0.12	-24.52
981.5	55	40.006	1,490	0.40	-24.76
684	56	40.033	222	0.07	-24.78
694.36	57	39.974	289	0.09	-24.22
1015	58	39.982	3,831	1.03	-26.16
<b>Run 4</b>					
1018.5	59	40.039	430	0.12	-25.53
1022	60	40.037	14,226	4.96	-25.58
1025.5	61	40.045	1,114	0.33	-25.91
1090	63	40.103	1,820	0.51	-27.31
1098	64	40.025	2,897	0.80	-26.06
1119.5	66	40.05	275	0.08	-25.16
1165.32	69	40.101	303	0.09	-25.45
1174.23	70	40	243	0.07	-24.82
1188	72	40.097	245	0.07	-25.67
1250	73	40.099	199	0.06	-25.87
1256.5	74	40.014	236	0.07	-25.71
1262.5	75	39.902	467	0.14	-22.52
1268	76	39.945	275	0.08	-24.87
<b>Run 5</b>					
1275	77	40.089	294	0.10	-25.58
1281.5	78	40.113	457	0.15	-23.15

1328	79	39.907	903	0.29	-26.17
1337.5	80	40.104	276	0.09	-26.52
1347	81	40.063	255	0.09	-25.76
1356.5	82	39.906	545	0.18	-28.70
1366	83	40.002	197	0.06	-26.95
1370	84	40.1	655	0.21	-28.83

**Table S1. Isotopic analysis results of  $\delta^{13}\text{C}_{\text{TOM}}$**

Isotopic analysis results of  $\delta^{13}\text{C}_{\text{TOM}}$  for samples taken along the section from the Nuevo Mundo Syncline. Each sample has a stratigraphic height, weight, ID, amplitude of the sample  $\text{CO}_2$  peak, the recalculated percent of Carbon, and the  $\delta^{13}\text{C}_{\text{TOM}}$  ‰ vs. VPDB.

**Table S2. Values of in-house standards**

Values of in-house standards for normalization correction and precision purposes obtained for each run for

<b>Run 1</b>				
<b>Quality Control Data</b>				
<b>std CBT</b>				
<i>In-house standards used for normalization correction</i>				
Sample ID	Weight (mg)	CO2 Amp	%C	$\delta^{13}\text{C}$ vs. VPDB
std CBT	1.038	4,371	49.82	-25.65
std CBT	1.016	4,340	50.36	-25.63
std CBT	1.037	4,439	50.35	-25.67
std CBT	1.040	4,522	50.82	-25.69
std CBT	0.971	4,165	50.74	-25.58
std CBT	1.030	4,415	50.79	-25.63
<b>Mean</b>			50.48	-25.64
<b>SD</b>			0.38	0.04
<b>std KCRN</b>				
<i>In-house standards used for normalization correction</i>				
Sample ID	Weight (mg)	CO2 Amp	%C	$\delta^{13}\text{C}$ vs. VPDB
std KCRN	2.964	10,347	44.23	-12.75
std KCRN	3.016	10,584	44.64	-12.75
std KCRN	3.012	10,538	44.59	-12.79
std KCRN	2.997	10,796	45.20	-12.74
std KCRN	3.058	10,992	45.17	-12.69
std KCRN	3.033	10,866	45.12	-12.71
<b>Mean</b>			44.82	-12.74
<b>SD</b>			0.40	0.04
<b>std BNPS</b>				
<i>In-house standard used for precision purposes</i>				
Sample ID	Weight (mg)	CO2 Amp	%C	$\delta^{13}\text{C}$ vs. VPDB
std BNPS	15.163	3,621	2.70	-23.08
std BNPS	15.07	3,695	2.80	-22.83
std BNPS	14.984	2,228	2.39	-23.06
<b>Mean</b>			2.63	-22.99
<b>SD</b>			0.22	0.14
<b>Run 2</b>				
<b>Quality Control Data</b>				
<b>std CBT</b>				

<i>In-house standards used for normalization correction</i>				
Sample ID	Weight (mg)	CO2 Amp	%C	$\delta^{13}\text{C}$ vs. VPDB
std CBT	1.031	4,498	47.43	-25.59
std CBT	1.004	4,442	48.10	-25.63
std CBT	1.034	4,556	47.75	-25.61
std CBT	1.030	4,457	47.14	-25.68
std CBT	1.006	4,336	47.22	-25.67
std CBT	1.023	4,368	46.86	-25.66
<b>Mean</b>			47.42	-25.64
<b>SD</b>			0.45	0.03
<b>std KCRN</b>				
<i>In-house standards used for normalization correction</i>				
Sample ID	Weight (mg)	CO2 Amp	%C	$\delta^{13}\text{C}$ vs. VPDB
std KCRN	3.003	10,716	41.93	-12.72
std KCRN	3.045	10,965	42.37	-12.78
std KCRN	2.995	10,777	42.30	-12.76
std KCRN	3.025	10,947	42.17	-12.69
std KCRN	3.027	10,791	41.73	-12.73
std KCRN	3.02	10,856	41.90	-12.77
<b>Mean</b>			42.07	-12.74
<b>SD</b>			0.25	0.03
<b>std BNPS</b>				
<i>In-house standard used for precision purposes</i>				
Sample ID	Weight (mg)	CO2 Amp	%C	$\delta^{13}\text{C}$ vs. VPDB
std BNPS	15.171	3,482	2.42	-23.17
std BNPS	14.961	3,857	2.67	-23.02
std BNPS	15.083	3,841	2.79	-22.91
<b>Mean</b>			2.63	-23.03
<b>SD</b>			0.19	0.13
<b>std methionine</b>				
<i>Chemical standard used to determine instrument linearity</i>				
Sample ID	Weight (mg)	CO2 Amp	%C	$\delta^{13}\text{C}$ vs. VPDB
std methionine	0.98	3,508	39.53	-25.31
std methionine	0.099	385	41.18	-24.87
std methionine	0.201	732	38.62	-25.17
std methionine	0.304	1,130	39.52	-25.09
std methionine	0.497	1,803	38.92	-25.22
std methionine	3.002	10,281	40.65	-25.93
std methionine	5.021	15,757	41.12	-25.19

	<b>Mean</b>		39.94		-25.25
	<b>SD</b>		1.05		0.33
<b>Run 3</b>					
<b>Quality Control Data</b>					
<b>std CBT</b>					
<i>In-house standards used for normalization correction</i>					
<b>Sample ID</b>	<b>Weight (mg)</b>	<b>CO2 Amp</b>	<b>%C</b>		<b>δ13C vs. VPDB</b>
std CBT	0.996	4,484	46.18		-25.73
std CBT	1.015	4,600	46.25		-25.69
std CBT	1.038	4,687	46.05		-25.70
std CBT	1.039	4,744	50.14		-25.58
std CBT	1.017	4,636	49.93		-25.56
std CBT	1.012	4,597	49.51		-25.58
	<b>Mean</b>		48.01		-25.64
	<b>SD</b>		2.04		0.07
<b>std KCRN</b>					
<i>In-house standards used for normalization correction</i>					
<b>Sample ID</b>	<b>Weight (mg)</b>	<b>CO2 Amp</b>	<b>%C</b>		<b>δ13C vs. VPDB</b>
std KCRN	2.96	10,860	41.10		-12.87
std KCRN	3.027	11,118	44.36		-12.76
std KCRN	3.03	11,038	43.92		-12.74
std KCRN	3.004	11,246	44.46		-12.69
std KCRN	2.966	11,064	44.47		-12.67
std KCRN	2.944	10,974	44.46		-12.72
	<b>Mean</b>		43.79		-12.74
	<b>SD</b>		1.34		0.07
<b>std BNPS</b>					
<i>In-house standard used for precision purposes</i>					
<b>Sample ID</b>	<b>Weight (mg)</b>	<b>CO2 Amp</b>	<b>%C</b>		<b>δ13C vs. VPDB</b>
std BNPS	14.995	3,744	2.65		-23.09
std BNPS	14.963	3,960	2.89		-22.97
std BNPS	15.027	3,219	2.38		-22.85
	<b>Mean</b>		2.64		-22.97
	<b>SD</b>		0.25		0.12
<b>Run 4</b>					
<b>Quality Control Data</b>					
<b>std CBT</b>					
<i>In-house standards used for normalization correction</i>					
<b>Sample ID</b>	<b>Weight (mg)</b>	<b>CO2 Amp</b>	<b>%C</b>		<b>δ13C vs. VPDB</b>

std CBT	1.032	4,700	50.72	-25.61
std CBT	1.045	4,798	51.05	-25.60
std CBT	1.023	4,698	51.08	-25.60
std CBT	1.003	4,543	51.03	-25.68
std CBT	1.038	4,691	50.92	-25.60
std CBT	1.036	4,677	50.93	-25.64
<b>Mean</b>			50.96	-25.62
<b>SD</b>			0.13	0.03
<b>std KCRN</b>				
<i>In-house standards used for normalization correction</i>				
<b>Sample ID</b>	<b>Weight (mg)</b>	<b>CO2 Amp</b>	<b>%C</b>	<b>δ13C vs. VPDB</b>
std KCRN	2.942	10,692	44.63	-12.72
std KCRN	3.028	10,960	44.69	-12.72
std KCRN	2.998	10,911	44.88	-12.73
std KCRN	2.987	10,803	44.82	-12.71
std KCRN	3.045	10,992	44.92	-12.72
std KCRN	2.977	10,747	44.85	-12.79
<b>Mean</b>			44.80	-12.73
<b>SD</b>			0.11	0.03
<b>std BNPS</b>				
<i>In-house standard used for precision purposes</i>				
<b>Sample ID</b>	<b>Weight (mg)</b>	<b>CO2 Amp</b>	<b>%C</b>	<b>δ13C vs. VPDB</b>
std BNPS	14.996	2,630	1.91	-23.07
std BNPS	14.973	3,339	2.49	-22.86
<b>Mean</b>			2.20	-22.97
<b>SD</b>			0.41	0.15
<b>std methionine</b>				
<i>Chemical standard used to determine instrument linearity</i>				
<b>Sample ID</b>	<b>Weight (mg)</b>	<b>CO2 Amp</b>	<b>%C</b>	<b>δ13C vs. VPDB</b>
std methionine	1.034	3,875	41.10	-25.20
std methionine	0.12	500	44.54	-24.84
std methionine	0.199	713	38.32	-25.12
std methionine	0.495	1,958	42.66	-25.12
std methionine	3.024	18,987		-24.99
std methionine	5.012	15,842	43.05	-25.13
<b>Mean</b>			41.93	-25.07
<b>SD</b>			2.36	0.13
<b>Run 5</b>				
<b>Quality Control Data</b>				

<b>std CBT</b>				
<i>In-house standards used for normalization correction</i>				
Sample ID	Weight (mg)	CO2 Amp	%C	$\delta^{13}\text{C}$ vs. VPDB
std CBT	1.086	4,931	61.52	-25.63
std CBT	0.979	5,310	73.75	-25.61
std CBT	0.988	4,602	62.70	-25.68
<b>Mean</b>			65.99	-25.64
<b>SD</b>			6.75	0.04
<b>std KCRN</b>				
<i>In-house standards used for normalization correction</i>				
Sample ID	Weight (mg)	CO2 Amp	%C	$\delta^{13}\text{C}$ vs. VPDB
std KCRN	3.035	11,032	54.62	-12.73
std KCRN	3.127	11,267	54.41	-12.74
std KCRN	2.993	10,850	54.18	-12.75
<b>Mean</b>			54.40	-12.74
<b>SD</b>			0.22	0.01
<b>std BNPS</b>				
<i>In-house standard used for precision purposes</i>				
Sample ID	Weight (mg)	CO2 Amp	%C	$\delta^{13}\text{C}$ vs. VPDB
std BNPS	15.059	3,696	3.22	-23.00
std BNPS	14.952	2,546	2.21	-22.88
<b>Mean</b>			2.71	-22.94
<b>SD</b>			0.72	0.08

## CHAPTER 3

# DALBERGIEAE (FABACEAE) SAMARA FRUITS FROM THE LATE EOCENE OF COLOMBIA

CAMILA MARTÍNEZ

*Notice*— Page, figure, table, and appendix numbers and formatting have been changed from the original to conform to dissertation requirements; also, several minor corrections made in page-proof stage in the published version are not included here. Any citations of this research should be made to the *International Journal of Plant Sciences* article. Access to the *International Journal of Plant Sciences* version of this article can be obtained at:

<https://www.journals.uchicago.edu/doi/10.1086/698937>

\* **Martínez, C.** 2018. Dalbergieae (Fabaceae) samara fruits from the late Eocene of Colombia. In press. *International Journal of Plant Sciences* 179: 541–553.

## ABSTRACT

**Premise of the research:** Species richness of Leguminosae (Fabaceae) is highest in the Neotropics today, but the fossil evidence of the family from this region remains sparse. The study of a fossilized indehiscent winged fruit (samara) from a recently discovered flora from the late Eocene Esmeraldas Formation in Colombia increases our understanding of the fossil record

of Leguminosae from the Neotropics and sheds light on the evolution and ecology of this emblematic angiosperm family.

**Methodology:** Plant fossils were collected from a new locality in the late Eocene Esmeraldas Formation. Fifteen fossilized samara fruits were described, and compared to fossil and extant angiosperm fruits based on herbarium collections and literature. Taxonomic affinities of the fossil fruits with the clade Dalbergieae (Papilionoideae, Fabaceae) were evaluated by a combined analysis of morphological and molecular data.

**Pivotal Results:** A new fossil fruit *Luckowcarpa gunnii* gen. and sp. nov. is described and associated with the *Pterocarpus* clade (Dalbergieae) based on the presence of two-seeded unicarpellate samaras with a proximal seed chamber and a style remnant at the distal end of the wing. *L. gunnii* represents the earliest fruit fossil record of the Dalbergieae clade.

**Conclusions:** The phylogenetic position of *L. gunnii*, nested within the clade Dalbergieae, supports the hypothesis that legume diversification occurred early in the Tertiary in low latitudes and suggests that this fossil taxon could have been adapted to tropical dry forest ecosystems.

**Key words:** Fabaceae, Dalbergieae, Colombia, fossil, samara, late Eocene

## INTRODUCTION

The family Fabaceae (Leguminosae) is the third largest flowering plant family, with ca. 770 genera and over 19,500 species (LPWG 2017). It has a worldwide distribution occurring across a broad range of geographical regions and ecological conditions. The family is characterized as a highly morphologically diverse group and include herbs, shrubs, lianas and trees (Group and others, 2013). Overall, Fabaceae is one of the most species-diverse families in the Neotropical region (Gentry, 1990; Terborgh and Andresen, 1998). Hypotheses based on the current distribution and the available fossil record suggest that the family originated in the tropics during the late Cretaceous and diversified during the Eocene (Herendeen et al., 1992; Lavin et al., 2005).

Globally, the Cenozoic fossil record of Fabaceae is rich compared to many other families, but its record in the Neotropics is still sparse. Some of the oldest possible records of the family come from the Maastrichtian of South America (~72–66 Ma (Muller, 1981; Herendeen et al., 1992; Caccavari, 1996), however, their validity has not been confirmed (Herendeen et al., 1992). The Maastrichtian Guaduas Flora from Colombia, currently being studied, completely lacks legume records, both at the micro and macrofossil level, despite the wide sampling (1200 macrofossils studied and 41 morphotypes recognized; Gutierrez and Jaramillo 2007; Field et al. 2011, Crifo et al., 2014), while the Paleocene Cerrejón Flora (~58 Ma) also from Colombia has an abundant fossil record of legume leaves and pods (Wing et al., 2009). Most of the modern Fabaceae clades are first documented based on fossil evidence during the Eocene to early Oligocene (~56–23 Ma; (Daghlian et al., 1980; Crepet and Taylor, 1985; Herendeen et al., 1992; Magallón-Puebla and Cevallos-Ferriz, 1994; Caccavari, 1996; Calvillo-Canadell and Cevallos-Ferriz, 2005). The temperature pulses that occurred during the Eocene have been hypothesized as

a possible trigger for legume diversity (Axelrod, 1992). Furthermore, the shift from rainforest type ecosystems to drier climates in what is now the southern and central United States during the middle Eocene has been correlated with the increasingly important role that legumes had in plant communities from that age (Axelrod, 1992). Through describing and identifying legume fossils from the Neotropics, is possible to test hypotheses related to the evolution of legumes and better understand the climatic and vegetation history of the region.

Recently discovered fossil material dated as late Eocene (~41–34 Ma) from the Esmeraldas Formation flora of Colombia provides an opportunity to increase our understanding of the fossil record from underrepresented regions, time intervals, and taxonomic groups in the Neotropics (Martínez, 2017; Pérez-Consuegra et al., 2017). Here, fossils of a new winged fruit attributable to Fabaceae are described. The fossils are compared with extant taxa and placed in a phylogenetic context using a cladistic analysis. Finally, the implications of this discovery for evolution of this family are discussed.

Winged fruits are adapted to wind dispersal and are commonly found in open forests, but also in emergent trees of closed forests (Herrera et al., 2014). They are among the more commonly fossilized fruit types because their inherent dispersal potential facilitates fossilization by increasing the probability that they will be deposited in bodies of water (Manchester and O’Leary, 2010). Samaras are dry, indehiscent winged fruits, and many have asymmetrical wings because the wing develops from only one side of the ovary wall (Mirle and Burnham, 1999). The fossil fruit described in this study corresponds to the definition of an asymmetrically winged samara. Asymmetrically winged samaras are only produced by a few families and genera of angiosperms. For example, in the western hemisphere, asymmetrically winged samaras are only known in 11 families and 39 genera of angiosperms (Mirle and Burnham, 1999).

## MATERIALS AND METHODS

### *Geological setting*

The fossil material was collected at the western flank of the Eastern Cordillera in Santander, Colombia, from a locality in the Esmeraldas Formation. The age of the Upper Esmeraldas Formation is late Eocene (Rodríguez-Forero et al., 2012); palynological zone T-07 of Jaramillo et al. (2011). The site is located in the Nuevo Mundo Syncline, Middle Magdalena Valley Basin, in the area of the Topocoro Dam near the road that leads from Bucaramanga to Barrancabermeja (fig. 1). Led by the Smithsonian Tropical Research Institute (STRI), the Colombian Geological Survey (SGC) and Isagen (a power generation company) the region was first explored in 2013 as a part of a paleontological rescue effort during the construction of the dam. The fossil material was collected on two field trips in 2013 and 2015. The locality has the identification number STRI-430134 and it is located at N 7°6'30.24" and W 73°25'45.12" (WGS84 18N), at 179 m of elevation, and it was not flooded after the filling of the dam. Approximately 400 specimens were collected from this locality including mostly compressions and impressions of angiosperm leaves, sometimes with cuticles preserved, but also seeds, fruits, and flowers (Pérez-Consuegra et al., 2017).

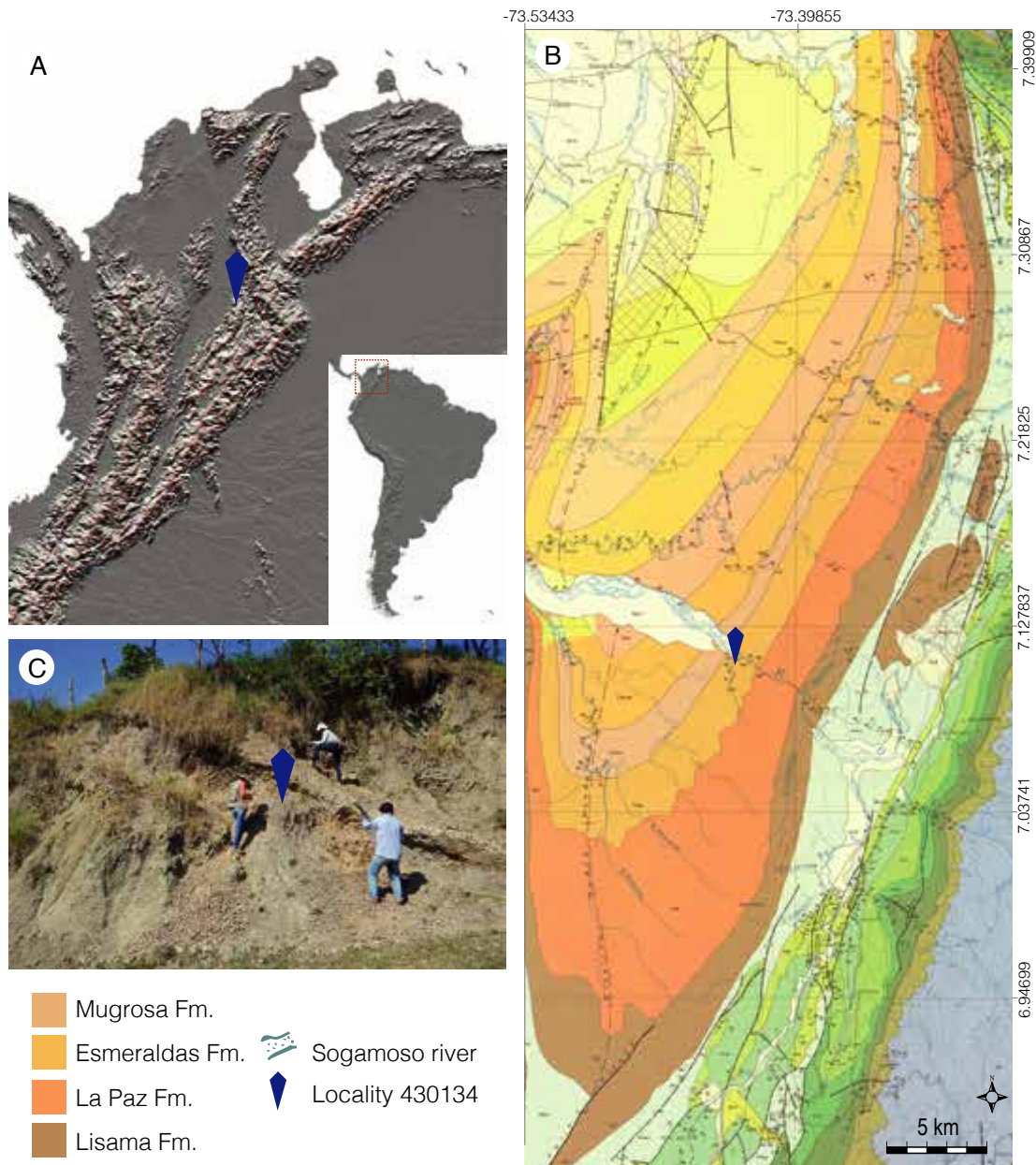


**Fig. 1. Geographic and geological location**

Geographic and geological location of the fossil plant locality “Topocoro dam: (ID: 430134). *A*, Relief map of South America and Colombia showing the geographic location of the outcrop. *B*, Geologic map modified from Ward et al. (1977) showing the Nuevo Mundo Syncline and the location of the fossil locality in the Esmeraldas Formation. *C*, Photograph of the 430134 locality.

Stratigraphically, the locality is near the top of the Esmeraldas Formation (885 m). The section of locality 430134 measured 17 m in thickness (fig. 2). The strata consist of interbedded

siltstone, sandstones, and sandy siltstone. The section is characterized by the presence of beds fining upwards from sandstone to siltstone, and by thick beds of grey siltstone with poor lamination. Plant remains were found at three horizons. Only those found at the top siltstone beds had good preservation. The remains found in the lower horizon preserved large cuticular fragments. Based on the characteristics described above the inferred depositional environment for the locality are floodplains associated with river channels (Reineck and Singh, 1980; Caballero et al., 2010). The preservation of delicate structures like large leaf cuticle fragments, flowers and relatively complete leaves, together with the lithology of the fossiliferous beds, could suggest that these remains were deposited close to the source plants, with minimal transport (Parautochthonous sensu Gastaldo et al. 1996).

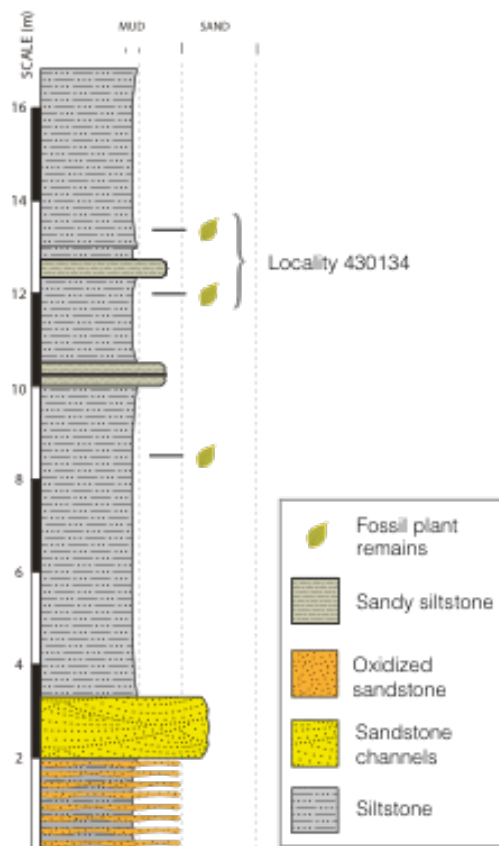


**Fig. 2 Stratigraphic section**

Stratigraphic section associated with fossil plant locality Topocoro dam (ID 430134).

The paleogeographic setting where the Esmeraldas Formation accumulated was very different compared to its current location in the foothills of the Eastern Cordillera of Colombia. During the Eocene the area where the Esmeraldas Formation was deposited was part of a larger basin that extended towards the Llanos regions of eastern Colombia and Venezuela, given that the Eastern Cordillera was not yet a barrier preventing this connection (Cooper et al., 1995; Gómez et al., 2005). Nevertheless, strata of the Esmeraldas Formation reflect the record of the initial rise of the Eastern cordillera (Caballero et al., 2010; Nie et al., 2012) so at least hills with perhaps a complex drainage patterns could have been present at that time creating landscape heterogeneity (Pérez-Consuegra et al., 2017).

#### ***Fossil description and comparisons***

Fifteen compressed and impressed specimens of complete and fragmented fruits were studied. Specimens were observed using a Zeiss StemI SV8 Stereo Microscope and photographed with a Nikon D200 camera with varied low-angle lighting. All the fossil material was studied at the Geosciences laboratory of the Universidad de los Andes, in Bogotá, Colombia. Specimens are deposited at the Paleontological Museum of the Colombian Geological Survey and Mapuka Museum (Universidad del Norte, Barranquilla, Colombia), indicated with the acronyms SGC STRI\_ID and Mapuka STRI\_ID.

The description follows the terminology used in the identification of asymmetrically winged samaras Mirle and Burnham (1999). To assess fossil's taxonomic affinities, I used the dichotomous key from Mirle and Burnham (1999) together with comparison tables of samara morphology included in Burnham (1995) and Burnham and Carranco (2004). In addition, the fossils were compared with digital collections from the Global Plants JSTOR and direct

observations from herbarium specimens from the Bailey Hortorium (BH) Cornell University, Ithaca, USA (appendix A1). Further comparisons were made only within the Fabaceae (alternatively Leguminosae) because the results of the previous comparisons suggested similarities with this family. The fossils were also compared with herbarium material, using fruit information published by Gunn (1984) and Kirkbride et al. (2003) and from the website created based on those publications (Kirkbride et al., 2012).

For comparison of the fossils with extant material a morphological matrix was constructed including 39 genera from 10 families of extant angiosperms: Anacardiaceae, Leguminosae, Malpighiaceae, Phytolaccaceae, Polygalaceae, Polygonaceae, Rutaceae, Sapindaceae, Trigonaceae and Ulmaceae.

Clade /subfamily classification for Leguminosae follows the classification system of the LPWG (2017), Cardoso et al. (2012, 2013), Lavin et al. (2001) and Klitgaard and Lavin (2005).

To determine the phylogenetic position of the new fossil taxon, a combined parsimony analysis of morphology and a molecular sequence data set for the clade Dalbergieae was performed. The molecular data set corresponded to a published alignment of *matK* sequences of 1785 nucleotides for 46 species (representing the 46 extant genera of the clade) included in the most recent molecular phylogeny of the clade Dalbergieae (Cardoso et al., 2013). The morphological data included 10 fruit characters (appendix A2) that were scored for both the fossil and 46 genera included in the molecular data set. The characters were coded from the morphologic information available at the Kirkbride et al. (2012) website (<https://data.nal.usda.gov/dataset/legume-fabaceae-fruits-and-seeds-version-2>) and from observation of herbarium material. The nucleotide characters were coded as missing for the fossil. The parsimony analysis was performed using TNT and the parsimony ratchet through

Winclada version 1.99 (Nixon, 2015). In the TNT analysis, 10 sets of 500 iterations using a 10% perturbation of characters were used for the ratchet analyses, and default values for drift, sectorial search, and tree fusion were used. A strict consensus and a bootstrap analysis were done to assess the coherence and support of the phylogenetic inference. The bootstrap was estimated using 100 replications in Winclada using NONA (Goloboff 1998).

In addition to fruit morphology, the ecology and geographic distribution for extant species of the Dalbergieae clade was derived from the book Legumes of the World and its website (Lewis et al., 2005; Legume Research Team at Kew, 2017).

## **RESULTS**

### ***Phylogenetic analyses***

The results from the comparison of the fossil with extant families (Table 1) and from the key for samaras from the Western Hemisphere (Mirle and Burnham, 1999) suggested that the fossil samara morphotype is more similar to those of Leguminosae based on the presence of unilocular fruits with style remnant at the distal side of the wing. In contrast, other unilocular samaras from families like Anacardiaceae, Phytolaccaceae and Ulmaceae, have a style remnant in the proximal side of the fruit.

**Table 1. Leguminosae genera with samara fruits.**

Leguminosae genera with generalized samaroid fruits and asymmetrically wing samaras.

Genera	Fruit type	Subfamily/Clade	Seed chamber	Distribution
<i>Amburana</i> Schwacke & Taub.	Samaroid	Papilionoideae/Amburaneae	NA	Neotropics
<i>Brandzeia</i> Baill.	AWS	Caesalpinioideae	Distal	Old-World Tropics
<i>Butea</i> Roxb. ex Willd.	AWS	Papilionoideae/NPAAA clade	Distal	Old-World Tropics
<i>Cascaronia</i> Griseb.	Samaroid	Papilionoideae/Dalbergieae	NA	Neotropics
<i>Centrolobium</i> Mart. ex Benth.	AWS	Papilionoideae/Dalbergieae	Proximal	Neotropics
<i>Dalbergiella</i> Baker f.	Samaroid	Papilionoideae/NPAAA clade	NA	Old-World Tropics
<i>Desmodium</i> Desv.	Samaroid	Papilionoideae/NPAAA clade	NA	Worldwide
<i>Fissicalyx</i> Benth.	Samaroid	Papilionoideae/Dalbergieae	NA	Neotropics
<i>Gossweilerodendron</i> Harms	AWS	Caesalpinioideae	Distal	Old-World Tropics
<i>Grazilodendron</i> H.C. Lima	Samaroid	Papilionoideae/Dalbergieae	NA	Neotropics
<i>Hylodendron</i> Taub.	AWS	Caesalpinioideae	Distal	Old-World Tropics
<i>Hymenolobium</i> Benth.	Samaroid	Papilionoideae/Andira	NA	Neotropics
<i>Luetzelburgia</i> Harms	AWS	Papilionoideae/Vataireoid	Proximal	Neotropics
<i>Machaerium</i> Pers.	AWS	Papilionoideae/Dalbergieae	Proximal	Neotropics
<i>Maraniona</i> C. E. Hughes, G. P. Lewis, Daza and Reynel	AWS	Papilionoideae/Dalbergieae	Proximal	Neotropics
<i>Meizotropis</i> Voigt	Samaroid	Papilionoideae	NA	Old-World Tropics
<i>Myrospermum</i> Jacq.	AWS	Papilionoideae/Amburaneae	Distal	Neotropics
<i>Myroxylon</i> L. f.	AWS	Papilionoideae/Amburaneae	Distal	Neotropics
<i>Neoapaloxylon</i> Rauschert	AWS	Caesalpinioideae	Distal	Old-World Tropics
<i>Nissolia</i> Jacq.	AWS	Papilionoideae/Dalbergieae	Proximal	Neotropics
<i>Onobrychis</i> Mill.	Samaroid	Papilionoideae/NPAAA clade	NA	Old-World Tropics
<i>Paramachaerium</i> Ducke	AWS	Papilionoideae/Dalbergieae	Proximal	Neotropics
<i>Platymiscium</i> Vogel	Samaroid	Papilionoideae/Dalbergieae	NA	Neotropics
<i>Platypodium</i> Vogel	AWS	Papilionoideae/Dalbergieae	Distal	Neotropics
<i>Pterocarpus</i> Jacq.	Samaroid	Papilionoideae/Dalbergieae	NA	Pantropical
<i>Pterogyne</i> Tul.	AWS	Caesalpinioideae	Distal	Neotropics
<i>Pterolobium</i> R. Br. ex Wight & Arn.	AWS	Caesalpinioideae	Proximal	Old-World Tropics
<i>Spatholobus</i> Hassk.	AWS	Papilionoideae	Distal	Old-World Tropics
<i>Steinbachiella</i> Harms	AWS	Papilionoideae/Dalbergieae	Proximal	Neotropics
<i>Sweetia</i> Spreng.	AWS	Papilionoideae/Vataireoid	Proximal	Neotropics
<i>Tachigali</i> Aubl.	Samaroid	Caesalpinioideae	NA	Neotropics
<i>Tipuana</i> (Benth.) Benth.	AWS	Papilionoideae/Dalbergieae	Proximal	Neotropics
<i>Vatairea</i> Aubl.	AWS	Papilionoideae/Vataireoid	Proximal	Neotropics
<i>Vataireopsis</i> Ducke	AWS	Papilionoideae/Vataireoid	Proximal	Neotropics
<i>Wiborgia</i> Thunb.	Samaroid	Papilionoideae/Crotalarieae	NA	Old-World Tropics

**Notes:** Information was taken from Cardoso et al. (2012, 2013); Kirkbride et al. (2017); Klitgaard and Lavin (2005); (Mirle and Burnham, 1999)). Abbreviations: Samaroid = generalized samaroid. AWS = asymmetrically wing samara. NA = not applicable.

Within Leguminosae there are 35 genera with samaroid-like fruits and 24 of them are present in the Neotropics (Kirkbride et al., 2012); table 1). Under the strict definition of asymmetrically winged samaras proposed by Mirle and Burnham (1999), only 22 genera were found to share characters with the fossil including the recently described genera *Maraniona* from Peru (Hughes et al., 2004) and *Steinbachiella* from Bolivia (Lewis et al., 2012). From those, 15 occur in the Neotropical region and seven in the Old-World Tropics (table 1). Asymmetrically winged samaras are present in two subfamilies, Caesalpinioideae (6 genera) and Papilionoideae (16 genera; Kirkbride et al., 2012). Within Papilionoideae most samaras are observed in clades Dalbergieae (8 genera out of 46), Vataireoid (4 genera out of 4) and Amburaneae (2 genera out of 7; table 1; Lavin et al. 2001; Kirkbride et al., 2003; Cardoso et al., 2013).

The second comparison step included only those legume samaras with a proximal seed chamber and distal wing (table 2). Amburaneae was therefore excluded from this comparison because its seed chamber is distal. Here, all except *Pterolobium* (Caesalpinioideae), are papilionoids restricted to the Neotropical region (table 2). Within Papilionoideae, seven genera were from Dalbergieae and four from Vataireoid (table 2). The third step of the comparison excluded *Pterolobium* because this genus has only one seed per seed chamber and subparallel venation, and the Vataireoid clade because these samaras have only one seed per seed chamber and are sub or non-stipitate, and also *Lutzelburgia* has a sulcus in the seed chamber.

**Table 2. Morphologic characters of Leguminosae samaras.**

Morphologic characters and distribution of Leguminosae genera with asymmetrically wing samaras and a proximal seed chamber

Genera	Clade	1	2	3	4	5	6	7	8	9	10	11	12
<i>Pterolobium</i> R. Br. ex Wight & Arn.	Caesalpinioideae	D	R	Sub/Non	–	3–6.5	0.8–2	A	C/L	A/P	1	P	Southern and eastern Africa, Arabia, southeastern Asia
<i>Centrolobium</i> Mart. ex Benth.	Dalbergieae	P	sP	Sub/Non	<2	–26	6–10	A	L	A	1(–5)	O or T	Panama to Ecuador, Bolivia, and Brazil
<i>Machaerium</i> Pers.	Dalbergieae	D	R	Sti/Sub	2.5–10	2–9.5	0.6–4	A/P	C/L	A	1(2)	P	Mexico, Central America to Argentina
<i>Maraniona</i> C. E. Hughes, G. P. et al.	Dalbergieae	D	sP	Non	–	2.7–3	1.5–1.7	P	L	A	1	O	Peru
<i>Nissolia</i> Jacq.	Dalbergieae	D	R/P	Sti/Sub/Non	<0.6	1.5–4.3	0.5–1.5	P	C	P	1–6	P	Mexico, West Indies, Central America, South America
<i>Steinbachiella</i> Harms	Dalbergieae	D	R	Sti	1.5–1.7	5.4	1.3	P		A	1	?	Bolivia
<i>Paramachaerium</i> Ducke	Dalbergieae	D	R	Sub/Non	–	2.5–12	2–6	A	C	A	1–2	T	Panama, Peru, Guianas, and Brazil
<i>Tipuana</i> (Benth.) Benth.	Dalbergieae	D	sP	Sti	1	4.5–8	2–3.2	A/P	L	A	1–4	T	Bolivia to northwestern Argentina and Brazil
<i>Luetzelburgia</i> Harms	Vataireoid	D	R	Sub	–	7–9	2.5–2.9	P	C	A	1	P	Brazil
<i>Sweetia</i> Spreng.	Vataireoid	D	I	Sub	0.3–0.4	4.5–6	1–1.3	P	Ch	A	1	P	Brazil, Bolivia, and Paraguay
<i>Vatairea</i> Aubl.	Vataireoid	D	I	Non	–	8.5–14	2.5–8	P	L	A	1	O	Mexico and Central America to Brazil.
<i>Vataireopsis</i> Ducke	Vataireoid	D	R	Sub/Non	–	8–12	2–3	P	C	A	1	O	Brazil, Surinam and French Guiana
Fossil Esmeraldas		D	R	Sti	0.8	4.1	0.9	P	–	A	2	P	Colombia

**Notes:** **1**=Style: D=distal, P=proximal; **2**=Wing venation: R=reticulate, P=parallel, sP=sub-parallel, I=irregular; **3**=Stipe: Sti=stipitate, Sub=substipitate, Non=nonstipitate; **4**=Stipe length (cm); **5**=Fruit length (cm); **6**=Fruit width (cm); **7**=Persistent calyx: A=absent, P=present; **8**=Texture: C=coriaceous, L=ligneous, Ch=chartaceous; **9**=Margin constricted: A=absent, P=present; **10**=Number of seeds; **11**=Seed orientation relative to backbone: P=parallel, O=oblique, T=transverse; **12**=Distribution. Information was taken from Lima (1989), (Lewis et al., 2005, 2012; Kirkbride et al., 2012)

The 46 genera of Dalbergieae vary greatly in fruit morphology (Lavin et al. 2001; fig. 3). Twenty-six genera have non-winged fruits, 12 genera have non-samaroid winged fruits, and 8 genera have samaras (fig. 3). The parsimony analysis of the combined molecular (Cardoso et al., 2013) and fruit morphological (table A1 and appendix A2) dataset for the clade Dalbergieae, resulted in 385 most-parsimonious trees of 1459 steps (CI: 63; RI: 68) and placed the fossil within the *Pterocarpus* subclade (fig. 4). The strict consensus tree collapsed 17 nodes. The bootstrap analysis provided strong support for the non-collapsed nodes of the strict consensus tree (>80, fig. 4). A hypothetical ancestral reconstruction of fruit morphological characters indicates that samaras and other winged fruits have evolved numerous times within Dalbergieae (fig. 4). The ecology and distribution of the extant species can be visualized in Figure 4. The *Pterocarpus* subclade can be found in a variety of settings, from exclusively tropical rainforest (9%) to exclusively seasonally dry forest in Neotropical and Old-World tropical regions (65%), warm temperate zones (4%) and both dry and rain forests (22%; fig. 4).

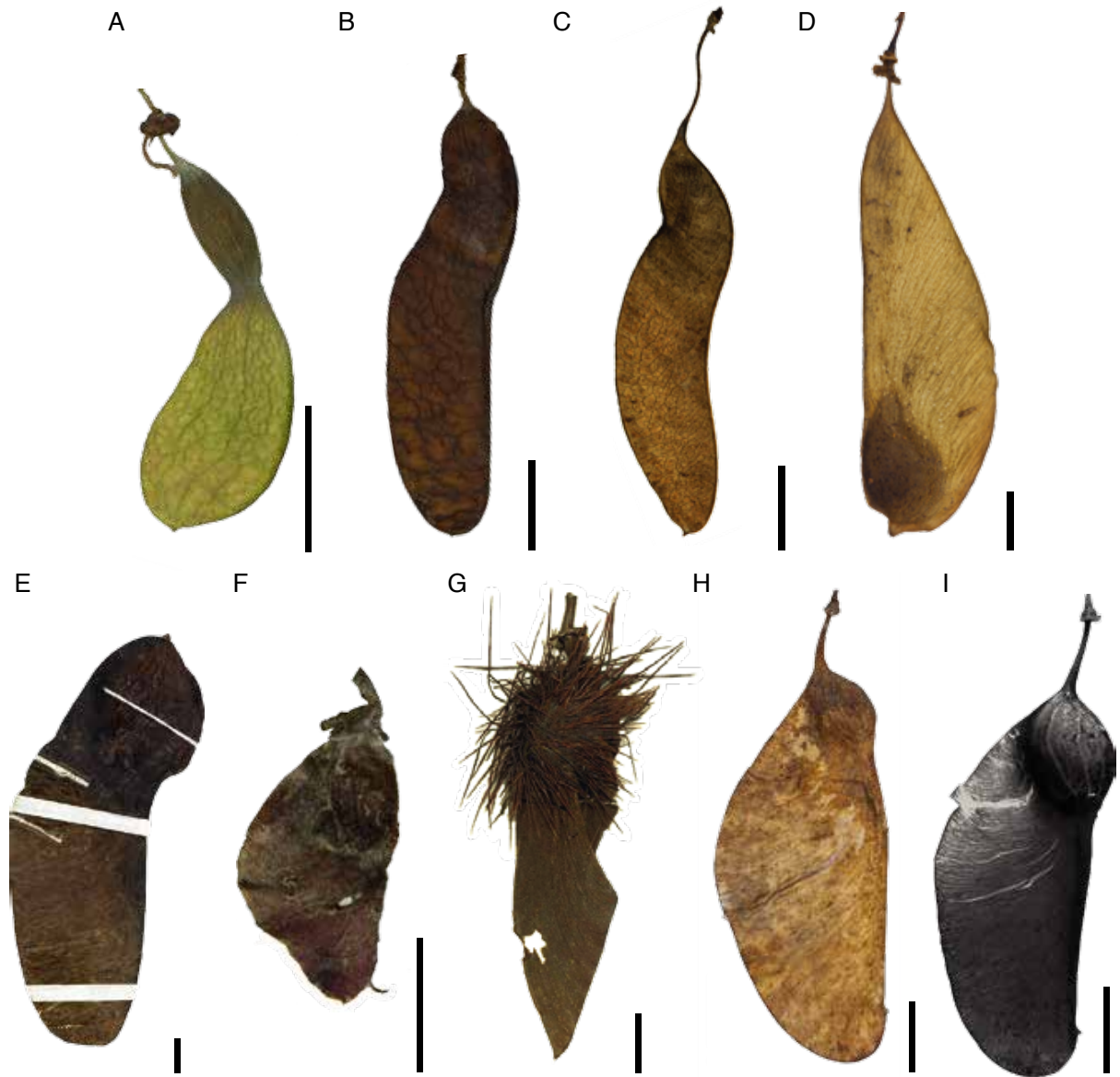


**Fig. 3. Extant samaras of the clade Dalbergieae**

Photographs of extant asymmetrically winged samaras of the clade Dalbergieae. *A*, *Nissolia* Jacq. *B*, *Machaerium* Pers. *C*, *Steinbachiella* Harms. *D*, *Platypodium* Vogel. *E*, *Paramachaerium* Ducke. *F*, *Maraniona* C.E. Hughes, G.P. Lewis, see Daza Yomona, Ancieto & Reynel. *G*, *Centrolobium* Mart. ex Benth. *H*, Cleared and stained *Tipuana* (Benth.) Benth. All scales are 1cm. Herbarium vouchers and species information corresponded to each genus listed here are in table B1, available online.

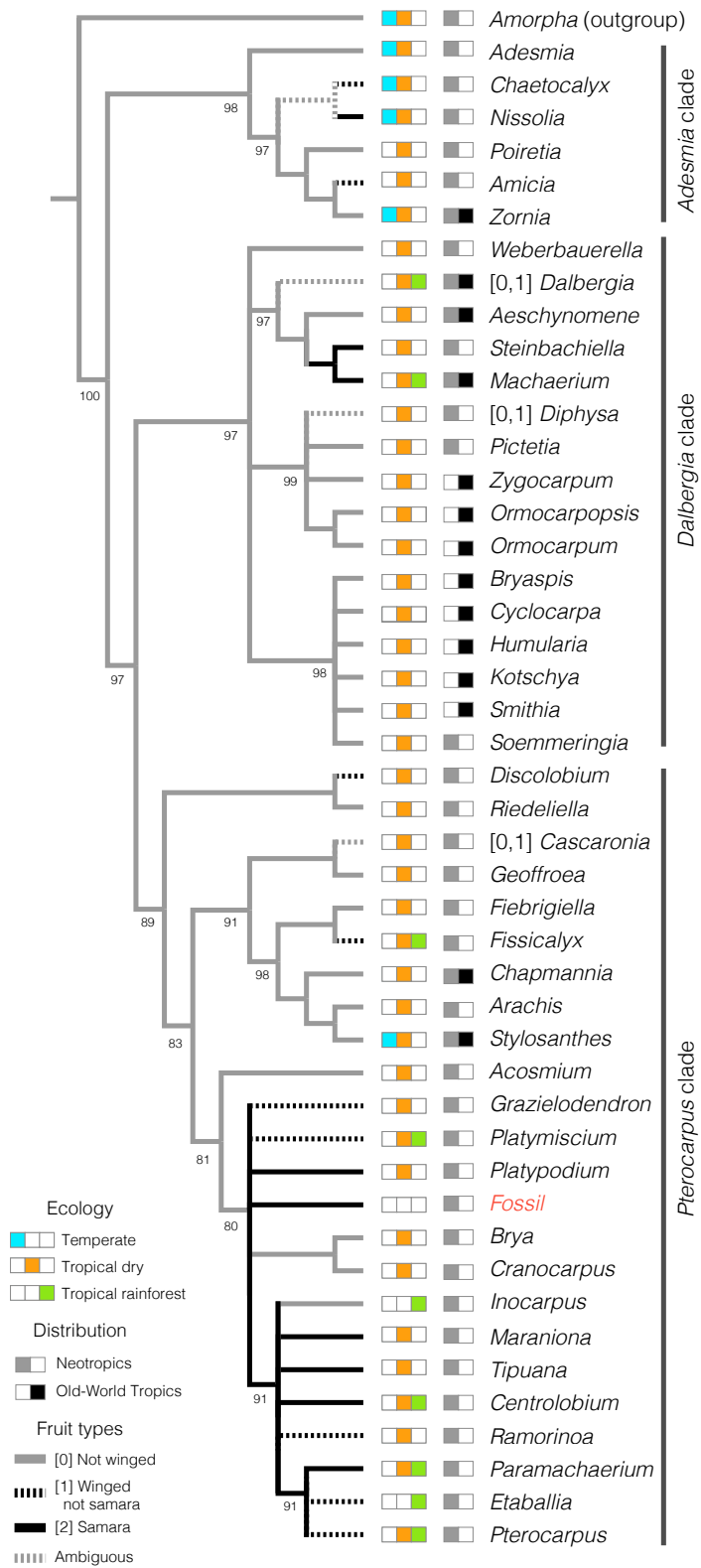


Fig. 4. Phylogenetic placement of the fossil samara

Strict consensus tree of the clade Dalbergieae from a parsimonious combined morphological and molecular analysis. The fossil *Luckowcarpa gunnii* (in red) is nested within the *Pterocarpus* subclade. The colors and patterns of the branches represent an ancestral character-state reconstruction for fruit type. The numbers below the main nodes branches represent bootstrap values. The first row of squares in front of each taxon corresponds to the ecology of where each genus is found today. The second row of squares corresponds to distribution of each genus.

### ***Taxonomy***

*Order*—*Fabales* Bromhead

*Family*—*Fabaceae* Lindl.

*Subfamily*—*Papilionoideae* DC.

*Clade*—*Dalbergieae* Bronn ex DC.

*Subclade*—*Pterocarpus* (*sensu* Lavin et al. 2001)

*Genus*—*Luckowcarpa* Martínez-A., *gen. nov.*

*Generic diagnosis.* Unicarpellate asymmetrically winged samara with a proximal seed chamber, single remnant style at the distal end of the wing. Stipe long, calyx remnant present along the stipe. Seed chamber with two seeds parallel to backbone. Wing with reticulate major venation.

*Type species.* *Luckowcarpa gunnii* Martínez-A., sp. nov. (fig. 5)

*Holotype.* STRI-Mapuka\_44057 (fig. 5A–C), here designated.

*Paratypes.* STRI-Mapuka\_44058–61 (fig. 5D–G)

*Studied material.* STRI-Mapuka\_44057–44068; STRI-SGC\_35550, 35650, 36162.

*Locality.* Topocoro dam, Santander, Colombia. STRI locality ID 430134, 7°6'30.24"N 73°25'45.12"W (WGS84 18N; fig. 1).

*Stratigraphic position and age.* Upper Esmeraldas Formation, Nuevo Mundo Syncline (fig. 1), Middle Magdalena Valley Basin. The age of the Upper Esmeraldas Formation is late Eocene (Rodríguez-Forero et al., 2012); palynological zone T-07 of Jaramillo et al (2011).

*Etymology, genus.* Named after Melissa Luckow, a botanist who has done great advances in legume systematics, and from Greek *-carpa* (fruit).

*Etymology, specific epithet.* Named after Charles Robert Gunn, a botanist expert in seeds, who made significant contributions to the multi-volume series of seeds and fruits of legumes.

*Repository.* Mapuka, Universidad del Norte, Barranquilla, Colombia and Museo José Royo y Gómez, Colombian Geological Survey, Bogota, Colombia.

*Species*— *Luckowcarpa gunnii* Martínez-A., *sp. nov.* (fig. 5)

*Species diagnosis.* Same as for the genus

*Description.* Fossil specimens are fruits with a single proximal seed chamber and a distal wing. The description is based on 15 specimens. The fruits have an average length of 4.1 cm from the pedicel attachment to the wing tip. Only one specimen (Mapuka STRI\_44057) was complete and measurements were only done on this specimen (fig. 5A–C). Eleven specimens have preserved wings or seed chambers but were not complete. I used the proportion of seed chamber length versus wing length measured on the complete specimen (seed chamber/wing ratio: 1.8), to estimate the length of the eleven incomplete specimens that ranged from 2.7 to 6.1 cm. The broadest point of the fruit is located in the seed chamber area and has an average of 0.9 cm of width ranging between 0.6–1.2 cm. The ratio of the fruit length to width is 4.5:1. The wing is between 1.4 to 2.2 cm in length measured from the distal margin of the seed chamber to the distal margin of the wing, and it is between 0.6 to 0.9 mm in width at its broadest point. The seed chamber is oval to circular in shape, and varies in length from 0.8 to 1 cm and width from 0.5 to

0.7 mm. There is a style remnant at the distal end of the wing (fig. 5D,E). The wing extends and tapers proximally along the entire length of the seed chamber and part of the stipe (fig. 5A–D). There is a long stipe 0.8 cm long (fig. 5F). The remnant of the calyx is present along the stipe (fig. 5F). The seed chamber has parallel venation. One specimen (fig. 5A–C) has the preserved impression of two non-overlapping seeds parallel to backbone (backbone is defined by Mirle and Burnham (1999) as the placental suture of the legume pod that corresponds to the thickest part of the wing). Both seeds have the same size, with a length of 0.42 cm and a width of 0.18 cm. The boundary between the seed chamber and the wing is transitional and then there is not a clear demarcation line between the two. The wing has reticulate major venation with stronger veins investing the backbone of the wing (fig. 5A,B). The primary veins of the wing are strong proximally, densely distributed and parallel to the backbone; distally they spread and diminish in thickness forming the reticulum. The primary veins have dichotomous branching proximally. The minor venation is reticulate. The fossils have a smooth margin along the wing.

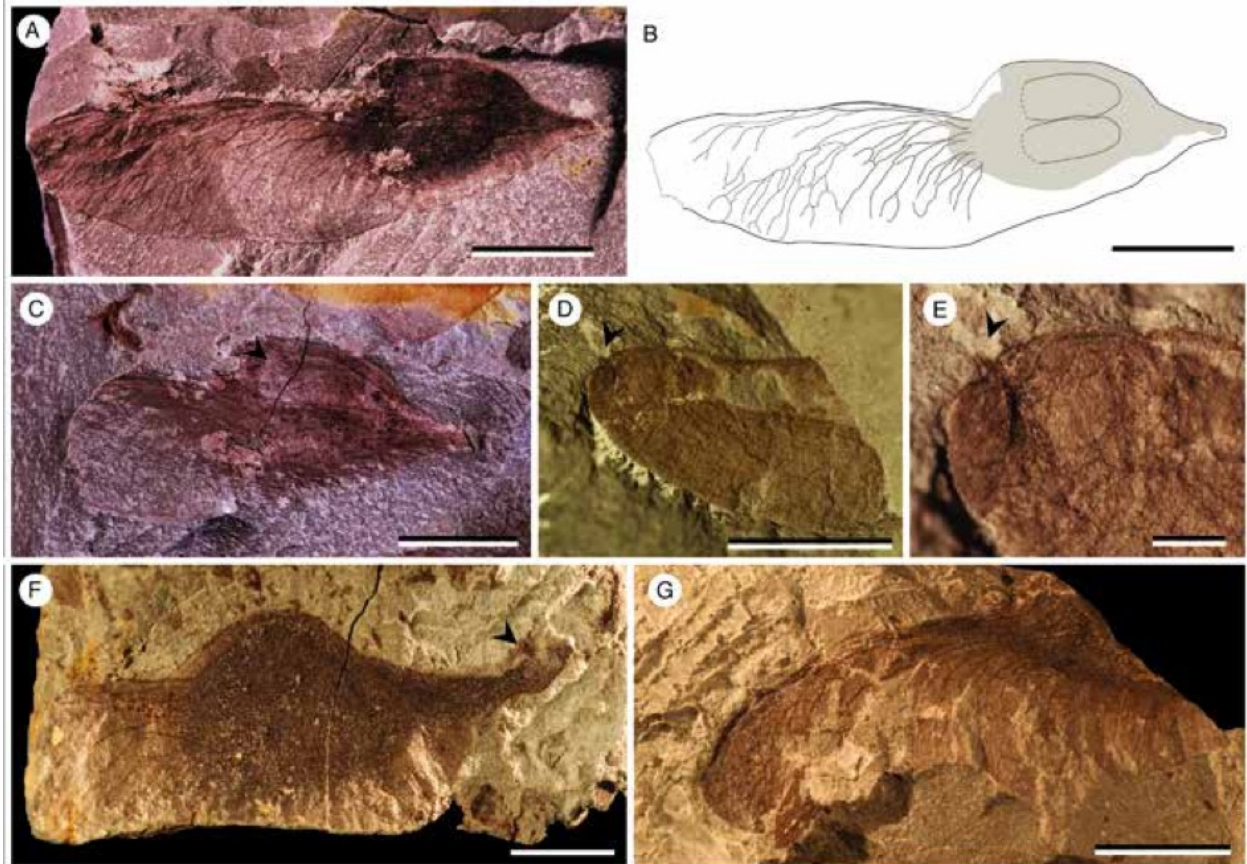


**Fig. 5. Fossil samara fruit *Luckowcarpa gunnii* gen. and sp. nov.**

*A–C*, Holotype STRI-Mapuka\_44057. *B*, Holotype sketch. *C*, Holotype counterpart, arrow shows the impression of the two seeds *D, E*, STRI-Mapuka\_44060. *E*, Close-up of the distal part of the wing, arrow shows the distal style remnant; scale is 0.1 cm. *F*, STRI-Mapuka\_44061. *G*, STRI-Mapuka\_44058. Scales from *A–D* and *F, G* are 0.5 cm.

#### *Comparison with other fossils*

Fossilized asymmetrically winged samaras have been described from numerous sites mostly in northern high latitudes. The majority of these records are from the Eocene of Japan, China, and United States and correspond mainly to the fossil genus *Deviacer* Manchester (Manchester, 1994; Chen and Manchester, 2015; Myers and Erwin, 2015) and to *Paleosecuridaca* Pigg, DeVore, and Wojciechowski (Pigg et al., 2008). These two morphogenera differ from *Luckowcarpa gunnii* in its proximal style remnant located at the end of the seed chamber, a more oval locular shape, a larger length to width ratio, and a more parallel wing venation. Recently a

fossilized legume samara was described from China: *Pterolobium punctatopsis* L.B. Jia, Y.J. Huang et Z.K. Zhou ((Jia et al., 2017). *Pterolobium* differs from *L. gunnii* by having only one seed per fruit and parallel wing venation. At lower latitudes only two fossil species based on asymmetrically winged samaras have been described, and both are from the Miocene of Ecuador. One them was identified to the modern genus *Loxopterygium* (Anacardiaceae;(Burnham and Carranco, 2004)) and differs from *L. gunnii* because it has a proximal style remnant. The other samara has been identified to the extant legume genus *Tipuana* (*Tipuana ecuatoriana*; (Burnham, 1995). This fruit shares with *L. gunnii* the presence of a long stipe, a distal style remnant, a similar seed chamber and wing shape, and size and length/width proportion. However, despite these similarities, *Tipuana* has a different seed orientation compared with *L. gunnii* (perpendicular vs. parallel to the backbone, respectively; fig. 6) and *Tipuana ecuatoriana* has a more parallel wing venation, a weaker backbone, and a shorter stipe compared with *L. gunnii*.



**Fig. 6. Dissected modern Dalbergieae samaras.**

Dissected samaras showing some variability of seed number and orientation within Dalbergieae. *A*, *Tipuana* has 1–4 perpendicular seeds (showing 4 in this specimen); *B*, *Platypodium* has 1(-2) parallel seeds (showing 1 in this specimen). *C*, *Machaerium* has 1 parallel seed.

## DISCUSSION

The new fossil genus and species *Luckowcarpa gunnii* provides an example of how fossil samara fruits retain sufficient relevant morphologic characters for allowing confident determination of their taxonomic affinity. Although Fabaceae are often recognized by their typical two valved dehiscent pods, winged fruits are also present in 18% of its genera, and asymmetrically winged samaras occur in only 3% of the genera (Kirkbride et al. 2017). This small percentage of Fabaceae with asymmetrically winged samaras facilitated the comparisons and taxonomic placement of *Luckowcarpa gunnii* within this large family. Within Papilionoideae the clade Dalbergieae includes the most samaroid taxa (Kirkbride et al., 2012), with seven genera having samaras that are asymmetrically winged. The Dalbergieae includes 46 genera and ca. 1367 species; it is subdivided into three subclades based on molecular markers, morphology, wood anatomy and palynology: *Pterocarpus*, *Dalbergia* and *Adesmia* (Cardoso et al., 2013). The comparisons of *L. gunnii* with extant and fossil material and the phylogenetic analysis placed this fossil taxon within the *Pterocarpus* subclade of the clade Dalbergieae of Papilionoideae.

The combined morphological and molecular parsimonious analysis, resulted in a topology that is similar to that based only on molecular data using Bayesian analytical methods (Cardoso et al., 2013). The subclades *Adesmia*, *Dalbergia* and *Pterocarpus* were recovered and share the same phylogenetic relationships. The main differences between both results are the number of polytomies, which in the strict consensus of the parsimonious analysis are 17, while in the Bayesian majority-rule consensus are 5 (Cardoso et al., 2013), and also the phylogenetic position of *Platymiscium*, which appears in another node within the *Pterocarpus* subclade. These differences could be attributed to methodological differences between the type of consensus used, the instability (Hermsen and Hendricks, 2008) caused by missing morphological data for

those genera that do not have asymmetrically winged samaras, and also by the incongruence of some samara characters, like stipe length and seed orientation (fig. 6).

The phylogenetic position of the fossil within the *Pterocarpus* subclade is supported by the presence of asymmetrically wing samaras (fig. 4), two seeds, and a persistent calyx.

Asymmetrically winged samaras have evolved independently in all three of the traditional subfamilies. The presence of asymmetrically winged samaras in distantly related taxa within Dalbergieae suggests that this fruit type has evolved numerous times within the clade as well, as Lavin et al. suggested (2001; fig. 4). Despite the similarities between *Luckowcarpa gunnii* and the extant genus *Tipuana* (figs. 3 and 5), they are separated by seed orientation and the venation patterns, which in *L. gunnii* is parallel to the backbone and reticulate (fig. 5A–C) while in *Tipuana* is perpendicular to the backbone and subparallel, respectively (Kirkbride et al., 2012).

The taxonomic affinity proposed for the fossil *Luckowcarpa gunnii* with the subclade *Pterocarpus* acknowledges the fact that there is not an extant genus that shares all the characters with the fossil, but instead the combination of the samara characters of the genera within this group are shared with the fossil *L. gunnii*. Although within the material available for dissection I was not able to find specimens within Dalbergieae with two or more seeds parallel to the backbone, Kirkbride et al. (2017) reports that the genus *Platypodium* can present sometimes two seeds parallel to the backbone. Figure 6 shows some of the variability in seed number and orientation present in Dalbergieae.

Within Dalbergieae numerous fossil fruits and leaflets have been described, however most of these records need careful reevaluation (Herendeen et al., 1992). Recently, three Dalbergieae fossil taxa have been described and consist of fossil leaflets from the middle Eocene of the United States with affinities to *Machaerium* (Herendeen, 1992), winged fruits from the

Oligocene-Miocene boundary of the Czech Republic with affinities to the genera *Pterocarpus* and *Riedeliella* (Buzek, 1992), and one samara from the Miocene of Ecuador which is similar to *Tipuana* (Burnham, 1995). Being Eocene, the fossil *Luckowcarpa gunnii* represents the earliest fruit record of the Dalbergieae clade.

Dalbergieae is pantropical in distribution, although some species reach subtropical regions. Species from 95% of the genera are found (exclusively and not exclusively) in tropical dry forest ecosystems, such as seasonally dry tropical forests or savannas (fig. 4). Only the monospecific genera *Inocarpus* and *Etaballia* are exclusively found in tropical rainforest, while 20% of the genera are found in both rain- and dry forests, and 67% of the genera are exclusively found in dry forest ecosystems (fig. 4). Based on the phylogenetic position of *Luckowcarpa gunnii* within the *Pterocarpus* subclade, it is reasonable to propose that *L. gunnii* was also adapted to tropical dry forest conditions (fig. 4). A biogeographic analysis for the genus *Platysmiscium*, a member of the *Pterocarpus* subclade, which is today adapted to tropical dry and rainforest ecosystems, suggests an ancestral dry forest distribution and a later expansion towards rainforest conditions (Saslis-Lagoudakis et al., 2008), supporting the hypothesis of an ancestral dry forest distribution for the *Pterocarpus* subclade.

The estimated age, based on molecular calibration, for the crown node of the *Pterocarpus* subclade is between 39.2 Ma (Saslis-Lagoudakis et al., 2008) to 41.2–49.6 Ma (Lavin et al., 2005). These age estimations roughly agree with the late Eocene age of *Luckowcarpa gunnii*. Fossil, climatic, and molecular phylogenetic evidence suggest that seasonally dry tropical forests date at least to the middle Eocene (Graham and Dilcher, 1995; Pennington et al., 2006; Schrire et al., 2009). Correlated with the expansion of seasonally dry tropical forests and strong temperature pulses during the Eocene, one of the main hypotheses related to the diversification

of Leguminosae suggests that these had an important role in its diversification (Axelrod, 1992; Herendeen, 1992). In addition to the *L. gunnii* record, fragments of legume-like pods and leaves have also been found in the same locality of the Esmeraldas Formation; therefore it is possible that legumes could have been already an important component of the Esmeraldas flora. However, more evidence from the Esmeraldas macro and microfloras is necessary to fully assess the habitat of *L. gunnii*.

### ***Conclusions***

The description of *Luckowcarpa gunnii* within a phylogenetic context, enhances our understanding of the evolution and biogeography of third largest flowering plant family, Leguminosae, and specifically, of the history of the clade Dalbergieae, a group having diverse fruit morphology, that is adapted to tropical dry forest ecosystems.

## REFERENCES

- Axelrod, D. I. 1992. Climatic pulses, a major factor in legume evolution. *Advances in legume systematics*. 4. The fossil record, 259–279.
- Burnham, R. J. 1995. A New Species of Winged Fruit from the Miocene of Ecuador: *Tipuana ecuatoriana* (Leguminosae). *American Journal of Botany* 82: 1599–1607.
- Burnham, R. J., and N. L. Carranco. 2004. Miocene winged fruits of *Loxopterygium* (Anacardiaceae) from the Ecuadorian Andes. *American journal of Botany* 91: 1767–1773.
- Buzek, C. 1992. Fruits of *Pterocarpus tertiaris* Weyland from the North-Bohemian Basin, Czechoslovakia. *Advances in legume systematics*. 4. The fossil record, 19–31. The Royal Botanic Garden, Kew, United Kingdom.
- Caballero, V., M. Parra, M. Bohorquez, and A. Roberto. 2010. Levantamiento de la Cordillera Oriental de Colombia durante el Eoceno tardío - Oligoceno temprano: proveniencia sedimentaria en el Sinclinal de Nuevo Mundo, Cuenca Valle Medio del Magdalena. *Boletín de Geología* 32: 45–77.
- Caccavari, M. A. 1996. Analysis of the South American fossil pollen record of Mimosoideae (Leguminosae). *Review of Palaeobotany and Palynology* 94: 123–135.
- Calvillo-Canadell, L., and S. R. S. Cevallos-Ferriz. 2005. Diverse Assemblage of Eocene and Oligocene Leguminosae from Mexico. *International Journal of Plant Sciences* 166: 671–692.
- Cardoso, D., R. T. Pennington, L. P. de Queiroz, J. S. Boatwright, B.-E. Van Wyk, M. F. Wojciechowski, and M. Lavin. 2013. Reconstructing the deep-branching relationships of the papilionoid legumes. *South African Journal of Botany* 89: 58–75.
- Chen, Y., and S. R. Manchester. 2015. Winged Fruits of *Deviacer* in the Oligocene from the Ningming Basin in Guangxi, South China W. O. Wong [ed.], *PLoS ONE* 10: e0144009.
- Cooper, M. A., F. T. Addison, R. Alvarez, M. Coral, R. H. Graham, A. B. Hayward, S. Howe, et al. 1995. Basin Development and Tectonic History of the Llanos Basin, Eastern Cordillera, and Middle Magdalena Valley, Colombia. *AAPG Bulletin* 79: 1421–1442.
- Crepet, W. L., and D. W. Taylor. 1985. The Diversification of the Leguminosae: First Fossil Evidence of the Mimosoideae and Papilionoideae. *Science* 228: 1087–1089.
- Daghlian, C. P., W. L. Crepet, and T. Delevoryas. 1980. Investigations of Tertiary Angiosperms: A New Flora Including *Eomimosoidea plumosa* from the Oligocene of Eastern Texas. *American Journal of Botany* 67: 309–320.

- Gentry, A. H. 1990. Floristic Similarities and Differences between Southern Central America and Upper and Central Amazonia. Four Neotropical Rainforests, 141–157. Yale University Press.
- Gómez, E., T. E. Jordan, R. W. Allmendinger, K. Hegarty, and S. Kelley. 2005. Syntectonic Cenozoic sedimentation in the northern middle Magdalena Valley Basin of Colombia and implications for exhumation of the Northern Andes. *Geological Society of America Bulletin* 117: 547.
- Graham, A., and D. Dilcher. 1995. The Cenozoic record of tropical dry forest in northern Latin America and the southern United States. Seasonally dry tropical forests, 124–145. Cambridge University Press, Cambridge, UK.
- Group, L. P. W., and others. 2013. Legume phylogeny and classification in the 21st century: progress, prospects and lessons for other species-rich clades. *Taxon* 62: 217–248.
- Gunn, C. R. 1984. Fruits and seeds of genera in the subfamily Mimosoideae (Fabaceae). United States Department of Agriculture, Washington, D.C.
- Herendeen, P., W. L. Crepet, and David L. Dilcher. 1992. The fossil history of the Leguminosae: phylogenetic and biogeographical implications. Advances in legume systematics. 4. The fossil record, 303–316. The Royal Botanic Garden, Kew, United Kingdom.
- Herendeen, P. S. 1992. The fossil history of the Leguminosae from the Eocene of southeastern North America. Advances in legume systematics. 4. The fossil record, 85–160. The Royal Botanic Garden, Kew, United Kingdom.
- Hermesen, E. J., and J. R. Hendricks. 2008. W(h)ither Fossils? Studying Morphological Character Evolution in the Age of Molecular Sequences. *Annals of the Missouri Botanical Garden* 95: 72–100.
- Herrera, F., S. R. Manchester, M. R. Carvalho, C. Jaramillo, and S. L. Wing. 2014. Paleocene wind-dispersed fruits and seeds from Colombia and their implications for early Neotropical rainforests. *Acta Palaeobotanica* 54: 197–229.
- Hughes, C. E., G. P. Lewis, A. D. Yomona, and C. Reynel. 2004. *Maraniona*. A new dalbergioid legume genus (Leguminosae, Papilionoideae) from Peru. *Systematic Botany* 29: 366–374.
- Jaramillo, C. A., M. Rueda, and V. Torres. 2011. A palynological zonation for the Cenozoic of the Llanos and Llanos Foothills of Colombia. *Palynology* 35: 46–84.
- Jia, L.-B., Y.-J. Huang, H. Sun, T. Su, J. Huang, and Z.-K. Zhou. 2017. First fossil of *Pterolobium* (Leguminosae) from the Middle Miocene Yunnan, South China. *Review of Palaeobotany and Palynology* 242: 21–32.
- Kirkbride, J. H., C. R. Gunn, and A. L. Weitzman. 2003. Fruits and seeds of genera in the subfamily Faboideae (Fabaceae). United States Department of Agriculture, Washington DC, USA.

- Kirkbride, J. H., C. R. Gunn, A. L. Weitzman, and M. J. Dallwitz. 2012. Legume (Fabaceae) Fruits and Seeds, version 2. *United States Department of Agriculture*. Website <http://nt.ars-grin.gov/seedsfruits/keys/fabaceae/Index.cfm> [accessed 23 January 2017].
- Lavin, M., P. Herendeen, and M. Wojciechowski. 2005. Evolutionary Rates Analysis of Leguminosae Implicates a Rapid Diversification of Lineages during the Tertiary. *Systematic Biology* 54: 575–594.
- Legume Research Team at Kew. 2017. Legumes of the World Online. Website <http://www.kew.org/science-conservation/research-data/resources/legumes-of-the-world> [accessed 1 February 2017].
- Lewis, G. P., B. D. Schrire, B. Mackinder, and M. Lock. 2005. Legumes of the world. Royal Botanic Gardens, Kew, Richmond, U.K.
- Lewis, G. P., J. R. I. Wood, and M. Lavin. 2012. *Steinbachiella* (Leguminosae: Papilionoideae: Dalbergieae), endemic. *Kew Bulletin* 67: 4.
- Magallón-Puebla, S., and S. R. S. Cevallos-Ferriz. 1994. Fossil legume fruits from tertiary strata of Puebla, Mexico. *Canadian Journal of Botany* 72: 1027–1038.
- Manchester, S. R. 1994. Fruits and seeds of the Middle Eocene nut beds flora, Clarno Formation, Oregon. Paleontological Research Institution.
- Manchester, S. R., and E. L. O’Leary. 2010. Phylogenetic Distribution and Identification of Fin-winged Fruits. *The Botanical Review* 76: 1–82.
- Martínez, C. 2017. Passifloraceae seeds from the late Eocene of Colombia. *American Journal of Botany* 104: 1857–1866.
- Mirle, C., and R. J. Burnham. 1999. Identification of asymmetrically winged samaras from the Western Hemisphere. *Brittonia* 51: 1–14.
- Muller, J. 1981. Fossil Pollen Records of Extant Angiosperms. *Botanical Review* 47: 1–142.
- Myers, J. A., and D. M. Erwin. 2015. *Deviacer pidemarmanii* sp. nov. (Polygalaceae) from the Late Eocene–Early Oligocene Badger’s Nose Paleoflora, Modoc County, California. *International Journal of Plant Sciences* 176: 259–268.
- Nie, J., B. K. Horton, J. E. Saylor, A. Mora, M. Mange, C. N. Garziona, A. Basu, et al. 2012. Integrated provenance analysis of a convergent retroarc foreland system: U–Pb ages, heavy minerals, Nd isotopes, and sandstone compositions of the Middle Magdalena Valley basin, northern Andes, Colombia. *Earth-Science Reviews* 110: 111–126.
- Nixon, K. C. 2015. Winclada ver. 1.99. Ithaca, New York, USA.

- Pennington, R. T., J. A. Ratter, and G. P. Lewis. 2006. Neotropical savannas and seasonally dry forests: plant diversity, biogeography, and conservation. CRC Press, Boca Raton, Florida, USA.
- Pérez-Consuegra, N., A. Cuervo-Gómez, C. Martínez, C. Montes, F. Herrera, S. Madriñán, and C. Jaramillo. 2017. Paleogene *Salvinia* (Salviniaceae) from Colombia and their paleobiogeographic implications. *Review of Palaeobotany and Palynology* 246: 85–108.
- Pigg, K. B., M. L. DeVore, and M. F. Wojciechowski. 2008. *Paleosecuridaca curtisii* gen. et sp. nov., *Securidaca* -Like Samaras (Polygalaceae) from the Late Paleocene of North Dakota and Their Significance to the Divergence of Families within the Fabales. *International Journal of Plant Sciences* 169: 1304–1313.
- Reineck, H.-E., and I. B. Singh. 1980. Depositional sedimentary environments: With reference to terrigenous clastics. Springer-Verlag, Berlin, Germany.
- Rodríguez-Forero, G., F. E. Oboh-Ikuenobe, C. Jaramillo-Munoz, M. J. Rueda-Serrano, and E. Cadena-Rueda. 2012. Palynology of the Eocene Esmeraldas Formation, Middle Magdalena Valley Basin, Colombia. *Palynology* 36: 96–111.
- Saslis-Lagoudakis, C., M. W. Chase, D. N. Robinson, S. J. Russell, and B. B. Klitgaard. 2008. Phylogenetics of neotropical *Platymiscium* (Leguminosae: Dalbergieae): systematics, divergence times, and biogeography inferred from nuclear ribosomal and plastid DNA sequence data. *American Journal of Botany* 95: 1270–1286.
- Schrire, B. D., M. Lavin, N. P. Barker, and F. Forest. 2009. Phylogeny of the tribe Indigofereae (Leguminosae–Papilionoideae): Geographically structured more in succulent-rich and temperate settings than in grass-rich environments. *American Journal of Botany* 96: 816–852.
- Terborgh, J., and E. Andresen. 1998. The Composition of Amazonian Forests: Patterns at Local and Regional Scales. *Journal of Tropical Ecology* 14: 645–664.
- Ward, D. E., R. Goldsmith, A. Jimeno, J. Cruz, H. Restrepo, and E. Gómez. 1977. Geologic map of the Bucaramanga Quadrangle (H-12), Colombia.

## APPENDIX A1

Extant species observed from herbarium specimens for comparison with the fossil

*Luckowcarpa gunnii*.

**Anacardiaceae:** *Loxopterygium* sp. Hook. f., USM-118113; **Fabaceae:** *Centrolobium minus* C. Presl, GPJD-K-000530331; *Luetzelburgia andrade-limae* H.C. Lima, GPJD-RB-00540304; *Machaerium oblongifolium* Vogel, BH-000120448; *Myrospermum frutescens* Jacq., BH-000120449; *Myroxylon balsamum* (L.) Harms, BH-000120450; *Nissolia fruticosa* Jacq., BH-000120548; *Paramachaerium gruberi* Brizicky, GPJD-US-00002385; *Platypodium elegans* Vogel, BH-000120447; *Pterogyne nitens* Tul., BH-00007268; *Tipuana tipu* (Benth.) Kuntze, USM-23035 and fresh material; *Vatairea paraensis* Ducke, GPJD-P-02767800; *Vataireopsis iglesiasii* Ducke, GPJD-F-0059965f. **Malpighiaceae:** *Banisteriopsis laevifolia* A. Juss., BH-000120451; *Barnebya harleyi* W.R. Anderson & B. Gates, GPJD-K-000427476; *Ectopopterys soejartoi* W.R. Anderson, GPJD-HUA-0000528; *Gaudichaudia* sp. Kunth, BH-000120452; *Heteropsis aureo-sericea* Cuatre., BH-000120453; *Janusia gracilis* Gray, BH-000123004; *Peixotoa magnifica* C.E. Anderson, BH-000123005; *Stigmaphyllon emarginatum* (Cav.) A. Juss., BH-000123006. **Phytolaccaceae:** *Gallesia gorarema* (Vell.) Moq., BH-000120457; *Seguiera guaranitica* Speg., BH-000120459. **Polygalaceae:** *Securidaca virgata* Sw., BH-000120455. **Polygonaceae:** *Brunnichia cirrhosa* Gaertn., BH-000120454. **Rutaceae:** *Helietta lucida* Brandegee, BH-000120460. **Sapindaceae:** *Acer* sp. L., Fresh material; *Athyana weinmannifolia* (Griseb.) Radlk., GPJD-K-000542540; *Diatenopteryx sorbifolia* Radlk., BH-000120461; *Lophostigma schunkei* (Acev.-Rodr.) Acev.-Rodr., GPJD-NO-0109903; *Serjania rufa* Radlk., BH-000120462; *Thouinia acuminata* S. Watson, BH-000120463; *Thouinidium decandrum* (Bonpl.) Radlk., BH-000120464; *Toulicia guianensis* Aubl., BH-000123006. **Trigoniaceae:** *Trigoniastrum hypoleucum* var. *viride* Airy Shaw, GPJD-M-0239862. **Ulmaceae:** *Phyllostylon rhamnoides* (J. Poiss.) Taub., BH-000120456.

**Notes:** Herbaria abbreviations. BH: L. H. Bailey Hortorium Herbarium; USM: Herbario Universidad Nacional Mayor de San Marcos; GPJD: Global Plants JSTOR Database; F: Field Museum of Natural History, Chicago; HUA: Herbario Universidad de Antioquia; K: Royal Botanic Gardens, Kew; M: Botanische Staatssammlung München; NO: Tulane University Herbarium; P: Muséum National d'Histoire Naturelle; RB: Jardim Botânico do Rio de Janeiro; US: United States National Herbarium, Smithsonian Institution.

### TABLE A1

Morphological matrix of extant genera of the tribe Dalbergieae and the fossil *Luckowcarpa gunnii*. Numbers in the headings of the columns and the matrix correspond to the morphological characters and characters states defined in Appendix A2.

<b>Genus</b>	<b>1</b>	<b>2</b>	<b>3</b>	<b>4</b>	<b>5</b>	<b>6</b>	<b>7</b>	<b>8</b>	<b>9</b>	<b>10</b>
<i>Amorpha</i>	0	-	-	-	0/1	-	-	1	0	-
<i>Adesmia</i>	0	-	-	-	1	-	-	0	2	-
<i>Chaetocalyx</i>	1	-	-	0	0/1/2	-	-	0/1	2	-
<i>Nissolia</i>	2	0	0	0/1	0/1/2	0	0	1	2	0
<i>Poiretia</i>	0	-	-	-	0	-	-	0/1	2	-
<i>Amicia</i>	1	-	-	0/3	0	-	-	0/1	2	-
<i>Zornia</i>	0	-	-	-	0	-	-	1	2	-
<i>Weberbauerella</i>	0	-	-	-	1	-	-	?	2	-
<i>Dalbergia</i>	0/1	-	2	0/3	2	-	-	0	2	-
<i>Aeschynomene</i>	0	-	-	-	1/2	-	-	0/1	2	-
<i>Steinbachiella</i>	2	0	0	0	2	0	0	1	0	?
<i>Machaerium</i>	2	0	0	0	1/2	0	0/1	0/1	0	0
<i>Diphysa</i>	0/1	-	2	0/1	1/2	-	-	1	2	-
<i>Pictetia</i>	0	-	-	-	0/1/2	-	-	0/1	2	-
<i>Zygocarpum</i>	0	-	-	-	1/2	-	-	0	2	-
<i>Ormocarpopsis</i>	0	-	-	-	2	-	-	1	2	-
<i>Ormocarpum</i>	0	-	-	-	1/2	-	-	0/1	2	-
<i>Humularia</i>	0	-	-	-	0	-	-	1	1	-
<i>Smithia</i>	0	-	-	-	1	-	-	1	2	-
<i>Bryaspis</i>	0	-	-	-	0	-	-	0	1	-
<i>Kotschya</i>	0	-	-	-	1	-	-	1	2	-
<i>Cyclocarpa</i>	0	-	-	-	1	-	-	0	2	-
<i>Soemmeringia</i>	0	-	-	-	0	-	-	1	2	-
<i>Discolobium</i>	1	-	-	0	0	-	-	1	0	-
<i>Riedeliella</i>	0	-	-	-	1/2	-	-	0/1	0	-
<i>Platymiscium</i>	1	-	-	0	2	-	-	0	0	-
<i>Cascaronia</i>	0/1	-	-	0/1	1	-	-	1	1	-
<i>Geoffroea</i>	0	-	-	-	0/1	-	-	0	1	-
<i>Fiebrigiella</i>	0	-	-	-	1	-	-	0/1	2	-
<i>Fissicalyx</i>	1	-	-	0/1	1	-	-	0	0	-
<i>Chapmannia</i>	0	-	-	-	0	-	-	0	2	-
<i>Arachis</i>	0	-	-	-	0	-	-	0	2	-
<i>Stylosanthes</i>	0	-	-	-	0	-	-	0/1	1	-
<i>Grazilodendron</i>	1	-	-	0	1	-	-	0	1	-
<i>Platypodium</i>	2	1	0	4	2	?	1	0	1	0
<i>Brya</i>	0	-	-	-	0	-	-	0/1	1	-
<i>Cranocarpus</i>	0	-	-	-	0	-	-	1	1	-
<i>Acosmium</i>	0	-	-	-	0/1/2	-	-	0/1	2	-

<i>Paramachaerium</i>	2	0	0	0	0/1	1	1	0	1	2
<i>Etaballia</i>	1	-	-	0/3	0	-	-	0	0	-
<i>Pterocarpus</i>	1	-	-	0/3	1/2	-	-	0	2	-
<i>Maraniona</i>	2	0	0	4	0	1	1	1	0	1
<i>Ramorinoa</i>	1	-	-	0	1	-	-	0	2	-
<i>Centrolobium</i>	2	0	1	4	0/1/2	0/1	1	0	2	1
<i>Inocarpus</i>	0	-	-	-	1	-	-	0	1	-
<i>Tipuana</i>	2	0	0	4	2	0/1	1	0/1	2	2
<i>Luckowcarpa gunnii</i>	2	0	0	0	2	1	1	1	1	0

## APPENDIX A2

List of characters and character states included in the matrix

1. Fruit type: not winged = 0; symmetrically winged = 1; asymmetrically winged samara.
2. Locule position: proximal = 0; distal = 1.
3. Style position: distal = 0; proximal = 1.
4. Wing venation: reticulate = 0; parallel = 1; irregular = 2; no venation = 3; subparallel = 4.
5. Stipe: nonstipitate = 0; substipitate = 1; stipitate = 2.
6. Wing along the locule: absent = 0; present = 1.
7. Ovary-wing distinction: absent = 0; present = 1.
8. Persistent calyx: absent = 0; present = 1.
9. Seed number: always one = 0; one or two = 1; one to numerous = 2.
10. Seed orientation relative to the backbone: parallel = 0; oblique = 1; transverse = 2.

## CHAPTER 4

### PASSIFLORACEAE SEEDS FROM THE LATE EOCENE OF COLOMBIA

CAMILA MARTÍNEZ

*Notice*—Page, figure, table, and appendix numbers and formatting have been changed from the original to conform to dissertation requirements. Any citations of this research should be made to the *American Journal of Botany* article. Access to the *American Journal of Botany* version of this article can be obtained at <https://doi.org/10.3732/ajb.1700224>

\* **Martínez, C.** 2017. Passifloraceae seeds from the late Eocene of Colombia. *American Journal of Botany* 104: 1857–1866.

#### ABSTRACT

**Premise of the study:** The plant fossil record for the neotropics is still sparse and temporally discontinuous. The location and description of new fossil material are fundamental for understanding evolutionary and biogeographic patterns of lineages. A new fossil record of Passifloraceae from the late Eocene of Colombia is described in this study.

**Methods:** Plant fossils were collected from a new locality from the Eocene Esmeraldas Formation. Eighteen fossil seeds were selected, described, and compared with fossil and extant angiosperm seeds based on the literature and herbarium collections. Taxonomic affinities of the

fossil seeds within Passifloraceae s.l. were evaluated by comparing morphological characters of the seeds in a phylogenetic context. Stratigraphic information associated with the fossil locality was used to interpret the environment and taphonomic processes associated with fossil deposition.

**Key results:** A new seed fossil genus and species, *Passifloroidesperma sogamosense* gen. and sp. nov., is described and associated with the subfamily Passifloroideae based on the presence of a foveolate seed surface, ruminant endosperm, and a seed coat with prismatic palisade cells. The depositional environment of the locality is described as a floodplain associated with river channels.

**Conclusions:** A detailed review of the Passifloraceae fossil record indicates that *P. sogamosense* is the oldest confirmed record of Passifloraceae. Its late Eocene age provides a minimum age that can be used as a calibration point for the crown Passifloroideae node in future dating analyses that together with its neotropical geographic location can shed light on the origin and diversification of the subfamily.

**Key words:** Esmeraldas Formation; fossil seeds; macrofossils; minimum age; neotropics; paleobotany; Passifloroideae; Middle Magdalena Valley Basin; ruminant endosperm; seed coat

## INTRODUCTION

The plant fossil record for the Neotropics remains inadequately known due to the few fossil localities that have been discovered and properly studied in the present day (Kidwell and Holland, 2002; Burnham and Johnson, 2004). Efforts to find and describe new fossil material are, in general, fundamental to understanding biogeographic and evolutionary patterns in plant lineages. The macrofossil record of the Eocene (56–33.9 Ma) of tropical America, despite a few

reports (e.g. Duarte and Mello Filha, 1980; Mello et al., 2000; Burnham and Johnson, 2004), remains poorly understood. Dramatic global changes in temperature took place during the Eocene with a transition from a warm “greenhouse” in the early Eocene to a cooler climate in the late Eocene and early Oligocene (Zachos et al., 2008). This climatic change, together with tectonic changes related to the onset of the uplift of the Andes in northern South America (Gómez et al., 2005; Bayona et al., 2008; Mora et al., 2010; Nie et al., 2010; Ochoa et al., 2012) could have driven numerous changes in the ecosystems during that time. The study of fossil material from a recently discovered locality in the late Eocene Esmeraldas Formation in Colombia increases our understanding of the paleoflora of an underrepresented region during a climatically significant time interval. Specifically, the identification of a new fossil seed from this formation, which clearly shows characteristics of the family Passifloraceae, sheds light into the evolution of this lineage.

Passifloraceae Juss. ex Roussel. *sensu lato* is mainly a pantropical family, with 28 genera and approximately 950 species (Tokuoka, 2012). The Angiosperm Phylogeny Group (APG III, 2009) includes Passifloraceae *sensu stricto* (now Passifloroideae Burnett), together with former Turneraceae Kunth ex DC. (now Turneroideae Eaton) and former Malesherbiaceae D. Don (now Malesherbioideae Burnett) in a single family, Passifloraceae s.l., based on results of large-scale molecular analyses (e.g. Soltis et al., 2000, 2007; Chase et al., 2002). More recently, studies at a smaller scale have confirmed Passifloraceae s.l. as a monophyletic group with several morphological characters supporting the molecular affinities among these former families (Tokuoka, 2012; Krosnick et al., 2013). Malesherbioideae has only one genus restricted to the Pacific coastal desert and the adjacent arid Andes of Chile, Peru and Argentina (Gengler-Nowak, 2002). Turneroideae and Passifloroideae have a wider distribution that includes tropical regions

of Africa and America with a few species reaching warm temperate regions (Feuillet and MacDougal, 2007; Thulin et al., 2012). Calibrated molecular phylogenies estimate ages of divergence for Passifloraceae s.l. as Early to Late Cretaceous (Davis et al., 2005; Magallón et al., 2015) and for Passifloroideae Late Cretaceous to Paleocene (Hearn, 2006; Muschner et al., 2012). Passifloroideae are mostly tendrillate climbers with a broad habitat distribution, from deserts to humid forests, with the highest diversity in tropical rainforests at low and middle elevations (Feuillet and MacDougal, 2007).

Despite the wide distribution, economic importance (passion fruit) and high diversity of Passifloroideae (comprising about 70% of the total diversity of the family), its fossil record is sparse. A review of the available literature shows records of possible Passifloroideae pollen, leaves, and seeds in Europe, America, and Africa, from the Cretaceous to the Miocene (Table 1). In this paper, a new fossil genus and species of Passifloroideae, *Passifloroidesperma sogamosense* gen. and sp. nov. are described based on seed remains from a newly discovered locality in the late Eocene Esmeraldas Formation in Colombia. The exploration of new Cenozoic plant localities from the Neotropics is an important step on providing evidence relevant to understanding the evolutionary, biogeographic, and past climatic events that lead to the creation of the most biodiverse region on Earth.

**Table 1. Fossil record of Passifloroideae**

Name	Organ	Taxonomic assignment	Reliability* *	Locality	Country	Age	Reference
<i>Passiflora antiqua</i> Newberry 1895	Leaf	<i>Passiflora</i>	Low	Fl. Amboy Clays, Raritan Formation, New Jersey	United States	Late Cretaceous	Newberry, 1895; Berry, 1911
<i>Passifloraephyllum kraeuseli</i> Rasky 1960	Leaf	<i>Passiflora</i>	Low	Budapest, Óbuda	Hungary	Late Eocene	Rásky, 1960

<i>Passiflora</i> L. 1753	Pollen	<i>Passiflora</i>	Low	Paraje Solo Formation, Veracruz	Mexico	Middle Miocene	Graham, 1976
<i>Spirosyncolpites spiralis</i> González-Guzmán 1967	Pollen	Passifloraceae	Not Passifloraceae	Mar 2x core, Zulia	Venezuela	Late Paleocene	Jaramillo et al., 2010
<i>Syncolpites</i> sp. Hammen 1954	Pollen	<i>Passiflora</i>	Medium	Barranca Final Formation, Patagonia	Argentina	Late Miocene	Palazzesi et al., 2014
<i>Passiflora heizmannii</i> Gregor 1982	Seed	<i>Passiflora</i> *	Medium	Langenau near Ulm, Baden-Württemberg	Germany	Early Miocene	Gregor, 1982
<i>Passiflora kirchheimeri</i> Mai 1960	Seed	<i>Passiflora</i> *	High	Wiesa, Kamenz	Germany	Early Miocene	Mai, 1960
<i>Passiflora kirchheimeri</i> Mai subsp. <i>bulgarica</i> Palam. 1971	Seed	<i>Passiflora</i> *	High	Schwandorf, Oberpfalz, Bavaria	Germany	Middle Miocene	Gregor, 1978
				Saxony and Brandenburg, Lusatia	Germany	Early Miocene	Mai, 2000
				Coalbearing Formation, Choukourovo	Bulgaria	Middle Miocene	Palamarev, 1971
<i>Carpolithus passifloriformis</i> Chesters 1955	Seed	Passifloraceae?	Low	Gbonoko, North-west Igala Division, Kabba	Nigeria	Maastrichtian	Chesters, 1955

**Notes:** \*The taxonomic assignment of *Passiflora kirchheimeri*, *Passiflora kirchheimeri* subsp. *bulgarica* and *Passiflora heizmannii*, is Passifloroideae, not *Passiflora* as originally proposed by the species authors, and should be transferred to the new genus *Passifloroidesperma*. \*\*The reliability of the Passifloroideae record was determined based on the preservation of the relevant fossils, the completeness of their description, and the correspondence between the fossil description and the extant putatively related assigned taxonomic groups.

## MATERIALS AND METHODS

### *Geologic setting—*

The fossil seeds were collected from a paleobotanically rich site in the upper Esmeraldas Formation on the western side of the Eastern Cordillera in Santander, Colombia. The age of the

upper Esmeraldas Formation is estimated as late Eocene (Jaramillo et al., 2011; Rodríguez-Forero et al., 2012). This formation is located in Nuevo Mundo Syncline, Middle Magdalena Valley Basin, in the area of the Topocoro Dam, near the road that leads from Bucaramanga to Barrancabermeja (Fig. 1). The region was first explored in 2013 as part of a paleontological rescue effort led by the Smithsonian Tropical Research Institute, the Colombian Geological Survey and Isagen (power generation company). The fossil material was collected during two field trips in 2013 and 2015. The locality is assigned #110026 of the Smithsonian Tropical Research Institute's (STRI) Sample Database. The locality occurs at 7°6'25.20"N, 73°25'22.84"W, at 211 m above sea level.

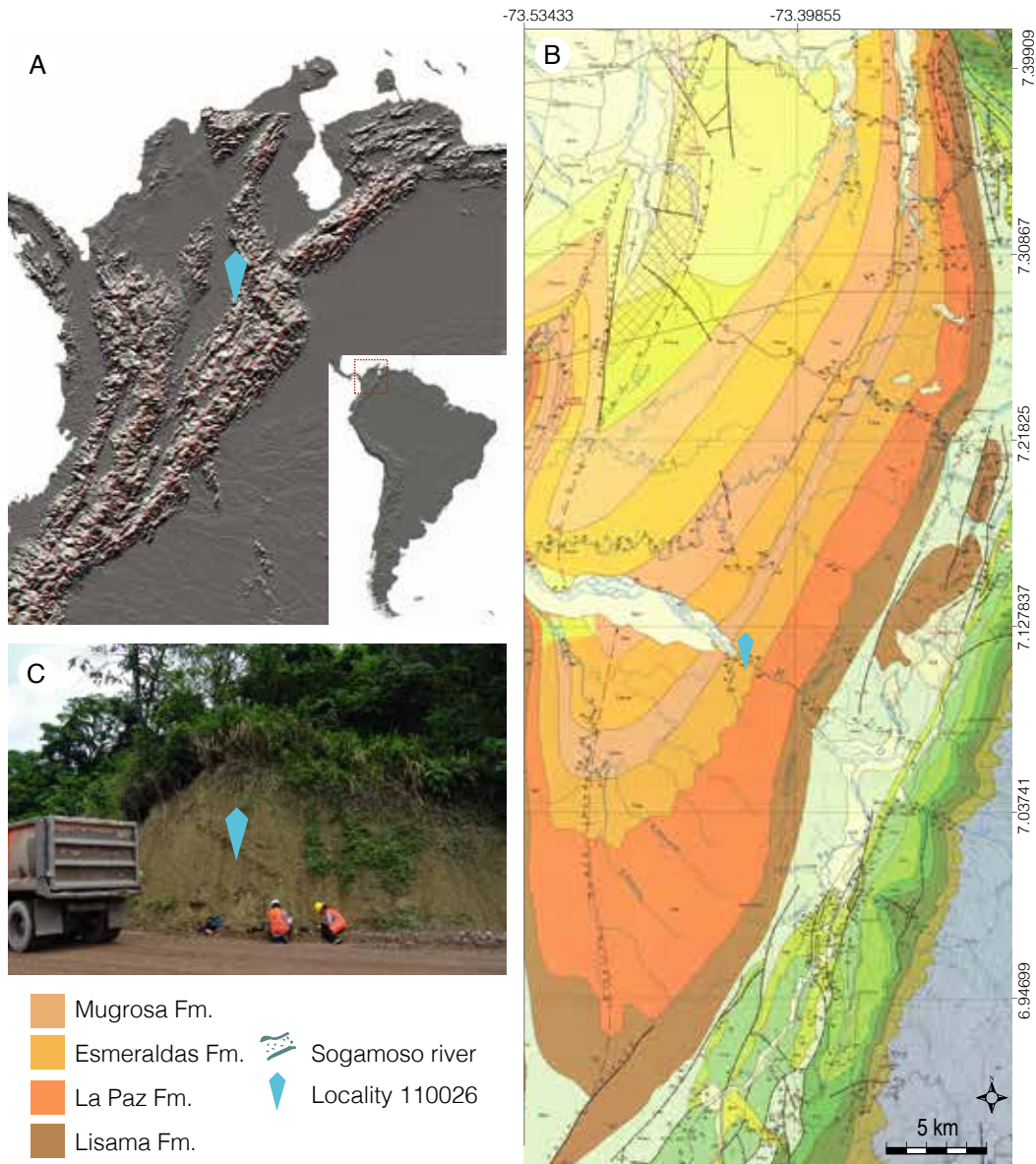


**Fig. 1. Geographic and geological location.**

Geographic and geological location of the Topocoro Dam fossil plant locality STRI-110026. (A) Relief map of South America and Colombia showing the geographic location of the outcrop. (B) Geologic map modified from Ward et al. (1977) showing the Nuevo Mundo Syncline and the location of the fossil locality in the Esmeraldas Formation (Fm.). (C) Photograph of the locality.

The stratigraphic section of locality 110026 measured 38 m in thickness (Fig. 2). The strata consist of interbedded sandstone, mudstone, and muddy sandstone, with lithologic changes at

vertical spacings that range between 10 cm to 6 m. The beds are parallel to the paleo-horizontal except the thick sandstone channel deposits, which have truncations and or toplaps that laterally terminate beds. Some of these channels reach up to 2 m in thickness. Other thinner sandstone beds at the base of the section are concordant. Some mudstone beds are grey, purple or greenish. Root traces are expressed by color and material variation, and they are ubiquitous in varicolored mudstone and muddy sandstone beds. Bed contacts are mostly non-erosive, except the upper surfaces of mudstones overlain directly by sandstone beds, which are slightly erosive. The section is characterized by the presence of beds fining upwards from sandstones to mudstones, and of thick beds of muddy sandstone with poor lamination. Plant remains were found in four horizons, however, only those found in the top muddy sandstone bed had good preservation. The remains in those upper muddy sandstones preserve large cuticles fragments.

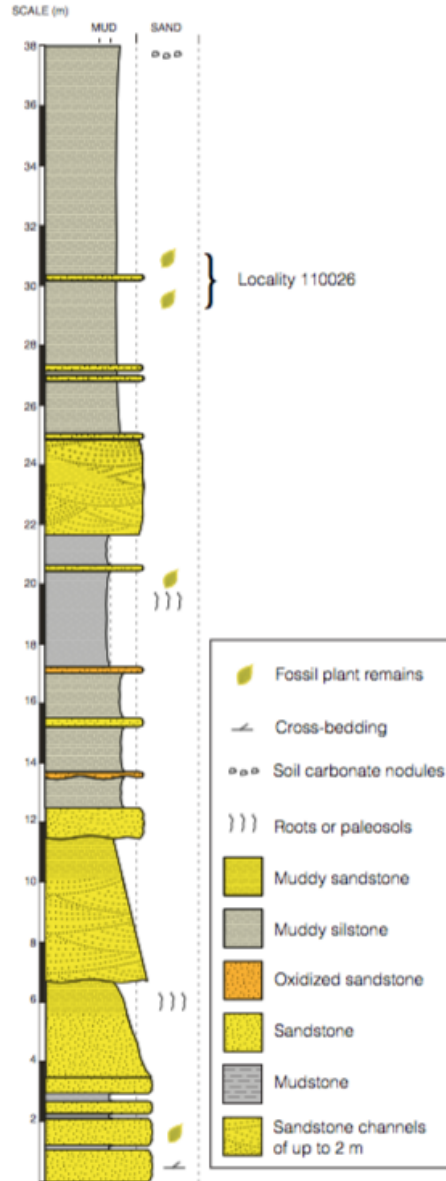


**Fig. 2. Stratigraphic section.**

Stratigraphic section traversing the fossil plant locality STRI-110026.

The varicolored mudstones in which most of the fossil flora occurs, locally contain root traces and carbonate nodules and are interpreted as paleosols. Specifically, towards the top of the section a thick bed of muddy sandstone is interpreted as having been exposed for an uncommonly long period between the time of its deposition and the next event of river-derived

sedimentation. That period of exposure to weathering and vegetation favored the formation of soil carbonate nodules. Most of the sandstone beds correspond to in-channel deposition. Nevertheless, thin concordant sandstone beds at the base of the section represent deposition outside of channels. The lithology, the bed geometry, the bounding contacts and the bed sorting described above provide evidence to infer a depositional environment of floodplains associated with river channels (Reineck and Singh, 1980; Caballero et al., 2010). The preservation of delicate structures like large leaf cuticle fragments and relatively complete leaves, together with the lithology of the fossiliferous bed could suggest that this locality corresponded to a parautochthonous assemblage (Gastaldo et al., 1996). Features like root traces, soil carbonate nodules, and formation of paleosols could indicate a paleoclimate characterized by rainfall seasonality.

#### *Fossil description and comparisons—*

Approximately 167 specimens were collected from this locality. Most of the material consists of compressions and impressions of angiosperm leaves, sometimes with cuticles preserved, and about 22% of the fossils are seeds and fruits.

The collection includes eighteen compression and impression specimens of complete and fragmented seeds of the fossil morphotype described here. Each specimen was observed using a Zeiss StemI SV8 Stereo Microscope (Jena, Thuringia, Germany) and photographed with a Nikon D200 camera (Tokyo, Japan) with varied low-angle lighting. All the fossil material was studied at the Geosciences laboratory of the Universidad de los Andes, Bogotá, Colombia and it is stored at the Paleontological Museum of the Colombian Geological Survey and the Mapuka Museum (Universidad del Norte, Barranquilla, Colombia). The description of the fossil seeds was done following the terminology of Corner (1976) and Werker (1997).

Comparisons with extant seeds were made with those of angiosperm families having seeds with ruminant endosperm and seed coats with palisade cells, given that these two characteristics were the most diagnostic characters of the fossil seeds. The comparisons were based on literature reports of Corner (1976) and Werker (1997). Further comparisons at the family level were also done using literature digital collections from the JSTOR Global Plants database (JSTOR), and direct observations from herbarium specimens from the Bailey Hortorium (BH) Cornell University, Ithaca, USA (see Supplemental Data with this article: Appendix S1 and S2). A fresh seed of *Passiflora tripartita* (Juss.) Poir. collected in Bogotá, Colombia; and a seed of *Adenia* sp. Forssk. from a herbarium specimen were also used for comparison. The fossil record of Passifloroideae was reviewed using the available literature, and ranked based on the quality of evidence supporting the assignments of the fossils to the subfamily.

The taxonomic affinities of the fossil seeds from Colombia within Passifloraceae s.l. were evaluated by comparing the seed morphological characters of each subfamily using literature and herbarium specimens (Appendix S1 and S2).

## RESULTS

### *Taxonomic summary—*

Order— Malpighiales Martius

Family—Passifloraceae Roussel

Genus—*Passifloroidesperma* Martínez-A., gen. nov.

Generic diagnosis: Seeds compressed; shape ovoid, obovoid or elliptic, bilaterally symmetrical or slightly asymmetrical; apex with a prominent to inconspicuous apical appendage, with or without lateral protrusions; base acute, obtuse, truncated or rounded; length less than 20

mm; length-width ratio around 1:1 to 2:1; seed surface foveolate, coarsely foveolate, reticulate-foveolate or transversally grooved; seed endosperm ruminant; seed coat with prismatic palisade cells.

Type species—*Passifloroidesperma sogamosense* Martínez-A., sp. nov. (Fig. 3).

Holotype: STRI-Mapuka\_43982 (Fig. 3A–C), here designated.

Paratype: STRI-Mapuka\_43987 (Fig. 3D).

Studied material: STRI-Mapuka\_43979–92, STRI-SGC\_35066, 350067, 35147, 35212

Locality: Topocoro Dam, Santander, Colombia. STRI locality ID 110026, 7°6'25.20"N, 73°25'22.84"W (WGS84 18N).

Stratigraphic position and age: Upper Esmeraldas Formation, Nuevo Mundo Syncline (Fig. 1), Middle Magdalena Valley Basin. The age of the Upper Esmeraldas Formation is late Eocene (Rodríguez-Forero et al., 2012); palynological zone T-07 of Jaramillo et al (2011).

Etymology, genus: Referring to Passifloroideae, the extant group to which the fossil is assigned and from Greek—*sperma* (seed).

Etymology, specific epithet: Referring to the Sogamoso River that flows near the fossil locality where the Topocoro Dam was built.

Repository: Mapuka, Universidad del Norte, Barranquilla, Colombia and Museo José Royo y Gómez, Colombian Geological Survey, Bogota, Colombia.

Species—*Passifloroidesperma sogamosense* Martínez-A., sp. nov. (Fig. 3).

Species diagnosis: Seeds compressed; shape obovoid; bilaterally slightly asymmetrical; apex with prominent apical appendage; base truncate to rounded; length less than 10 mm; length-

width ratio around 1.7:1; surface reticulate-foveolate; endosperm ruminant; seed coat with prismatic palisade cells.

Description: This description is based on 18 specimens. The seed size is 6.75 mm long (4–9 mm) and 3.88 mm wide (2.2–4.5 mm). The shape varies from elliptic to obovoid and is bilaterally slightly asymmetric; its apex is characterized by the presence of the chalaza, which is prominent and central, and its base is truncate to rounded, and corresponds to the micropylar end (Fig. 3D). The surface is reticulate-foveolate and has on each side approximately 40 pits (Fig. 3A,B); the seed coat is approximately 0.3 mm thick and is characterized by a uniseriate layer of palisade cells that are prismatic, elongated, and angular, with a length of 0.3 mm and a width of 0.02 mm (Fig. 3C). The seed contains ruminant endosperm (Fig. 3A).

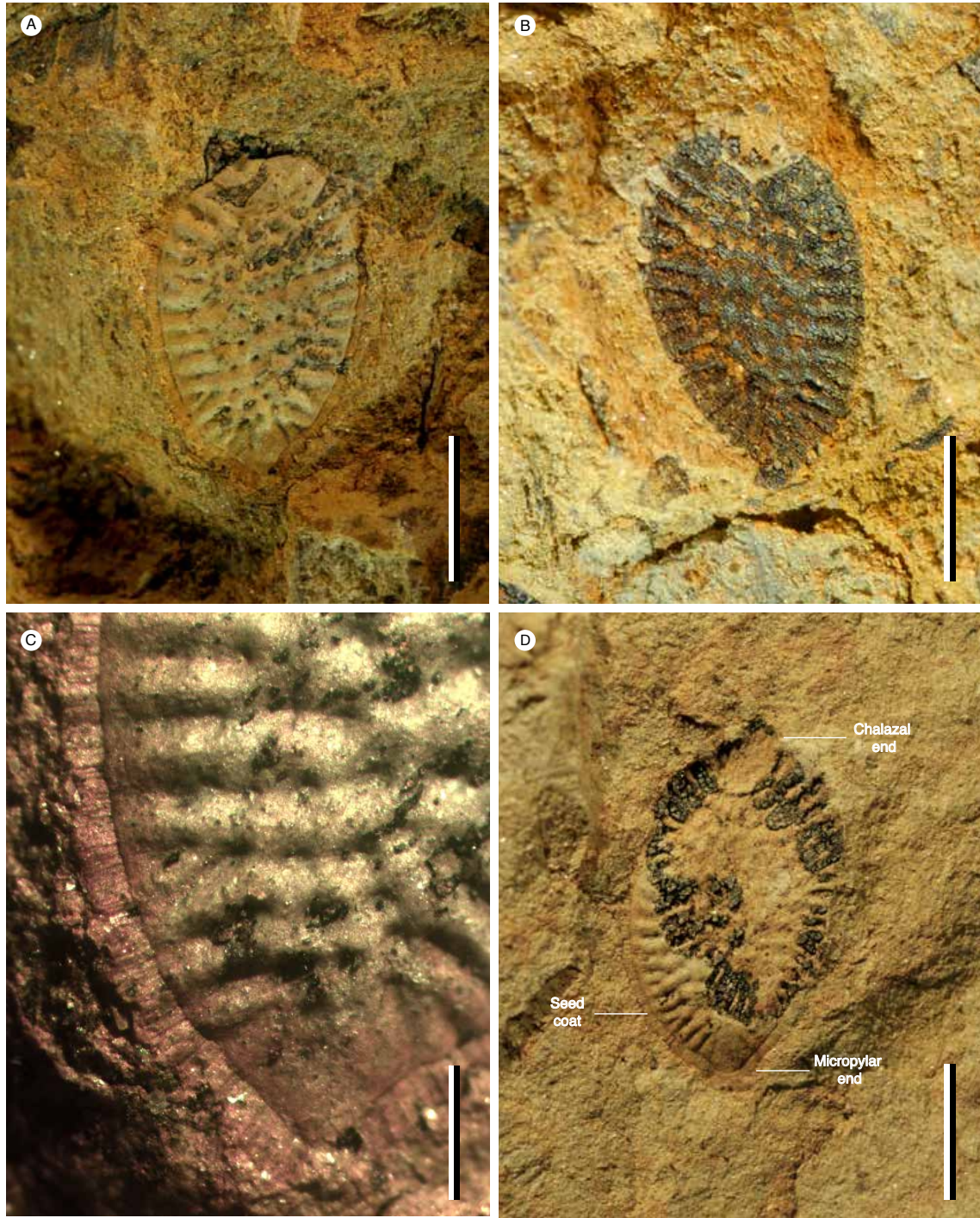


**Fig. 3. Fossil seed of *Passifloroidesperma sogamosense* sp. nov.**

(A–C) STRI-Mapuka\_43982 (Holotype). (A) Inside surface of the seed coat impressed into the sediment; scale = 3 mm. (B) Counterpart; scale = 3 mm. (C) Palisade seed coat close-up; scale = 1 mm. (D) STRI-Mapuka\_43987 (Paratype); scale = 3 mm.

Comparisons: Comparisons were initially made with seeds having ruminant endosperm (Table 2) and seed coats with palisade cells (Table 3), given that these two features are the most diagnostic characters of the fossil seeds described herein. Seeds with ruminant endosperm have been separated into seven types based on the tissue layers taking part in the formation of the seed coat, the presence or absence of ingrowths of surrounding tissue in the endosperm, and presence of one or two layers in the tegmen (Periasamy, 1962; Werker, 1997; Table 2). Unfortunately, the state of preservation of the fossils does not allow discriminating between unitegmic and bitegmic seeds, but it does allow the observation of ingrowths or infoldings of the seed coat, which in *Passifloroidesperma sogamosense*, are definitely absent (Fig. 3A). The lack of infoldings of surrounding tissues excludes affinities with the seed types: *Annona*, *Myristica*, *Coccoloba*, *Spigelia*, and *Elytraria* that are characterized by the presence of infoldings (Table 2).

**Table 2. Families with ruminant endosperm.**

Classified by types based on Periasamy (1962) and Werker (1997).

Type	Family
<i>Annona</i>	Annonaceae
	Arecaceae
	Aristolochiaceae
	Degeneriaceae
	Dipterocarpaceae
	Ebenaceae
	Menispermaceae
Vitaceae	
<i>Coccoloba</i>	Polygonaceae
<i>Elytraria</i>	Acanthaceae
<i>Myristica</i>	Arecaceae
	Myristicaceae
<i>Passiflora</i>	Oxalidaceae
	Passifloraceae
<i>Spigelia</i>	Apocynaceae
	Araliaceae
	Caprifoliaceae

	Loganiaceae
	Rubiaceae
<i>Verbascum</i>	Scrophulariaceae

**Table 3. Families with palisade seed coat.**

Classified based on whether the seed is testal or tegmic and location of the mechanical layer following Corner (1976).

Seed coat	Mechanical layer	Family
Testal	Endotestal	Cruciferae
		Dilleniaceae
		Myristicaceae
	Exotestal	Leguminosae
Ranunculaceae Rhamnaceae Winteraceae		
	Mesotestal	Paeoniaceae
Tegmic	Exotegmic with prismatical cells	Bixaceae
		Bombacaceae
Cistaceae		
Dipterocarpaceae		
Euphorbiaceae- Phyllanthoideae		
Gonystylaceae		
Malvaceae		
Passifloraceae		
<i>Perrotetia</i> (Celestraceae)		
Piperaceae		
Sterculiaceae		
Thymelaeaceae		
Tiliaceae		
Turneraceae?		
	Exotegmic with tubular cells	<i>Actephila</i> (Euphorbiaceae- Phyllanthoideae)
		Sterculiaceae
		Thymelaeaceae
		Tiliaceae
		Turneraceae?

Corner (1976) reported the presence of palisade cells in the seed coat of dicots. Palisade cells can be present in either the tegmen (exotegmic) or the testa (exotestal, mesotestal, or endotestal) of the seed (Table 3; Corner 1976). Families with exotegmic palisade seeds are split in two groups depending on the shape of the palisade cells that can be prismatic with angular, isodiametric or shortly oblong facets, vs. tubular with stellate-undulate or lobate facets (Table 3). *P. sogamosense* clearly has prismatic cells and angular oblong facets (Fig. 3C).

A comparison among families listed in tables 2 and 3 shows that families having seed coats with both ruminant endosperm and palisade cells include only Myristicaceae and Passifloraceae. Seeds of Myristicaceae, however, differ morphologically from the fossil seeds in the presence of ingrowths of surrounding tissue in the endosperm (Corner, 1976). Annonaceae seeds show very similar morphology to the fossil seed surface, nevertheless Annonaceae seed coats are characterized by the presence of fibers instead of a palisade layer, and most have ingrowths of surrounding tissue in the endosperm (Corner, 1976). These differences indicate that *Passifloroidesperma sogamosense* does not belong to Annonaceae.

Within Passifloraceae s.l., subfamilies can be easily differentiated based on their seed morphology. Malesherbioideae has small seeds, of 1.3 to 2.7 mm, with a globose shape; a ridged-reticulate seed coat organized in vertical and horizontal tiers, and a prominent chalaza (Ricardi, 1967; Kubitzki, 2007). Turneroideae has small seeds, of approximately 1.2 to 5 mm long, elongated in shape and often curved with ridged-reticulate or striate coats, and a prominent or inconspicuous chalaza (Arbo, 2007; Arbo et al., 2015; Fig. 5; Appendix S2). Passifloroideae has compressed seeds that are larger than seeds of the other subfamilies, ranging from approximately 1.4 to 14 mm long, with ovoid, obovoid or elliptic shape and foveolate, coarsely foveolate, reticulate-foveolate, or transversally grooved hard seed coats (e.g. de Wilde, 1972,

1974, 1976; Feuillet and MacDougal, 2007; Pérez-Cortéz, 2007; Mezzonato-Pires et al., 2017; Fig. 4 and 5). *Passifloroidesperma sogamosense* can be easily differentiated from Malesherbioideae and Turneroideae seeds, by its larger size, its foveolate or grooved hard seed coat and bilaterally-compressed appearance.

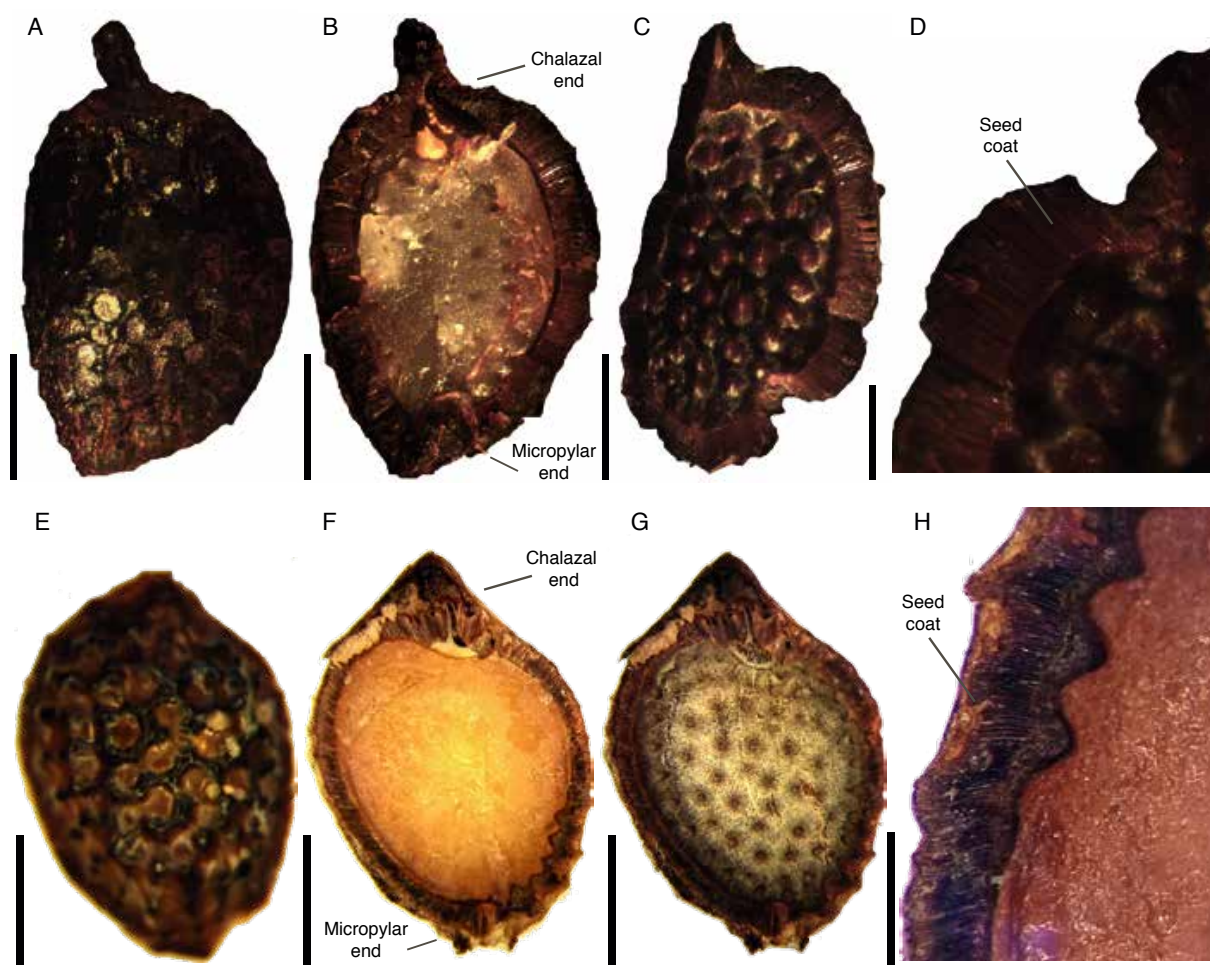


**Fig. 4. Extant seeds of Passifloroideae.**

Dissected for comparison with the fossil specimens. (A–D) *Passiflora tripartita* (Juss.) Poir.; (E–H) *Adenia* sp. Forssk.; (A, E) Seed external surface; (B, F) Longitudinal section of the seed; (C, G) inside surface of the seed coat; (D, H) close-up of palisade seed coat; scales = 0.5mm; (A–C and E–G) scales = 2mm.

A detailed examination of the seeds of the genera of Passifloroideae shows that, despite some variation in the seed length (1.4 to 14 mm), shape (ovoid, obovoid, elliptic), surface (foveolate, coarsely foveolate, reticulate-foveolate or transversally grooved), and size of the apical appendage, the seed morphology of the two included tribes (Passiflorae and Paroposieae) and their genera are very similar and cannot be distinguished based solely on morphological characters (Appendix S2; Fig. 4). The overall variation observed in *Passiflora* L., the largest genus of the subfamily (~525 species), is almost as wide as the variation observed in all Passifloroideae. Unfortunately, the restricted distribution and small number of species of some of the other genera (e.g. *Ancistrothyrsus*, *Androsiphonia*, *Crossostemma*, *Efulensia*, *Schlechterina*, *Smeathmannia*, and *Viridivia*) limit the availability of herbarium specimens and detailed descriptions of seed characters. As a consequence it was not possible to carry out a morphological phylogenetic analysis to provide more resolution to the taxonomic affinity of the fossil. The two dissected seeds of *Passiflora tripartita* and *Adenia* sp. illustrate the shared presence of chalazal and micropylar ends, prismatic palisade cells in the seed coat, and ruminant endosperm, as in *Passifloroidesperma sogamosense* (compare Fig. 3 and 4).

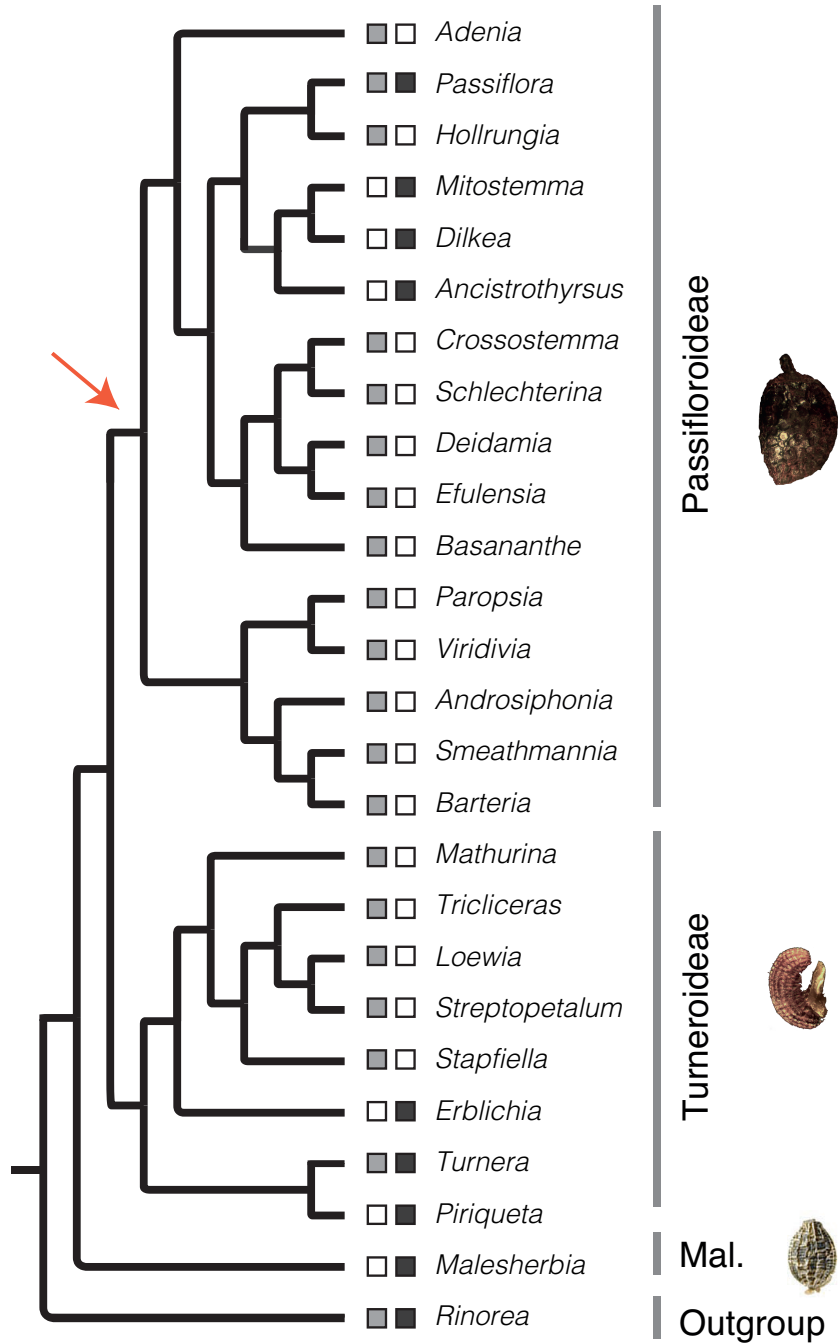


**Fig. 5. Phylogenetic tree of Passifloraceae.**

Topology from Tokuoka (2012). The squares at the right of the generic names indicate their general distribution; dark gray indicates the neotropical region; light gray indicates the Old World tropics region. The red arrow indicates the node to which *Passifloroidesperma sogamosense* is assigned. Photograph for Passifloroideae corresponds to *Passiflora tripartita* (Juss.) Poir. Photograph for Turneroideae corresponds to *Turnera hassleriana* Urb. Photograph for Malesherbioideae (Mal.) corresponds to *Malesherbia paniculata* D. Don (photograph courtesy of the U. S. Department of Agriculture, 2015).

## DISCUSSION

*Passifloroidesperma sogamosense* provides the earliest confirmed fossil record for Passifloraceae. Although the taxonomic affinity of *P. sogamosense* could not be assigned to a particular extant tribe or genus, the congruence in characters between the fossils and extant members of Passifloroideae, suggests that *P. sogamosense* belongs to the crown node of the subfamily (Fig. 5) and supports the establishment of the new fossil genus, *Passifloroidesperma*. This new fossil genus can also accommodate fossil seeds with similar morphology in future findings. This new record provides a minimum age for Passifloroideae in the Neotropical region that can be used for future molecular calibration analyses and biogeographic studies.

Older or contemporaneous records of Passifloraceae include fossil leaves from the Cretaceous of North America and the late Eocene of Hungary, assigned to *Passiflora* (Newberry, 1895; Rásky, 1960). These records are superficially similar to some extant *Passiflora* leaves, however, the leaf architecture of these fossils were not examined in detail and compared with enough extant material to clearly support the proposed affinity. Additionally, several pollen species from the late Eocene of Nigeria including *Retitricolpites abakensis*, *R. crassireticulatus*, *R. ituensis*, and *R. pseudosphaericus* have been related to Turneraceae but also to Nyctaginaceae (Jan du Chêne et al., 1978); more comprehensive studies including scanning and transmission electron microscopy are needed to verify the purported affinities. The only older reproductive macrofossil previously described as possibly belonging to Passifloraceae is a Maastrichtian (70.6–65.5 Ma) seed from Nigeria (Chesters, 1955); however, its description and preservational quality leave doubts as to its affinities with the family, given that the palisade seed coat is not described nor observed in the photograph, the seed surface is described as presenting fewer pits

than extant Passifloraceae, and the specimen has a central longitudinal groove that is not present in extant Passifloraceae.

The presence of *Passifloroidesperma sogamosense* in Colombia indicates that Passifloroideae were present during the late Eocene in the Neotropics. The later occurrence of the fossil seeds of Passifloroideae in the Miocene of Germany and Bulgaria (Mai, 1960; Palamarev, 1971; Gregor, 1978, 1982), suggests that the family had a broader distribution during that time, perhaps as a result of higher temperatures reported worldwide during the Miocene (Zachos et al., 2008) consistent with the presence of some tropical elements in higher latitudes (Mai, 1995). Today only four genera in Passifloroideae (out of 17) are present in the Neotropics: *Passiflora*, *Mitostemma*, *Dilkea*, and *Ancistrothyrsus* (Tokuoka, 2012; Fig. 5). *Passiflora* is also distributed in the Old World tropics, and *Hollrungia*, which is shown as the sister group of *Passiflora* (Fig. 5), was a monotypic genus from the Old World tropics that has been recently transferred to *Passiflora* (Krosnick et al., 2009). Although this predominant Neotropical clade share seed characters with *P. sogamosense*, its overlapped Neotropical distribution cannot be used as the unique argument to place the fossil within this clade, given the similarities of *P. sogamosense* with other genera outside this clade (e.g. *Adenia*; Fig. 4E–H) and because long-distance dispersal events have been reported in numerous plant groups and even in *Passiflora* (Renner et al., 2001; Muschener et al., 2012; Krosnick et al., 2013). However, the Neotropical distribution and late Eocene age of *P. sogamosense* provide physical evidence for future analyses that addresses the complex biogeographic distribution of the family.

The late Eocene (~45–34 Ma) age of the fossil *Passifloroidesperma sogamosense* provides a minimum age for the crown Passifloroideae and therefore it can be used as a calibration point for future analyses of diversification. Previously, Hearn (2006) and Muschner (2012) did molecular

dating analyses for Passifloroideae, and used the *Passiflora* fossil seed reported by Mai (1967) as the main calibration point. However, they assigned an age of 37 million years (my) to the fossil but Mai (1967) does not include a description of the fossil species and does not provide a 37 my age for the fossil. The only fossil seed species of *Passiflora* described by Mai, is *Passiflora kirchheimeri* Mai, and was collected from early Miocene (~23–15 Ma) deposits of Germany (Mai, 1960). In addition, there are reports of additional species and subspecies assigned to *Passiflora* from several Miocene (23.03–5.3 Ma) localities in Germany and Bulgaria: *Passiflora kirchheimeri* Mai subsp. *bulgarica* Palmarev and *Passiflora heizmannii* Gregor (Palamarev, 1971; Gregor, 1978, 1982; Mai, 2000; Table 1). Both fossil seeds (*P. kirchheimeri* and *P. heizmannii*) have been related to *Passiflora* (Mai, 1960; Gregor, 1982), however, they are very similar to *Passifloroidesperma sogamosense*, and therefore, their interpreted affinity to *Passiflora* should be reconsidered because genera of Passifloroideae cannot be distinguished solely by seed morphological features, and can only be assigned to Passifloroideae.

The habitat in which some Passifloroideae species are found today is similar to the depositional environment inferred for the fossil (e.g. *Passiflora bicornis* Mill., *P. serrulata* Jacq., *P. subpeltata* Ortega). Given that today most Passifloroideae are tendrillate climbers, one could hypothesize that *Passifloroidesperma sogamosense* was also a climber. A climbing habit could have played an advantageous role in re-colonization following flooding events. Only angiosperms were found in this locality, and preliminary studies of this material suggest the presence of leaf fossil morphotypes associated with Fabaceae, Malvaceae, and possibly Myrtaceae, and a fossil endocarp morphotype is indicative of Menispermaceae. Microphyll and notophyll leaves with entire margins dominate the fossil assemblage, again indicating a paleoclimate with rainfall seasonality.

The recognition of *Passifloroidesperma sogamosense* enhances our understanding of the evolution and biogeography of an important tropical lineage, Passifloroideae, and its habitat, and it raises the possibility that the climbing habit could have been an important life form by that time. The revision of the fossil record of Passifloroideae highlights the critical importance of careful examination of the literature where fossils were described and their precise taxonomic placement in the context of molecular related calibration.

## REFERENCES

- Arbo, M.M. 2007. Turneraceae. *In* Flowering plants · Eudicots, the families and genera of vascular plants, 458–466. Springer, Berlin, Heidelberg. Available at: [https://link.springer.com/chapter/10.1007/978-3-540-32219-1\\_53](https://link.springer.com/chapter/10.1007/978-3-540-32219-1_53) [Accessed August 21, 2017].
- Arbo, M.M., A.M. Gonzalez, and S.M. Sede. 2015. Phylogenetic relationships within Turneraceae based on morphological characters with emphasis on seed micromorphology. *Plant Systematics and Evolution* 301: 1907–1926.
- Bayona, G., M. Cortés, C. Jaramillo, G. Ojeda, J.J. Aristizabal, and A. Reyes-Harker. 2008. An integrated analysis of an orogen–sedimentary basin pair: Latest Cretaceous–Cenozoic evolution of the linked Eastern Cordillera orogen and the Llanos foreland basin of Colombia. *Geological Society of America Bulletin* 120: 1171–1197.
- Berry, E.W. 1911. The Flora of the Raritan Formation. *Geological Survey of New Jersey* 3: 1–233.
- Burnham, R.J., and K.R. Johnson. 2004. South American palaeobotany and the origins of neotropical rainforests. *Philosophical Transactions of the Royal Society B: Biological Sciences* 359: 1595–1610.
- Caballero, V., M. Parra, M. Bohorquez, and A. Roberto. 2010. Levantamiento de la cordillera oriental de Colombia durante el Eoceno tardío - Oligoceno temprano: proveniencia sedimentaria en el Sinclinal de Nuevo Mundo, Cuenca Valle Medio del Magdalena. *Boletín de Geología* 32: 45–77.

- Chase, M.W., S. Zmarzty, M.D. Lledó, K.J. Wurdack, S.M. Swensen, and M.F. Fay. 2002. When in doubt, put it in Flacourtiaceae: a molecular phylogenetic analysis based on plastid *rbcL* DNA sequences. *Kew Bulletin* 57: 141–181.
- Chesters, K.I.M. 1955. LXI.—Some plant remains from the upper Cretaceous and tertiary of West Africa. *Journal of Natural History Series 12* 8: 498–504.
- Corner, E.J.H. 1976. *The Seeds of Dicotyledons*. Cambridge University Press, Cambridge, UK.
- Davis, C.C., C.O. Webb, K.J. Wurdack, C.A. Jaramillo, and M.J. Donoghue. 2005. Explosive radiation of Malpighiales supports a Mid-Cretaceous origin of modern tropical rain forests. *The American Naturalist* 165: E36–E65.
- Duarte, L., and M. da C. Mello Filha. 1980. Florula Cenozoica de Gandarela, MG. I. *Anais da Academia Brasileira de Ciências* 52: 77–91.
- Feuillet, C., and J.M. MacDougal. 2007. Passifloraceae. In P. D. K. Kubitzki [ed.], *Flowering plants · Eudicots, the families and genera of vascular plants*, 270–281. Springer Berlin Heidelberg. Available at: [http://link.springer.com/chapter/10.1007/978-3-540-32219-1\\_35](http://link.springer.com/chapter/10.1007/978-3-540-32219-1_35) [Accessed December 6, 2016].
- Gastaldo, R.A., D.K. Ferguson, H. Walther, and J.M. Rabold. 1996. Criteria to distinguish parautochthonous leaves in Tertiary alluvial channel-fills. *Review of Palaeobotany and Palynology* 91: 1–21.
- Gengler-Nowak, K. 2002. Reconstruction of the biogeographical history of Malesherbiaceae. *Botanical Review* 68: 171–188.

- Gómez, E., T.E. Jordan, R.W. Allmendinger, K. Hegarty, and S. Kelley. 2005. Syntectonic Cenozoic sedimentation in the northern middle Magdalena Valley Basin of Colombia and implications for exhumation of the Northern Andes. *Geological Society of America Bulletin* 117: 547.
- Graham, A. 1976. Studies in neotropical paleobotany. II. The Miocene communities of Veracruz, Mexico. *Annals of the Missouri Botanical Garden* 63: 787–842.
- Gregor, H.-J. 1978. Die miozänen Frucht- und Samen-Floren der Oberpfälzer Braunkohle. I. Funde aus den sandigen Zwischenmitteln. *Palaeontographica Abteilung B* 167: 8–103.
- Gregor, H.-J. 1982. Die jungtertiären Floren Süddeutschlands. Ferdinand Enke Verlag, Stuttgart, Germany.
- Hearn, D.J. 2006. *Adenia* (Passifloraceae) and its adaptive radiation: phylogeny and growth form diversification. *Systematic Botany* 31: 805–821.
- Jan du Chêne, R., M. Onyike, and M. Sowunmi. 1978. Some new Eocene pollen of the Ogwashi-Asaba Formation, southeastern Nigeria. *Revista Espanola de Micropaleontologia* 10: 285–322.
- Jaramillo, C., D. Ochoa, L. Contreras, M. Pagani, H. Carvajal-Ortiz, L.M. Pratt, S. Krishnan, et al. 2010. Effects of rapid global warming at the Paleocene-Eocene boundary on Neotropical vegetation. *Science* 330: 957–961.
- Jaramillo, C.A., M. Rueda, and V. Torres. 2011. A palynological zonation for the Cenozoic of the Llanos and Llanos Foothills of Colombia. *Palynology* 35: 46–84.

- Kidwell, S.M., and S.M. Holland. 2002. The quality of the fossil record: Implications for evolutionary analyses. *Annual Review of Ecology and Systematics* 33: 561–588.
- Krosnick, S.E., A.J. Ford, and J.V. Freudenstein. 2009. Taxonomic revision of *Passiflora* subgenus *Tetrapathea* including the monotypic genera *Hollrungia* and *Tetrapathea* (Passifloraceae), and a new species of *Passiflora*. *Systematic Botany* 34: 375–385.
- Krosnick, S.E., K.E. Porter-Utley, J.M. MacDougal, P.M. Jørgensen, and L.A. McDade. 2013. New Insights into the evolution of *Passiflora* subgenus *Decaloba* (Passifloraceae): phylogenetic relationships and morphological synapomorphies. *Systematic Botany* 38: 692–713.
- Kubitzki, K. 2007. Malesherbiaceae. In *Flowering plants · Eudicots, the families and genera of vascular plants*, 247–249. Springer, Berlin, Heidelberg. Available at: [https://link.springer.com/chapter/10.1007/978-3-540-32219-1\\_31](https://link.springer.com/chapter/10.1007/978-3-540-32219-1_31) [Accessed Dec 10, 2016].
- Magallón, S., S. Gómez-Acevedo, L.L. Sánchez-Reyes, and T. Hernández-Hernández. 2015. A metacalibrated time-tree documents the early rise of flowering plant phylogenetic diversity. *New Phytologist* 207: 437–453.
- Mai, D.H. 1960. Über neue Früchte und Samen aus dem deutschen Tertiär. *Paläontologische Zeitschrift* 34: 73–90.
- Mai, D.H. 1967. Die Florenzonen, der Florenwechsel und die Vorstellungen über den Klimaablauf im Jungtertiär der Deutschen Demokratischen Republik. *Abhandlungen des Zentralen Geologischen Institutes* 10: 55–81.

- Mai, D.H. 1995. Tertiäre Vegetationsgeschichte Europas: Methoden und Ergebnisse. Gustav Fischer, Stuttgart, Germany.
- Mai, D.H. 2000. Die untermiozänen Floren aus der Spremberger Folge und dem 2. Flözhorizont der Lausitz. Teil III. Dialypetalae und Sympetalae. *Palaeontographica Abteilung B* 253: 1–106.
- Mello, C.L., L.G. Sant’Anna, and L.P. Bergqvist. 2000. The palaeontological site of Fonseca, Minas Gerais state, Brazil (fossil plants of the Tertiary of Brazil). *Sítios geológicos e paleontológicos do Brasil [online]*. Available at: [www.unb.br/ig/sigep/sitio086/sitio086.htm](http://www.unb.br/ig/sigep/sitio086/sitio086.htm) [Accessed December 1, 2017].
- Mezzonato-Pires, A.C., C.B.F. Mendonça, M.A. Milward-De-Azevedo, V. Gonçalves-Esteves, A.C. Mezzonato-Pires, C.B.F. Mendonça, M.A. Milward-De-Azevedo, and V. Gonçalves-Esteves. 2017. The taxonomic significance of seed morphology in the *Passiflora* subgenus *Astrophea* (Passifloraceae). *Acta Botanica Brasilica* 31: 68–83.
- Miall, A. 1996. The Geology of Fluvial Deposits: Sedimentary Facies, Basin Analysis. Springer, Berlin, Germany.
- Mora, A., P. Baby, M. Roddaz, M. Parra, S. Brusset, W. Hermoza, and N. Espurt. 2010. Tectonic history of the Andes and sub-Andean zones: implications for the development of the Amazon drainage basin. In *Amazonia, Landscape and Species Evolution, a Look into the Past* In C. Hoorn, and F. P. Wesselingh [eds.], 38–60. Blackwell Publishing Ltd., Oxford, UK.

- Muschner, V.C., P.M. Zamberlan, S.L. Bonatto, and L.B. Freitas. 2012. Phylogeny, biogeography and divergence times in *Passiflora* (Passifloraceae). *Genetics and molecular biology* 35: 1036–1043.
- Newberry, J.S. 1895. The Flora from the Amboy Clays. United States Geological Survey, Washington, USA.
- Nie, J., B.K. Horton, A. Mora, J.E. Saylor, T.B. Housh, J. Rubiano, and J. Naranjo. 2010. Tracking exhumation of Andean ranges bounding the Middle Magdalena Valley Basin, Colombia. *Geology* 38: 451–454.
- Ochoa, D., C. Hoorn, C. Jaramillo, G. Bayona, M. Parra, and F. De la Parra. 2012. The final phase of tropical lowland conditions in the axial zone of the Eastern Cordillera of Colombia: Evidence from three palynological records. *Journal of South American Earth Sciences* 39: 157–169.
- Palamarev, E. 1971. Diasporen aus der miozänen Braunkohle des Cukurovo-Beckens (West-Bulgarien). *Palaeontographica Abteilung B* 153–164.
- Palazzesi, L., V.D. Barreda, J.I. Cuitiño, M.V. Guler, M.C. Tellería, and R. Ventura Santos. 2014. Fossil pollen records indicate that Patagonian desertification was not solely a consequence of Andean uplift. *Nature Communications* 5: Article number: 3558.
- Pérez-Cortéz, S. 2007. Atlas morfológico de semillas en especies del género *Passiflora* L. presentes en Venezuela. Fundación Instituto Bótanico de Venezuela, Caracas, Venezuela.

- Pérez-Cortéz, S., M. Escala, and S. Tillett. 2009. Morfoanatomía de la cubierta seminal en siete especies de *Passiflora* L., subgénero *Passiflora* (Passifloraceae). *Hoehnea* 36: 131–137.
- Pérez-Cortéz, S., S. Tillett, and M. Escala. 2002. Estudio morfológico de la semilla de 51 especies del género *Passiflora* L. *Acta Botánica Venezuelica* 67–96.
- Periasamy, K. 1962. Studies on seeds with ruminant endosperm. *Proceedings of the Indian Academy of Sciences - Section B* 56: 13–26.
- Rásky, K. 1960. Pflanzenreste aus dem Obereozän Ungarns. *Senckenbergiana lethaea* 41: 423–449.
- Reineck, H.-E., and I.B. Singh. 1980. Depositional sedimentary environments: With reference to terrigenous clastics. Springer-Verlag, Berlin, Germany.
- Renner, S.S., G. Clausen, and K. Meyer. 2001. Historical biogeography of Melastomataceae: the roles of Tertiary migration and long-distance dispersal. *American Journal of Botany* 88: 1290–1300.
- Ricardi, S.M. 1967. Revisión taxonómica de las Malesherbiaceas. *Gayana* 16: 3–139.
- Rodríguez-Forero, G., F.E. Oboh-Ikuenobe, C. Jaramillo-Munoz, M.J. Rueda-Serrano, and E. Cadena-Rueda. 2012. Palynology of the Eocene Esmeraldas Formation, Middle Magdalena Valley Basin, Colombia. *Palynology* 36: 96–111.
- Soltis, D.E., M.A. Gitzendanner, and P.S. Soltis. 2007. A 567-taxon data set for angiosperms: the challenges posed by bayesian analyses of large data sets. *International Journal of Plant Sciences* 168: 137–157.

- Soltis, D.E., P.S. Soltis, M.W. Chase, M.E. Mort, D.C. Albach, M. Zanis, V. Savolainen, et al. 2000. Angiosperm phylogeny inferred from 18S rDNA, *rbcL*, and *atpB* sequences. *Botanical Journal of the Linnean Society* 133: 381–461.
- The Angiosperm Phylogeny Group. 2009. An update of the Angiosperm Phylogeny Group classification for the orders and families of flowering plants: APG III. *Botanical Journal of the Linnean Society* 161: 105–121.
- Thulin, M., S.G. Razafimandimbison, P. Chafe, N. Heidari, A. Kool, and J.S. Shore. 2012. Phylogeny of the Turneraceae clade (Passifloraceae s.l.): Trans-Atlantic disjunctions and two new genera in Africa. *Taxon* 61: 308–323.
- Tokuoka, T. 2012. Molecular phylogenetic analysis of Passifloraceae sensu lato (Malpighiales) based on plastid and nuclear DNA sequences. *Journal of Plant Research* 125: 489–497.
- United States Department Of Agriculture. 2015. Germplasm Resources Information Network. Available at: <http://www.ars-grin.gov/~sbmljw/images.html>.
- Ward, D.E., R. Goldsmith, A. Jimeno, J. Cruz, H. Restrepo, and E. Gómez. 1977. Geologic map of the Bucaramanga Quadrangle (H-12), Colombia.
- Werker, E. 1997. Seed Anatomy. Gebrüder Borntraeger, Stuttgart, Germany.
- de Wilde, W.J.J.O. 1972. Passifloraceae. *Flora Malesiana - Series 1, Spermatophyta* 7: 405–434.
- de Wilde, W.J.J.O. 1974. Account of *Efulensia* (Passifloraceae). *Blumea* 22: 31–35.
- de Wilde, W.J.J.O. 1976. Passifloraceae. In *Flora of Southern Africa*, Government Printer, Pretoria, by Cape & Transvaal Printers, Ltd., Parow, C.P., South Africa.

Zachos, J.C., G.R. Dickens, and R.E. Zeebe. 2008. An early Cenozoic perspective on greenhouse warming and carbon-cycle dynamics. *Nature* 451: 279–283.

## APPENDIX S1

Subfamily	Tribe	Genus	Species observed	Reference
Malesherbioideae	NA	<i>Malesherbia</i> Ruiz & Pav.	see Ricardi, 1967	Kubitzki, 2007; Ricardi, 1967
Passifloroideae	Passifloreae	<i>Adenia</i> Forssk.	<i>Adenia</i> sp., <i>Adenia lobata</i> (Jacq.) Engl.	Corner, 1976; de Wilde, 1972; Feuillet and MacDougal, 2007; BH-000052487
Passifloroideae	Passifloreae	<i>Ancistrothyrsus</i> Harms	<i>Ancistrothyrsus hirtellus</i> A.H. Gentry	Feuillet and MacDougal, 2007; Gentry, 1992
Passifloroideae	Paropsieae	<i>Androsiphonia</i> Stapf	<i>Androsiphonia adenostegia</i> Stapf	Feuillet and MacDougal, 2007; Schmelzer et al., 2008
Passifloroideae	Paropsieae	<i>Barteria</i> Hook. f.	<i>Barteria nigriflora</i> Hook. f.	Feuillet and MacDougal, 2007; Masters, 1871
Passifloroideae	Passifloreae	<i>Basananthe</i> Peyr.	<i>Basananthe lanceolata</i> (Engl.) W.J. de Wilde	Feuillet and MacDougal, 2007; Masters, 1871
Passifloroideae	Passifloreae	<i>Crossostemma</i> Benth.	<i>Crossostemma laurifolium</i> Planch. ex Benth.	Feuillet and MacDougal, 2007; Masters, 1871
Passifloroideae	Passifloreae	<i>Deidamia</i> Thouars	<i>Deidamia clematoides</i> Harms, <i>D. setigera</i> Tul.	Feuillet and MacDougal, 2007; Humbert and Leroy, 1945; JSTOR-K-000311046
Passifloroideae	Passifloreae	<i>Dilkea</i> Mast.	<i>Dilkea acuminata</i> Mast., <i>D. hebes</i> Feuillet	Feuillet and MacDougal, 2007; Feuillet, 2011; JSTOR-HUA-0008478
Passifloroideae	Passifloreae	<i>Efulensia</i> C. H. Wright	<i>Efulensia clematoides</i> C. H. Wright, <i>E. montana</i> W.J. de Wilde	de Wilde, 1974; Feuillet and MacDougal, 2007; JSTOR-RB-0000006953614
Passifloroideae	Passifloreae	<i>Hollrungia</i> K. Schum.	<i>Hollrungia aurantioides</i> K. Schum.	de Wilde, 1972; Feuillet and MacDougal, 2007
Passifloroideae	Passifloreae	<i>Mitostemma</i> Mast.	<i>Mitostemma brevifilis</i> Gontsch., <i>M. jenmanii</i> Mast., <i>M. glaziovii</i> Mast.	Feuillet and MacDougal, 2007; Killip, 1938
Passifloroideae	Paropsieae	<i>Paropsia</i> Thouars	<i>Paropsia grewoides</i> Welw. ex Mast.	Feuillet and MacDougal, 2007; Masters, 1871; Schmelzer et al., 2008
Passifloroideae	Passifloreae	<i>Paropsiopsis</i> Engl.	<i>Paropsiopsis decandra</i> Sleumer	de Vos and Breteler, 2009; Feuillet and MacDougal, 2007
Passifloroideae	Passifloreae	<i>Passiflora</i> L.	See references	Mezzonato-Pires et al., 2017; Pérez-Cortéz, 2007; BH-000128952; BH-000128953
Passifloroideae	Passifloreae	<i>Schlechterina</i> Harms	<i>Schlechterina mitostemmatoides</i> Harms	de Wilde, 1976; Feuillet and MacDougal, 2007
Passifloroideae	Paropsieae	<i>Smeathmannia</i> R. Brown	<i>Smeathmannia pubescens</i> Sol. ex R. Br.	Feuillet and MacDougal, 2007; Masters, 1871; Schmelzer et al., 2008
Passifloroideae	Paropsieae	<i>Viridivia</i> Hemsl. & Verdc.	<i>Viridivia suberosa</i> Hemsl. & Verdc.	Feuillet and MacDougal, 2007; JSTOR-K-000311341
Turneroideae	NA	<i>Adenoa</i> Arbo	<i>Adenoa cubensis</i> (Britton & P. Wilson) Arbo	Arbo, 2007; Arbo et al., 2015
Turneroideae	NA	<i>Afroqueta</i> Thulin & Razafim.	<i>Afroqueta capensis</i> (Harv.) Thulin & Razafim.	Arbo et al., 2015
Turneroideae	NA	<i>Arboa</i> Thulin & Razafim.	see Arbo et al., 2015	Arbo et al., 2015
Turneroideae	NA	<i>Erblichia</i> Seem.	see Arbo et al., 2015	Arbo, 2007; Arbo et al., 2015
Turneroideae	NA	<i>Hyalocalyx</i> Rolfe	see Arbo et al., 2015	Arbo, 2007; Arbo et al., 2015
Turneroideae	NA	<i>Loewia</i> Urb.	<i>Loewia glutinosa</i> Urb.	Arbo, 2007; Arbo et al., 2015
Turneroideae	NA	<i>Mathurina</i> Balf. f.	<i>Mathurina penduliflora</i> Balf. f.	Arbo, 2007; Arbo et al., 2015
Turneroideae	NA	<i>Piriqueta</i> Aubl.	see Arbo, 1995	Arbo, 1995; Arbo, 2007; Arbo et al., 2015; BH-000120581
Turneroideae	NA	<i>Stapfiella</i> Gilg	see Arbo et al., 2015	Arbo, 2007; Arbo et al., 2015
Turneroideae	NA	<i>Streptopetalum</i> Hochst.	<i>Streptopetalum serratum</i> Hochst.	Arbo, 2007; Arbo et al., 2015
Turneroideae	NA	<i>Tricliceras</i> Thonn. ex DC.	<i>Tricliceras pilosum</i> (Willd.) R.Fern.	Arbo, 2007; Arbo et al., 2015
Turneroideae	NA	<i>Turnera</i> L.	see Arbo et al., 2015	Bailey; Arbo, 2007; Arbo et al., 2015; BH-000120582

**Appendix S1.** List of species observed and literature used for the morphological comparison of Passifloraceae genera. **Notes:** Herbaria abbreviations. BH: L. H. Bailey Hortorium Herbarium; HUA: Herbario Universidad de Antioquia; K: Royal Botanic Gardens, Kew; RB: Jardim Botânico do Rio de Janeiro.

## REFERENCES APPENDIX S1

- Arbo, M.M. 1995. Turneraceae: Parte I Piriqueta. *Flora Neotropica* 67: 1–156.
- Arbo, M.M. 2007. Turneraceae. In K. Kubitzki [ed.], Flowering plants · Eudicots, The families and genera of vascular plants, 458–466. Springer, Berlin, Heidelberg. Available at: [https://link.springer.com/chapter/10.1007/978-3-540-32219-1\\_53](https://link.springer.com/chapter/10.1007/978-3-540-32219-1_53) [Accessed Dec 10, 2016].
- Arbo, M.M., A.M. Gonzalez, and S.M. Sede. 2015. Phylogenetic relationships within Turneraceae based on morphological characters with emphasis on seed micromorphology. *Plant Systematics and Evolution* 301: 1907–1926.
- Corner, E.J.H. 1976. The seeds of Dicotyledons. Cambridge University Press, Cambridge, UK.
- Feuillet, C. 2011. Two new species of *Dilkea* subgenus *Dilkea* (Passifloraceae) from Loreto, Peru. *PhytoKeys* 2: 1–8.
- Feuillet, C., and J.M. MacDougal. 2007. Passifloraceae. In K. Kubitzki [ed.], Flowering plants · Eudicots, The families and genera of vascular plants, 270–281. Springer, Berlin, Heidelberg. Available at: [https://link.springer.com/chapter/10.1007/978-3-540-32219-1\\_35](https://link.springer.com/chapter/10.1007/978-3-540-32219-1_35) [Accessed Dec 6, 2016].
- Gentry, A.H. 1992. New species of woody plants from Amazonian Peru. *Novon* 2: 333–338.
- Humbert, H., and J.-F. Leroy. 1945. Passifloraceae. Flore de Madagascar et des Comores (plantes vasculaires), vol. 143. Gouvernement general de Madagascar.

- Imprimerie officielle. Tananarive, Madagascar. Available at:  
<http://archive.org/details/mobot31753003400311>.
- Killip, E.P. 1938. The American species of Passifloraceae. Publications of the Field Museum of Natural History, Chicago, USA. Available at:  
<http://www.biodiversitylibrary.org/item/19699>.
- Kubitzki, K. 2007. Malesherbiaceae. In K. Kubitzki [ed.], Flowering plants · Eudicots, The families and genera of vascular plants, 247–249. Springer, Berlin, Heidelberg. Available at: [https://link.springer.com/chapter/10.1007/978-3-540-32219-1\\_31](https://link.springer.com/chapter/10.1007/978-3-540-32219-1_31) [Accessed Dec 10, 2017].
- Mezzonato-Pires, A.C., C.B.F. Mendonça, M.A. Milward-De-Azevedo, V. Gonçalves-Esteves, A.C. 2017. The taxonomic significance of seed morphology in the *Passiflora* subgenus *Astrophea* (Passifloraceae). *Acta Botanica Brasilica* 31: 68–83.
- Masters, D. 1871. Passiflorae. In D. Oliver [ed.], Flora of Tropical Africa. Part LXIII. 503–520. L. Reeve & Co., London, UK. Available at: <http://biodiversitylibrary.org/page/18088618>
- Pérez-Cortéz, S. 2007. Atlas morfológico de semillas en especies del género *Passiflora* L. presentes en Venezuela. Fundación Instituto Bótanico de Venezuela, Caracas, Venezuela.
- Ricardi, S.M. 1967. Revisión taxonómica de las Malesherbiaceas. *Gayana* 16: 3–139.
- Schmelzer, G.H., G.H. Schmelzer, and A. Gurib-Fakim. 2008. Plant resources of Tropical Africa 11 (1). Medicinal Plants 1. PROTA Foundation. Wageningen, Netherlands.

- Vos, J.M. de, and F.J. Breteler. 2009. A revision of the African genera *Paropsiopsis* and *Smeathmannia* (Passifloraceae – Paropsieae), including a new species of *Paropsiopsis* from Cameroon. *Edinburgh Journal of Botany* 66: 27–49.
- de Wilde, W.J.J.O. 1972. Passifloraceae. *Flora Malesiana - Series 1, Spermatophyta*. vol. 7: 405–434. Noordhoff Int. Publ., Leiden. Netherlands.
- de Wilde, W.J.J.O. 1974. Account of *Efulensia* (Passifloraceae). *Blumea* 22: 31–35.
- de Wilde, W.J.J.O. 1976. Passifloraceae. *In* Flora of Southern Africa, Government Printer, Pretoria, by Cape & Transvaal Printers, Ltd., Parow, C.P., South Africa.

## APPENDIX S2

**Appendix S2.** Comparison table of seed morphological characters, geographic distribution and number of species of Passifloraceae genera. The species observed and literature used to compile the table are listed in Appendix S1.

Genus	Shape	Compressed	Length (mm)	Chalaza	Hard seed coat	Ornamentation	No. spp	Distribution
<i>Malesherbia</i>	Obovoid to elliptic	Absent	1.3–2.7	Prominent	Absent	Reticulate in vertical and horizontal tiers	24	Central Peru to Central Chile and adjacent Argentina
<i>Adenia</i>	Obovoid to elliptic	Present	7–8	Prominent	Present	Foveolate	~100	Africa, Madagascar, Southeast Asia, Malesia and Australia
<i>Ancistrothyrus</i>	Obovoid	Present	12–14	?	?	Shallowly foveolate	2	Tropical South America
<i>Androsiphonia</i>	?	?	?	?	?	Foveolate	1	Liberia
<i>Barteria</i>	Obovoid	Present	?	Not prominent	?	Coarsely foveolate	4	Central Africa
<i>Basananthe</i>	Ellipsoid to reniform	Present	?	Prominent	Present	Rugose?	30	Central, eastern and southern Africa
<i>Crossostemma</i>	?	?	?	?	?	?	1	West Africa
<i>Deidamia</i>	Obovoid	?	?	Not prominent	Present	Coarsely foveolate	5	Madagascar
<i>Dilkea</i>	Obovoid	Present	7–9	Prominent with protrusions	Present	Coarsely foveolate	6	South America and Panama
<i>Efulensia</i>	Subellipsoid	Present	6–8	Rounded with protrusions	Present	Coarsely foveolate	2	Equatorial Africa
<i>Hollrungia</i>	Ellipsoid to obovoid	Present	5.5–7	Prominent	?	Coarsely foveolate or grooved	2	Borneo, New Guinea and northern Australia
<i>Mitostemma</i>	?	?	?	?	?	?	3	Tropical South America
<i>Paropsia</i>	Obovoid to ovoid	Present	5–7	Inconspicuous	Present	Grooved and foveolate	11	Tropical Africa, Madagascar and Malesia
<i>Paropsiopsis</i>	Ovoid to ellipsoid	?	4–5(–7)	?	?	Foveolate	7	Tropical west Africa
<i>Passiflora</i>	Obovoid, ellipsoid and ovoid	Present	1.4–9.1	Rounded, truncate, prominent with or without protrusions, or inconspicuous	Present	Shallowly to coarsely foveolate and transversally grooved	~525	America, India and south China to Australia and Samoa
<i>Schlechterina</i>	Ellipsoid	Present	6–8	?	?	Foveolate	1	Tropical East Africa
<i>Smeathmannia</i>	Ellipsoid to obovoid	Present	?	?	Present	Foveolate	2	Tropical West Africa
<i>Viridivia</i>	Ovoid to ellipsoid	Present	8–9	Prominent	Present	Shallowly foveolate	1	Tanzania and Zambia
<i>Adenoa</i>	Obovoid, slightly curved	Absent	4.7	Rounded, not prominent	Absent	Striate	1	Southeast Cuba
<i>Afroqueta</i>	Slightly curved	Absent	3.6	Prominent and concave	Absent	Reticulate	1	Africa
<i>Arboa</i>	Slightly curved	Absent	2.5–4	Rounded, not prominent	Absent	Striate	4	Madagascar
<i>Erblichia</i>	Slightly curved	Absent	4–5	Rounded	Absent	Striate	5	Madagascar and Mesoamerica
<i>Hyalocalyx</i>	Obovoid, curved	Absent	1.5–1.6	Rounded	Absent	Reticulate	1	Madagascar and south-eastern Africa
<i>Loewia</i>	Obovoid, usually straight	Absent	3.6	Prominent and concave	Absent	Reticulate	3	East Africa
<i>Mathurina</i>	Straight	Absent	4.2	Rounded, not prominent	Absent	Striate	1	Mascarenes (Rodrigues Island)
<i>Piriqueta</i>	Curved, occasionally straight	Absent	1.8–3.6	Obtuse	Absent	Reticulate	45	America and South Africa
<i>Stapfiella</i>	Straight, concave	Absent	3–4.6	Somewhat prominent	Absent	Striate-reticulate	6	Tropical Africa
<i>Streptopetalum</i>	Curved	Absent	3.4	Prominent and concave	Absent	Reticulate	6	East tropical and southern Africa

<i>Tricliceras</i>	Obovoid, usually straight	Absent	3.4	Prominent and concave	Absent	Reticulate	16	Central and southern Africa
<i>Turnera</i>	Curved	Absent	1.2–4.9	Obtuse or prominent and concave	Absent	Striate or reticulate	143	America and Africa

---